Biogeochemical assessments of rapidly changing glacial rivers on the eastern slopes of the Canadian Rocky Mountains

by

Jessica A. Serbu

A thesis submitted in partial fulfillment of the requirements for the degree of

Doctor of Philosophy

in

Ecology

Department of Biological Sciences
University of Alberta

Abstract

Climate change is driving the loss of alpine glaciers globally, yet investigations about the water quality of rivers stemming from them are few. In Chapter 2, we provide an overview of a biogeochemical dataset containing 200+ parameters that we collected between 2019-2021 from 14 sampling sites along the headwaters of three such rivers (Sunwapta-Athabasca, North Saskatchewan, and Bow). Notably, their watersheds spanned glacierized to montane altitudinal life zones over 100 km reaches on the eastern slopes of the Canadian Rocky Mountains in Banff and Jasper National Parks, Alberta. We used regional hydrometric datasets to accurately model discharge at our sampling sites. We created a Local Meteoric Water Line (LMWL) using riverine water isotope signatures and compared it to collected regional rain, snow, and glacial ice signatures. Principal component analyses of physicochemical measures revealed distance from glacier explained more data variability than other spatiotemporal factors (i.e., season, year, or river). Discharge, chemical concentrations, and watershed areas were then used to model site-specific open water season yields for 25 parameters. Chemical yields followed what would generally be expected along river continuums from glacierized to montane altitudinal life zones, with landscape characteristics driving chemical sources and sinks. Particulate chemical yields were generally highest near source glaciers with proglacial lakes acting as settling ponds, whereas most dissolved chemical yields varied by parameter and site. As these headwaters continue to evolve with glacier mass loss, the dataset and analyses presented here can be used as a contemporary baseline to mark future change against.

Geochemical weathering is especially pronounced in glacierized watersheds due to large quantities of fresh glacial flour. In Chapter 3, we assessed types and magnitude of geochemical weathering in the same three Canadian Rocky Mountain eastern slope rivers described in

Chapter 2. We used multiple lines of evidence to quantify geochemical weathering along our ecologically complex river transects and across seasons and years. CO_2 was highly undersaturated, and CO_2 fluxes most negative, at sampling sites nearest source glaciers, while calcite saturation indices were mostly below zero. The chemostatic behavior of Ca^{2+}, Mg^{2+} and dissolved inorganic carbon (DIC) indicated carbonate weathering at all sites, though relative Si inputs increased downriver. Molar concentration ratios showed H_2CO_3 was the key proton donor to weathering reactions. The range of $^{87}Sr/^{86}Sr$ ratios indicated a lack of lithological contrasts, while $\delta^{34}S\text{-}SO_4$ was similar to global evaporites, and $\delta^{13}C$-DIC was the most isotopically heavy at sites nearest source glaciers. Organic matter and silicate weathering contributions to the DIC mass balance increased moving downriver. Yet, carbonate weathering and atmospheric CO_2 remained the dominant sources of DIC throughout our rivers, with >50% contribution even 100 km downriver of source glaciers. On a global scale, we suspect these patterns in types and magnitude of geochemical weathering are common across glacierized watersheds. As glaciers retreat due to climatic warming and we see an encroachment of downriver altitudinal life zones, sources of DIC may shift.

Finally, in Chapter 4, which was initiated during the 2020 COVID-19 shutdown, we quantified how efficiently the contaminants total mercury (THg) and methylmercury (MeHg) were removed from North Saskatchewan River water along the different stages of drinking water production at the E.L. Smith Drinking Water Treatment Plant in the municipality of Edmonton, Alberta. Water treatment processes involved chemical additions for flocculation, followed by clarification, filtration, and UV treatment prior to water being stored in reservoirs for later distribution. 75% THg and 66% MeHg were removed from river water following chemical additions and clarification. A further 9.8% THg and 31.8% MeHg was removed during the filtration stage,

while 1.5% THg and 0.8% MeHg more was removed during UV treatment. The final product water was an order of magnitude less than Canada's maximum allowable concentration for drinking water. We also examined how yields of Hg changed along the North Saskatchewan River as it flowed from its glacial headwaters described in Chapter 2 to where water was removed for drinking water production 534 km downriver. In 2020, mean open water season (1 May to 31 October) THg yields varied greatly from 0.127 to 1.29 g km^{-2} at headwater and mid-river sites but increased to 1.89 g km^{-2} at Edmonton, suggesting value in the protection of source watersheds.

Preface

Science is nothing if not collaborative. Due to the inherently interdisciplinary nature of this field of study, collaborations were necessary and welcome. Throughout this thesis, I use the term “we” to depict this.

Chapter 1 includes an introduction to the Canadian Rocky Mountains and downstream environments, the field sites where data was collected for this thesis, the objectives of this thesis, and is my original work.

Chapter 2 was published as: Serbu, J. A., St.Louis, V. L., Emmerton, C. A., Tank, S. E., Criscitiello, A. S., Silins, U, Bhatia, M. P., Cavaco, M. A., Christenson, C., Cooke, C. A., Drapeau, H. F., Enns, S. J. A., Flett, J. E., Holland, K. M., Lavallee-Whiffen, J., Ma, M., Muir, C. E., Poesch, M., & Shin, J. A comprehensive biogeochemical assessment of the headwaters of three major glacier-fed rivers on the eastern slopes of the Canadian Rocky Mountains under the threat of climate change. (2024). Journal of Geophysical Research: Biogeosciences. 129, e2023JG007745. https://doi. org/10.1029/2023JG007745

Chapter 3 will be submitted to Global Biogeochemical Cycles as: Serbu, J. A., Tank, S. E., Peucker-Ehrenbrink, B., & St.Louis, V. L. Spatiotemporal patterns of geochemical weathering along rivers spanning glacierized to montane altitudinal life zones.

Chapter 4 will be submitted to Environmental Science & Technology Letters as: Serbu, J. A., Graydon, J. A., Charrois, J. W. A., Emmerton, C. A., & St.Louis, V. L. Removal of total and methyl mercury from North Saskatchewan River water during the production of municipal drinking water in Edmonton, Alberta, Canada.

Chapter 5 concludes my thesis and is my original work.

Acknowledgements

First and foremost, thank you to my supervisor Vince St.Louis. You believed in me when I often didn't believe in myself and I'm not sure I could have gotten through this without you. Thank you also to my supervising committee Drs. Suzanne Tank and Craig Emmerton for your guidance and reassurance along the arduous journey that was my PhD. I was lucky enough to be a guest student in three academic laboratories during my PhD – with Drs. Jemma Wadham and Moya Macdonald at the Bristol Glaciology Centre, Dr. Kyra St.Pierre in Vancouver, BC, and Dr. Bernhard Peucker-Ehrenbrink at the Woods Hole Oceanographic Institution – which allowed me to expand the breadth and depth of my learning. So many people contributed to the projects of my thesis. I am deeply, deeply indebted to the four superstar undergraduate students that worked with me through my PhD and who never fail to be awe-inspiring to me - Sydney Enns, Janelle Flett, Jessie Lavallee-Whiffen, and Conall Muir. All the field and laboratory work that went into this thesis would just not have been possible without you. Thank you also to my close collaborators Hayley Drapeau and Maya Bhatia for their roles in making the mountain project a success and contributing data to this thesis. To all the coauthors who also contributed time, data, or expertise to my research chapters – I will never be able to express how thankful I am. A special shout out to two former St.Louis Lab members, who I am lucky to call friends and mentors, Maria Cavaco and Kyra St.Pierre. Thank you Bobbi, Shelby, Dale, Jen, and all my other amazing friends that only want the best for me and lift me up when I am down. Thank you to my family, particularly my mom Kathy, an absolute generous force, and my much, much older and only somewhat wiser sisters (I had to) Christie (Tanner, Evann, James) and Amy (Brent, Charlize, Sianne), and extended family including my worldly and intelligent Gramma (Ann) and Grampa (James), and down-to-earth and loving Mémère (Marie) and Pépère (Gene). To the four-legged animals in my life – Puma Canoe, Indigo, Bolt, Blackey – thank you for all the unconditional love. To my inner saboteur, which controlled me more than I would have liked, you can only imagine what I think of you.

Many laboratories were instrumental (pun!) in the analysis of samples for my projects, but I would be remiss if I didn't highlight Dr. Mingsheng Ma and the Biogeochemical Analytical Service Laboratory (BASL) at the UofA. Their support of me over the years was unmatched and so greatly appreciated. Data collected via fieldwork was approved under permits JNP-2018-

29597 (Jasper National Park) and LL-2019-32266 (Banff National Park). Funding for this thesis was provided by the Canadian Mountain Network (Chapters 2 & 3), Natural Sciences and Engineering Research Council of Canada (NSERC) Discovery Grant (all chapters) and the Alberta Conservation Association Biodiversity Grant (Chapters 2 & 3). I was personally funded through an NSERC CGS-M, NSERC PGS-D, Henry Kroeger Memorial Graduate Scholarship, and Government of Alberta Women in STEM Scholarship.

We acknowledge that the University of Alberta is on Treaty 6 Territory and fieldwork was conducted on Treaty 7 and 8 Territories. Jasper and Banff National Parks are located on the lands of the Ktunaxa ʔamakʔis (Ktunaxa), As’in’i’wa’chi Niy’yaw Askiy (Rocky Mountain Cree), Ĩyãħé Nakón mąkóce (Stoney), Niitsítpiis-stahkoii ᖹᐟᒧᐧᐨᑯᐧ ᓴᐦᖾᐟ (Blackfoot / Niitsítapi ᖹᐟᒧᐧᒣᑯ), Secwepemcúl’ecw (Secwépemc), Tsuut’ina, Michif Piyii (Métis), and Mountain Métis people.

Inspirational Quotes

“If they got to the moon with less technology than you have in your phone, you can figure out how to sample DIC.” [after I messed up ^{13}C-DIC during my first field trip] – Dr. Vincent St.Louis

“This doesn’t give me heartburn.” [in reference to how I did hydrology for Chapter 2] – Dr. Uldis Silins

“There is no funny business here.” [in reference to the CQ graphs in Chapter 3] – Dr. Bernhard Peucker-Ehrenbrink

“Science without publication is just recreation.” – Dr. Rolf Vinebrooke, as told by Shelby Stenerson

Table of Contents

List of Tables

List of Figures

Chapter 1: General introduction

Current perspectives on climate change

The “Anthropocene” is a term famously promoted by Crutzen & Stoermer (2000) to define a new contemporary epoch that is irrefutably influenced by human activities. Though recently rejected as a formal geological epoch (Witze, 2024), it is expected to prevail as a concept that prevails in both the hard and soft sciences (Malhi, 2017; Witze, 2024). Now, nearly a quarter of a century since its introduction into the scientific lexicon, the onset of the Anthropocene is still greatly debated (Zalasiewicz et al., 2010, 2020), but has been argued to capture the start of The Great Acceleration (Lewis & Maslin, 2015; Steffen et al., 2015). The Great Acceleration refers to the post-1950 rapid exponential increase in human population size, socio-economic trends like transportation and energy and water use, and Earth system trends like surface temperature and land use change (Steffen et al., 2015). A particularly important post-1950s upward Earth system trend is the release of strong greenhouse gases (GHGs), such as carbon dioxide and methane, to the atmosphere due to various human activities. Once in the atmosphere, GHGs have the capacity to warm the planet (IPCC, 2023).

Mean global temperatures were 1.1°C warmer in 2011-2020 compared to 1850-1900, a mark of anthropogenic climate change (IPCC, 2023). How much the planet will warm in the future will depend on continued GHG emissions, with the ideal limit to warming of 1.5°C above preindustrial levels. Yet, 2023 was the hottest year on record globally, and nearly 1.5°C warmer compared to 1850-1900 (Copernicus, 2024). Even if GHG emissions were curbed today, the accumulation of GHGs in the atmosphere, and their continued cycling between Earth’s biogeochemical reservoirs – including the atmosphere, ocean, and terra – will likely result in a global temperature “overshoot”, an uncertain excess in temperature that would be difficult to recover from (Hoegh-Guldberg et al., 2019). Some adverse impacts of climate change on global ecosystem health include sea level rise (Karl & Trenberth, 2003), loss of biodiversity (Habibullah et al., 2022), and more extreme temperature and precipitation events (Madakumbura et al., 2019).

The increase in GHGs emissions from human activities that forms the basis of rapid climate change has long been examined by the scientific community (Houghton & Woodwell, 1989;

Keeling, 1960). Yet, the scientific methodologies we apply to it and the way we approach it has evolved over time. Additional to Representative Concentration Pathways (RCPs), which are GHG emission scenarios used by climate modelers, the latest Intergovernmental Panel on Climate Change Report included Shared Socio-economic Pathways (SSPs) (IPCC, 2023). The introduction of SSPs to the 2021 IPCC Report cements the role that national and international socioeconomics play in GHG emissions and the importance of widescale concerted efforts for mitigation and adaptation. However, regardless of which SSP is followed, not all communities will be impacted by climate change equally. For instance, global sea level rose an average of 3.7 mm yr^{-1} from 2006 to 2018 (IPCC, 2023), disproportionally affecting high populous coastal regions (Nicholls, 2011). Extreme events like heatwaves, droughts, and wildfires are also expected to increase globally (IPCC, 2023), with desert and forested communities bearing the brunt of the impact (Halofsky et al., 2020; Race et al., 2023). Water resources in mountains, including predictable precipitation, snowpacks, and glaciers, are at also risk (Pepin et al., 2022; Viviroli et al., 2011). Within the mountains, water quality and trophic structures will change, while beyond the mountains, clean water for drinking, infrastructure, and recreation will diminish (**Figure 1.1**) (Huss et al., 2017). It follows that individuals that live on the margins or in the lowlands of mountains are particularly prone to the effects of climate change (Beniston, 2003; Knight, 2022).

Climate change in glacierized mountains

Glaciers, ice caps, and ice sheets store approximately 75% of the Earth's freshwater (Jansson et al., 2003). With seasonal fluctuations in temperature and precipitation, glaciers gain mass in winter and lose it in summer (Bennet & Glasser, 2009). Because nearly a fourth of the world's population depends on clean mountain freshwaters for survival, the alteration of glacial water sources will leave vulnerable populations with freshwater insecurity (Immerzeel et al., 2020). Human-induced climate warming is, however, amplified at high latitudes (Arctic and Antarctic) and in high altitude (alpine) regions (IPCC, 2023). As a result, global glacier (non-ice sheet) volume is expected to decline up to 41% by 2100 as glacier mass losses exceed mass gains (Radić et al., 2014), with coincident changes to downstream runoff (Bliss et al., 2014; Huss & Hock, 2018).

As glaciers melt, new and biogeochemically reactive areas, called proglacial landscapes, form in front of the retreating ice mass. Although proglacial landscapes are some of the most rapidly emerging and evolving regions on the planet, they are little studied and poorly understood. The terrestrial portions of these proglacial landscapes consist of exposed bedrock and fine mineral sediments formed by glacial erosion. They tend to be sparsely vegetated with poorly developed organic soils in the early successional stages of glacial retreat (Cauvy-Fraunié & Dangles, 2019). The meltwaters that converge in proglacial zones originate from channels along the edge of glaciers, from over the glacier surface, or through and beneath the glaciers (Bhatia et al., 2011; Dubnick et al., 2017; Raiswell, 1984). Hence, glacial mass loss will also result in the downstream release of archived nutrients (Hood et al., 2015; Warner et al., 2017) and legacy contaminants (Beal et al., 2015; Fernández et al., 2003; Schuster et al., 2015) that were transported and deposited to high latitude and alpine regions over previous decades or centuries (Boutron, 1995; Legrand & Mayewski, 1997), as well as previously stored old and potentially labile organic carbon and nutrients from underneath glaciers (Barker et al., 2006; Hood et al., 2015; Hood & Scott, 2008).

Mineral sediment, derived from the physical abrasion and grinding of underlying bedrock, is also expulsed from subglacial environments with glacial meltwaters (Bennet & Glasser, 2009). This sediment, known as glacial flour, is freshly ground and ultra-fine grained. Thus, glacial meltwaters laden with these sediments are ideal locations for geochemical weathering reactions to take place. The type of geochemical weathering that may occur is dependent on the minerals present and the acid that acts to transform that mineral. For example, the weathering of carbonate and silicate minerals with the weak carbonic acid consumes carbon dioxide (CO_2) on short and long geological timescales, respectively (Eq. 1 & 2), while the weathering of carbonates with sulfuric acid via sulfide oxidation (Eq. 3) releases $CO_{2(g)}$ (Eq. 4).

$$CaCO_{3(s)} + H_2O + CO_{2(g)} \rightarrow Ca^{2+} + 2HCO_3^- \textbf{ (Eq. 1)}$$

$$CaAl_2Si_2O_{8(s)} + 3H_2O + 2CO_{2(g)} \rightarrow Ca^{2+} + 2HCO_3^- + Al_2Si_2O_5(OH)_{4(s)} \textbf{ (Eq. 2)}$$

$$4FeS_2 + 15O_2 + 14H_2O \rightarrow 4Fe(OH)_3 + 8H_2SO_4 \textbf{ (Eq. 3)}$$

$$CaCO_3 + H_2SO_4 \rightarrow CO_{2(g)} + H_2O + Ca^{2+} + SO_4^{2-} \textbf{ (Eq. 4)}$$

Prominent landscape features across proglacial watersheds can further help define the biogeochemical load of glacial meltwaters, and in turn, their geochemical reactivity. Proglacial lakes, carved from the recession of a glacier, are known to be strong sinks of sediment carried with glacial meltwaters (Carrivick & Tweed, 2013). Further, sediment-bound chemicals such as some nutrients and contaminants that were released during glacial melt will also be sequestered in proglacial lakes (Zhou et al., 2024; Zhu et al., 2020), and may have important implications for the biological species that live there (Vorobyeva et al., 2015). As meltwaters traverse immediate proglacial landscapes in braided river systems, they can also entrain vast quantities of additional sediments (Malard et al., 2006; Schroth et al., 2011). Glacial outwash floodplains are, for example, areas of loose sediment that can be moved by, and transferred in, glacial meltwaters to downstream locales (Goff & Ashmore, 1994). Glacial outwash floodplains, also known as sandurs, have been noted to be hotspots of geochemical exchanges (Deuerling et al., 2018), in part due to the pulsing of meltwaters and their biogeochemical constituents.

Overall, we know little about hydrological-biogeochemical couplings across rapidly changing proglacial landscapes and the impact of these on the ecosystem goods and services associated with downstream freshwaters (Milner et al., 2017). Thus, part of the purpose of my dissertation was to begin addressing some of these knowledge gaps by collecting, recording, and analyzing a comprehensive water quality dataset for the eastern slopes of the Canadian Rocky Mountains, an alpine region vulnerable to climate change.

The Canadian Rocky Mountains

Formidable against the adjacent western prairies, the Canadian Rocky Mountains have long been a focus of cultural and scientific interest. On the eastern slopes, world-renowned Banff National Park was founded in 1885 as Canada's first National Park, while its northern sibling Jasper National Park was founded in 1907. Both are steeped in rich histories with deep Indigenous roots and settler narratives. For example, archeological evidence in the form of spearheads, knives, and animal bones scarred with deliberate cut marks date early human occupation of the Canadian Rocky Mountains to 11,000 BP (Gadd, 2009). Today, Jasper and Banff National Parks are recognized to be located on Treaty 7 and 8 territories covering the lands of the Ktunaxa ʔamakʔis (Ktunaxa)**,** As'in'i'wa'chi Niy'yaw Askiy (Rocky Mountain Cree), Ĩyãħé Nakón mąkóce (Stoney), Niitsítpiis-stahkoii ᖹᐟᒧᐧᖿᐧ ᓴᐦᖾᐟ (Blackfoot / Niitsítapi ᖹᐟᒧᐧᒣᑯ),

Secwepemcúl’ecw (Secwépemc), Tsuut’ina**,** Michif Piyii (Métis), and Mountain Métis people (Ruka et al., 2024).

It is on these lands where historic and current scientific exploration have occurred. Early in the 20th century, much scientific inquiry focused on the geological make up and landforms of the Canadian Rocky Mountains (Clark, 1949; Heusser, 1956), or the practical business of land surveying (**Figure 1.2**). By comparison, recent research has generally focused on the rapid diminishment of the icefields and outlet glaciers in this region (e.g., Marshall et al., 2011; Tennant et al., 2012). However, with few exceptions (e.g., Blais et al., 2001; Lafrenière & Sharp, 2004; Staniszewska et al., 2021), the biogeochemistry of the meltwaters that stem from these glaciers have rarely been examined in a comprehensive manner.

Downstream freshwaters

Glacier-fed meltwaters of the Canadian Rocky Mountains form the proglacial headwaters of three primary river watersheds in Alberta – the Athabasca, North Saskatchewan, and Bow. These headwaters originate in the icefields of Jasper and Banff National Parks that are rapidly losing mass due to climate warming. In Alberta, annual glacial meltwater contributions to river flow may be reduced 10-fold, from 1.1 km^3 in the early 2000s to only 0.1 km^3 by 2100 (Gardner et al., 2013). Meltwater stemming from these headwater regions establishes the watersheds’ initial nutrient, contaminant, and sediment loads and thus impact downstream resident primary producers and microbial communities. These rivers are also the source of drinking water to major municipalities in Alberta, and contribute to agricultural, recreational, and traditional practices across Canada (Anderson & Radić, 2020). For example, the North Saskatchewan Watershed is the drinking water source of Edmonton and surrounding municipalities amounting to 1.4 million people (EPCOR, personal comm.), contributes freshwater for domestic animals and crop irrigation across the rural prairie provinces of Alberta, Saskatchewan, and Manitoba, and acts as an invaluable clean water resource for Indigenous communities along its route (Schindler & Donahue, 2006). However, since these downstream environments have only been studied sparingly, the characterization of the chemical and biological components of these rapidly changing systems is crucial to understand how changing headwater conditions will affect downstream water quality and the biodiversity that it shapes, as these systems flow eastward through the Province of Alberta.

Objectives

To address gaps in the literature, a water quality dataset focused on the biogeochemistry of meltwaters stemming from the eastern slopes of the Canadian Rocky Mountains was collected and investigated. Data collection for the Chapters 2 and 3 of my PhD dissertation research was conducted over three years (2019-2021) at 14 sites established along the Sunwapta-Athabasca, North Saskatchewan, and Bow rivers, beginning near their source glacier and then at multiple sites up to 100 kilometers downriver. Data was collected for Chapter 4 of my PhD dissertation over a one-year period (2020-2021) at the E.L. Smith Drinking Water Treatment Plant (DWTP) in Edmonton, a facility designed to process raw, untreated North Saskatchewan River water into clean municipal drinking water. Given the importance of these major Albertan rivers, the objectives of my PhD research program were to:

Objective 1: Quantify spatial, seasonal, and interannual patterns in proglacial freshwater physicochemistry and quality;

Objective 2: Determine if geochemical weathering is driving a portion of the CO_2 cycling in these rivers, and how the magnitude of geochemical weathering changes spatially, seasonally, and interannually; and

Objective 3: Establish how efficiently total and methyl mercury are removed from raw river water during the water treatment process, and compare mercury yields from source headwaters to further downriver at the point of consumption.

To accomplish **Objective 1**, four distinct sub-objectives were completed. First, extensive sampling of 200+ basic water physicochemical parameters, including contaminants, was an integral part of my overall research program. Concentrations of water quality parameters were compared between sites, seasons, and years using multivariate statistics. Second, the hydrology for our 14 sampling sites was modeled using watershed area-discharge relationships based on Water Survey of Canada (WSC) gauged Albertan mountain rivers. Third, point concentration data and discharge estimates were then combined to calculate continuous export and yield data for 25 sampled parameters at all 14 sampling sites in 2019 and 2020. Finally, water isotopes collected from riverine, precipitation (snow and rain), and glacial ice samples were used to assess source water contributions to our sites and create a Local Meteoric Water Line (LMWL). This led to a peer-reviewed publication in the Journal of Geophysical Research: Biogeosciences (Serbu et al., 2024) and a peer-reviewed dataset publication in the PANGAEA data repository (Serbu et al., 2023).

Objective 2 was a similarly large undertaking as multiple lines of evidence were used to assess the type and magnitude of geochemical weathering along our ecologically complex study transects, that included glacierized, alpine, subalpine, and montane altitudinal life zones. First, percent saturation, calcite saturation indices, calculated instantaneous CO_2 fluxes, concentration-discharge graphs and molar ratio relationships were assessed. A large suite of stable and radio-isotopes were then used to place our data within a regional and global context. Lastly, a mass balance of DIC sources to our sampling sites was calculated.

For **Objective 3**, research commenced spring 2020 at the onset of the COVID-19 pandemic when my regular field and laboratory work were restricted. We targeted the North Saskatchewan River in Edmonton for its accessibility and collected total and methyl mercury samples from five stages along the water treatment process to determine how this environmental contaminant is removed from human drinking water supplies at the E.L. Smith DWTP. We additionally compared total and dissolved (filtered) mercury yields from the source waters in the Canadian Rocky Mountains (from **Objective 1**) to the point of consumption in Edmonton. Finally, we discuss the benefits of source water protection, including the preservation of whole watersheds, as a known way to mitigate costs associated with building and operating components of the water treatment process.

Ultimately, my dissertation research will identify key impacts of glacial melt on downstream freshwater quality and ecosystem services of importance to Canada, and increase our ability to predict the impact of climate change on the quality of surface waters originating in glacierized landscapes (Milner et al., 2017). The water security and livelihoods of many populations depend on clean freshwaters that originates from mountain regions, yet reliable access to this crucial resource is quickly becoming one of the leading human rights issues of my generation (Immerzeel et al., 2020). Further, accurately estimating geochemical weathering in these rivers is essential for understanding annual carbon budgets and GHG exchange at the watershed-scale in these rapidly changing regions (St. Pierre et al., 2019). The combined datasets from Objectives 1 & 2 will be the most comprehensive record of freshwater quality and health ever documented for the headwaters of these rivers, shaping watershed policy, and acting as a reference for those investigating changes to this vulnerable alpine region in the future (Schindler & Donahue, 2006). The dataset from Objective 3 provides insight into how the contaminant mercury is removed during the water treatment process and how mercury yields change across source water transects. Overall, these datasets will also be crucial for local governments and communities developing climate change management and mitigation plans, and legislation that could protect these resources for future generations.

References

Anderson, S., & Radić, V. (2020). Identification of local water resource vulnerability to rapid deglaciation in Alberta. *Nature Climate Change*, *10*(10), 933–938. https://doi.org/10.1038/s41558-020-0863-4

Barker, J. D., Sharp, M. J., Fitzsimons, S. J., & Turner, R. J. (2006). Abundance and dynamics of dissolved organic carbon in glacier systems. *Arctic, Antarctic, and Alpine Research*, *38*(2), 163–172. https://doi.org/10.1657/1523-0430(2006)38[163:AADODO]2.0.CO;2

Beal, S. A., Osterberg, E. C., Zdanowicz, C. M., & Fisher, D. A. (2015). Ice Core Perspective on Mercury Pollution during the Past 600 Years. *Environmental Science & Technology*, *49*(13), 7641–7647. https://doi.org/10.1021/acs.est.5b01033

Beniston, M. (2003). Climatic change in mountain regions: A review of possible impacts. *Climatic Change*, *59*, 5–31. https://doi.org/10.1007/978-94-015-1252-7_2

Bennet, M. R., & Glasser, N. F. (2009). Glacial geology: Ice sheets and landforms. In *Glacial Geology: Ice Sheets and Landforms* (2nd ed.). Wiley-Blackwell.

Bhatia, M. P., Das, S. B., Kujawinski, E. B., Henderson, P., Burke, A., & Charette, M. A. (2011). Seasonal evolution of water contributions to discharge from a Greenland outlet glacier: Insight from a new isotope-mixing model. *Journal of Glaciology*, *57*(205), 929–941. https://doi.org/10.3189/002214311798043861

Blais, J. M., Schindler, D. W., G Muir, D. C., Sharp, M., Donald, D., Lafrenière, M., Braekevelt, E., & J Strachan, W. M. (2001). Melting glaciers: A major source of persistent organochlorines to subalpine Bow Lake in Banff National Park, Canada. *Ambio*, *30*(7), 410–415.

Bliss, A., Hock, R., & Radić, V. (2014). Global response of glacier runoff to twenty-first century climate change. *Journal of Geophysical Research: Earth Surface*, *119*(4), 717–730. https://doi.org/10.1002/2013JF002931

Boutron, C. F. (1995). Historical reconstruction of the earth's past atmospheric environment from Greenland and Antarctic snow and ice cores. *Environmental Reviews*, *3*(1), 1–28. https://doi.org/10.1139/a95-001

Carrivick, J. L., & Tweed, F. S. (2013). Proglacial lakes: Character, behaviour and geological importance. *Quaternary Science Reviews*, *78*, 34–52. https://doi.org/10.1016/j.quascirev.2013.07.028

Cauvy-Fraunié, S., & Dangles, O. (2019). A global synthesis of biodiversity responses to glacier retreat. *Nature Ecology & Evolution*, *3*(12), 1675–1685. https://doi.org/10.1038/s41559-019-1042-8

Clark, L. M. (1949). Geology of Rocky Mountain front ranges near Bow River, Alberta. *Bulletin of the American Association of Petroleum Geologists*, *33*(4), 614–633. https://doi.org/10.1306/sv15347c2

Copernicus. (2024). *Global Climate Highlights 2023*. https://climate.copernicus.eu/copernicus-2023-hottest-year-record

Crutzen, P. J., & Stoermer, E. F. (2000). The "Anthropocene." *Global Change Newsletter*, *41*, 17–18.

Deuerling, K. M., Martin, J. B., Martin, E. E., & Scribner, C. A. (2018). Hydrologic exchange and chemical weathering in a proglacial watershed near Kangerlussuaq, west Greenland. *Journal of Hydrology*, *556*, 220–232. https://doi.org/10.1016/j.jhydrol.2017.11.002

Dubnick, A., Kazemi, S., Sharp, M., Wadham, J., Hawkings, J., Beaton, A., & Lanoil, B. (2017). Hydrological controls on glacially exported microbial assemblages. *Journal of Geophysical Research: Biogeosciences*, *122*(5), 1049–1061. https://doi.org/10.1002/2016JG003685

Fernández, P., Carrera, G., Grimalt, J. O., Ventura, M., Camarero, L., Catalan, J., Nickus, U., Thies, H., & Psenner, R. (2003). Factors governing the atmospheric deposition of polycyclic aromatic hydrocarbons to remote areas. *Environmental Science & Technology*, *37*(15), 3261–3267. https://doi.org/10.1021/es020137k

Gadd, B. (2009). *Handbook of the Canadian Rockies*. Corex Press.

Gardner, A. S., Moholdt, G., Cogley, J. G., Wouters, B., Arendt, A. A., Wahr, J., Berthier, E., Hock, R., Pfeffer, W. T., Kaser, G., Ligtenberg, S. R. M., Bolch, T., Sharp, M. J., Hagen, J. O., Van Den Broeke, M. R., & Paul, F. (2013). A reconciled estimate of glacier contributions to sea level rise: 2003 to 2009. *Science*, *340*(6134), 852–857. https://doi.org/10.1126/science.1234532

Goff, J. R., & Ashmore, P. (1994). Gravel transport and morphological change in braided Sunwapta River, Alberta, Canada. *Earth Surface Processes and Landforms*, *19*(3), 195–212. https://doi.org/10.1002/esp.3290190302

Habibullah, M. S., Din, B. H., Tan, S.-H., & Zahid, H. (2022). Impact of climate change on biodiversity loss: Global evidence. *Environmental Science and Pollution Research*, *29*(1), 1073–1086. https://doi.org/10.1007/s11356-021-15702-8

Halofsky, J. E., Peterson, D. L., & Harvey, B. J. (2020). Changing wildfire, changing forests: The effects of climate change on fire regimes and vegetation in the Pacific Northwest, USA. *Fire Ecology*, *16*(1), 4. https://doi.org/10.1186/s42408-019-0062-8

Heusser, C. J. (1956). Postglacial environments in the Canadian Rocky Mountains. *Ecological Monographs*, *26*(4), 263–302. https://doi.org/10.2307/1948543

Higgs, E. S. (2023). *Mountain Legacy Project*. https://explore.mountainlegacy.ca

Hoegh-Guldberg, O., Jacob, D., Taylor, M., Guillén Bolaños, T., Bindi, M., Brown, S., Camilloni, I. A., Diedhiou, A., Djalante, R., Ebi, K., Engelbrecht, F., Guiot, J., Hijioka, Y., Mehrotra, S., Hope, C. W., Payne, A. J., Pörtner, H.-O., Seneviratne, S. I., Thomas, A., … Zhou, G. (2019). The human imperative of stabilizing global climate change at 1.5°C. *Science*, *365*(6459), eaaw6974. https://doi.org/10.1126/science.aaw6974

Hood, E., Battin, T. J., Fellman, J., O'Neel, S., & Spencer, R. G. M. (2015). Storage and release of organic carbon from glaciers and ice sheets. *Nature Geoscience*, *8*(2), 91–96. https://doi.org/10.1038/ngeo2331

Hood, E., & Scott, D. (2008). Riverine organic matter and nutrients in southeast Alaska affected by glacial coverage. *Nature Geoscience*, *1*(9), 583–587. https://doi.org/10.1038/ngeo280

Houghton, R. A., & Woodwell, G. M. (1989). Global climatic change. *Scientific American*.

Huss, M., Bookhagen, B., Huggel, C., Jacobsen, D., Bradley, R. S., Clague, J. J., Vuille, M., Buytaert, W., Cayan, D. R., Greenwood, G., Mark, B. G., Milner, A. M., Weingartner, R.,

& Winder, M. (2017). Toward mountains without permanent snow and ice. *Earth's Future*, *5*(5), 418–435. https://doi.org/10.1002/2016EF000514

Huss, M., & Hock, R. (2018). Global-scale hydrological response to future glacier mass loss. *Nature Climate Change*, *8*(2), 135–140. https://doi.org/10.1038/s41558-017-0049-x

Immerzeel, W. W., Lutz, A. F., Andrade, M., Bahl, A., Biemans, H., Bolch, T., Hyde, S., Brumby, S., Davies, B. J., Elmore, A. C., Emmer, A., Feng, M., Fernández, A., Haritashya, U., Kargel, J. S., Koppes, M., Kraaijenbrink, P. D. A., Kulkarni, A. V., Mayewski, P. A., … Baillie, J. E. M. (2020). Importance and vulnerability of the world's water towers. *Nature*, *577*(7790), 364–369. https://doi.org/10.1038/s41586-019-1822-y

IPCC. (2023). *Climate Change 2023: Synthesis Report. Contribution of Working Groups I, II, and III to the Sixth Assessment Report of the Intergovernmental Panel on Climate Change*.

Jansson, P., Hock, R., & Schneider, T. (2003). The concept of glacier storage: A review. *Journal of Hydrology*, *282*(1–4), 116–129. https://doi.org/10.1016/S0022-1694(03)00258-0

Karl, T. R., & Trenberth, K. E. (2003). Modern global climate change. *Science*, *302*(5651), 1719–1723. https://doi.org/10.1126/science.1090228

Keeling, C. D. (1960). The concentration and isotopic abundances of carbon dioxide in the atmosphere. *Tellus*, *12*(2), 200–203. https://doi.org/10.1111/j.2153-3490.1960.tb01300.x

Knight, J. (2022). Scientists' warning of the impacts of climate change on mountains. *PeerJ*, *10*, e14253. https://doi.org/10.7717/peerj.14253

Lafrenière, M. J., & Sharp, M. J. (2004). The concentration and fluorescence of dissolved organic carbon (DOC) in glacial and nonglacial catchments: Interpreting hydrological flow routing and DOC sources. *Arctic, Antarctic, and Alpine Research*, *36*(2), 156–165. https://doi.org/10.1657/1523-0430(2004)036[0156:TCAFOD]2.0.CO;2

Legrand, M., & Mayewski, P. (1997). Glaciochemistry of polar ice cores: A review. *Reviews of Geophysics*, *35*(3), 219–243. https://doi.org/10.1029/96RG03527

Lewis, S. L., & Maslin, M. A. (2015). Defining the Anthropocene. *Nature*, *519*(7542), 171–180. https://doi.org/10.1038/nature14258

Madakumbura, G. D., Kim, H., Utsumi, N., Shiogama, H., Fischer, E. M., Seland, Ø., Scinocca, J. F., Mitchell, D. M., Hirabayashi, Y., & Oki, T. (2019). Event-to-event intensification of the hydrologic cycle from 1.5°C to a 2°C warmer world. *Scientific Reports*, *9*(1), 3483. https://doi.org/10.1038/s41598-019-39936-2

Malard, F., Uehlinger, U., Zah, R., & Tockner, K. (2006). Flood-pulse and riverscape dynamics in a braided glacial river. *Ecology*, *87*(3), 704–716. https://doi.org/10.1890/04-0889

Malhi, Y. (2017). The concept of the Anthropocene. *Annual Review of Environment and Resources*, *42*, 77–104. https://doi.org/10.1146/annurev- environ102016- 060854

Marshall, S. J., White, E. C., Demuth, M. N., Bolch, T., Wheate, R., Menounos, B., Beedle, M. J., & Shea, J. M. (2011). Glacier water resources on the eastern slopes of the Canadian Rocky Mountains. *Canadian Water Resources Journal*, *36*(2), 109–134. https://doi.org/10.4296/cwrj3602823

Milner, A. M., Khamis, K., Battin, T. J., Brittain, J. E., Barrand, N. E., Füreder, L., Cauvy-Fraunié, S., Gíslason, G. M., Jacobsen, D., Hannah, D. M., Hodson, A. J., Hood, E., Lencioni, V., Ólafsson, J. S., Robinson, C. T., Tranter, M., & Brown, L. E. (2017). Glacier shrinkage driving global changes in downstream systems. *Proceedings of the National Academy of Sciences*, *114*(37), 9770–9778. https://doi.org/10.1073/pnas.1619807114

Nicholls, R. (2011). Planning for the impacts of sea level rise. *Oceanography*, *24*(2), 144–157. https://doi.org/10.5670/oceanog.2011.34

Pepin, N. C., Arnone, E., Gobiet, A., Haslinger, K., Kotlarski, S., Notarnicola, C., Palazzi, E., Seibert, P., Serafin, S., Schöner, W., Terzago, S., Thornton, J. M., Vuille, M., & Adler, C. (2022). Climate changes and their elevational patterns in the mountains of the world. *Reviews of Geophysics*, *60*(1), e2020RG000730. https://doi.org/10.1029/2020RG000730

Race, D., Gentle, P., & Mathew, S. (2023). Living on the margins: Climate change impacts and adaptation by remote communities living in the Pacific Islands, the Himalaya and desert Australia. *Climate Risk Management*, *40*, 100503. https://doi.org/10.1016/j.crm.2023.100503

Radić, V., Bliss, A., Beedlow, A. C., Hock, R., Miles, E., & Cogley, J. G. (2014). Regional and global projections of twenty-first century glacier mass changes in response to climate scenarios from global climate models. *Climate Dynamics*, *42*(1–2), 37–58. https://doi.org/10.1007/s00382-013-1719-7

Raiswell, R. (1984). Chemical models of solute acquisition in glacial melt waters. *Journal of Glaciology*, *30*(104), 49–57. https://doi.org/10.3189/S0022143000008480

Ruka, T., Sauca, V., Rawlins, M., Haines, E., Banaszak, R., & Gutierrez, W. (2024). *Native Land Digital*. https://native-land.ca

Schindler, D. W., & Donahue, W. F. (2006). An impending water crisis in Canada's western prairie provinces. *Proceedings of the National Academy of Sciences*, *103*(19), 7210–7216. https://doi.org/10.1073/pnas.0601568103

Schroth, A. W., Crusius, J., Chever, F., Bostick, B. C., & Rouxel, O. J. (2011). Glacial influence on the geochemistry of riverine iron fluxes to the Gulf of Alaska and effects of deglaciation. *Geophysical Research Letters*, *38*(16), n/a-n/a. https://doi.org/10.1029/2011GL048367

Schuster, J. K., Harner, T., Su, K., Mihele, C., & Eng, A. (2015). First results from the oil sands passive air monitoring network for polycyclic aromatic compounds. *Environmental Science & Technology*, *49*(5), 2991–2998. https://doi.org/10.1021/es505684e

Serbu, J. A., St. Louis, V. L., Emmerton, C. A., Tank, S. E., Criscitiello, A. S., Silins, U., Bhatia, M. P., Cavaco, M. A., Christenson, C., Cooke, C. A., Drapeau, H. F., Enns, S. J. A., Flett, J. E., Holland, K. M., Lavallee-Whiffen, J., Ma, M., Muir, C. E., Poesch, M., & Shin, J. (2023). *Physicochemical, particulate matter, temperature, and hydrological datasets collected from climate-threatened glacial river headwaters on the eastern slopes of the Canadian Rocky Mountains (2019-2021)*.

Serbu, J. A., St. Louis, V. L., Emmerton, C. A., Tank, S. E., Criscitiello, A. S., Silins, U., Bhatia, M. P., Cavaco, M. A., Christenson, C., Cooke, C. A., Drapeau, H. F., Enns, S. J. A., Flett, J. E., Holland, K. M., Lavallee-Whiffen, J., Ma, M., Muir, C. E., Poesch, M., & Shin, J. (2024). A comprehensive biogeochemical assessment of climate-threatened glacial river headwaters on the eastern slopes of the Canadian Rocky Mountains. *Journal of Geophysical Research: Biogeosciences*, *129*(1), e2023JG007745. https://doi.org/10.1029/2023JG007745

St. Pierre, K. A., St. Louis, V. L., Schiff, S. L., Lehnherr, I., Dainard, P. G., Gardner, A. S., Aukes, P. J. K., & Sharp, M. J. (2019). Proglacial freshwaters are significant and previously unrecognized sinks of atmospheric CO $_2$. *Proceedings of the National Academy of Sciences*, *116*(36), 17690–17695. https://doi.org/10.1073/pnas.1904241116

Staniszewska, K. J., Cooke, C. A., & Reyes, A. V. (2021). Quantifying meltwater sources and contaminant fluxes from the Athabasca Glacier, Canada. *ACS Earth and Space Chemistry*, *5*(1), 23–32. https://doi.org/10.1021/acsearthspacechem.0c00256

Steffen, W., Broadgate, W., Deutsch, L., Gaffney, O., & Ludwig, C. (2015). The trajectory of the Anthropocene: The Great Acceleration. *The Anthropocene Review*, *2*(1), 81–98. https://doi.org/10.1177/2053019614564785

Tennant, C., Menounos, B., Wheate, R., & Clague, J. J. (2012). Area change of glaciers in the Canadian Rocky Mountains, 1919 to 2006. *The Cryosphere*, *6*(6), 1541–1552. https://doi.org/10.5194/tc-6-1541-2012

Trail to Peak. (2024). *Iceberg Lake + Bow Glacier's Big Toe* [Blog]. Trail to Peak: The Adventurous Path. https://trailtopeaktheadventurouspath.wordpress.com/2019/09/04/iceberg-lake-bow-glaciers-big-toe/

Viviroli, D., Archer, D. R., Buytaert, W., Fowler, H. J., Greenwood, G. B., Hamlet, A. F., Huang, Y., Koboltschnig, G., Litaor, M. I., López-Moreno, J. I., Lorentz, S., Schädler, B., Schreier, H., Schwaiger, K., Vuille, M., & Woods, R. (2011). Climate change and mountain water resources: Overview and recommendations for research, management and policy. *Hydrology and Earth System Sciences*, *15*(2), 471–504. https://doi.org/10.5194/hess-15-471-2011

Vorobyeva, S. S., Trunova, V. A., Stepanova, O. G., Zvereva, V. V., Petrovskii, S. K., Melgunov, M. S., Zheleznyakova, T. O., Chechetkina, L. G., & Fedotov, A. P. (2015). Impact of glacier changes on ecosystem of proglacial lakes in high mountain regions of East Siberia (Russia). *Environmental Earth Sciences*, *74*(3), 2055–2063. https://doi.org/10.1007/s12665-015-4164-6

Warner, K. A., Saros, J. E., & Simon, K. S. (2017). Nitrogen subsidies in glacial meltwater: Implications for high elevation aquatic chains. *Water Resources Research*, *53*(11), 9791–9806. https://doi.org/10.1002/2016WR020096

Witze, A. (2024). Geologists reject the Anthropocene as Easth's new epoch—After 15 years of debate. *Nature*, *627*, 249–250. https://doi.org/10.1038/d41586-024-00675-8

Zalasiewicz, J., Waters, C., & Williams, M. (2020). The Anthropocene. In *Geologic Time Scale 2020* (pp. 1257–1280). Elsevier. https://doi.org/10.1016/B978-0-12-824360-2.00031-0

Zalasiewicz, J., Williams, M., Steffen, W., & Crutzen, P. (2010). The new world of the Anthropocene. *Environmental Science & Technology*, *44*(7), 2228–2231. https://doi.org/10.1021/es903118j

Zhou, Y., Wang, X., Chen, M., Fu, J., Zhu, T., Wang, C., Gong, P., Wang, L., & Ren, J. (2024). Proglacial river sediments are a substantial sink of perfluoroalkyl substances released by glacial meltwater. *Communications Earth & Environment*, *5*(1), 68. https://doi.org/10.1038/s43247-024-01223-y

Zhu, T., Wang, X., Lin, H., Ren, J., Wang, C., & Gong, P. (2020). Accumulation of pollutants in proglacial lake sediments: Impacts of glacial meltwater and anthropogenic activities. *Environmental Science & Technology*, *54*(13), 7901–7910. https://doi.org/10.1021/acs.est.0c01849

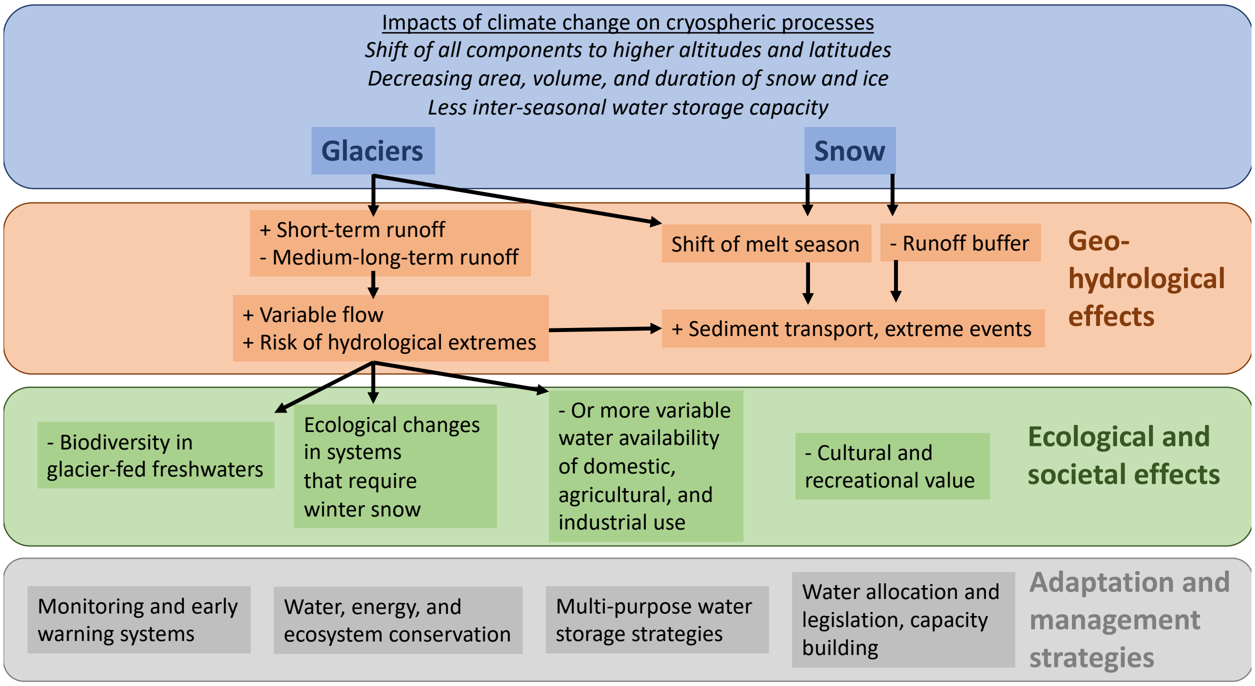

Figure 1.1. Loss of cryosphere components in mountains and their geo-hydrological, ecological, and societal effects. Adapted from Huss et al., 2017.

Figure 1.2. Bow Glacier, as captured by Arthur Oliver Wheeler in 1903 during an Interprovincial Boundary Survey and documented by the Mountain Legacy Project (Higgs, 2024) (left), and in 2019 (Trail to Peak, 2024) (right). Please note the development of proglacial Iceberg Lake in the current (right) photograph.

Chapter 2: A comprehensive biogeochemical assessment of climate-threatened glacial river headwaters on the eastern slopes of the Canadian Rocky Mountains

1 Introduction

Mountains are widely regarded as Earth's water towers, supplying up to 50% of global freshwaters for crucial ecosystem goods and services (Price, 2015). As climate change accelerates alpine glacier mass loss, there is an initial increase in meltwater output until reaching its "tipping point", or maximum discharge, followed by a waning as the smaller ice mass can no longer sustain the export of large water volumes (Bennet & Glasser, 2009). Newly emerging proglacial landscapes in the forefields of retreating glaciers are known to be hotspots of biogeochemical cycling (Tranter & Wadham, 2013; Wadham et al., 2001), and as a result, meltwaters moving across these landscapes tend to have biogeochemical constituents that differ in both concentration and speciation compared to freshwaters in non-glacierized watersheds (Hood & Scott, 2008; Lafrenière & Sharp, 2004). The unique biogeochemical fingerprint of glacial meltwaters is in part due to the various sources of chemicals to glacial environments. First, atmospheric constituents can be transported to ice via both wet and dry atmospheric deposition and trapped within ice, archiving past environmental conditions (Blais et al., 2001; Boutron, 1995; Pasteris et al., 2014). Second, as glaciers move, through basal ice deformation or the advance and retreat of their terminus, their heavy bodies physically weather underlying bedrock, creating characteristic till that includes fine-grained glacial flour ideally suited for geochemical reactions (S. P. Anderson, 2007; Tranter & Wadham, 2013). As alpine glaciers melt, biogeochemical constituents that were atmospherically deposited and archived within the ice or the result of subglacial grinding could be released downriver.

The downriver impacts of glacially derived biogeochemical constituents can be substantial. For instance, organic carbon and nutrients released from receding glaciers have the potential to drastically alter downstream productivity and riverine food webs (Hood et al., 2015; Hood & Scott, 2008). Contaminants like mercury and polycyclic aromatic hydrocarbons (PAHs) released to the atmosphere via anthropogenic activities and deposited to alpine glaciers could drive in-river toxicity (Beal et al., 2015; Fernández et al., 2003; Schuster et al., 2015). Even glacial flour can contribute not only to suspended sediment loads and turbidity of meltwaters, but to downriver biogeochemical reactions (St. Pierre et al., 2019). For instance, nutrients and other water quality parameters that are integral to freshwater biogeochemical cycling can be associated with sediment, impacting bioavailability and uptake by riverine organisms. Similarly, whether trace elements are associated with sediments helps define whether they are available for microbial use downriver (Hawkings et al., 2020). Yet, as mountain glaciers atrophy and meltwater-fed rivers are increasingly reliant on inputs from spring snowmelt and stochastic summer precipitation events, both the reliability of alpine freshwater resources and their biogeochemical make up become more uncertain (S. Anderson & Radić, 2020; Immerzeel et al., 2020; Schindler & Donahue, 2006). This makes it critical to investigate contemporary meltwater quality to establish baseline datasets that future researchers can use to monitor biogeochemical changes as mountain glaciers continue to transform under the pressures of climate change (Milner et al., 2017).

The total glacierized region of Western Canada and the US is the seventh smallest of 19 glacierized regions in the world by volume (Radić et al., 2014) and mass (Rounce et al., 2023). Given their relatively small size, these glaciers are therefore particularly sensitive to changes in temperature and atmospheric conditions (Menounos et al., 2019; Rounce et al., 2023). In part because of this, glacierized alpine regions of the Canadian Rocky Mountains have long been a point of scientific interest and inquiry with research generally focused on the rapid diminishment of the icefields and outlet glaciers there (e.g., Marshall et al., 2011; Tennant et al., 2012). For example, between 1919 and 2009, the mean area change of all outlet glaciers stemming from the Columbia Icefield was modeled at -2.4 km^2 (or -34%; Tennant & Menounos, 2013), with corresponding studies highlighting large-scale glacier termini thinning and recession during this century (see also **Figure 2.1** for a visual of Athabasca Glacier in 1918 and 2011; Ommanney, 2002; Rippin et al., 2020; Tennant & Menounos, 2013). On the eastern slopes, glacier volume is projected to decline 80-90% by 2100 with subsequent changes to the volume and timing of meltwater and biogeochemical inputs into downstream rivers (Clarke et al., 2015; Radić et al., 2014). It is no surprise, then, that the glaciers on the eastern slopes have been shown to be past their tipping point (Marshall et al., 2011).

Relatively little has been published on the meltwater-fed rivers that flow from the glacierized regions of the eastern slopes of the Canadian Rocky Mountains, or how the biogeochemistry of these rivers change across the open water season or as they traverse the downstream proglacial environment (e.g., Lafrenière & Sharp, 2005; Staniszewska et al., 2020). As such, we established 14 sampling sites along the Sunwapta, Athabasca, North Saskatchewan, and Bow rivers, which stem from outlet glaciers on the eastern slopes in Jasper and Banff National Parks, Alberta. Between 2019-2021, riverine measures were collected from glacier termini up to 100 kilometers downstream across all seasons to investigate spatiotemporal patterns in proglacial freshwater physicochemistry and quality. Given the importance of these headwaters in establishing the initial dissolved and particulate biogeochemical loads of three major Canadian watersheds, and the rapid glacier mass loss that indicates this region is presently on the brink of freshwater resource uncertainty (S. Anderson & Radić, 2020; Schindler & Donahue, 2006), water quality research in these vulnerable headwaters is especially important.

For each river sampling site, the overall objectives of this study were to: (1) produce biennial hydrographs using measured and modeled discharge data; (2) characterize water isotope signatures of river water, and compare those to water isotope signatures in rain, snow, and glacial ice; (3) quantify an array of 200+ physicochemical parameters, including *in situ*, basic water chemistry, nutrient, ion, trace element, contaminant, and particulate ion and trace element measures; and (4) combine hydrology and physicochemical measures to estimate chemical loads and yields. Spatial (within river transects and between rivers), seasonal, and interannual patterns are explored for each objective to determine the prominent factors driving data variability at our sampling sites. This interdisciplinary work lies at the intersection of biogeochemistry, limnology, glaciology, and hydrology and is the most comprehensive freshwater assessment ever documented for the headwater reaches of these rivers. As such, the spatiotemporal dataset presented here will provide an invaluable baseline reference for those investigating changes to this rapidly changing alpine region in the future, as well as increase our ability to predict the impact of climate change on the water quality of rivers originating in alpine glacierized regions.

2 Methods

2.1 Site description

The headwater regions of the Sunwapta, Athabasca, North Saskatchewan, and Bow rivers are contained within the montane cordillera ecozone and span glacierized, alpine, subalpine, and montane altitudinal life zones (Demuth & Horne, 2017). Broadly, they are underlain by calcite and dolomite bedrock, with various plagioclastic feldspars, phyllosilicates, and quartzes intermixed (Gadd, 2009; Pana & Elgr, 2013). In total, we established seven sampling sites along the Sunwapta-Athabasca River continuum, three sites along the North Saskatchewan River, and four sites along the Bow River (**Figure 2.2**; **Table A1.1**).

The Athabasca Glacier, a valley glacier of the Columbia Icefield, is the point of origin for the Sunwapta River (SR; Ommanney, 2002). The SR passes through a proglacial lake prior to braiding through a sparsely vegetated glacial outwash plain. The braids converge into one channel and further downstream merge into the Athabasca River (AR), which originates upriver of this juncture at the Columbia Glacier in the northwest margin of the Columbia Icefield (Ommanney, 2002). The large AR flows northeast towards our most northern sampling site 97.8 km downriver, upstream of Jasper Township (**Figure 2.3**).

The North Saskatchewan River (NSR) originates at the Saskatchewan Glacier on the southern edge of the Columbia Icefield (Ommanney, 2002). Meltwaters from the Saskatchewan Glacier, the largest outlet glacier of the Columbia Icefield, terminate into a large proglacial lake before flowing downriver through a glacial valley. From there, the NSR meanders through a prominent glacial floodplain area vegetated with low-lying shrubs and grasses before forming a single large channel that flows through montane forest until our last sampling site 46.3 km downriver (**Figure 2.3**).

The Bow River (BR) begins at the cirque Bow Glacier in the Wapta Icefield (Ommanney, 2002), flowing from proglacial Iceberg Lake, over a large waterfall, and into a braided forefield. The BR then feeds Bow Lake, a large subalpine lake surrounded by subalpine forest, before it passes through a forested wetland area. Dense montane forest lined the remainder of the headwaters of the BR towards our most southern sampling site 75.4 km downriver, upstream of Banff Township (**Figure 2.3**).

For each sampling site, the relative percent of its watershed area covered by major and minor land cover classes was determined with the Alberta Biodiversity Monitoring Institute (ABMI) Wall-to-Wall Land Cover Inventory and the relative percent of its watershed area covered by wetland type was determined with the ABMI Wetland Inventory (**Table A1.2**, Alberta Biodiversity Monitoring Institute, 2010, 2021). Of the 10 land cover classes, only three (snow and ice, rock and rubble, and coniferous forest) exceeded 10% cover of the watershed area at some of our sampling sites. Other land cover classes pertaining to diverse vegetation (e.g., grassland, broadleaf forest) or anthropogenic disturbance (i.e., developed, including roads) represented less than 10% of the land cover along our sampling reaches, highlighting the barren and pristine landscape of our study region. Intuitively, the relative percent of cumulative watershed area covered by snow and ice was highest at our sampling sites nearest glaciers (41.5-54.7%), whereas the relative percent of cumulative watershed area covered by coniferous forest was highest (29.7-41.3%) at our most distant sampling sites on each river. The proportion of cumulative watershed area covered by rock and rubble was relatively constant (35.7-55.3%) across river reaches, but interestingly slightly higher at the glacial outwash floodplain sites (**Figure 2.3**, **Table A1.2**).

2.2 River discharge

Mean daily river discharge ($m^3 s^{-1}$) was directly quantified at two of our 14 sampling sites (SR2 and BR3) by hydrometric gauging stations maintained by Water Survey of Canada (WSC; (Water Survey of Canada, 2021). To estimate daily discharge at the remaining 12 sampling sites, we used day-specific watershed area-discharge linear regression models derived from mean daily discharge measured at nine Albertan mountain river WSC hydrometric gauging stations (**Table A1.3**, **Figure A1.1**). More specifically, we downloaded WSC measured discharge from the nine gauging stations and created simple daily linear regressions for 2019 and 2020 (i.e., 730 linear regressions) in a spreadsheet program before applying the linear regression equations to the watershed areas for each sampling site and for each day of the year(s). The nine gauging stations, including those at our sampling sites SR2 and BR3, were selected because they were all within the SR-AR, NSR, and BR watersheds, had watershed areas (km^2) similar to those of our sampling sites, and were operational during our river physicochemistry sampling years of 2019 and 2020. Based on our calibration results (described below), one regression model included data from gauging stations where watershed areas were less than 630 km^2; this model was used to estimate daily discharge at our study sites where watershed areas were less than 150 km^2. The second regression model included data from all nine of the gauging stations; this model was used to estimate daily discharge at our study sites where watershed areas exceeded 150 km^2. When the regression models estimated negative discharges or discharges below 0.1 $m^3 d^{-1}$, discharge was set to 0.1 m^3 d^{-1}. Watershed areas for our sampling sites were obtained directly from WSC (SR2 and BR3) or delineated using the Alberta ArcHydro Phase 2 Dataset on ArcGIS (all other sites; Alberta Environment and Parks, 2018).

To determine the accuracy of our watershed area-discharge models, modeled discharge was compared to discharge obtained at the five WSC gauging stations along the main stem of our study rivers in 2019 and 2020. These calibration sites included SR2 and BR3, as well as three gauging stations within 12.8-41.0 km downriver of our sampling reaches (**Table A1.3**). Modeled data was compared to WSC measured data at multiple watershed area thresholds (e.g., 50, 150, 500, or 1000 km^2) during our calibration process. The best fit for all sites was a threshold of 150 km^2. Thus, the calibration site 07AA007 (Sunwapta River at Athabasca Glacier) with a watershed area less than 150 km^2 was compared to modeled discharge using the first linear model, whereas the other four calibration sites with watershed areas exceeding 150 km^2 were compared to modeled discharge using the second linear model.

2.3 Sample collection and chemical concentration analyses

Sampling sites were visited monthly in 2019 and 2020 during the open water season (OWS), beginning during snowmelt in late May/early June, through peak glacial melt in July/August, then during the receding flow period in September/October. Due to safety concerns of sampling fast flowing rivers in remote areas, all sample collection was done near the shoreline in the main flow of the river. However, turbulence and mixing are high in this high-slope region, and back-eddies, slumping shorelines, and areas where in-river sediment could be disturbed were strictly avoided, ensuring a representative sample. In braided river sections (i.e., SR3 and NSR2), the main channel was selected for sample collection. Additional samples were collected twice in winter (December 2019, January 2021) during base flow, but only at sites where (a) the sampling location was partially ice free, (b) the ice margin shelves were stable enough to support the weight of a person, and (c) a safety harness could be securely connected to an onshore anchor point.

River water sampling and analytical protocols are fully detailed in **Table A1.4**. In general, at each river sampling site and time, we deployed a YSI EXO2 multiparameter sonde to obtain instantaneous measures of optical dissolved oxygen (ODO; % saturation and concentration), conductivity, turbidity, pH, and temperature. Sondes were calibrated at each sampling site for ODO, and prior to each sampling campaign for all other parameters. Low ionic strength standards were not used for the calibration of pH or conductivity, and as a result, possible measurement biases may have occurred in our low ionic glacial meltwaters (Bagshaw et al., 2021). However, we calibrated often, opted for spot sampling over long term deployments, and eliminated the first five minutes of data at each site ensuring *in situ* equilibrium was reached, all of which help to reduce bias (Bagshaw et al., 2021). Using clean field sampling protocols, we also collected water samples for the analyses of total suspended solids (TSS); total dissolved solids (TDS); nutrients (total and dissolved phosphorus [TP, TDP] and nitrogen [TN, TDN], soluble reactive phosphorus [SRP; 2020 only], ammonium [NH_4^+], nitrite and nitrate [NO_2^- +NO_3^-], and dissolved silica [Si]); major cations (Ca^{2+}, K^+, Mg^{2+}, Na^+) and anions (Cl^-, SO_4^{2-}); trace elements; water isotopes (δ^2H-H_2O, $\delta^{18}O$-H_2O); particulate carbon (PC) and nitrogen (PN); dissolved inorganic and organic carbon (DIC, DOC); and the contaminants total and filtered mercury (THg, FHg), methyl- and filtered methyl-mercury (MeHg, FMeHg), and polycyclic aromatic hydrocarbons (PAHs) (2019 only). Henceforth, discussions of “total” chemicals include those that were not filtered prior to analyses, and thus contained non-dissolved (i.e., particulate) and dissolved (i.e., filtered) fractions. We correspondingly collected suspended sediments at each study site for total recoverable particulate cation and trace element concentrations (denoted as “parameter_PTL”, for e.g., Ca^{2+}_PTL). Depending on protocol, samples were either processed and preserved at the time of sampling or within 24h in a clean field laboratory or University of Alberta laboratory. All samples were then analyzed using standard protocols in Canadian Association for Laboratory Accreditation (CALA)-accredited and/or academic laboratories.

Integrated snow cores were collected with a stainless-steel corer once in March 2021 at peak snow accumulation. One fresh snow sample was also opportunistically collected by skimming the surface of the snowpack with a clean Whirl-Pak® bag during a snowfall event that occurred while sampling. Rain samples were collected during a multi-day regional precipitation event in June 2023 by setting out wide-mouthed clean buckets lined with clean plastic bags and placed on elevated surfaces in open areas to prevent ground-level splash back. Precipitation was originally collected for water isotope analyses and to estimate the potential influence of winter wet and dry deposition on chemical contributions to the rivers during snowmelt and rainfall; however, only water isotopes will be discussed in this text (chemical concentrations for precipitation are available in *Data Availability*). Water chemistry was also determined for a 10.2-meter ice core extracted from Mt. Snow Dome, the apex point of the Columbia Icefield, in April 2020 by the Canadian Ice Core Lab (CICL; University of Alberta). In January 2022, the CICL further collected surficial snow samples from longitudinal transects along the Athabasca and Saskatchewan outlet glaciers that were subsequently analyzed for water isotopes (**Figure A1.2**).

Concentration data that fell below analytical detection limits (DL) were modified to half DL values for statistical purposes (Antweiler & Taylor, 2008; Helsel, 1990). Further, all data from four sampling times at site AR1 were eliminated from statistical analyses when inputs from an upstream tributary disproportionately influenced the biogeochemical signal (see starred circles in **Figure 2.4**). Unless otherwise stated, physicochemical statistics were performed in base R and physicochemical graphs were built using *ggplot2* (R Core Team, 2022; Wickham, 2016).

2.4 Water sources

We used water isotope data from our river, precipitation, and the Mt. Snow Dome ice core samples to define water source contributions to our sampling sites. Analytical precision was ≤0.35 for $\delta^{18}O$ and ≤0.94 for $\delta^{2}H$. Linear regression statistics were performed on seasonal and bulk river water isotope signatures collected at our sampling sites throughout the study period to assess their overall difference relative to the Canadian Meteoric Water Line (CMWL; Gibson et al., 2020), as well as calculated deuterium-excess signatures (d-excess, where $d= \delta^{2}H-8\delta^{18}O$; Dansgaard, 1964; Pfahl & Sodemann, 2014). Water isotope signatures and d-excess from fresh snow (n=1) and rain (n=7) samples were used to represent new precipitation inputs, and integrated snowpack (n=7) and surficial glacier snow (n=8) samples were used to represent snowpack contributions, to the mountain region. The distinction between new precipitation inputs and snowpack contributions is important because post-depositional processes are known to enrich water isotope signatures and so do not represent the water isotopes of freshly fallen snow. However, for ease of interpretation, precipitation in the results and discussion refers to all combined rain and snow samples. Water isotope signatures and d-excess obtained from the ice core (n=360) were considered undisturbed firn or glacier ice. Freshly fallen and immediately sampled rain and snow that had not yet undergone post-depositional transformations were compared to riverine water, and elevational trends in precipitation, glacier ice, and river samples were determined to assess the impact of the mountain environment on the water isotope and d-excess signatures in our study region.

To further support the discussion of our water isotope data, water sources to our overall study region were examined by calculating ten-day air mass back trajectories with the National Oceanic and Atmospheric Administration (NOAA) HYSPLIT model using National Centers for Environmental Protection and Atmospheric Research (NCEP/NCAR) Reanalysis I data for 2019-2021 (Kalnay et al., 1996; Stein et al., 2015). Trajectories were launched twice daily (3:00am and 3:00pm local time) at half the height of the planetary boundary layer at Mt. Snow Dome. Residence time density analysis (e.g., Ashbaugh et al., 1985; Miller et al., 2002) determined precipitation source regions using highly frequented trajectory pathways. Trajectory endpoints over each grid cell were summed to determine total residence time densities, then normalized by multiplying each density value by the Euclidean distance between the center of the grid cell and receptor point (Ashbaugh et al., 1985). See Criscitiello et al., 2016 for further details.

2.5 Measures and patterns in physicochemical parameters

Principal Component Analyses (PCA) were used to assess measures of water quality parameters spatiotemporally (across seasons and years, between rivers, and within river transects). Parameters were included in PCAs if sampling of the parameter spanned both 2019 and 2020 and the number of analytical below-detects were less than 25% of the total number of samples taken (Antweiler & Taylor, 2008; Helsel, 1990). The R packages *FactoMineR* and *factoextra* were employed for detailed data interpretation and visualization (Kassambara & Mundt, 2020; Lê et al., 2008), with biplots of PC1-PC2 and PC1-PC3 pairs used to capture most of the variability explained by the PCA.

We were primarily interested in summarizing large-scale spatiotemporal patterns across all sampling sites and chemical parameters, so collinear variables were not removed from analyses, and PCAs were specifically chosen to address the high multicollinearity and associated variable inflation factor inherent to the measured physicochemical parameters. Importantly, we were able to exploit the collinearity for the interpolation of missing data. For the PCA run on the main physicochemical parameters that met the criteria outlined above, 1.5% of datapoints were missing (NA), which would have disproportionally reduced the number of sampling records included in the PCA by 17.2% (from n=151 sampling records to n=125). Thus, to circumvent the loss of 26 sampling records for use in the main physicochemical parameter PCA (i.e., **Figure 2.6**), missing untransformed concentration data was interpolated using the best correlation matrix relationships possible between parameters (**Figure A1.3**; correlation coefficients (r) for data interpolation ranged from 0.50 to 0.96). For example, we used Si to estimate five missing K concentrations based on their correlation relationship (r=0.79). In total, 10 of the 23 parameters included in the main physicochemical PCAs contained some interpolated data, filling anywhere from 1 to 13 NAs (PN and DOC, respectively).

For PCAs run on cations and trace element chemical concentrations (i.e., **Figures A1.9** and **A1.10,** respectively), only sites that had both complete PTL and dissolved cation and trace element concentrations were included (n=42). At a given sampling site, if there was not enough particulate matter for analyses, we sometimes combined the particulate matter from several seasonal sampling times at that site prior to digestion and analyses (denoted as such in dataset; see *Data Availability Statement*). Since measured particulate concentrations (e.g., mg g^{-1}) were converted to liquid concentrations (e.g., mg L^{-1}) using sample-specific TSS data (in mg L^{-1}), even if a site had two identical particulate concentrations, the PTL result included in the PCA was unique.

2.6 Chemical yields

Measured chemical concentrations and modeled discharge were combined to model OWS (May 1 to October 31) loads (total mass OWS^{-1}) at each of our sampling sites in 2019 and 2020. Chemical parameters were included in load modeling only if the number of analytical non-detects were less than 25% of the total number of samples taken for that parameter. Site AR1 was not included in chemical load modeling due to the removal of dissolved concentration data at four time points (see starred circles in **Figure 2.4**), leading to fewer sampling records (n=5) and the overfitting of load models.

Data from two parameters of differing concentrations (DIC in mg L^{-1} and NO_2^-+NO_3^- in µg L^{-1}) and two river sites of differing morphology and size (SR1, single-channel proglacial stream and SR3, braided and mid-river) were initially run through the U.S. Geological Survey's (USGS) *loadflex* package in R to test which modeling approach would be best applied to all sites (n=13) and parameters of interest (n=25) (Appling et al., 2015). In loadflex, we generated continuous load through four built-in and customizable models: (1) rectangular interpolation, (2) linear regression, (3) LOAD ESTimator (LOADEST) regression, and (4) composite, which applied a mathematical correction to a regression method of choice (in this study (3); (Appling et al., 2015). The four loadflex models produced comparable mean load results across parameters and sites (relative standard deviation ranged from 0.06-5.1%; **Table A1.5**), indicating little overall difference between models. However, rectangular interpolation consistently produced the largest mean standard errors when compared to the other three loadflex models and was thus eliminated from consideration. Manually calculated load datapoints (i.e., point sample concentrations multiplied by daily flow; n=11 for the parameter-site combinations) were then overlayed on modeled loads plotted against time for the remaining three loadflex models. The linear regression model consistently resulted in the most deviation between the manual and modeled load and was therefore excluded from further load calculations. Finally, to select between the LOADEST and composite models, the Durbin Watson statistic was performed on the regression residuals to determine the degree of autocorrelation (Appling et al., 2015). Autocorrelation was a requirement of the composite model and was determined to be weak to non-existent in the regression residuals (Durbin Watson ranged from 1.5-2.6). Because the LOADEST regression model was determined to be the overall best model to use for load calculations across all sites and parameters of interest in this study, loads were modeled in the USGS *rloadest* package (Lorenz et al., 2017; Runkel et al., 2004).

We followed conservative model elimination criteria to reduce the likelihood of overfit load models. As we did not collect time-series data in this study, we did not consider models where trigonometrically transformed time was not a component (i.e., LOADEST models 3, 5, 7-9). Out of LOADEST models 1, 2, 4, and 6, we chose the one with the lowest Akaike Information Criterion (AIC), which indicated the best regression fit. We then determined if the R^2 and percent bias (Bp) for the model was greater than 50 and lower than 25, respectively. If the model with the lowest AIC did not meet the statistical criteria or it resulted in a model error, it was eliminated from use (**Table A1.6**). In these cases, the next best models were assessed in the same way. Once models passed these criteria, we graphed manually calculated and LOADEST modeled loads against time to determine if any large deviations in load occurred in the model. All the selected models resulted in good or moderate fits (**Figure A1.4**). In total, we surveyed the statistics and time versus calculated/modeled load graphs of 345 LOADEST models to determine the best loads possible in this study (13 sampling sites x 25 parameters + 20 additional models from best model elimination; **Table A1.6**, **Table A1.7**). Open water season chemical yields (mass OWS^{-1} km^{-2}) for each site were then calculated by dividing the LOADEST-derived chemical load (mass OWS^{-1}) by the watershed area (km^2). While annual OWS chemical loads and yields were calculated for each sampling site, only yields will be reported and discussed to allow for standardized results between sites of differing watershed areas. To determine whether specific reaches along the rivers were sources or sinks of chemicals, we also calculated reach-specific yields between two neighboring sampling sites using the equation: [$Load_{Site2}$ – $Load_{Site1}$]/[Watershed $area_{Site2}$ – Watershed $area_{Site1}$].

3 Results & Discussion

3.1 River discharge

There were few overall discrepancies between WSC-measured discharge and our modeled discharge at the five calibration sites in 2019 and 2020 (R^2_{adj} ranged from 0.774 to 0.998; **Figure A1.5**). Measured and modeled discharge had the weakest statistical relationship at the calibration site with a watershed area less than 150 km^2, station 07AA007 (Sunwapta River at Athabasca Glacier, $R^2_{adj} = 0.774$, **Figure A1.5a**), compared to the four calibration sites with watershed areas exceeding 150 km^2 ($R^2_{adj} \geq 0.912$, **Figure A1.5b-e**). During the OWS, however, modeled discharge visually deviated from measured WSC station discharge at two of the large watershed calibration sites: 1) station 05DA009 (North Saskatchewan River at Whirlpool Point) located approximately 20 km downstream of our sampling site NSR3; and 2) station 05BB001 (Bow River in Banff) located approximately 40 km downstream of our sampling site BR4. Station 05DA009 recorded average to above average discharge from March to September 2019 (106-127% basin-wide) and 2020 (115-155% basin-wide) relative to long-term discharge records (Alberta Environment and Parks, 2019a, 2020a). During 2019 and 2020, our model underestimated discharge at this station (**Figure A1.5c**), possibly due to higher-than-expected snow and glacier melt hydrologic inputs from the Howse and Mistaya, two large glacial rivers, that entered the NSR upstream of station 05DA009, although the Mistaya River was hydrometrically gauged by WSC upstream of NSR3 and included in our model (station 05DA007, **Table A1.3**). The southernmost WSC hydrometric gauging station in our model, station 05BB001 recorded average discharge from March to September 2019 (81-103% basin-wide) and 2020 (87-118% basin-wide) relative to long-term discharge records (Alberta Environment and Parks, 2019a, 2020a). During 2019 and 2020 our model overestimated discharge at station 05BB001 (**Figure A1.5e**), potentially because of the abnormally large variability of flow noted throughout the downstream reaches of the Bow River basin during these two years (Alberta Environment and Parks, 2019a, 2020a). Regardless, because stations 05DA009 and 05BB001 were high volume downstream stations, the deviations between modelled and actual discharge described here were small ($R^2_{adj} = 0.966$ and 0.912, respectively) and were not considered an issue when applying our discharge models to the 12 ungauged sampling sites to calculate chemical loads and yields.

Biennial (January 2019 to January 2021) WSC-measured and modeled hydrographs for the Sunwapta, Athabasca, North Saskatchewan, and Bow rivers sampling sites are shown in **Figure 2.4**. The hydrographic profiles of our 14 sampling sites generally displayed steep rising limbs in spring, notable spring and mid- to late-summer discharge peaks, gradual receding limbs in early fall, and low winter baseflow. The roughly two-peaked, right skewed distribution of the annual hydrographs in our study system was the result of a rapid snowmelt freshet in the spring associated with the onset of warmer temperatures, and the combined influence of summer precipitation and expulsion of glacier meltwaters from supra-, en-, and sub-glacial meltwater channels that were hydrologically active in the summer and early fall (Demuth & Pietroniro, 2003; Marshall & White, 2010). The hydrology of our sampling sites is thus reflective of a characteristic mid-latitude glacierized alpine hydrograph (Comeau et al., 2009; Demuth & Pietroniro, 2003; Marshall & White, 2010). Even so, some spatiotemporal trends did emerge in our biennial hydrographs (**Figure 2.4**). Total discharge increased downstream in conjunction with the greater capacity of larger watershed areas to funnel winter melt and summer precipitation to the downstream sites. Meltwater peaks appeared slightly later in 2020, yet it was an overall higher flow year. For example, summing the total discharge of the most downstream sampling sites (i.e., AR3, NSR3, BR4), total OWS Q_{2020} was 4.22 km^3 compared to total OWS Q_{2019} at 3.79 km^3. The difference in the timing and magnitude of flow in 2019 and 2020 may have been partially due to the prevailing regional meteorological conditions during those years. Winter 2020 experienced a mild February (**Table A1.8**; Environment and Climate Change Canada, 2019, 2020) and above normal precipitation (approximately 115-200% when compared to the mean winter precipitation over the previous 30 years; Alberta Environment and Parks, 2020b). More winter precipitation in 2020 compared to 2019 could have delayed the onset of flow as deeper, better insulated snowpacks and glaciers required more energy to melt (Alberta Environment and Parks, 2019b). Once landscape melt was triggered, the larger snowpacks combined with higher temperatures recorded in Jasper and Banff National Parks in July and August 2020 compared to July and August 2019 (**Table A1.8**) likely contributed to the larger flow volumes seen in the 2020 hydrographs.

At sampling sites close to their source glacier, namely SR1, SR2, NSR1, and BR1 (**Figure 2.2**, **Table A1.1**), the difference in discharge between the height of annual snowmelt and glacier meltwater discharge peaks was small. Moving downstream, glacier melt peaks decreased relative to snowmelt peaks, a reflection of the glacierized area making up progressively less of the total watershed area at those sites (**Table A1.2**; Marshall & White, 2010). Even though glacier meltwaters make up only a small proportion of the overall annual riverine flow at downstream sites in glacierized alpine basins, that proportion increases in the peak glacial melt months of July to September. For example, on an annual basis, the mean proportion of glacier meltwaters to Bow River at the WSC hydrometric gauging station 05BA001 (Bow River at Lake Louise) between 1975 and 1998 was 4.2% whereas the mean July to September proportion of glacier meltwaters was over double that at 8.7% (Comeau et al., 2009). The same study also noted strong positive correlations between the total glacierized area of a watershed and the glacial melt contributions to river flow across the eastern slopes of the Canadian Rocky Mountains (Comeau et al., 2009). This correlation supports the relative decrease in summer discharge peaks (driven by glacial melt) compared to spring discharge peaks (driven by snow melt) with increasing distance downstream observed along each study river (**Figure 2.4**; also see Marshall, 2014), and suggested that the proportional glacier meltwater outputs from the Sunwapta-Athabasca and North Saskatchewan watersheds, where nearly 77% of Alberta's glacierized area is located (Marshall & White, 2010), are likely far greater than glacier meltwater outputs from the less glacierized Bow Watershed (Comeau et al., 2009; Demuth & Pietroniro, 2003; Marshall et al., 2011; Marshall & White, 2010).

The hydrology of this region is rapidly evolving. Conservative climate models (RCP 4.5) predict that glacial mass loss in western Canada may reach 85% by 2100 (Radić et al., 2014). As glacier melt contributions to headwater river discharge continue to decrease, the relative importance of snow and summer precipitation to sustaining flow will increase (Comeau et al., 2009; Marshall et al., 2011; Marshall & White, 2010) and the right skewed distribution of hydrographs produced in deglaciated alpine regions could become more exaggerated. Yet, despite the research regarding future hydrological changes to the eastern slopes described above, far less has been documented regarding the consequent impact of waning glacier flow to riverine water physicochemistry.

3.2 Water sources

The water isotope signatures of riverine samples ranged from -23.1 to -19.1‰ $\delta^{18}O$ and -176.0 to -143.4‰ $\delta^{2}H$ (n=151), with the lowest signatures recorded in spring and the highest signatures recorded in autumn. A Local Meteoric Water Line (LMWL) based on the riverine samples was calculated to be $\delta^{2}H = 8.0*\delta^{18}O + 8.9$ ($r_{Pearson} = 0.98$) and was nearly identical to the CMWL at δ2H = 8.0*δ18O + 8.5 (**Figure 2.5a**; Gibson et al., 2020), suggesting no major in-river fractionations such as evaporation or condensation were occurring during our sampling period (Beria et al., 2018; Mahindawansha et al., 2022). Minor deviations from our riverine LMWL and the CMWL were observed for river samples binned by season with the highest slope in winter (8.8, $r_{Pearson} = 0.97$), followed by autumn (8.5, $r_{Pearson} = 0.98$), spring (7.6, $r_{Spearman} = 0.96$), and summer (7.4, $r_{Pearson} = 0.96$). There were also no discernable patterns in d-excess signatures across seasons (**Figure 2.5b**). Riverine d-excess ranged from 6.2 to 11.1‰ except for NSR3 in spring of 2019 which produced a d-excess value of 4.2‰, potentially due to instantaneous evaporation during a major spring rain event (Pfahl & Sodemann, 2014). The similar slopes and d-excess signatures across seasons were not surprising given the considerable overlap and small isotopic range of seasonal riverine water isotope measures (**Figure 2.5c-d**).

We further collected precipitation (rain and snow) and glacial ice core samples to identify the isotope signatures of water that fed our rivers. Isotope signatures spanned a range from -25.5 to -7.3‰ $\delta^{18}O$ and -201.8 to -73.2‰ $\delta^{2}H$ for precipitation (n=22) and from -30.7 to -13.8‰ $\delta^{18}O$ and -231.0 to -118.9‰ $\delta^{2}H$ for the 10 m glacial ice core collected on Mt. Snow Dome (n=360). Snow isotopes tended to sit near or below the CMWL with a slope of 8.7 ($r_{Pearson} = 0.98$), typical of cold environments (Mahindawansha et al., 2022), but adding rain samples to the analysis changed the precipitation slope to 7.3 ($r_{Spearman} = 0.98$; **Figure 2.5e**). This slope was more similar to that produced using glacial ice core samples, which sat near or above the CMWL with a slope of 7.5 ($r_{\text{Spearman}} = 0.98$; **Figure 2.5g**). The difference between the slope produced using snow samples compared to the slope produced using ice core samples may have been due to post-depositional transformation processes (Penn et al., 2023). The two most enriched water isotope signatures, which diverged from the other precipitation samples (**Figure 2.5e**), were in rain collected near the terminus of the Athabasca Glacier at the onset of a severe thunderstorm with strong katabatic winds. We also observed negative d-excess signatures in precipitation. The negative d-excess value of the snow sample could have been the product of sublimation or freeze-thaw events and the negative d-excess signatures of the rain samples could have been due to sub-cloud evaporation (Bershaw et al., 2020), as rain samples were collected and immediately processed during rain events (**Figure 2.5f**; Beria et al., 2018; Dansgaard, 1964; Hu et al., 2022; Penn et al., 2023). In contrast, the d-excess signatures of the ice core skewed more positively than the river or precipitation data and contained signatures up to 20.5‰ (**Figure 2.5h**).

Detailed descriptions of atmospheric water transport, including air mass back trajectory residence time density analysis, for our study region can be found in the SI. We also explored water transformations pre- and post-deposition and how water isotopic signatures changed with elevation at our study sites and at sampled sites from atop the Columbia Icefield in the SI. Ultimately, given the complexity of water transport and transformation processes to and within mountain watersheds (Sinclair & Marshall, 2008), our limited number of precipitation samples relative to the large range of air mass sources, and the large overlap in isotope signatures of river waters, precipitation, and glacier ice at our study sites, presenting a water isotope mixing model to apportion river isotopic signatures to specific water sources is outside the scope of this study. Regardless, our combined riverine, precipitation, and ice core water isotope dataset greatly expands on the existing literature on, and the characterization of, water isotopes in our study region (Arendt et al., 2015; Lafrenière & Sinclair, 2011; Niu et al., 2017).

3.3 Measures and patterns in physicochemical parameters

The physicochemical measures explored in the main PCA are summarized as yearly means in **Table A1.9**. Dissolved cations were included in the main physicochemical PCA, but trace elements were not because only few, correlated trace elements met the criteria for inclusion. The cation- and trace element-specific PCAs included only sampling points when both PTL and dissolved concentration data were available. Further, while the BR is represented in the main physicochemical PCA, it was wholly excluded from the cation and trace element PCAs because at no sampling times was enough suspended particulate material obtained for PTL digestions and analysis. For each PCA, we visualized PC scores by season and year, river, and distance from glacier (km) to assess if these spatiotemporal factors drove the variation in measures of the physicochemistry presented on the loading plots. Please see the SI for a further discussion on parameters included in the PCA analyses.

3.3.1 Main physicochemical PCA

The first three principal components (PC) explained 67.1% of the variation in measures for the main physicochemical parameters among all our river sampling sites and times (PC1=37.1, PC2=19.2, PC3=10.9; **Figure 2.6** with loadings summarized in **Table A1.10a**). There was a distinct grouping of dissolved parameters (e.g., dissolved carbon, ions, and nutrients) and particulate and unfiltered parameters (e.g., TSS, PC, and THg) along the PC1 axis (**Figure 2.6a**). The bulk of dissolved chemical parameters were negatively correlated with pH, as might be expected due to carbonate or silicate geochemical weathering consuming CO_2 and driving up pH (Brown et al., 1996). *In situ* temperature was negatively correlated with ODO concentrations along PC2 in line with the known inverse relationship between oxygen solubility and temperature in aquatic systems (Figure 6a; Dodds & Whiles, 2020). PC3 further separated the nitrogen species from most of the dissolved parameters and accentuated the negative correlation between temperature and ODO concentrations (**Figure 2.6b**).

The spatiotemporal factor that captured the most variation in this PCA was distance from glacier. While mid- to far-downstream sampling site (approximately 25-100 km) scores tended to overlap, the river sampling site scores closest to their source glacier (approximately 0-25 km) clearly differed on the PC1 axis (**Figure 2.6g-h**). River sampling sites closest to the source glacier tended to have the highest particulate and total concentrations and the lowest dissolved concentrations, with less obvious differences among downstream sites (**Figure 2.6g-h**). This aligns with the understanding that untransformed glacial meltwaters tend to have high sediment loads but are dilute in dissolved chemistry (S. P. Anderson et al., 1997), whereas various sources and sinks to the meltwater as it flows downriver across differing landscape types can alter the relative proportion of the particulate, total, and dissolved constituents in less predictable ways (Deuerling et al., 2018; Kohler et al., 2022). We also found that samples collected during spring, when river chemistry was largely driven by snowmelt runoff, stood out from samples collected in the other seasons on PC2 (**Figure 2.6c**). During spring 2019, river samples had higher concentrations of dissolved chemical parameters than during the rest of the year, whereas during spring 2020 when snowmelt runoff volume was greater than in 2019 (**Figure 2.4**), river samples had higher concentrations of particulates and particle bound chemicals, possibly because there was heavy rainfall and overland flooding during our late June 2020 sampling trip (**Figure A1.8**). The rivers' contact with, and mobilization of, sediments during this extreme flow event indicate that an erosion threshold was crossed and that is likely the reason we see the highest particulate and total chemical concentrations during that period. By comparison, river (**Figure 2.6e-f**) poorly explained differences in variation in physicochemical measures on all the PCs.

3.3.2 Particulate and dissolved cation PCA

The first three PCs explained 93.5% of the variation in PTL and dissolved cation concentrations (PC1=57.3, PC2=29.4, PC3=6.8; **Figure A1.9** with loadings summarized in **Table A1.10b**). Along PC1, the PTL cations grouped at a nearly 90° angle from the dissolved cations, indicating a lack of correlation between the two groups (**Figure A1.9a**). Their similar deviation from zero along the PC1 axis (~-5 for PTL and ~+5 for dissolved) and similar vector lengths on PC2 suggested relatively equal contributions of these groups to the variation captured by this ordination (**Figure A1.9a**). Yet, the PTL and dissolved cations showed a pattern along PC3 that was not captured by PC1 or PC2 (**Figure A1.9b**). The PTL cations grouped close together on PC3, which suggested that PC3 was a poor explainer of the PTL cation concentration variability, while the dissolved cations split between Ca^{2+}/Mg^{2+} and Na^{+}/K^{+} in the top right and bottom left quadrants of the loading plot, respectively (**Figure A1.9b**).

The bulk of PTL and dissolved data were from summer when glacial melt resulted in rivers being turbid enough to obtain enough material for PTL analysis. A sample from the outwash floodplain along the NSR, NSR2, during the high flow spring of 2020 drove much of the variation in PTL cation concentrations along PC1 and PC2 (**Figure A1.8**; **Figure A1.9c-d**). Along PC1 and PC2, the dissolved cation concentrations were more influenced by river (**Figure A1.9e-f**) and distance from glacier (**Figure A1.9g-h**) as the lowest concentrations occurred at SR sampling sites closest to the source glacier. Along PC3, all spatiotemporal factors clustered closely around zero and it was consequently not considered important in explaining cation concentration variation (**Figure A1.9d, f, h**).

3.3.3 Particulate and dissolved trace element PCA

The trace element PCA was conducted the same way as the cation PCA with both PTL and dissolved constituents. In the PCA of PTL and dissolved trace elements, the first three PCs explained 87.2% of the variation in concentrations (PC1=65.9, PC2=11.2, PC3=9.4; **Figure A1.10** with loadings summarized in **Table A1.10c**). The variation captured by PC1 was largely accounted for by the short-vectored PTL samples as the dissolved trace elements did not deviate far from zero on the PC1 axis (**Figure A1.10a-b**). The opposite trend was observed on PC2 where PTL trace elements remained clustered around zero on the PC2 axis and the dissolved trace elements Cr, Mo, Sr and Al, Ba, Mn were separated by PC2 (**Figure A1.10a**). PC3 also captured more variation in dissolved species, separating Cr from the other dissolved trace elements (**Figure A1.10b**). Hence, PC1 captured more variation in PTL trace element concentrations while PC2 and PC3 captured similar variations in dissolved trace element concentrations.

Though both river (**Figure A1.10e**) and distance from glacier (**Figure A1.10g**) appeared to capture some variation in dissolved trace element concentrations, particularly at AR sampling sites far from the source glacier, PC2 contributed only approximately 1/6th the amount of PC1 to the explanation of variation in our data. Thus, it was season and year that explained the most variation in PC1 versus PC2 with spring 2020 dominating the PC1 axis (**Figure A1.10c**). Spring 2020 particulate samples along the PC1 axis again drove the bulk of variation in PC1 versus PC3 (**Figure A1.10d**). Apart from Cr, dissolved trace elements vectored away from SR sampling sites (**Figure A1.10f**) close to the source glacier (**Figure A1.10h**) where the lowest dissolved trace elements would exist. This trend was presumably due to the high quantity of snow and glacier meltwaters diluting dissolved chemistry at glacier forefield sampling sites (S. P. Anderson, 2007; S. P. Anderson et al., 1997).

3.4 Chemical yields

Chemical concentrations in themselves only represent a sample-specific mass of chemical in a given volume of water and thus inherently reduces the discussion to specific sampling sites and times. Because snow and glacier melt-fed systems are characterized by high summer flow that drive downstream mobilization of chemicals (S. P. Anderson et al., 1997), to determine the watershed-scale load of our sampled chemical parameters, we now discuss chemical yields.

Year-specific 2019 and 2020 OWS chemical yields for each sampling site (except AR1, please see *Section 2.6* for details) and parameter of study are summarized in **Table A1.11**. Basic chemical parameters TSS, TDS, PC, and DIC (**Table A1.11a**) and ions Ca^{2+}, Mg^{2+}, and SO_4^{2-} (**Table A1.11c**) had the highest chemical yields (reported in Mg OWS^{-1} km^{-2}), while trace elements Cr and Mo (**Table A1.11d**) and contaminants THg and FHg (**Table A1.11e**) had the lowest (reported in g OWS^{-1} km^{-2}). All other chemical parameters, including nutrients (**Table A1.11b**), had moderate chemical yields (reported in kg OWS^{-1} km^{-2}). Water yields were reported in m^3 OWS^{-1} km^{-2} (**Table A1.11e**). With only the exceptions of Na at BR2 (97%) and Cr at SR3 and SR4 (93% and 95%, respectively), all chemical yields were greater in 2020 than in 2019. Because year had little overall influence on the variation of the concentrations assessed in the main physicochemical PCA as indicated by the overlap of data in temporal space (**Figure 2.6d-f**), we can likely account for the majority of the difference in yearly chemical yields from the difference in yearly discharge. Total OWS discharge of the most downstream sampling sites in 2020 exceeded that of 2019 by approximately 0.44 km^3 (see *Section 3.1*), resulting in larger loads and yields of chemical constituents in our study rivers. To identify spatial differences in chemical yields between our study rivers and sampling sites, mean 2019 and 2020 (±SD) OWS chemical yields for each sampling site and parameter of study were graphed (**Figure 2.7**). We also graphed mean 2019 and 2020 (±SD) OWS chemical yields between two neighboring sampling sites to assess whether discrete river reaches were sources or sinks of chemicals in our study rivers (**Figure A1.11**). Please note that because AR1 was removed from analysis, SR4 and AR2 are neighboring sites in **Figure A1.11** and its discussion.

Along the SR-AR and BR, chemical yields of all parameters were generally highest at the sampling sites closest to the source glacier (i.e., SR1 and BR1) then decreased or stabilized at downstream sampling sites (**Figure 2.7**). Glaciers of the Canadian Rockies are warm-based, which allows for basal sliding in addition to subglacial abrasion, and potentially high sediment formation (S. P. Anderson, 2007). It is thus unsurprising that the strongest source of particulate (e.g., TSS, PN, PC) and total (e.g., TP, THg) chemicals was at the most upstream sampling sites along the SR-AR and BR, dwarfing sources of the same chemicals at downstream sites (**Figure A1.11**). This pattern was not consistent along the NSR which tended to have the highest chemical yields at the mid-river glacial outwash plain site, NSR2 (**Figure 2.3**). Here, river waters increased their surface area with extensive braiding and had the potential to entrain more underlying and adjacent sediments, primarily creating a spike in particulate and total chemical yields (Goff & Ashmore, 1994). Along the NSR, the area between NSR1 and NSR2 was consistently the greatest source of particulate and total chemicals and contributed to the elevated chemical yields along the river, highlighting the importance of glacial outwash plains to riverine sediment loads and distribution (**Figure A1.11**)

The greatest decline of particulate and total chemical yields typically occurred along the upper reaches of the SR-AR and this loss was not recovered at downstream sampling sites. Between SR1 and SR2 sits Sunwapta Lake, a proglacial lake fed directly by sediment-laden glacial meltwaters flowing from the Athabasca Glacier (**Figure 2.3**). Sunwapta Lake has been shown to have extremely high sedimentation rates typical of proglacial lakes (Gilbert & Shaw, 1981; Wankiewicz, 1979), and accordingly acted as an initial settling pond for particulate and total chemicals suspended in meltwaters (Carrivick & Tweed, 2013). Importantly, the AR, NSR, and BR similarly have substantial proglacial lakes. However, the effects of sedimentation on particulate and total chemical yields are not explored there as our first sampling sites along those rivers occurred downstream of their proglacial lakes due to sampling access limitations (**Figure 2.3**). Given the dramatic decline of particulate and total chemical yields due to sedimentation in Sunwapta Lake, reason follows that the particulate and total chemical yields of the AR, NSR, and BR were likely highest between the glacier toe and their respective proglacial lakes and that this study consequently only captured some of the more chemically subdued glacial meltwaters that are possible along those rivers. For instance, Geilhausen et al., 2013 found that a proglacial lake in Austria reduced the TSS of a glacial river by over 85% during normal flow conditions and Bogen et al., 2015 found a similar 80% loss of TSS in proglacial lakes in Norway. River reach-specific chemical yields confirmed that not only did particulate and total yields decrease from SR1 and SR2, but that the area between SR1 and SR2 acted as a large sink of those chemicals (**Figure A1.11**).

The loss of a large portion of particulate and total chemistry in proglacial lakes may be most pronounced within the NSR. The Saskatchewan Glacier was the largest of the source glaciers in this study with an area of 38.3 km^2 and a length of 12.2 km (Tennant & Menounos, 2013). Despite NSR1 being sampled 5.6 kms downstream of the glacier tongue (**Table A1.1**), the relative percent snow and ice land cover was the highest of all sites at 54.7% (**Table A1.2**). This compares to SR1 which was sampled only 0.2 kms from the Athabasca Glacier tongue (**Table A1.1**) yet, had a slightly lower relative percent snow and ice land cover of 50.7% (**Table A1.2**). Theoretically, with more glacier area in direct contact with underlying bedrock, more subglacial grinding and abrasion could occur, and more sediment-laden meltwaters could be expelled from the system. Bedrock hardness is a key factor in how much abrasion, and consequent sediment export, can occur in a subglacial system. The bedrock underlying our study glaciers is relatively consistent, with Middle Cambrian limestone and dolostones, including those of the Pika Formation (Arendt et al., 2016), underlying the Athabasca, Saskatchewan, and Bow glaciers (Pana & Elgr, 2013), with Bow Glacier also partially underlain by the Lower Cambrian Gog Group consisting of limestone and dolostone beds with some quartzose sandstone (Pana & Elgr, 2013). Yet, the chemical yields along the NSR consistently fall low- to mid-range compared to the other rivers of study, suggesting that the deposition of material in the North Saskatchewan proglacial lake was likely the highest of all the proglacial lakes in this study and that the chemical signature of the NSR downstream of the proglacial lake was markedly different from what would be measured coming from the glacier. Further, the proglacial lakes of the NSR and AR are more than twice the surface area of the proglacial lakes of the SR and BR, so size differences could play a role in sedimentation rates as well.

Bow River sampling sites BR2, BR3, and BR4 generally had the lowest particulate and total chemical yields of all rivers (**Figure 2.6**), following the low concentrations of particulate matter at these sites (**Figure A1.9, A1.10**). The decrease of those same chemical yields from BR1 to BR2 may have been due to the presence of Bow Lake, a large subalpine lake (2.8 km^2 surface area; Blais et al., 2001) between the two sampling sites. The reduction in particulate and total chemical yields is not as apparent in Bow Lake as it was for Sunwapta Lake, likely due to its position downstream of BR's proglacial Iceberg Lake which would have been the site of the most substantial glacial sediment settling (**Figure 2.3**). The BR1-BR2 river reach-specific yields for particulate and total chemicals were neutral to slightly positive, suggesting that the area between BR1 and BR2, including Bow Lake and a small wetland, had very little impact on the chemical load into lower reaches of the BR despite a decrease in chemical yield values from BR1 to BR2 described above (**Figure A1.11**). Yet, our chemical yields suggest that Bow Lake impacted the dissolved chemistry. Most dissolved (e.g., TDS, DOC, TDN, all trace elements, FHg) chemical yields decreased from BR1 to BR2 and never recovered to their pre-lake levels at downstream sites (**Figure 2.7**). This trend was especially evident as the BR tended to have the highest dissolved chemical yields compared to the other rivers of study, in part due to the elevated dissolved loads estimated for BR1. As our most southern study river and the only one not to originate from the prominent Columbia Icefield, the BR was arguably our most atypical glacial river. Thick subalpine forests began to line the waters midway along Bow Lake, a relatively more upstream locale for the onset of substantial vegetation than the other rivers in this study, and wetland zones were present at downstream sites (**Figure 2.3**, **Table A1.2**). Nitrogen species yields decreased from BR1 to BR2 suggesting lake and/or wetland processes may have been using TDN and NO_2^-+NO_3^- faster than they could be replenished (**Figure 2.7b; Figure A1.11b**), while DOC (**Figure 2.7a; Figure A1.11a**) and Na^+ (**Figure 2.7c; Figure A1.11c**) yields peaked at BR2, a site with wetland regions along the river's edge, suggesting site-specific inputs.

When chemical yields were considered by parameter grouping, few anomalies stood out. Water yields were greatest at the most upstream site and leveled out at downstream sites along each river (**Figure 2.7e**). Following this, yields of basic chemical parameters mostly decreased along the SR-AR and BR, but DOC increased from the most upstream sites to the most downstream sites along all three rivers (**Figure 2.7a**). The increase in DOC yields with distance from glacier can potentially be explained by the transition from a glacierized altitudinal life zone with fast-flowing cold, turbid meltwaters to an alpine altitudinal life zone with freshwaters more hospitable to *in situ* biological productivity and/or more additions of allochthonous terrestrial organic matter (Robison et al., 2023). Dissolved Si yields also increased with distance downstream and was the only nutrient to do so (**Figure 2.7b**). An increase in water temperature and terrestrial-sourced organic acids can have a stimulatory effect on the erosion of silicates from surrounding soils and minerals, which may account for the higher Si yields at downstream sites (S. P. Anderson, 2005). Further, amorphous silica bound to suspended sediment has been found in glacial regions (Pryer et al., 2020), and the dissolution of bound silica along our rivers could have also contributed to higher Si yields at downstream sites. And while related ions such as Ca^{2+} and Mg^{2+} paralleled each other's downstream yield patterns (**Figure 2.7c**), trace element yields were found to be more element- and site-specific potentially due to the influence of geology or *in situ* ion exchange processes, for example (**Figure 2.7d**). Ultimately, sources and sinks of dissolved chemicals varied with parameter and site (**Figure A1.11**). Apart from the area between SR1 and SR2 acting as a minor sink for Ba, Mo, and FHg, river reaches were sources of dissolved chemicals. For instance, every river reach was a source of DOC, though as we would expect, downstream watershed DOC contributions were greater than upstream ones (**Figure A1.11a**); Ca^{2+} contributions across all rivers and river reaches were steady (**Figure A1.11c**); and the strongest sources of Sr were midstream for the SR-AR, mid- and down-stream for the NSR, and upstream for the BR, and thus river-specific (**Figure A1.11d**). In summary, the patterns in yields explored here were intuitively impacted by the diverse landscape features of our sampling reach (**Figure 2.3**; Dixon & Thorn, 2005). Proglacial lakes acted as settling ponds for turbid meltwaters coming from glacier drainage systems (Gilbert & Shaw, 1981; Wankiewicz, 1979), while braided glacial outwash floodplains contributed more particulate and total chemicals to the rivers (Goff & Ashmore, 1994). As you move downriver, the warmer climate, development of soils, and introduction of more montane vegetation in adjacent off-channel areas increased riverine yields of key dissolved parameters.

4 Conclusions

The objectives of our research in the glacial headwaters of the Sunwapta-Athabasca, North Saskatchewan and Bow rivers on the eastern slopes of the Canadian Rocky Mountains were to: (1) produce biennial hydrographs; (2) characterize water isotope signatures; (3) provide a general analysis of a 200+ parameter physicochemical dataset; and (4) estimate chemical yields for each sampling site and assess the spatiotemporal factors that drove data variability. We found that we could accurately model the hydrology at our sampling sites using existing regional discharge datasets, and that the hydrographs we produced showed the roughly bimodal shape typical in a snow- and glacier-melt hydrological regime during the open water season. Back trajectories from 2019 to 2021 showed that air masses traveled to our study region from western North America, circumpolar Arctic, and the North Pacific Ocean, explaining some of the diversity in precipitation and glacial ice water isotope signatures that we measured. The LMWL produced from our riverine water isotope signatures was similar to the CMWL (Gibson et al., 2020) and reflected a mix of inputs. Principal component analyses of physicochemical measures revealed that of all the spatiotemporal factors examined, distance from glacier had the overall greatest impact on the variability of physicochemistry in our system. Yet, that may rapidly change as the glaciers disappear from the landscape and extreme precipitation events, such as those experienced in June 2020, become more prevalent. Chemical yields followed what would generally be expected for rivers flowing through glacierized, alpine, subalpine, and montane altitudinal life zones. For example, particulate and total yields were highest at sampling sites nearest their source glacier and along glacial outwash plains. And apart from DOC and Si, whose yields increased with distance downstream, dissolved yields were parameter and site specific.

As mountain glaciers disappear due to climate change on a global scale, proglacial landscapes are expanding past their current areal boundaries and evolving biogeochemically. Further, the hydrology of the rivers that once stemmed from glaciers will become increasingly reliant on snowmelt and summer precipitation for their flow. Hence, chemical yields will likely become more reflective of non-glacierized systems, making it especially important to provide detailed scientific evaluations in these regions. We provided an initial high-level assessment of such a dataset here, at the intersection of biogeochemistry, limnology, glaciology, and hydrology. Thus, the analyses explored here can also be considered a contemporary baseline reference for those investigating river headwaters stemming from the eastern slopes of the Canadian Rocky Mountains in the future. However, the dataset is expansive with over 260,000 datapoints, and as such, we encourage other to mine and analyze it in ways we did not here. For example, water apportionment via isotope mixing models could be investigated using the water isotope signatures of our river water, precipitation, and glacier ice. Further, data on dissolved phosphorus concentrations, MeHg, and PAHs were not discussed in detail here, yet they could provide new biogeochemical information potentially important for gauging productivity and toxicity in glacier rivers. We believe the possibilities for data exploration are numerous and support further investigations given the lack of biogeochemical studies in these river systems and the collective effort in producing this dataset.

Data Availability Statement

All datasets used in this work are open source. The "Physicochemical, particulate matter, temperature, and hydrological datasets collected from climate-threatened glacial river headwaters on the eastern slopes of the Canadian Rocky Mountains (2019-2021)" that form the basis of this manuscript are available in the PANGAEA data repository (Felden et al., 2023) at https://doi.org/10.1594/PANGAEA.963863 (Serbu et al., 2023). Map base layers produced by Alberta Environment and Parks are from Alberta ArcHydro Phase 2 Data (https://open.alberta.ca/opendata/gda-d22f5906-358e-47b9-9259-02702932a7a0#summary; Alberta Environment and Parks, 2018). Land cover classes for each sampling site were obtained with the 2010 ABMI Wall-to-Wall Land Cover Inventory (https://abmi.ca/home/data-analytics/da-top/da-product-overview/Data-Archive/Land-Cover.html; Alberta Biodiversity Monitoring Institute, 2010) and the 2021 ABMI Wetland Inventory (https://abmi.ca/home/data-analytics/da-top/da-product-overview/Advanced-Landcover-Prediction-and-Habitat-Assessment--ALPHA--Products/ABMI-Wetland-Inventory.html; Alberta Biodiversity Monitoring Institute, 2021). Monthly climate summaries for Alberta were made available by Environment and Climate Change Canada (https://climate.weather.gc.ca/prods_servs/cdn_climate_summary_e.html; Environment and Climate Change Canada, 2019, 2020). Lastly, discharge measures from the National Water Data Archive: HYDAT were obtained by Water Survey of Canada and were invaluable to this study (https://www.canada.ca/en/environment-climate-change/services/water-overview/quantity/monitoring/survey/data-products-services/national-archive-hydat.html; Water Survey of Canada, 2021).

References

Alberta Biodiversity Monitoring Institute. (2010). ABMI Wall-to-Wall Land Cover Inventory. [Dataset]. https://abmi.ca/home/data-analytics/da-top/da-product-overview/Data-Archive/Land-Cover.html. Retrieved March 2023.

Alberta Biodiversity Monitoring Institute. (2021). ABMI Wetland Inventory. [Dataset]. https://abmi.ca/home/data-analytics/da-top/da-product-overview/Advanced-Landcover-Prediction-and-Habitat-Assessment--ALPHA--Products/ABMI-Wetland-Inventory.html. Retrieved March 2023.

Alberta Environment and Parks. (2018). Alberta ArcHydro Phase 2 Data. [Dataset]. Government of Alberta. https://open.alberta.ca/opendata/gda-d22f5906-358e-47b9-9259-02702932a7a0#summary. Retrieved February 2023.

Alberta Environment and Parks. (2019a). *Water supply outlook for Alberta*. Edmonton, AB: Government of Alberta. https://rivers.alberta.ca. Retrieved April 2023.

Alberta Environment and Parks. (2019b). Winter precipitation percent of normal. Edmonton, AB: Government of Alberta.

Alberta Environment and Parks. (2020a). *Water supply outlook for Alberta*. Edmonton, AB: Government of Alberta. https://rivers.alberta.ca. Retrieved April 2023.

Alberta Environment and Parks. (2020b). Winter precipitation percent of normal. Edmonton, AB: Government of Alberta.

Anderson, S. P. (2005). Glaciers show direct linkage between erosion rate and chemical weathering fluxes. *Geomorphology*, *67*(1-2 SPEC. ISS.), 147–157. https://doi.org/10.1016/j.geomorph.2004.07.010

Anderson, S. P. (2007). Biogeochemistry of glacial landscape systems. *Annual Review of Earth and Planetary Sciences*, *35*, 375–399. https://doi.org/10.1146/annurev.earth.35.031306.140033

Anderson, S. P., Drever, J. I., & Humphrey, N. F. (1997). Chemical weathering in glacial environments. *Geology*, *25*(5), 399–402.

Anderson, S., & Radić, V. (2020). Identification of local water resource vulnerability to rapid deglaciation in Alberta. *Nature Climate Change*, *10*(10), 933–938. https://doi.org/10.1038/s41558-020-0863-4

Antweiler, R. C., & Taylor, H. E. (2008). Evaluation of statistical treatments of left-censored environmental data using coincident uncensored data sets: I. Summary statistics. *Environmental Science and Technology*, *42*(10), 3732–3738. https://doi.org/10.1021/acs.est.5b02385

Appling, A. P., Leon, M. C., & McDowell, W. H. (2015). Reducing bias and quantifying uncertainty in watershed flux estimates: The R package loadflex. *Ecosphere*, *6*(12). https://doi.org/10.1890/ES14-00517.1

Arendt, C. A., Aciego, S. M., & Hetland, E. A. (2015). An open source Bayesian Monte Carlo isotope mixing model with applications in Earth surface processes. *Geochemistry, Geophysics, Geosystems*, *16*(5), 1274–1292. https://doi.org/10.1002/2014GC005683

Arendt, C. A., Stevenson, E. I., & Aciego, S. M. (2016). Hydrologic controls on radiogenic Sr in meltwater from an alpine glacier system: Athabasca Glacier, Canada. *Applied Geochemistry*, *69*, 42–49. https://doi.org/10.1016/j.apgeochem.2016.04.002

Ashbaugh, L. L., Malm, W. C., & Sadehs, W. Z. (1985). A residence time probability analysis of sulfur concentrations at Grand Canyon National Park. *Atmospheric Environment*, *19*(8), 1263–1270.

Bagshaw, E. A., Wadham, J. L., Tranter, M., Beaton, A. D., Hawkings, J. R., Lamarche-Gagnon, G., & Mowlem, M. C. (2021). Measuring pH in low ionic strength glacial meltwaters using ion selective field effect transistor (ISFET) technology. *Limnology and Oceanography: Methods*, *19*(3), 222–233. https://doi.org/10.1002/lom3.10416

Beal, S. A., Osterberg, E. C., Zdanowicz, C. M., & Fisher, D. A. (2015). Ice core perspective on mercury pollution during the past 600 years. *Environmental Science and Technology*, *49*(13), 7641–7647. https://doi.org/10.1021/acs.est.5b01033

Bennet, M. R., & Glasser, N. F. (2009). Glacial geology: Ice sheets and landforms. In *Glacial Geology: Ice Sheets and Landforms* (2nd ed.). Wiley-Blackwell.

Beria, H., Larsen, J. R., Ceperley, N. C., Michelon, A., Vennemann, T., & Schaefli, B. (2018). Understanding snow hydrological processes through the lens of stable water isotopes. *Wiley Interdisciplinary Reviews: Water*, *5*(6), 1–23. https://doi.org/10.1002/wat2.1311

Bershaw, J., Hansen, D. D., & Schauer, A. J. (2020). Deuterium excess and 17O-excess variability in meteoric water across the Pacific Northwest, USA. *Tellus B: Chemical and Physical Meteorology*, *72*(1), 1–17. https://doi.org/10.1080/16000889.2020.1773722

Blais, J. M., Schindler, D. W., G Muir, D. C., Sharp, M., Donald, D., Lafrenière, M., Braekevelt, E., & J Strachan, W. M. (2001). Melting glaciers: A major source of persistent organochlorines to subalpine Bow Lake in Banff National Park, Canada. *Ambio*, *30*(7), 410–415.

Bogen, J., Xu, M., & Kennie, P. (2015). The impact of pro-glacial lakes on downstream sediment delivery in Norway. *Earth Surface Processes and Landforms*, *40*(7), 942–952. https://doi.org/10.1002/esp.3669

Boutron, C. F. (1995). Historical reconstruction of the earth's past atmospheric environment from Greenland and Antarctic snow and ice cores. *Environmental Reviews*, *3*(1), 1–28. https://doi.org/10.1139/a95-001

Bowman, M. F., Chambers, P. A., & Schindler, D. W. (2005). Epilithic algal abundance in relation to anthropogenic changes in phosphorus bioavailability and limitation in mountain rivers. *Canadian Journal of Fisheries and Aquatic Sciences*, *62*(1), 174–184. https://doi.org/10.1139/f04-244

Brown, G. H., Tranter, M., & Sharp, M. J. (1996). Experimental investigations of the weathering of suspended sediment by alpine glacial meltwater. *Hydrological Processes*, *10*(4), 579–597. https://doi.org/10.1002/(SICI)1099-1085(199604)10:4<579::AID-HYP393>3.0.CO;2-D

Campbell, É. M. S., & Ryan, M. C. (2021). Nested recharge systems in mountain block hydrology: High-elevation snowpack generates low-elevation overwinter baseflow in a Rocky Mountain river. *Water (Switzerland)*, *13*(16). https://doi.org/10.3390/w13162249

Carroll, R. W. H., Deems, J., Maxwell, R., Sprenger, M., Brown, W., Newman, A., Beutler, C., Bill, M., Hubbard, S. S., & Williams, K. H. (2022). Variability in observed stable water isotopes in snowpack across a mountainous watershed in Colorado. *Hydrological Processes*, *36*(8). https://doi.org/10.1002/hyp.14653

Carroll, R. W. H., Deems, J., Sprenger, M., Maxwell, R., Brown, W., Newman, A., Beutler, C., & Williams, K. H. (2022). Modeling snow dynamics and stable water isotopes across mountain landscapes. *Geophysical Research Letters*, *49*(20). https://doi.org/10.1029/2022GL098780

Carrivick, J. L., & Tweed, F. S. (2013). Proglacial lakes: Character, behaviour and geological importance. *Quaternary Science Reviews*, *78*, 34–52. https://doi.org/10.1016/j.quascirev.2013.07.028

Clarke, G. K. C., Jarosch, A. H., Anslow, F. S., Radić, V., & Menounos, B. (2015). Projected deglaciation of western Canada in the twenty-first century. *Nature Geoscience*, *8*(5), 372–377. https://doi.org/10.1038/ngeo2407

Comeau, L. E. L., Pietroniro, A., & Demuth, M. N. (2009). Glacier contribution to the North and South Saskatchewan rivers. *Hydrological Processes*, *23*, 2640–2653. https://doi.org/10.1002/hyp.7409

Criscitiello, A. S., Marshall, S. J., Evans, M. J., Kinnard, C., Norman, A. L., & Sharp, M. J. (2016). Marine aerosol source regions to prince of Wales Icefield, Ellesmere Island, and influence from the tropical Pacific, 1979-2001. *Journal of Geophysical Research*, *121*(16), 9492–9507. https://doi.org/10.1002/2015JD024457

Dansgaard, W. (1964). Stable isotopes in precipitation. *Tellus*, *16*(4), 436–468. https://doi.org/10.1111/j.2153-3490.1964.tb00181.x

Demuth, M. N., & Horne, G. (2017). *Decadal-centenary glacier mass changes and their variability, Jasper National Park of Canada, Alberta, including the Columbia Icefield region* (Issue December). https://doi.org/10.4095/302705

Demuth, M. N., & Pietroniro, A. (2003). *The impact of climate change on the glaciers of the Canadian Rocky Mountain eastern slopes and implications for water resource-related adaptation in the Canadian prairies 'Phase I'- Headwaters of the North Saskatchewan River Basin*.

Deuerling, K. M., Martin, J. B., Martin, E. E., & Scribner, C. A. (2018). Hydrologic exchange and chemical weathering in a proglacial watershed near Kangerlussuaq, west Greenland. *Journal of Hydrology*, *556*, 220–232. https://doi.org/10.1016/j.jhydrol.2017.11.002

Dixon, J. C., & Thorn, C. E. (2005). Chemical weathering and landscape development in mid-latitude alpine environments. *Geomorphology*, *67*(1-2 SPEC. ISS.), 127–145. https://doi.org/10.1016/j.geomorph.2004.07.009

Dodds, W. K., & Whiles, M. R. (2020). Freshwater Ecology. *Aquatic Ecology* (3rd Edition). Cambridge, MA: Academic Press.

Environment and Climate Change Canada. (2019). Monthly climate summaries Alberta [Dataset]. https://climate.weather.gc.ca/prods_servs/cdn_climate_summary_e.html. Retrieved April 2023.

Environment and Climate Change Canada. (2020). Monthly climate summaries Alberta [Dataset]. https://climate.weather.gc.ca/prods_servs/cdn_climate_summary_e.html. Retrieved April 2023.

Felden, J., Möller, L., Schindler, U., Huber, R., Schumacher, S., Koppe, R., Diepenbroek, M., & Glöckner, F. O. (2023). PANGAEA - Data Publisher for Earth & Environmental Science. *Scientific Data*, *10*(1), 347. https://doi.org/10.1038/s41597-023-02269-x

Fernández, P., Carrera, G., Grimalt, J. O., Ventura, M., Camarero, L., Catalan, J., Nickus, U., Thies, H., & Psenner, R. (2003). Factors governing the atmospheric deposition of polycyclic aromatic hydrocarbons to remote areas. *Environmental Science and Technology*, *37*(15), 3261–3267. https://doi.org/10.1021/es020137k

Gadd, B. (2009). *Handbook of the Canadian Rockies*. Corex Press.

Geilhausen, M., Morche, D., Otto, J.-C., & Schrott, L. (2013). Sediment discharge from the proglacial zone of a retreating Alpine glacier. *Zeitschrift Für Geomorphologie, Supplementary Issues*, *57*(2), 29–53. https://doi.org/10.1127/0372-8854/2012/s-00122

Gibson, J. J., Holmes, T., Stadnyk, T. A., Birks, S. J., Eby, P., & Pietroniro, A. (2020). 18O and 2H in streamflow across Canada. In *Journal of Hydrology: Regional Studies* (Vol. 32). Elsevier B.V. https://doi.org/10.1016/j.ejrh.2020.100754

Gilbert, R., & Shaw, J. (1981). Sedimentation in proglacial Sunwapta Lake, Alberta. *Canadian Journal of Earth Sciences*, *18*(1), 81–93. https://doi.org/10.1139/e81-007

Goff, J. R., & Ashmore, P. (1994). Gravel transport and morphological change in braided Sunwapta River, Alberta, Canada. *Earth Surface Processes and Landforms*, *19*(3), 195–212. https://doi.org/10.1002/esp.3290190302

Hawkings, J. R., Benning, L. G., Raiswell, R., Kaulich, B., Araki, T., Abyaneh, M., Stockdale, A., Koch-Müller, M., Wadham, J. L., & Tranter, M. (2018). Biolabile ferrous iron bearing nanoparticles in glacial sediments. *Earth and Planetary Science Letters*, *493*, 92–101. https://doi.org/10.1016/j.epsl.2018.04.022

Hawkings, J. R., Skidmore, M. L., Wadham, J. L., Priscu, J. C., Morton, P. L., & Hatton, J. E. (2020). Enhanced trace element mobilization by Earth's ice sheets. *Proceedings of the*

National Academy of Sciences of the United States of America, 1–12. https://doi.org/10.1073/pnas.2014378117

Hayashi, M. (2020). Alpine hydrogeology: The critical role of groundwater in sourcing the headwaters of the world. *Groundwater*, *58*(4), 498–510. https://doi.org/10.1111/gwat.12965

Helsel, D. R. (1990). Less than obvious: Statistical treatment of data below the detection limit. *Environmental Science & Technology*, *24*(12), 1766–1774.

Higgs, E. S. (n.d.). *Mountain Legacy Project*. University of Victoria, Canada. Retrieved 28 June 2023, from https://explore.mountainlegacy.ca

Holdsworth, G., Fogarasi, S., & Krouse, H. R. (1991). Variation of the stable isotopes of water with altitude in the Saint Elias Mountains of Canada. *Journal of Geophysical Research*, *96*(D4), 7483–7494. https://doi.org/10.1029/91JD00048

Hood, E., Battin, T. J., Fellman, J., O’neel, S., & Spencer, R. G. M. (2015). Storage and release of organic carbon from glaciers and ice sheets. *Nature Geoscience*, *8*(2), 91–96. https://doi.org/10.1038/ngeo2331

Hood, E., & Scott, D. (2008). Riverine organic matter and nutrients insoutheast Alaska affected by glacial coverage. *Nature Geoscience*, *1*(9), 583–587. https://doi.org/10.1038/ngeo280

Hopwood, M. J., Statham, P. J., Tranter, M., & Wadham, J. L. (2014). Glacial flours as a potential source of Fe(II) and Fe(III) to polar waters. *Biogeochemistry*, *118*(1–3), 443–452. https://doi.org/10.1007/s10533-013-9945-y

Hu, J., Yan, Y., Yeung, L. Y., & Dee, S. G. (2022). Sublimation origin of negative deuterium excess observed in snow and ice samples from McMurdo Dry Valleys and Allan Hills blue ice areas, East Antarctica. *Journal of Geophysical Research: Atmospheres*, *127*(11). https://doi.org/10.1029/2021JD035950

Immerzeel, W. W., Lutz, A. F., Andrade, M., Bahl, A., Biemans, H., Bolch, T., Hyde, S., Brumby, S., Davies, B. J., Elmore, A. C., Emmer, A., Feng, M., Fernández, A., Haritashya, U., Kargel, J. S., Koppes, M., Kraaijenbrink, P. D. A., Kulkarni, A. V., Mayewski, P. A., … Baillie, J. E. M. (2020). Importance and vulnerability of the world’s water towers. *Nature*, *577*(7790), 364–369. https://doi.org/10.1038/s41586-019-1822-y

International Atomic Energy Agency. (2009). Laser spectroscopic analysis of liquid water samples for stable hydrogen and oxygen isotopes. In IAEA, *Training Course Series No. 35*.

Kalnay, E., Kanamitsu, M., Kistler, R., Collins, W., Deaven, D., Gandin, L., Iredell, M., Saha, S., White, G., Woollen, J., Zhu, Y., Chelliah, M., Ebisuzaki, + W, Higgins, + W, Janowiak, + J, Mo, + K C, Ropelewski, + C, Wang, + J, Leetmaa, + A, … Joseph, D. (1996). The NCEP/NCAR 40-Year Reanalysis Project. *Bulletin of the American Meteorological Society*, *77*(3), 437–471.

Kassambara, A., & Mundt, F. (2020). *factoextra: Extract and visualize the results of multivariate data analyses*. R package version 1.0.7, https://CRAN.R-project.org/package=factoextra

Kohler, T. J., Fodelianakis, S., Michoud, G., Ezzat, L., Bourquin, M., Peter, H., Busi, S. B., Pramateftaki, P., Deluigi, N., Styllas, M., Tolosano, M., de Staercke, V., Schön, M., Brandani, J., Marasco, R., Daffonchio, D., Wilmes, P., & Battin, T. J. (2022). Glacier shrinkage will accelerate downstream decomposition of organic matter and alters microbiome structure and function. *Global Change Biology*, *28*(12), 3846–3859. https://doi.org/10.1111/gcb.16169

Lafrenière, M. J., & Sharp, M. J. (2004). The concentration and fluorescence of dissolved organic carbon (DOC) in glacial and nonglacial catchments: Interpreting hydrological flow routing and DOC sources. *Arctic, Antarctic, and Alpine Research*, *36*(2), 156–165. https://doi.org/10.1657/1523-0430(2004)036[0156:TCAFOD]2.0.CO;2

Lafrenière, M. J., & Sharp, M. J. (2005). A comparison of solute fluxes and sources from glacial and non-glacial catchments over contrasting melt seasons. *Hydrological Processes*, *19*(15), 2991–3012. https://doi.org/10.1002/hyp.5812

Lafrenière, M. J., & Sinclair, K. E. (2011). Snowpack and precipitation chemistry at a high altitude site in the Canadian Rocky Mountains. *Journal of Hydrology*, *409*(3–4), 737–748. https://doi.org/10.1016/j.jhydrol.2011.09.007

Lê, S., Josse, J., & Husson, F. (2008). FactoMineR: An R package for multivariate analysis. *Journal of Statistical Software*, *25*(1), 1–18. https://doi.org/10.18637/jss.v025.i01

Lorenz, D., Runkel, R., De Cicco, L., Watkins, D., & Stachelek, J. (2017). *rloadest: River load estimation, version 0.4.5*. U.S. Geological Survey.

Mahindawansha, A., Jost, M., & Gassmann, M. (2022). Spatial and temporal variations of stable isotopes in precipitation in the mountainous region, North Hesse. *Water (Switzerland)*, *14*(23). https://doi.org/10.3390/w14233910

Mansilha, C., Carvalho, A., Guimarães, P., & Marques, J. E. (2014). Water quality concerns due to forest fires: Polycyclic aromatic hydrocarbons (PAH) contamination of groundwater from mountain areas. *Journal of Toxicology and Environmental Health - Part A: Current Issues*, *77*(14–16), 806–815. https://doi.org/10.1080/15287394.2014.909301

Marshall, S. J. (2014). Meltwater run-off from Haig Glacier, Canadian Rocky Mountains, 2002-2013. *Hydrology and Earth System Sciences*, *18*(12), 5181–5200. https://doi.org/10.5194/hess-18-5181-2014

Marshall, S. J., White, E. C., Demuth, M. N., Bolch, T., Wheate, R., Menounos, B., Beedle, M. J., & Shea, J. M. (2011). Glacier water resources on the eastern slopes of the Canadian Rocky Mountains. *Canadian Water Resources Journal*, *36*(2), 109–134. https://doi.org/10.4296/cwrj3602823

Marshall, S., & White, E. (2010). *Alberta glacier inventory and ice volume estimation* (Issue December).

Marvin, C. H., Berthiaume, A., Burniston, D. A., Chibwe, L., Dove, A., Evans, M., Hewitt, L. M., Hodson, P. V., Muir, D. C. G., Parrott, J., Thomas, P. J., & Tomy, G. T. (2021). Polycyclic aromatic compounds in the Canadian Environment: Aquatic and terrestrial environments. In *Environmental Pollution* (Vol. 285). Elsevier Ltd. https://doi.org/10.1016/j.envpol.2021.117442

Menounos, B., Hugonnet, R., Shean, D., Gardner, A., Howat, I., Berthier, E., Pelto, B., Tennant, C., Shea, J., Noh, M. J., Brun, F., & Dehecq, A. (2019). Heterogeneous changes in western North American glaciers linked to decadal variability in zonal wind strength. *Geophysical Research Letters*, *46*(1), 200–209. https://doi.org/10.1029/2018GL080942

Miller, J. E., Kahl, J. D. W., Heller, F., & Harris, J. M. (2002). A three-dimensional residence-time analysis of potential summertime atmospheric transport to Summit, Greenland. *Annals of Glaciology*, *35*. https://www.cambridge.org/core.

Milner, A. M., Khamis, K., Battin, T. J., Brittain, J. E., Barrand, N. E., Füreder, L., Cauvy-Fraunié, S., Gíslason, G. M., Jacobsen, D., Hannah, D. M., Hodson, A. J., Hood, E., Lencioni, V., Ólafsson, J. S., Robinson, C. T., Tranter, M., & Brown, L. E. (2017). Glacier shrinkage driving global changes in downstream systems. *Proceedings of the National Academy of Sciences of the United States of America*, *114*(37), 9770–9778. https://doi.org/10.1073/pnas.1619807114

Niu, Y., Castro, M. C., Hall, C. M., Aciego, S. M., & Arendt, C. A. (2017). Characterizing glacial meltwater sources in the Athabasca Glacier, Canada, using noble gases as tracers. *Applied Geochemistry*, *76*, 136–147. https://doi.org/10.1016/j.apgeochem.2016.11.015

Ommanney, C. S. L. (2002). Glaciers of the Canadian Rockies. In *Glaciers of North America*.

Pana, D. I., & Elgr, R. (2013). Geology of the Alberta Rocky Mountains and Foothills (Map No. 560). Edmonton, AB: Alberta Geological Survey.

Pasteris, D. R., McConnell, J. R., Das, S. B., Criscitiello, A. S., Evans, M. J., Maselli, O. J., Sigl, M., & Layman, L. (2014). Seasonally resolved ice core records from West Antarctica indicate a sea ice source of sea-salt aerosol and a biomass burning source of ammonium. *JGR: Atmospheres*, *119*(14), 9168–9182. https://doi.org/10.1002/2013JD020720

Paznekas, A., & Hayashi, M. (2016). Groundwater contribution to winter streamflow in the Canadian Rockies. *Canadian Water Resources Journal*, *41*(4), 484–499. https://doi.org/10.1080/07011784.2015.1060870

Penn, K., Marshall, S. J., & Sinclair, K. E. (2023). Seasonal enrichment of heavy isotopes in meltwater runoff from Haig Glacier, Canadian Rocky Mountains. *Frontiers in Earth Science*, *11*. https://doi.org/10.3389/feart.2023.1125877

Pfahl, S., & Sodemann, H. (2014). What controls deuterium excess in global precipitation? *Climate of the Past*, *10*(2), 771–781. https://doi.org/10.5194/cp-10-771-2014

Price, M. F. (2015). Mountains: A very short introduction. In *Mountains: A Very Short Introduction*. Oxford University Press.

Pryer, H. V., Hawkings, J. R., Wadham, J. L., Robinson, L. F., Hendry, K. R., Hatton, J. E., Kellerman, A. M., Bertrand, S., Gill-Olivas, B., Marshall, M. G., Brooker, R. A., Daneri, G., & Häussermann, V. (2020). The influence of glacial cover on riverine silicon and iron exports in Chilean Patagonia. *Global Biogeochemical Cycles*, *34*(12). https://doi.org/10.1029/2020GB006611

R Core Team. (2022). *R: A language and environment for statistical computing*. R Foundation for Statistical Computing. https://www.R-project.org/

Radić, V., Bliss, A., Beedlow, A. C., Hock, R., Miles, E., & Cogley, J. G. (2014). Regional and global projections of twenty-first century glacier mass changes in response to climate scenarios from global climate models. *Climate Dynamics*, *42*(1–2), 37–58. https://doi.org/10.1007/s00382-013-1719-7

Rippin, D. M., Sharp, M., Van Wychen, W., & Zubot, D. (2020). ‘Detachment’ of icefield outlet glaciers: Catastrophic thinning and retreat of the Columbia Glacier (Canada). *Earth Surface Processes and Landforms*, *45*(2), 459–472. https://doi.org/10.1002/esp.4746

Robison, A. L., Deluigi, N., Rolland, C., Manetti, N., & Battin, T. (2023). Glacier loss and vegetation expansion alter organic and inorganic carbon dynamics in high-mountain streams. *Biogeosciences*, *20*(12), 2301–2316. https://doi.org/10.5194/bg-20-2301-2023

Rounce, D. R., Hock, R., Maussion, F., Hugonnet, R., Kochtitzky, W., Huss, M., Berthier, E., Brinkerhoff, D., Compagno, L., Copland, L., Farinotti, D., Menounos, B., & Mcnabb, R. W. (2023). Global glacier change in the 21st century: Every increase in temperature matters. In *Science* (Vol. 379). https://www.science.org

Runkel, B. R. L., Crawford, C. G., & Cohn, T. A. (2004). Load Estimator (LOADEST): A FORTRAN program for estimating constituent loads in streams and rivers. In *Techniques and Methods Book 4*.

Schindler, D. W., & Donahue, W. F. (2006). An impending water crisis in Canada’s western prairie provinces. *Proceedings of the National Academy of Sciences of the United States of America*, *103*(19), 7210–7216. https://doi.org/10.1073/pnas.0601568103

Schuster, J. K., Harner, T., Su, K., Mihele, C., & Eng, A. (2015). First results from the oil sands passive air monitoring network for polycyclic aromatic compounds. *Environmental Science and Technology*, *49*(5), 2991–2998. https://doi.org/10.1021/es505684e

Serbu, J. A., St.Louis, V. L., Emmerton, C. A., Tank, S. E., Criscitiello, A. S., Silins, U, Bhatia, M. P., Cavaco, M. A., Christenson, C., Cooke, C. A., Drapeau, H. F., Enns, S. J. A., Flett, J. E., Holland, K. M., Lavallee-Whiffen, J., Ma, M., Muir, C. E., Poesch, M., & Shin, J. Physicochemical, particulate matter, temperature, and hydrological datasets collected from climate-threatened glacial river headwaters on the eastern slopes of the Canadian Rocky Mountains (2019-2021). PANGAEA. https://doi.org/10.1594/PANGAEA.963863

Sharma, B. M., Nizzetto, L., Bharat, G. K., Tayal, S., Melymuk, L., Sáňka, O., Přibylová, P., Audy, O., & Larssen, T. (2015). Melting Himalayan glaciers contaminated by legacy atmospheric depositions are important sources of PCBs and high-molecular-weight PAHs for the Ganges floodplain during dry periods. *Environmental Pollution*, *206*, 588–596. https://doi.org/10.1016/j.envpol.2015.08.012

Sinclair, K. E., & Marshall, S. J. (2008). Post-depositional modification of stable water isotopes in winter snowpacks in the Canadian Rocky Mountains. *Annals of Glaciology*, *49*, 96–106. https://doi.org/10.3189/172756408787814979

Sinclair, K. E., & Marshall, S. J. (2009). Temperature and vapour-trajectory controls on the stable-isotope signal in Canadian Rocky Mountain snowpacks. *Journal of Glaciology*, *55*(191), 485–498. https://doi.org/10.3189/002214309788816687

Somers, L. D., & McKenzie, J. M. (2020). A review of groundwater in high mountain environments. In *Wiley Interdisciplinary Reviews: Water* (Vol. 7, Issue 6). John Wiley and Sons Inc. https://doi.org/10.1002/wat2.1475

Standard Methods Committee of the American Public Health Association, American Water Works Association, & Water Environment Federation. (a). Method 3125: Metals by Inductively Coupled Plasma-Mass Spectrometry (ICP-MS). In W. C. Lipps, T. E. Baxter, & E. Braun-Howland (Eds.), *Standard Methods for the Examination of Water and Wastewater*. APHA Press. https://doi.org/10.2105/smww.2882.048

Standard Methods Committee of the American Public Health Association, American Water Works Association, & Water Environment Federation. (b). Method 4500-NH3 (Ammonia). In W. C. Lipps, T. E. Baxter, & E. Braun-Howland (Eds.), *Standard Methods for the Examination of Water and Wastewater*. APHA Press. https://doi.org/10.2105/SMWW.2882.087

Standard Methods Committee of the American Public Health Association, American Water Works Association, & Water Environment Federation. (c). Method 4500-P (Phosphorus). In W. C. Lipps, T. E. Baxter, & E. Braun-Howland (Eds.), *Standard Methods for the Examination of Water and Wastewater*. APHA Press.

Standard Methods Committee of the American Public Health Association, American Water Works Association, & Water Environment Federation. (d). Method 4500-SiO2 (Silica). In W. C. Lipps, T. E. Baxter, & E. Braun-Howland (Eds.), *Standard Methods for the Examination of Water and Wastewater*. APHA Press. https://doi.org/10.2105/SMWW.2882.095

Standard Methods Committee of the American Public Health Association, American Water Works Association, & Water Environment Federation. (e). Method 5310 - TOC (Total organic carbon). In W. C. Lipps, T. E. Baxter, & E. Braun-Howland (Eds.), *Standard*

Methods for the Examination of Water and Wastewater. APHA Press. https://doi.org/10.2105/SMWW.2882.104

St. Pierre, K. A., St. Louis, V. L., Schiff, S. L., Lehnherr, I., Dainard, P. G., Gardner, A. S., Aukes, P. J. K., & Sharp, M. J. (2019). Proglacial freshwaters are significant and previously unrecognized sinks of atmospheric CO2. *Proceedings of the National Academy of Sciences of the United States of America*, *116*(36), 17690–17695. https://doi.org/10.1073/pnas.1904241116

Staniszewska, K. J., Cooke, C. A., & Reyes, A. V. (2020). Quantifying meltwater sources and contaminant fluxes from the Athabasca Glacier, Canada. *ACS Earth and Space Chemistry*. https://doi.org/10.1021/acsearthspacechem.0c00256

Stein, A. F., Draxler, R. R., Rolph, G. D., Stunder, B. J. B., Cohen, M. D., & Ngan, F. (2015). NOAA's HYSPLIT atmospheric transport and dispersion modeling system. In *Bulletin of the American Meteorological Society* (Vol. 96, Issue 12, pp. 2059–2077). American Meteorological Society. https://doi.org/10.1175/BAMS-D-14-00110.1

Tennant, C., & Menounos, B. (2013). Glacier change of the Columbia Icefield, Canadian Rocky Mountains, 1919-2009. *Journal of Glaciology*, *59*(216), 671–686. https://doi.org/10.3189/2013JoG12J135

Tennant, C., Menounos, B., Wheate, R., & Clague, J. J. (2012). Area change of glaciers in the Canadian Rocky Mountains, 1919 to 2006. *Cryosphere*, *6*(6), 1541–1552. https://doi.org/10.5194/tc-6-1541-2012

Tranter, M., & Wadham, J. L. (2013). Geochemical weathering in glacial and proglacial environments. In *Treatise on Geochemistry: Second Edition* (2nd ed., Vol. 7, pp. 157–173). Elsevier Ltd. https://doi.org/10.1016/B978-0-08-095975-7.00505-2

U.S. Environmental Protection Agency. (1989). Method 1625C: Semivolatile organic compounds by isotope dilution GCMS. U.S. EPA Federal Registry.

U.S. Environmental Protection Agency. (2014). Method 8270E (SW-846): Semivolatile organic compounds by Gas Chromatography/Mass Spectrometry (GC/MS). U.S. EPA Federal Registry.

U.S. EPA. (1971a). Method 160.1: Total dissolved solids. In *Methods for Chemical Analysis of Water and Wastes (EPA 600/4-79-020)*. U.S. EPA Federal Registry.

U.S. EPA. (1971b). Method 160.2: Non-filterable residue and total suspended solids. In *Methods for Chemical Analysis of Water and Wastes (EPA 600/4-79-020)*. U.S. EPA Federal Registry.

U.S. EPA. (1993a). Method 300.1: Determination of anions in drinking water by ion chromatography. In *Methods for the Determination of Organic and Inorganic Compounds in Drinking Water (EPA 815/R-00-014)*. U.S. EPA Federal Registry.

U.S. EPA. (1993b). Method 353.2: Determination of nitrate-nitrite nitrogen by automated colorimetry. In *Methods for Chemical Analysis of Water and Wastes (EPA 600/4-79-020)*. U.S. EPA Federal Registry.

U.S. EPA. (1994). *Method 200.7, Revision 4.4: Determination of metals and trace elements in water and wastes by Inductively Coupled Plasma-Atomic Emission Spectrometry (ICP-AES)*. U.S. EPA Federal Registry.

U.S. EPA. (1997). Method 440.0: Carbon and nitrogen in sediments and particulates. In *Methods for the Determination of Chemical Substances in Estuarine Environmental Matrices (EPA 600/R-97-072)*. U.S. EPA Federal Registry.

U.S. EPA. (1998). *Method 1630: Methyl mercury in water by distillation, aqueous ethylation, purge and trap, and cold vapor atomic fluorescence spectrometry*. U.S. EPA Federal Registry.

U.S. EPA. (2002). *Method 1631, Revision E: Mercury in water by oxidation, purge and trap, and cold vapor atomic fluorescence spectrometry*. U.S. EPA Federal Registry.

Wadham, J. L., Cooper, R. J., Tranter, M., & Hodgkins, R. (2001). Enhancement of glacial solute fluxes in the proglacial zone of a polythermal glacier. *Journal of Glaciology*, *47*(158), 378–386. https://doi.org/10.3189/172756501781832188

Wang, Z. A., Lawson, G. L., Pilskaln, C. H., & Maas, A. E. (2017). Seasonal controls of aragonite saturation states in the Gulf of Maine. *Journal of Geophysical Research: Oceans*, *122*(1), 372–389. https://doi.org/10.1002/2016JC012373

Wankiewicz, P. M. (1979). *Sedimentation in Sunwapta Lake, Jasper National Park, Alberta* (Master's thesis). Edmonton, AB: University of Alberta.

Water Survey of Canada. (2021). National Water Data Archive: HYDAT [Dataset]. Environment and Climate Change Canada, Government of Canada. https://www.canada.ca/en/environment-climate-change/services/water-overview/quantity/monitoring/survey/data-products-services/national-archive-hydat.html. Retrieved January 2021.

Wickham, H. (2016). *ggplot2: Elegant graphics for data analysis*. Springer-Verlag.

Figure 2.1. Side-by-side comparisons of historic and contemporary photographs of Athabasca Glacier, Jasper National Park. All 1918 scenes were captured by Arthur Oliver Wheeler during an Interprovincial Boundary Survey and archived by the Mountain Legacy Project team (Higgs, 2023). Sampling sites SR1 and SR2 and the Sunwapta River proglacial lake are labeled in the top right image. For site abbreviations, please see **Table A1.1**.

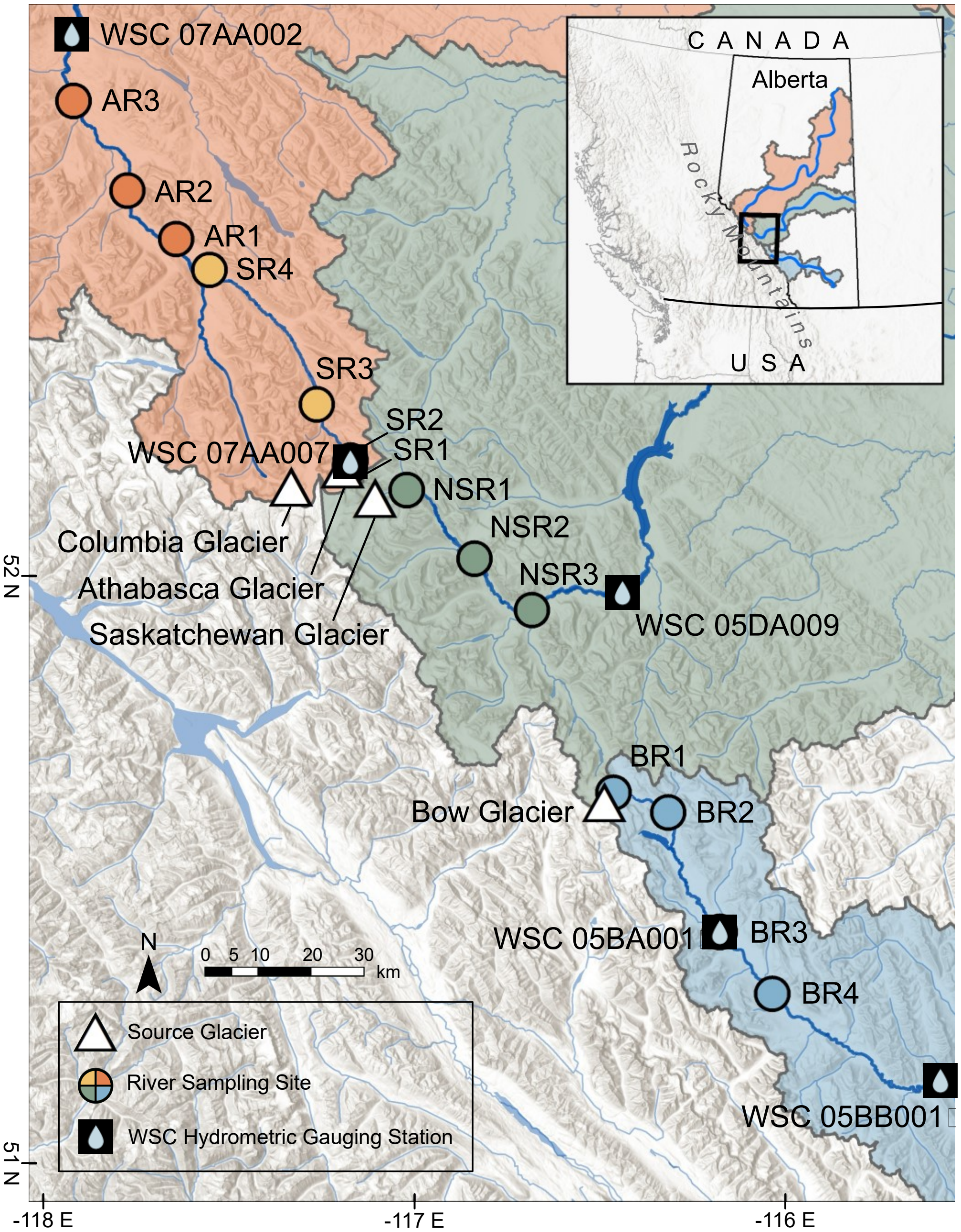

Figure 2.2. Map of source glaciers, our sampling sites on the Sunwapta (SR), Athabasca (AR), North Saskatchewan (NSR), and Bow (BR) rivers, and Water Survey of Canada (WSC) hydrometric gauging stations that were used as hydrology calibration sites in this study (see **Table A1.1** and **Table A1.3**). Sampled watersheds are color-coded and match the watersheds depicted on the inset map of Alberta, Canada. All sampling was conducted in the headwaters of these major river systems in Jasper and Banff National Parks (Park boundaries are not shown). Base map imagery from Esri, Government of Canada (Alberta Project NA1) 1983 Transverse Mercator.

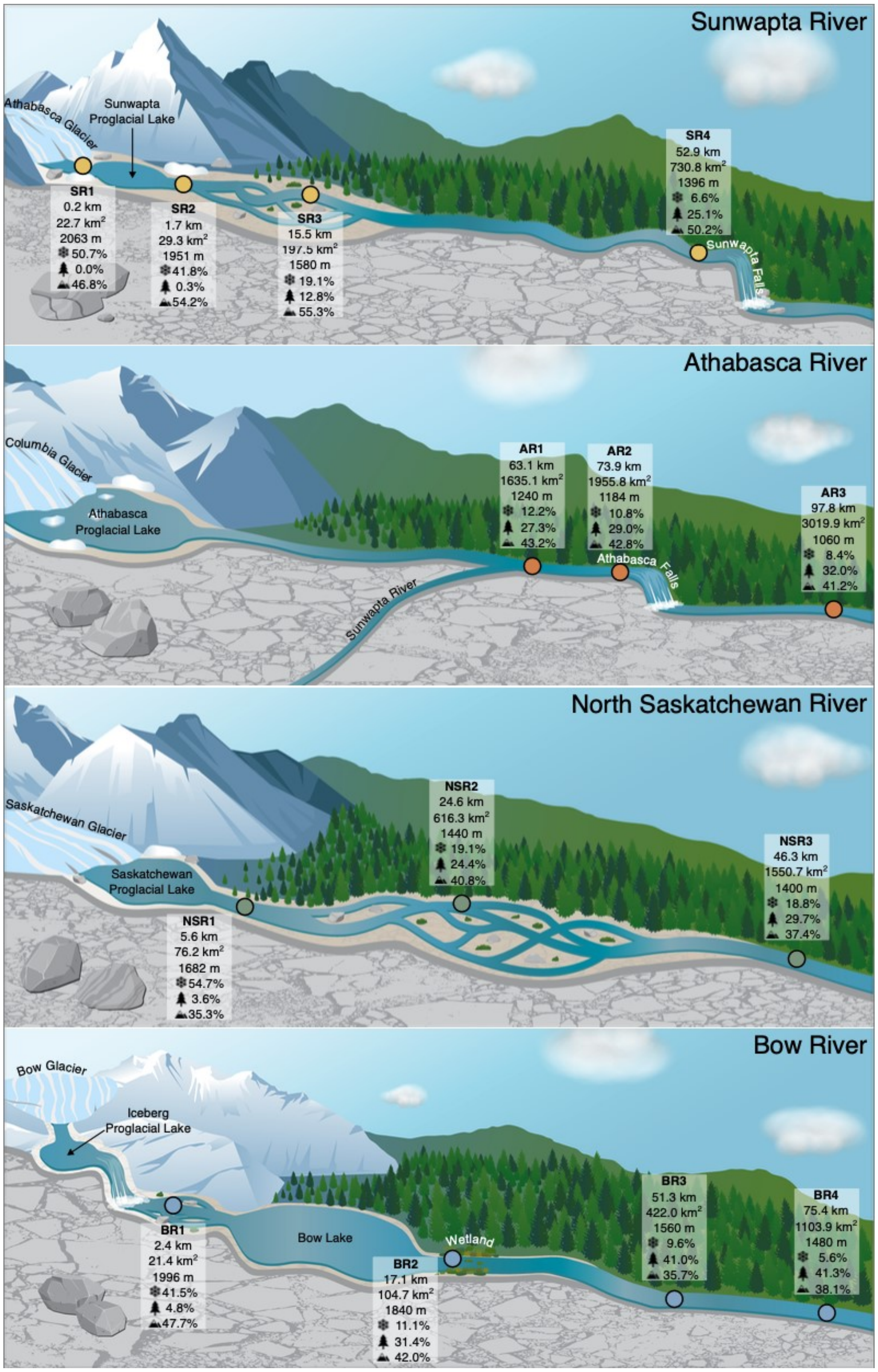

Figure 2.3. Profiles of the (a) Sunwapta, (b) Athabasca, (c) North Saskatchewan, and (d) Bow rivers with sampling sites, distance from glacier, watershed area, elevation, and notable river features included. Relative percent watershed area covered by major land cover classes in our study system (snow and ice [snowflake], coniferous forest [tree], and rock and rubble [mountain]) are listed for each site. For further site descriptions, including river abbreviations, exact sampling locations, and relative percent land covered by minor land cover classes, please see **Table A1.1** and **Table A1.2**. Distances and elevations are not precisely to scale.

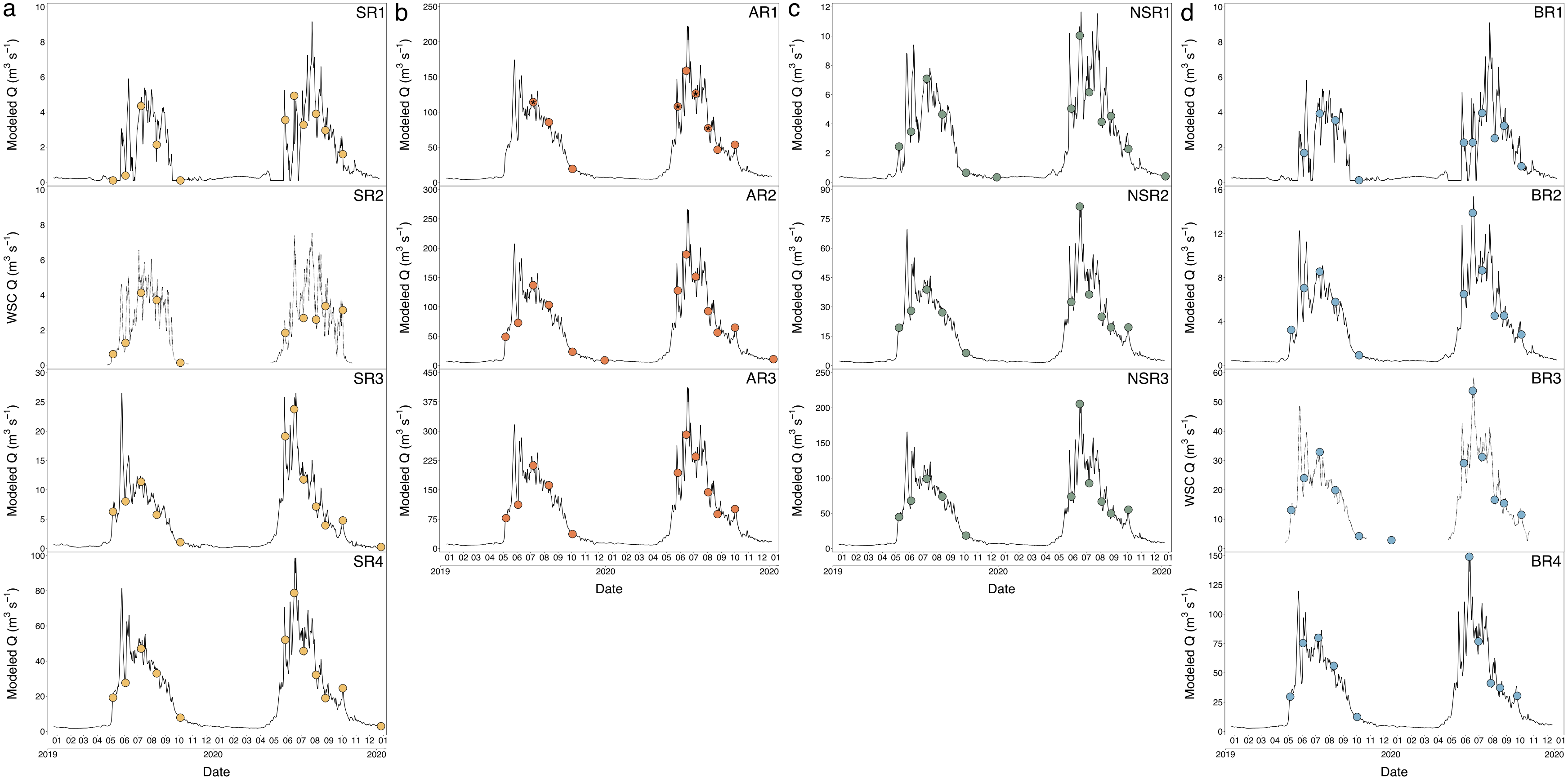

Figure 2.4. Modeled (solid line) and measured Water Survey of Canada (WSC; dotted line) discharge (Q; m^3 s^{-1}) and physicochemical sampling dates (colored circles) at the 14 sampling sites along the (a) Sunwapta (SR), (b) Athabasca (AR), (c) North Saskatchewan (NSR), and (d) Bow (BR) rivers for 2019 through early 2021. Stars in the orange circles for AR1 symbolize sampling dates where dissolved concentration data was eliminated from all data analyses. For site abbreviations, please see **Table A1.1**. Please note different y-axis scales.

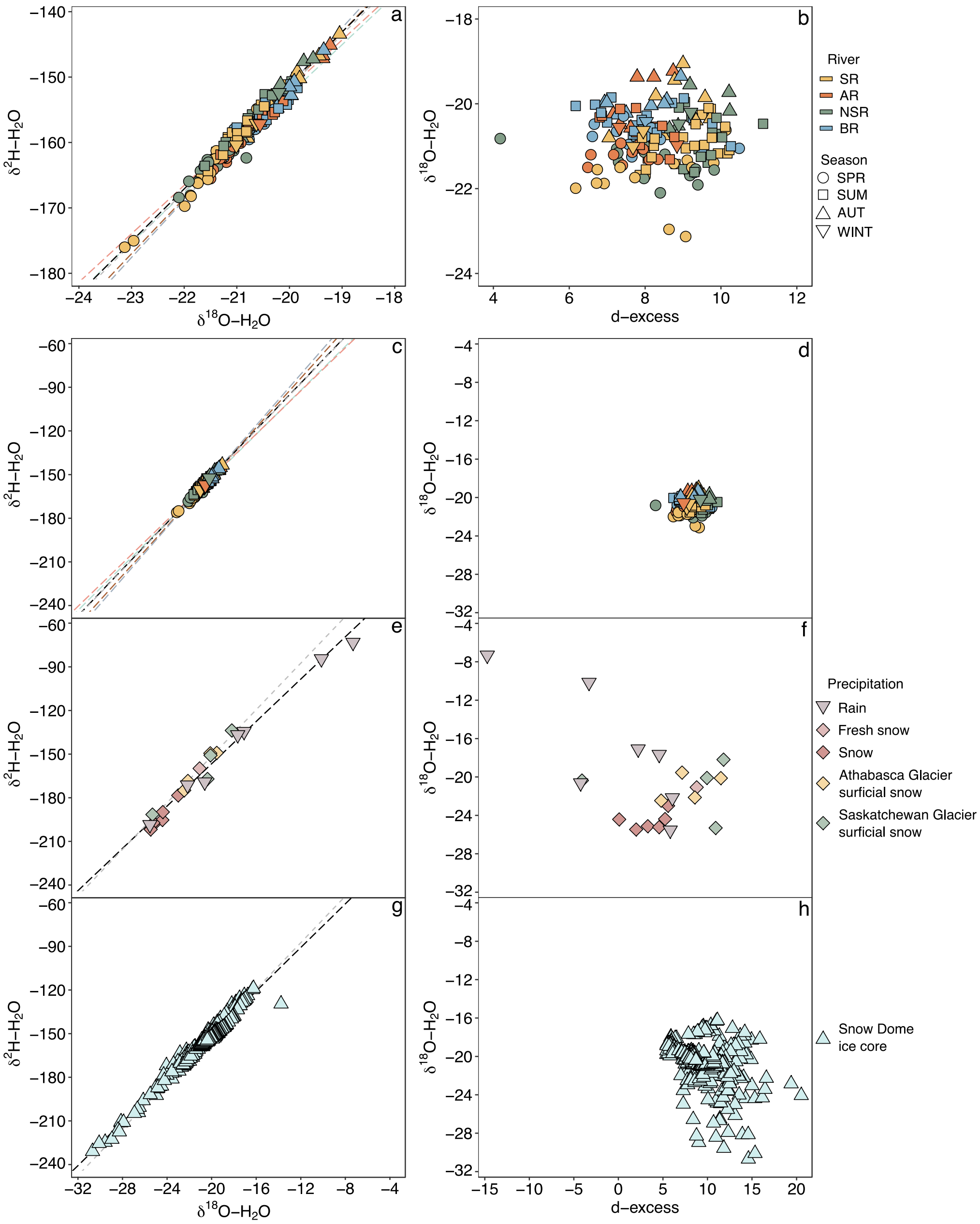

Figure 2.5. The $\delta^{18}O$ and δ^2H of water for river (a, c), precipitation (e), and the Mt. Snow Dome ice core (g) samples (left column), and d-excess and $\delta^{18}O$ of water for river (b, d), precipitation (f), and the Mt. Snow Dome ice core (h) samples (right column). Water source is color-coded and the grey dashed line is the Canadian Meteoric Water Line (CMWL), while the black long dashed line is the line of best fit for all the data on each graph. Seasons are abbreviated as SPR (spring; May 14 – June 25), SUM (summer; July 14 – September 3), AUT (autumn; October 9 – 14), and WINT (winter; December 20 – January 29). Season specific lines of best fit are colored by season as teal (SPR), pink (SUM), brown (AUT), and blue (WINT). Rivers are abbreviated as SR (Sunwapta River), AR (Athabasca River), NSR (North Saskatchewan River), and BR (Bow River).

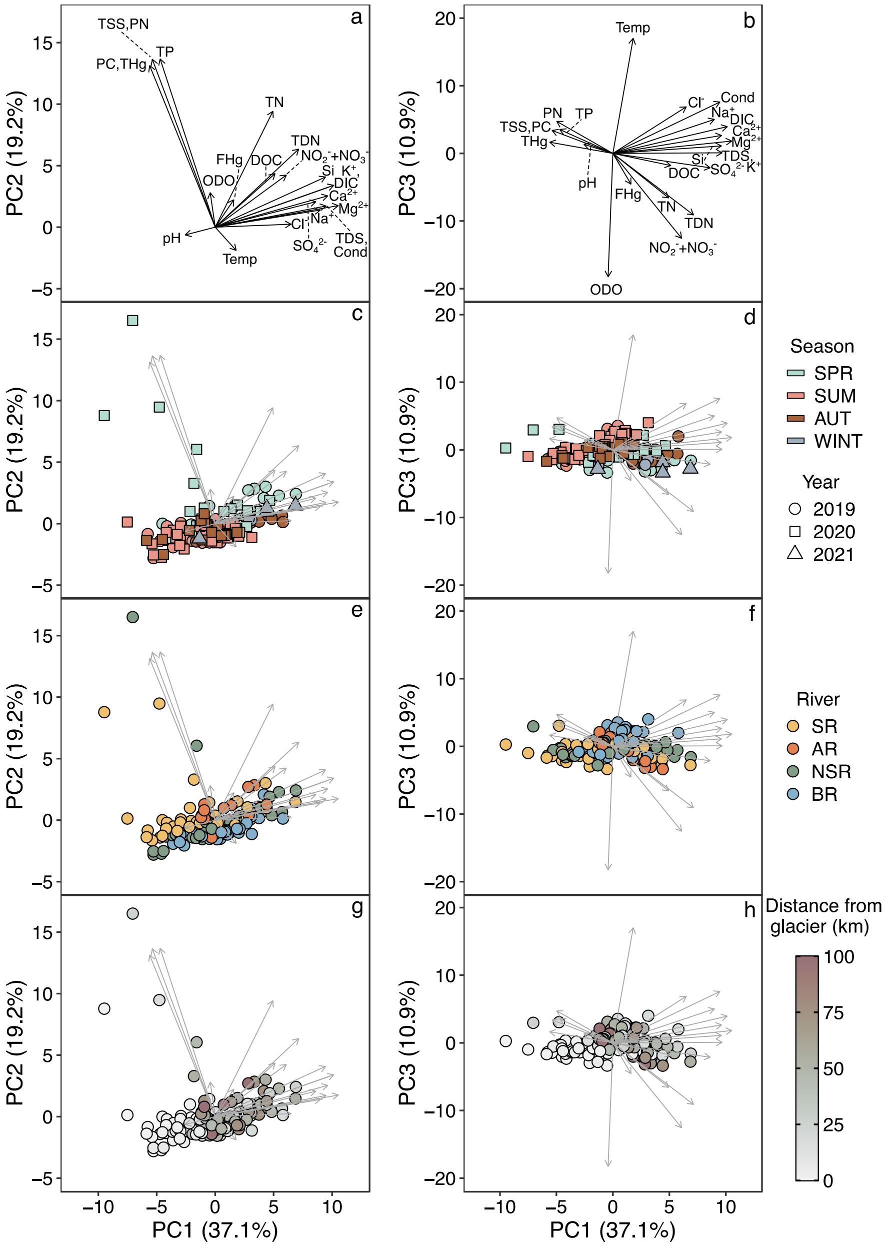

Figure 2.6. Principal Component Analyses (PCA) of the main physicochemical parameter measures quantified among all our river sampling sites and times. Shown are biplots of PC1 versus PC2 (left column) and PC1 versus PC3 (right column), with parameters and scaled vectors (a-b), and sampling sites color-coded spatiotemporally by season and year (c-d), river (e-f), and distance from glacier (km; g-h) for visual comparison. The first three PCs account for 67.1% of the variation in measures of the main physicochemical parameters. Seasons are abbreviated as SPR (spring; May 14 – June 25), SUM (summer; July 14 – September 3), AUT (autumn; October 9 – 14), and WINT (winter; December 20 – January 29). Rivers are abbreviated as SR (Sunwapta River), AR (Athabasca River), NSR (North Saskatchewan River), and BR (Bow River). For parameter abbreviations, please see *Section 2.3*.

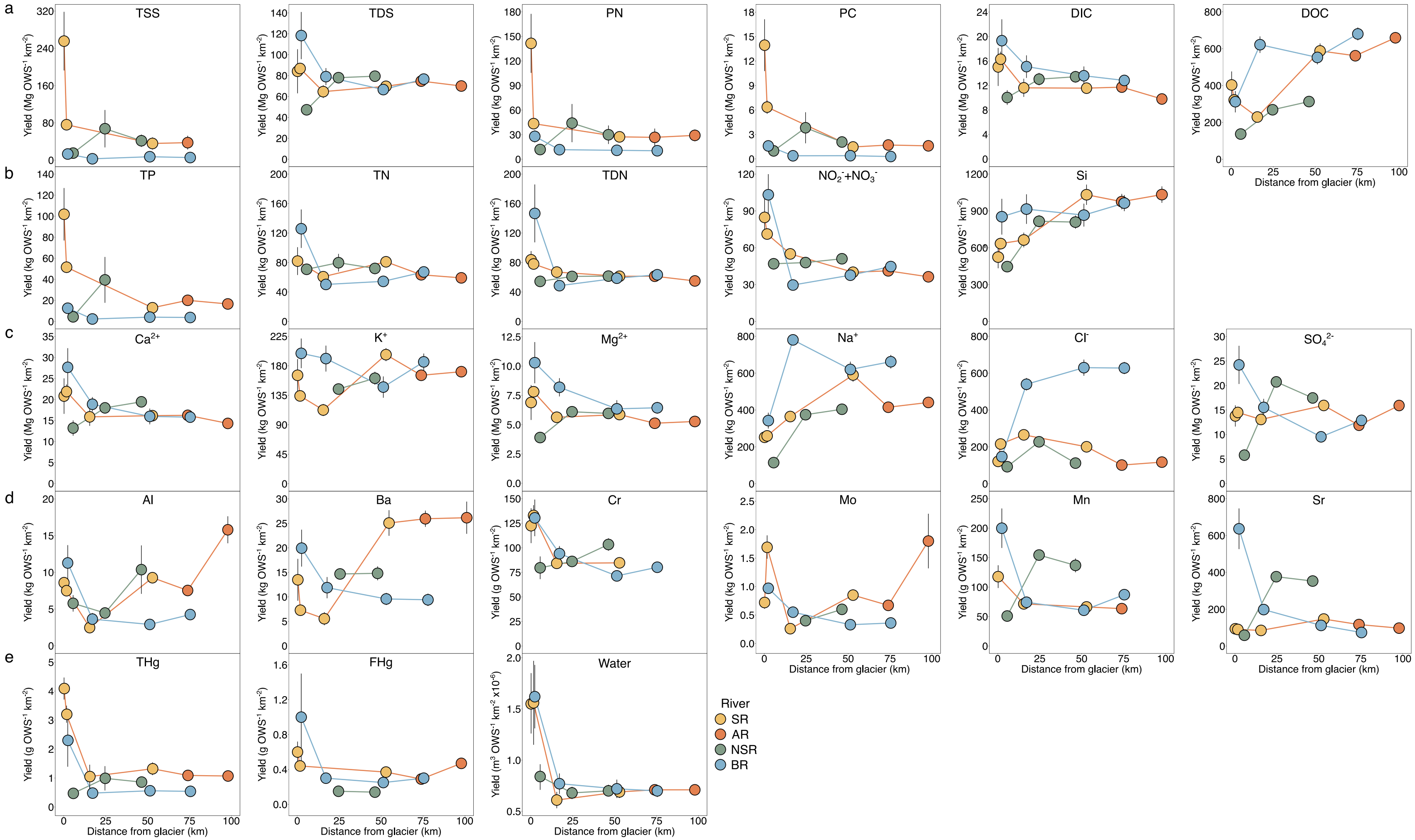

Figure 2.7. Mean 2019 and 2020 (±SD) open water season (OWS; May 1 to October 31) chemical yields for (a) basic chemical parameters, (b) nutrients, (c) ions, (d) trace elements, and (e) contaminants and water. Year-specific data is summarized in **Table A1.11**. Rivers are abbreviated as SR (Sunwapta River), AR (Athabasca River), NSR (North Saskatchewan River), and BR (Bow River). For parameter abbreviations, please see *Section 2.3*.

Chapter 3: Spatiotemporal patterns of geochemical weathering along rivers spanning glacierized to montane altitudinal life zones

1 Introduction

Geochemical weathering plays an important role in local (Kempe, 1988) to global (Isson et al., 2020) carbon cycling. However, the direction and magnitude of the effect on the carbon cycle depends on both the source of protons and the minerals they act upon (S.-L. Li et al., 2008; Viers et al., 2007). For instance, carbonate weathering by carbonic acid consumes one mole of CO_2 for every mole of carbonate mineral (Mackenzie & Garrels, 1966; Meybeck, 1993; Rubey, 1951; Urey, 1952). This is significant because carbonate is an easily weatherable mineral compared to many rock-forming silicates, and often dominates weathering reactions, even when carbonates are present in minor amounts (Blum et al., 1998). However, carbonate weathering is atmospheric CO_2 net neutral on geological timescales (Liu et al., 2011). Consequently, many studies focus on silicate weathering and sulfide oxidation-carbonate dissolution, which are net consumers and emitters of CO_2, respectively (Berner, 1992; Torres et al., 2017). Hence, site specific quantification of all forms of geochemical weathering is crucial to determining accurate regional CO_2 budgets (Khadka et al., 2014; St. Pierre et al., 2019) and our full understanding of the global carbon cycle (Donnini et al., 2016; Robison et al., 2023).

The magnitude of geochemical weathering is particularly pronounced in glacierized watersheds, in part due to the high exposure and discharge of weatherable materials associated with glacial melt (Anderson et al., 1997; Sharp et al., 1995). Geochemical weathering in glacierized watersheds are supported by heightened physical weathering of bedrock in subglacial environments (Anderson et al., 2000; Sharp et al., 1995; St. Pierre et al., 2019) that produce ultra-fine grained glacial flour with high surface area:volume ratios (Raiswell, 1984) and low weathering maturity (Deuerling et al., 2019). Once transport in meltwater discharge removes these sediments from the cold temperatures and restricted atmospheric exposure of subglacial environments (Tranter & Wadham, 2014), their potential for chemical weathering increases (Anderson et al., 2000). Yet, most research thus far on geochemical weathering in glacial systems has been conducted subglacially (Graly et al., 2014; X. Li et al., 2022; Tranter et al., 2002), in immediate proglacial environments (Hodson et al., 2000; Sharp et al., 1995; Urra et al., 2019), or over summer field campaigns when sampling sites were accessible (Deuerling et al., 2019; St. Pierre et al., 2019). Despite glaciers serving as a hotspot of chemical weathering globally, we still know little about how the type and magnitude of various geochemical weathering reactions change downriver, and how this effect may change seasonally or interannually.

The goals of this study were to quantify changing types and rates of geochemical weathering spatiotemporally along the Sunwapta (SR), Athabasca (AR), North Saskatchewan (NSR), and Bow (BR) proglacial rivers in Jasper and Banff National Parks along the eastern slopes of the Canadian Rocky Mountains. This mid-latitude alpine region is home to small warm-based glaciers with moderate discharge and sediment transport potentials. River transects (0.2 to 100 km) began in glacierized regions near the rivers' source glaciers, then moved downriver through alpine, subalpine, and montane altitudinal life zones, resulting in an underlying ecological complexity that shaped our study of geochemical weathering in this region. To overcome this complexity, multiple lines of evidence were used to assess the type and magnitude of geochemical weathering as one moved downriver. First, dissolved CO_2 and dissolved O_2 saturation and saturation indices, along with instantaneous CO_2 fluxes, were calculated to determine the extent to which weathering was occurring in our study rivers. Second, concentration-discharge (CQ) and molar ratio relationships were used to assess overall sources and types of geochemical weathering, while strontium isotopes were used to aid in determining lithological endmembers; sulfate isotopes were used to determine the presence of sulfide oxidation; and carbon isotopes were used to determine direct carbonate, silicate, and atmospheric contributions to the DIC pool. Finally, an inorganic-organic carbon mass balance model was used to estimate the proportions of riverine DIC that resulted from carbonate weathering, the atmosphere, respiration of organic matter (OM), and silicate weathering (Voss et al., 2023) in these ecologically complex river systems.

2 Methods

2.1 Sampling site descriptions and underlying geology

The headwater regions of the SR, AR, NSR, and BR span glacierized, alpine, subalpine, and montane altitudinal life zones within the montane cordillera ecozone (Demuth & Horne, 2017). We established seven sampling sites along the SR-AR continuum, three sampling sites along the

NSR, and four sampling sites along the BR (**Figure 3.1**). The relative percent of watershed area covered by major and minor land cover classes can be found in **Table A2.1** (see also Serbu et al., 2024). For more information about our sampling sites along these rivers, please see **Appendix 2**.

The watersheds of our study rivers are underlain by bedrock composed of calcite and dolomite, plagioclase and other feldspars, phyllosilicates, and quartz (Gadd, 2009; Pana & Elgr, 2013). The Columbia Icefield is underlain by multiple geological formations mostly comprised of Middle Cambrian limestone with some dolostone and shale (Pana & Elgr, 2013; Price, 2000). An example is the Pika Formation (Mountjoy, 1962), which underlies the Athabasca Glacier (Arendt et al., 2016). The SR is in contact with the Upper Cambrian Lynx Group consisting of limestone and dolostone beds with siltstone at upriver sites, and the Lower Cambrian Gog Formation of limestone and dolostone alternating with quartzite at downriver sites (Mountjoy, 1962; Pana & Elgr, 2013). Downriver of where the SR joins the AR, the Lower Cambrian Gog Group is replaced as bedrock by the Neo-Proterozoic Miette Group consisting of quartzite and argillite with conglomerates (Pana & Elgr, 2013; Price, 2000). The geology of the NSR watershed consists of various formations, ranging in age from the Devonian to Middle Cambrian (Pana & Elgr, 2013). Across the NSR watershed, limestone dominates with some dolostone, chert, argillite, and quartzites (Pana & Elgr, 2013). The Wapta Icefield is underlain by various formations of the Middle Cambrian and the Lower Cambrian Gog Group, all of which are comprised of primarily limestone, with some dolostone and quartzose sandstones (Mountjoy, 1962). Downriver, the BR is predominantly underlain by the Neo-Proterozoic Miette Group like the AR but is secondarily lined by various Middle Cambrian formations of limestone and dolomitic sandstones and the Lower Cambrian Gog Group (Pana & Elgr, 2013).

2.2 Sample collection and analyses

2.2.1 Collection of samples for analyses of basic chemistry and stable and radiogenic isotopes

Sampling sites were visited monthly in 2019 and 2020 during the open water season, beginning during snowmelt in late May/early June, through peak glacial melt in July/August, then during the receding flow period in September/October (**Figure A2.1**; Serbu et al. 2024). Due to safety concerns of sampling fast flowing rivers in remote areas, all sample collection was done near shorelines in the main flow of rivers. However, turbulence and mixing are high in this steep-slope region, and back-eddies, slumping shorelines, and areas where in-river sediment could be disturbed were strictly avoided, ensuring a representative sample. In braided river sections (i.e., SR3 and NSR2), the main channel was selected for sample collection. Additional samples were collected twice in winter (December 2019, January 2021) during base flow, but only at sites that were partially ice free and safe to sample when harnessed in.

At each river sampling site and time, we deployed a YSI Inc. EXO2 multiparameter sonde to obtain instantaneous measures of optical dissolved oxygen (ODO; % saturation and concentration), conductivity, turbidity, pH, and temperature. Atmospheric $CO_{2(g)}$ and dissolved in situ riverine $CO_{2(aq)}$ concentrations were directly measured with a Vaisala CARBOCAP® GM70 Hand-Held CO_2 Meter fitted with a 0 – 2000 ppm GMP222 CO_2 probe sealed in a tight Teflon sleeve. Water samples were collected for major cations (Ca^{2+}, K^+, Mg^{2+}, Na^+), anions (Cl^-, SO_4^{2-}), and trace elements; dissolved silica (Si); dissolved inorganic carbon (DIC), δ^{13}C-DIC, and Δ^{14}C-DIC; particulate inorganic carbon (PIC) and δ^{13}C-PIC; particulate and dissolved organic carbon (POC and DOC, respectively) and their isotopes (δ^{13}C-POC, Δ^{14}C-POC, δ^{13}C-DOC, Δ^{14}C-DOC) (Drapeau et al., 2023); sulfate isotopes ($\delta^{34}S-SO_4$, $\delta^{18}O-SO_4$), and radiogenic strontium ($^{87}Sr/^{86}Sr$). X-Ray Diffraction (XRD) was conducted on suspended river sediment collected at our sampling sites to determine which minerals were being eroded within the watershed and suspended in the river water during our sampling times (**Figure A2.2**). Measurements were conducted during the daytime when weathering and photosynthesis were theoretically at their peak, so $CO_{2(aq)}$ concentrations may be bias lower. Details on the collection and analysis of each parameter is outlined in **Appendix 2**.

3 Results & Discussion

We begin this section by providing a schematic (**Figure 3.2**) to ease the interpretation of the multiple lines of evidence for geochemical weathering presented and discussed below.

3.1 Determining weathering feasibility with CO_2 saturation, calcite saturation indices, and instantaneous CO_2 fluxes

Measurements revealed that $CO_{2(aq)}$ was highly undersaturated at some sampling sites along our study rivers, especially those nearest source glaciers. To determine if waters already undersaturated in $CO_{2(aq)}$ emerged from subglacial environments where there was little atmospheric exchange (Tranter & Wadham, 2014), we compared site and time specific saturation of dissolved O_2 with saturation of $CO_{2(aq)}$ (St. Pierre et al., 2019).

Mean ± SD O_2 percent saturation was 102 ± 3%, with the minimum value observed in autumn at SR1 (94%) and the maximum value observed in early spring at BR4 (112%). Saturation of O_2 never showed strong deviation from atmospheric equilibrium, and was thus similar across all sampling sites, rivers, and seasons (**Figure A2.3**). The relative stability of O_2 percent saturation around atmospheric equilibrium (100%) suggested that diffusive and turbulent exchange of O_2 between the atmosphere and rivers played a large and equalizing role in O_2 cycling, even at sampling sites closest to source glaciers where potential subglacial O_2 consumption by sulfide oxidation or microbial respiration would be strongest (Brown et al., 1994; Sharp et al., 1995; St. Pierre et al., 2019).

By comparison, $CO_{2(aq)}$ saturation showed overall more variability than O_2 saturation (**Figure A2.3**), hinting at multiple processes at work in CO_2 cycling. Mean ± SD $CO_{2(aq)}$ percent saturation was 106 ± 34%, with the minimum value recorded in spring at SR1 (16%) and the maximum value recorded in early spring at BR2 (222%). Regardless of season, SR1, the site closest to a source glacier, consistently had the lowest $CO_{2(aq)}$ percent saturation, whereas BR2, a wetland site (Serbu et al., 2024), consistently had the highest $CO_{2(aq)}$ percent saturation (**Figure A2.3**). The SR-AR and NSR exhibited similar patterns in $CO_{2(aq)}$ percent saturation with the upriver sites being the most undersaturated before increasing to, or above, saturation at their respective glacial outwash plain sites (i.e., SR3, NSR2) (**Figure A2.3**). This pattern diverged along the BR, as all sites were oversaturated in $CO_{2(aq)}$ at all sampling times (**Figure A2.3**). Notably, BR1 is immediately downriver of a waterfall, a discontinuity to river flow (Hall & Ulseth, 2020). The river-atmosphere equilibration at this discontinuity may have then masked any in situ gaseous signatures of weathering. Seasonal variability was also observed in $CO_{2(aq)}$ percent saturation (**Figure A2.3**). $CO_{2(aq)}$ percent saturation decreased from spring through summer before increasing in early autumn and staying at an elevated percent saturation until early spring (**Figure A2.3**; **Table A2.2**). Even with half the year represented by higher $CO_{2(aq)}$ percent saturations, undersaturation was captured at all times of year except winter (**Table A2.2**), when groundwater feeds the hydrologic system, even immediately downriver of glacial influence

(Hayashi, 2020; Paznekas & Hayashi, 2016). Seasonal trends in $CO_{2(aq)}$ percent undersaturation were especially prominent at SR1, SR2, and NSR1.

Following observations of $CO_{2(aq)}$ undersaturation along our river transects, we calculated saturation indices (SIs) of calcite, which assess the over- or under-saturation of Ca^{2+} and HCO_3^- ions in a given solution relative to equilibrium (Joint Task Group on Calcium Carbonate Saturation, 1990; Neal, 2002; Wojtowicz, 2001) (for details on calculations, please see **Appendix 2**). Carbonate and calcium-bearing silicate mineral dissolution that produces Ca^{2+} and HCO_3^- ions is more likely to occur in a state of calcite undersaturation. The SIs of calcite ranged from log -1.33 to log 0.66 across all sampling sites and times (**Figure A2.4**). Of the 146 calcite SIs calculated, only 14 (9.6%) were above zero (i.e., saturation equilibrium) (Wojtowicz, 2001). Calcite undersaturation is common in reactions controlled by kinetics, such as carbonate weathering in waters hydrologically influenced by glacial melt (Brown et al., 1996). In glacierized systems, high TSS concentrations are often correlated to high discharge (Q), whereby meltwaters flush the subglacial environment of finely comminuted glacial sediments (Anderson, 2007). At elevated Qs, abundant chemically reactive sediments can be weathered more quickly than saturation equilibrium can occur (Skidmore et al., 2004). Calcite undersaturation was observed multiple times at all sampling sites and across all seasons (**Figure A2.4**). The SIs of calcite varied across seasons at each site, with more undersaturated values occurring during summer (**Figure A2.4; Table A2.2**). The hydrology of our sampling sites was characteristic of mid-latitude glacierized systems, marked by Q peaks during the snowmelt freshet and in summer when glacial meltwater channels were developed enough for sustained glacial melt flow (**Figure A2.1**) (Comeau et al., 2009; Demuth & Pietroniro, 2003; Marshall & White, 2010). The elevated glacial meltwater flow in summer, and its associated increased in glacial flour discharge (Serbu et al., 2023), corresponded to the most calcite undersaturated conditions observed during the year. Additionally, though calcite undersaturation was recorded at every site, the most negative values were generally observed at sites closest to source glaciers, where TSS concentrations were greatest (Serbu et al. 2024).

Calcite oversaturation primarily occurred at the three downriver BR sites (i.e., BR2, BR3, BR4) and in autumn or winter (**Figure A2.4**; **Table A2.2**). The BR differed from the other study rivers in several ways that could have contributed to a state of calcite oversaturation. For instance, the

BR is the only river to initially flow through both a proglacial and large subalpine lake. Both proglacial Iceberg Lake and subalpine Bow Lake would have acted as sediment traps to the sediment-rich glacial meltwaters flowing from cirque Bow Glacier (Geilhausen et al., 2013).

Following the interpretation of $CO_{2(aq)}$ percent saturation and calcite SIs in our study system, we calculated instantaneous CO_2 fluxes, which provide a more accurate quantification of net CO_2 exchange across the air-water interface than $CO_{2(aq)}$ percent saturation. Instantaneous fluxes were calculated from our measured atmospheric and $CO_{2(aq)}$ concentrations, modeled energy dissipation rates (eD) and modeled gas exchange velocities (k_{600}) (Ulseth et al., 2019) after substantial efforts to measure k_{600} directly were unsuccessful (**Appendix 2**; **Figure A2.5**). Once eD and k_{600} were calculated (Ulseth et al., 2019), Schmidt scaling was applied to k_{600} to convert it to k_{CO2} (Wanninkhof, 2014), and instantaneous flux was determined (Bade, 2009, Hall & Ulseth, 2020, Robison et al., 2023).

Instantaneous fluxes ranged from -149 to 56 g CO_2 m^{-2} d^{-1} across the open water season (May 1 to October 31). Instantaneous fluxes were generally most negative at SR1 and NSR1, sites closest to source glaciers (**Figure 3.3**). Fluxes quickly leveled out at or near zero at sites immediately downriver, for example at SR2 (**Figure 3.3**). The SR2 site was the outflow of the Sunwapta proglacial lake, a known sediment trap (Wankiewicz, 1979); this rapid change in flux from negative at SR1 to positive at SR2 could indicate the potential loss of easily weatherable material that initially emerged from the Columbia Icefield subglacial environment (Mancini et al., 2023). By comparison, the Saskatchewan Glacier was the largest of the source glaciers in this study. Theoretically, with more glacier area in direct contact with underlying bedrock, more subglacial grinding and abrasion could occur, and more sediment-laden meltwaters could be expelled from the system. The NSR1 site was approximately 5.6 km downriver of its glacial tongue and after Saskatchewan proglacial lake (Serbu et al. 2024), yet we generally saw greater negative instantaneous CO_2 fluxes at this site than others in the study (**Figure 3.3**). None of the sites along the BR had negative instantaneous CO_2 fluxes, and similar to CO_2 saturation, several BR sites had the highest positive fluxes in this study (**Figure 3.3**). For example, the wetland site BR2 produced the highest instantaneous CO_2 fluxes in spring while BR1 had the highest in early autumn (**Figure 3.3**).

Instantaneous CO_2 fluxes also showed distinct seasonality. Fluxes from all sites were closest to net equilibrium in early spring and late autumn, and furthest from equilibrium during summer, with late spring and early autumn representing a transition between these two states. This seasonal effect was most prominent at SR1 and NSR1, where CO_2 influx increased in summer, but also at sites such as AR2, whose efflux increased in summer (**Figure 3.3**). Fluxes at AR2 remained close to neutral across all seasons except during summer 2020, where they increased to the highest positive instantaneous flux calculated in this study (**Figure 3.3**). Site AR2 is likely affected by in situ biological productivity because it is receiving more allochthonous terrestrial organic matter (Robison et al., 2023) than upriver sites along the SR-AR, leading to the observed net efflux of CO_2. The same trend, though muted compared to AR2, is observed at other downriver sampling sites such as SR3 and BR4 (**Figure 3.3**), indicating that the majority of our downriver sampling sites behave similarly to other mountain rivers, acting as net sources of CO_2 to the atmosphere (Horgby et al., 2019).

3.2 Evaluating major ion concentrations and molar ratios to assess sources and types of weathering

Ternary diagrams indicate that, in general, all our sampling sites contained similar ratios of dissolved cations and anions (**Figure 3.4**), and that calcium bicarbonate dominated the ion pool. This is indicative of similar lithologies across all sampling sites, which was supported in part by local lithologic maps (Pana & Elgr, 2013) and the general consistency across sites in our XRD results (**Figure A2.2**). Concentrations of these ions, in addition to DIC and Si, were further interpreted in relation to river Q at our sampling sites (**Figure A2.1**) using CQ diagrams.

Site-specific semi-log CQ diagrams help examine seasonal trends in dissolved ion concentrations, though it should be noted that there was not enough data per site to define seasonal hysteresis (**Figure A2.6**). Discharge in our study system was overall greater in 2020 than 2019 (**Figure A2.1**) with spring 2020 experiencing particularly high Q due to a multi-day torrential rain event (Serbu et al., 2024); accordingly, both spring and summer 2020 data skews right of their 2019 equivalents on the Q axis regardless of parameter, with the highest Qs most often from spring 2020 (**Figure A2.6**). Within each sampling site, the effects of solute dilution with increasing Q were also apparent (**Figure A2.6**), indicating lower dissolved concentrations during spring freshet and the summer meltwater season, and high concentrations during winter base flow (Comeau et al., 2009; Demuth & Pietroniro, 2003; Marshall & White, 2010). Ultimately, shoulder- and off-season sampling in autumn and winter allowed us to extend our CQ observations into the lowest Qs recorded at our sites, supporting the importance of year-round glacial river sampling (Sharp et al., 1995).

Log-log CQ diagrams show that Ca^{2+} and Mg^{2+} exhibited chemostasis (slope = 0, linear regression; $p > 0.05$) and comprised the greatest portion of the total ion pool regardless of Q (**Figure 3.5A**), indicating the presence of carbonate weathering along the entirety of the river transects (Winnick et al., 2017). Additionally, molar K^+/Na^+ values ranged widely in our system but included numerous values exceeding one-third, above which is a hallmark signature of glacial meltwaters (Anderson et al., 1997). There was a slight positive relationship between Cl^- concentration and Q ($p < 0.05$), but the same trend was not observed for SO_4^{2-} ($p > 0.05$), (**Figure 3.5B**). Notably, DIC concentrations were chemostatic across all Qs ($p > 0.05$) while Si concentrations had a strong positive relationship with Q ($p < 0.001$) (**Figure 3.5C**), suggesting that high Qs resulted in the access of new Si sources. Overall, the chemostatic behavior of Ca^{2+}, Mg^{2+}, and DIC concentrations suggests the maintenance of carbonate weathering across our sites, even as water inputs (Q) increased downriver, while the chemodynamic behaviour of Si concentrations suggests relative input with transit downriver.

To determine the relative contributions of H_2CO_3 and H_2SO_4 to geochemical weathering reactions in our study system, molar ratios of HCO_3^-/SO_4^{2-} were calculated (Deuerling et al., 2018; Tranter et al., 2002). Mean HCO_3^-/SO_4^{2-} was 7.9 ± 3.3, ranging from 2.1 to 18.6 and never falling below the 2:1 molar ratio indicative of H_2SO_4 contributions to weathering (**Figure 3.6A**) (Deuerling et al., 2018; Wadham et al., 2001). We therefore conclude that H_2CO_3 was the key proton donor to weathering reactions in our study systems.

With HCO_3^- as the dominant anion, we calculated $(Ca^{2+}+Mg^{2+})/HCO_3^-$ molar ratios to determine whether $Ca^{2+}+Mg^{2+}$ was in excess of that expected from H_2CO_3 driven carbonate weathering reactions alone (Deuerling et al., 2018). H_2CO_3 driven carbonate reactions produce half the $Ca^{2+}+Mg^{2+}$ than HCO_3^- so their molar $(Ca^{2+}+Mg^{2+})/HCO_3^-$ ratio should be near 0.5:1 (Deuerling et al., 2018). HCO_3^- and $Ca^{2+}+Mg^{2+}$ had a significant positive relationship ($R^2_{adj} = 0.85$, $p < 0.001$) and all data fell close to the 0.5:1 molar ratio line with a slope of 0.64 (**Figure 3.6B**). Generally, sites closest to source glaciers were close and parallel to the 0.5:1 molar line, but sites farther from glaciers on each river slightly diverged from it (**Figure 3.6B**), suggesting the presence of more Ca^{2+}+Mg^{2+} in the downriver river reaches than expected from carbonate weathering alone. The overall difference between expected (Ca^{2+}+Mg^{2+})/HCO_3^- molar ratios given pure carbonate weathering and observed (Ca^{2+}+Mg^{2+})/HCO_3^- molar ratios in our rivers was small. The excess Ca^{2+}+Mg^{2+} could be from weathering reactions involving H_2SO_4 or dissolution of localized sulfate and/or carbonate salts, both of which could add free cations to the rivers. Yet, downriver sites had the greatest Qs, and sulfide oxidation-carbonate dissolution becomes slightly less effective with increasing Q (Sharp et al., 1995). Additionally, **Figure 3.6A** implies that H_2SO_4 is not the major driver of weathering in our study region, further pointing to salts and/or non-salt evaporite dissolution as the most likely source of excess Ca^{2+}+Mg^{2+}.

Concluding that the primary weathering reactions in our study system were carbonate and/or silicate via H_2CO_3, we next used the non-sea salt (nss) $Ca^{2+}_{nss}/Na^{+}_{nss}$ and $Mg^{2+}_{nss}/Na^{+}_{nss}$ molar ratios to estimate the relative contribution of carbonate and silicate weathering to those dissolved ions in our rivers. $Ca^{2+}_{nss}/Na^{+}_{nss}$ molar ratios ranged from 8.2 to 678 and $Mg^{2+}_{nss}/Na^{+}_{nss}$ molar ratios ranged from 5.5 to 405, with values never deviating far from the line of best fit (**Figure A2.7**). Higher molar ratios are indicative of carbonate weathering as Na^{+}_{nss} is not produced with carbonate weathering (Millot et al., 2002), whereas values positioning along the line of best fit suggests a close adherence to a two endmember system. Generally, the most downriver sites along each river had relatively lower molar ratios, whereas sites closer to their source glacier had relatively higher molar ratios (**Figure A2.7A**), indicating that carbonate weathering dominated in glacier forefields, but silicate weathering increased with distance downriver.

As expected, the largest ranges of $Ca^{2+}_{nss}/Na^{+}_{nss}$ and $Mg^{2+}_{nss}/Na^{+}_{nss}$ molar ratios occurred in the spring and autumn shoulder seasons (**Figure A2.7B**). In spring, snowmelt drives the hydrology of glacial systems (**Figure A2.1**) (Marshall et al., 2011), and the resultant large volumes of water traversing watersheds through the upper portions of soil profiles can access new pools of solutes such as fresh glacial sediment (Deuerling et al., 2018; St. Pierre et al., 2019). The two highest $Ca^{2+}_{nss}/Na^{+}_{nss}$ and $Mg^{2+}_{nss}/Na^{+}_{nss}$ molar ratios were from spring 2020 when we sampled during torrential rains (Serbu et al., 2024). High discharge resulted in breached river channels, and along the NSR, flowed across glacial outwash plains, increasing the TSS concentrations, turbidity, and solute loads by possibly resuspending recently deposited glacial sediment (Serbu et al., 2024).

Thus, the two most extreme spring $Ca^{2+}_{nss}/Na^{+}_{nss}$ and $Mg^{2+}_{nss}/Na^{+}_{nss}$ molar ratios (**Figure A2.7B**) were removed from consideration for endmember compositions for the mass balance of DIC sources (Gaillardet et al., 1999). In autumn, Q was driven by a deceleration of glacier melt combined with new precipitation and baseflow inputs (**Figure A2.1**) (Marshall et al., 2011; Marshall & White, 2010). Dry summers may lead to evaporation and the isolation of residual water pockets that increased rock:water contact time. The pulse of water in autumn from fall rains could then allow for new solute release. Sediment erosion would then decrease considerably in winter as temperatures and Q drop (Viers et al., 2007).

3.3 Isotope compositions and evidence for weathering

To aid in defining the most appropriate carbonate and silicate endmembers in our system for a mass balance of DIC sources, $^{87}Sr/^{86}Sr$ values from each river aligning with the lowest and highest $Ca^{2+}_{nss}/Na^{+}_{nss}$ and $Mg^{2+}_{nss}/Na^{+}_{nss}$ molar ratios were quantified (n=8; **Figure A2.7**). However, we ultimately decided that $^{87}Sr/^{86}Sr$ ratios were not suitable to use as endmembers for the mass balance of DIC because our study region did not have lithological contrast like some regions (e.g., Muñoz et al., 2024). This resulted in $^{87}Sr/^{86}Sr$ values only ranging from 0.7099 to 0.7199 (**Figure A2.8**), with a mean of 0.7126, across all rivers. It is thought that the high physical weathering and sediment loads of glacier-fed systems generate $^{87}Sr/^{86}Sr$ that exceed non-glacial rivers (Anderson et al., 1997; Hindshaw et al., 2014; Vance et al., 2009). Yet, the mean $^{87}Sr/^{86}Sr$ in our rivers was similar to that of large rivers globally (0.7120) (Gaillardet et al., 1999; Millot et al., 2003). The exception was AR3, our most downriver sampling site, with an $^{87}Sr/^{86}Sr$ value of 0.7199 (**Figure A2.8**). Despite being within the Sr concentration range of the other sampling sites, AR3's $^{87}Sr/^{86}Sr$ exceeded all others (**Figure A2.8A**), possibly because sampling this downriver site captured weathered biotite from upriver sites. Biotite, like muscovite, is common at our sampling sites (**Figure A2.2**) and could have contributed more radiogenic Sr to AR3 (Anderson et al., 1997; Hindshaw et al., 2014). By comparison, our most upriver sampling site, SR1, fit within the majority of $^{87}Sr/^{86}Sr$ ratios, but was higher in 1/Sr (**Figure A2.8A**), Ca/Mg (**Figure A2.8B**) , and Ca/K values (**Figure A2.8C**). To aid in the interpretation of our data, matching data from Arendt et al. (2016) collected proximal to SR1 was included in **Figure A2.8**. Our SR1 data fell within the range of summer data presented in Arendt et al. (2016) (**Figure A2.8**).

The $\delta^{34}S-SO_4$ (VCDT) of our rivers ranged from 8 to 29 ‰, with a small yet distinct grouping of values between rivers. The most isotopically light values were from the SR, followed by the AR, BR, and NSR, which had the most isotopically heavy values overall (**Figure A2.9**, **Figure A2.10**). Across all sampling sites and times, $(Na^+-Cl^-)/Cl^-$ molar ratios were only once less than 0.1, the threshold for polluted rivers (Burke et al., 2018). We can therefore classify our rivers as relatively pristine. The closest $\delta^{34}S-SO_4$ value to the less-polluted global river mean of 4.8 ± 4.9‰ defined in Burke et al., 2018 was our most isotopically light value at 8 ‰ (**Figure A2.9**).

The $\delta^{34}S-SO_4$ values measured in this study were similar to global evaporites (10-30 ‰), with our mean value of 17 ‰ aligning with the global evaporite mean of 17 ‰ (Burke et al., 2018) (**Figure A2.9**). However, microbial sulfate reduction and lithogenic sulfides encompass a wide span of $\delta^{34}S-SO_4$ values (Burke et al., 2018; Kemeny et al., 2021; Relph et al., 2021). Therefore, contributions from pyrite oxidation cannot be excluded based on an evaluation of $\delta^{34}S-SO_4$ alone (Relph et al., 2021). To determine if the $\delta^{34}S-SO_4$ in this study were mainly derived from pyrite oxidation, the relationship between $\delta^{18}O-H_2O$ and $\delta^{18}O-SO_4$ was explored (Calmels et al., 2007). A strong linear relationship between $\delta^{18}O-H_2O$ and $\delta^{18}O-SO_4$ is indicative of integration of surface H_2O into sulfate formed by oxidation of pyrite (Calmels et al., 2007). We observe that $\delta^{18}O-SO_4$ increased independently of $\delta^{18}O-H_2O$ ($R^2_{adj}=0.0019$, $p > 0.05$) (**Figure A2.10**). The weak relationship does not support pyrite oxidation as a primary source of sulfate in our systems. Though pyrite is present along the NSR (Pana & Elgr, 2013), there was no evidence of sulfides in sampled minerology (**Figure A2.2**).

$\delta^{13}C$-PIC ranged from -3.18 to 0.55 ‰ with no discernable downriver trends (**Figure A2.11**). The small spread of $\delta^{13}C$-PIC (**Figure A2.11**) aligned with the isotope value of weathered carbonates, consistent with other alpine locales as documented by Aucour et al. (1999) on the Rhône River system. Matching $\delta^{13}C$-DIC had an overall larger range from -7.32 to -2.08 ‰ (**Figure A2.11**) and were isotopically heaviest at sites closest to their source glacier, suggesting relatively more carbonate contributions to the DIC pool at these sites (**Figure A2.11**, **Figure 3.7**) (Marwick et al., 2015). Downriver sites were generally isotopically lighter, indicating contributions from organic sources to the DIC pool (Marwick et al., 2015), or possibly through greater contributions from silicate weathering, which would have a DIC value reflective of a mixture of soil carbon and atmospheric CO_2 (**Figure 3.7**). An equal contribution of carbonates and C3 plants, which dominate vegetated landscapes of the Canadian Rocky Mountains, would have an approximate isotopic value of -10 ‰ (Aucour et al., 1999). Yet, even with the downriver isotopic shift, δ^{13}C-DIC values never fell below -8 ‰ along any river (**Figure A2.11**), suggesting an overall larger contribution of carbonate sources to the DIC pool at all sites. Additionally, although periphyton (benthic algae) in our study rivers (Bowman et al., 2005, 2007) may contribute to the downriver shift in δ^{13}C-DIC (**Figure 3.7**), as the isotope values of periphyton are difficult to constrain (Ishikawa et al., 2012) we do not discuss them in detail here.

Δ^{14}C-DIC spanned from -644 to -205 ‰, though samples were only collected from the first two sites on each river (except for an individual datapoint at AR1). Downriver sites typically also had Δ^{14}C-DIC indicative of more modern sources than sampling sites closer to their source glacier (**Figure 3.7**). SR1 had the lowest Δ^{14}C-DIC value, closest to Δ^{14}C-dead $CaCO_3$ sources than any other site (**Figure 3.7**). All other sites were clustered less negatively, and reflect a transition towards a mixture of atmospheric and terrestrial organic contributions to the DIC pool (**Figure 3.7**). **Figure 3.7** summarizes results discussed above that indicate that the isotopic value of inorganic carbon at upriver sites were driven primarily by inorganic carbon sources, and that downriver sites were also influenced by organic contributions.

3.4 Mass balance estimates of riverine DIC sources

We diverged from mass balance models traditionally used in glaciology (e.g., Deuerling et al., 2019; Hodson et al., 2000; St. Pierre et al., 2019) because they exclusively focused on inorganic biogeochemical constituents. Instead, we took an integrative approach using models that included both inorganic and organic constituents due to an assumed increase in both autochthonous and allochthonous organic matter inputs with increasing distance downriver from source glaciers (Anderson, 2007; Robison et al., 2023). We followed the inorganic-organic carbon mass balance model detailed by Voss et al., 2023, with one exception: in calculating the fraction of H_2SO_4 involved in weathering (f_S), the formula (($[SO_4^{2-}]/\Sigma[\text{ions}]$) x $\delta^{34}S\text{-}SO_4/10$) was used in place of the Fraser River basin-specific estimate of $f_S = 0.08$ (Voss et al., 2023). The fraction of H_2CO_3 driving weathering (f_C) remained $1\text{-}f_S$.

We acknowledge that in applying a mass balance model developed for downriver freshwater systems on the western side of the Canadian Cordillera (Fraser River), we potentially overestimate the role organics had in defining the biogeochemistry of our most upriver sites (i.e., SR1, SR2, NSR1, and BR1). However, we consider an overestimation of the influence of DOC in our study system as less egregious than overestimating the combined influence of carbonate and silicate weathering, which is the focus of this study. Consequently, calculated weathering outputs are likely underestimated. On the few occasions the model estimated percent values of DIC from various sources below 0% or slightly above 100%, those data were set to 0% and 100%, respectively, for ease of interpretation. As the inorganic-organic mass balance model described by Voss et al., 2023 used both ^{13}C and ^{14}C values of DIC and DOC, and ^{14}C samples were not collected at all sampling sites and times, only 86 of 155 samples were included in the mass balance results and discussion.

The relative percent of DIC derived from carbonate weathering and atmospheric $CO_{2(g)}$, OM, and silicate weathering varied with distance downriver (**Figure 3.8**). Sampling sites closest to their source glacier along each river transect had the highest percent of total DIC from carbonate weathering and the atmosphere, and the lowest percent of total DIC from OM (**Figure 3.8**). However, we believe that the mass balance model likely overestimated DOC contributions to DIC concentration and isotope values at the most upriver sampling sites (i.e., SR1, SR2, NSR1, BR1) where DOC concentrations and yields were lowest (Serbu et al., 2024). The mass balance model we used (Voss et al., 2023) likely provided a better fit to our system with increasing distance downriver and the corresponding transition from glacierized to montane altitudinal life zones. Intimately related to the downward transition of altitudinal life zones within our river catchments was an increase in temperatures, the development of landscape soils, and an increase in the potential allochthonous organic matter inputs into our rivers (Anderson, 2007; Robison et al., 2023). The sampling site with the highest percent of total DIC from OM was BR2 (**Figure 3.8**), which had the greatest relative percent wetland cover in its watershed of all sites (2.1 %). Otherwise, the percent total DIC that was derived from OM increased with distance downriver, as expected (**Figure 3.8**) (Robison et al., 2023).

Concurrently, carbonate and silicate weathering contributions to percent of total DIC at the most upriver sampling sites may be underestimated since some data was likely erroneously allocated to OM contributions within the mass balance model. The percent total carbonate and atmospheric contributions to DIC was large (>50 %) at all sampling sites, but greatest (>75 %) at sites closest to their source glacier (**Figure 3.8**). This was the case even at BR1 where $CO_{2(aq)}$ was near saturation, emphasizing the importance of river topography, such as waterfalls, in mixing and gas equilibration. The dominant carbonate and atmospheric contributions to DIC across all sites was supported by relatively constant Ca^{2+} concentrations regardless of the percent contributions of carbonate versus non-carbonate to DIC in the mass balance model (**Figure A2.6**). Sites closest to their source glacier had some of the highest TSS concentrations (Serbu et al., 2024), a consequence of subglacial grinding and sediment expulsion with meltwaters (Comiti et al., 2019). Finely ground sediments facilitate weathering reactions (Brown et al., 1996). Carbonates tend to dominate weathering outputs (Blum et al., 1998) regardless of the dominant geology in a region. By comparison, Si concentrations increased with distance downriver (Serbu et al., 2024). An increase in water temperature and terrestrially-sourced organic acids stimulate weathering of silicates in surrounding soils, which may account for the higher Si concentrations at downriver sites (Anderson, 2005). Further, amorphous Si bound to suspended sediments has been found in glacial regions (Pryer et al., 2020), and the release of bound Si during transport along our rivers could have also contributed to higher Si concentrations at downriver sites.

The results of our mass balance support our interpretation that some of the increasing Si concentrations with distance downriver was caused by greater contributions from silicate weathering (**Figure 3.8B**). The proportion of DIC from silicate weathering is positively correlated to distance downriver after the most upriver sites ($R^2_{adj} = 0.109$, $p < 0.001$) (**Figure 3.8B**). Na^+ concentrations and yields support this conclusion as they increased downriver from glacier sources (Serbu et al., 2024) in conjunction with an increase in modeled non-carbonate fractions (**Figure 3.8**). Although silicate weathering is depressed in cold environments due to the higher activation energy required to bring the geochemical reaction to completion (Anderson, 2005), it is expected to increase downriver of glacierized zones as temperatures increase and organic acids from more developed soils and their associated organic matter become available (Anderson et al., 2000; Jenckes et al., 2024; Tranter & Wadham, 2014). Our study confirms and illuminates such processes.

4 Conclusion

Multiple lines of evidence were investigated to determine the carbon balance and type and magnitude of geochemical weathering along ecologically complex river transects. Sites closest to source glaciers experienced the lowest $CO_{2(aq)}$ percent saturation and most negative calcite saturation indices and CO_2 fluxes. Temporal trends also showed that the most extreme values observed for each line of evidence occurred in the summer when glacier meltwater Q, and their associated TSS loads, were greatest. Combined, this suggests the potential presence of carbonate or silicate weathering contributing to CO_2 drawdown at immediate proglacial sites.

The CQ relationships documented that the chemostatic behavior of Ca^{2+}, Mg^{2+}, and DIC concentrations suggest the maintenance of carbonate weathering across our sites, even as water inputs increase downriver, while the chemodynamic behaviour of Si concentrations suggests relative increases in Si input with transit downriver. H_2CO_3 was determined to be the main acid driving weathering in our study system. $Ca^{2+}_{nss}/Na^{+}_{nss}$ and $Mg^{2+}_{nss}/Na^{+}_{nss}$ molar ratios ranged widely, particularly across seasons, but showed more contributions from carbonate weathering at sites closest to source glaciers and relatively more silicate weathering contributions at downriver sites. $^{87}Sr/^{86}Sr$ and elemental ratios were not used to define endmembers for carbonate and silicate weathering given their small range, but instead suggested the lithological consistency of our study region. $\delta^{34}S\text{-}SO_4$ values close to the global evaporite mean in these anthropogenically pristine rivers, coupled with a lack of relationship between $\delta^{18}O\text{-}H_2O$ and $\delta^{18}O\text{-}SO_4$, were used to reject pyrite oxidation as a large source of sulfate to any of our sites. Lastly, $\delta^{13}C$-DIC and $\Delta^{14}C$-DIC showed that sites closest to source glaciers were more influenced by older carbonate sources to DIC than sites downriver. Moving downriver from glacierized to montane altitudinal life zones, OM and silicate weathering become more influential compared to upriver sites. Yet, carbonate weathering and atmospheric $CO_{2(g)}$ remain the dominant sources of DIC in our rivers, with >50 % contribution even 100 km downriver of the source glaciers. Thus, as glaciers disappear as a result of climate change, we may expect a shift of the alpine and montane altitudinal life zones to higher altitudes, along with river DIC being more influenced by OM and silicate weathering. Further, given the ecological complexity of rapidly evolving proglacial landscapes, we recommend multiple lines of evidence for studying patterns in geochemical weathering.

References

Anderson, S. P. (2005). Glaciers show direct linkage between erosion rate and chemical weathering fluxes. *Geomorphology*, *67*(1–2), 147–157. https://doi.org/10.1016/j.geomorph.2004.07.010

Anderson, S. P. (2007). Biogeochemistry of glacial landscape systems. *Annual Review of Earth and Planetary Sciences*, *35*(1), 375–399. https://doi.org/10.1146/annurev.earth.35.031306.140033

Anderson, S. P., Drever, J. I., Frost, C. D., & Holden, P. (2000). Chemical weathering in the foreland of a retreating glacier. *Geochimica et Cosmochimica Acta*, *64*(7), 1173–1189. https://doi.org/10.1016/S0016-7037(99)00358-0

Anderson, S. P., Drever, J. I., & Humphrey, N. F. (1997). Chemical weathering in glacial environments. *Geology*, *25*(5), 399–402.

Arendt, C. A., Stevenson, E. I., & Aciego, S. M. (2016). Hydrologic controls on radiogenic Sr in meltwater from an alpine glacier system: Athabasca Glacier, Canada. *Applied Geochemistry*, *69*, 42–49. https://doi.org/10.1016/j.apgeochem.2016.04.002

Aucour, A.-M., Sheppard, S. M. F., Guyomar, O., & Wattelet, J. (1999). Use of 13C to trace origin and cycling of inorganic carbon in the Rhone river system. *Chemical Geology*, *159*, 87–105.

Bade, D. L. (2009). Gas Exchange at the Air–Water Interface. In *Encyclopedia of Inland Waters* (pp. 70–78). Elsevier. https://doi.org/10.1016/B978-012370626-3.00213-1

Berner, R. A. (1992). Weathering, plants, and the long-term carbon cycle. *Geochimica et Cosmochimica Acta*, *56*(8), 3225–3231. https://doi.org/10.1016/0016-7037(92)90300-8

Blum, J. D., Gazis, C. A., Jacobson, A. D., & Page Chamberlain, C. (1998). Carbonate versus silicate weathering in the Raikhot watershed within the High Himalayan Crystalline Series. *Geology*, *26*(5), 411. https://doi.org/10.1130/0091-7613(1998)026<0411:CVSWIT>2.3.CO;2

Bowman, M. F., Chambers, P. A., & Schindler, D. W. (2005). Epilithic algal abundance in relation to anthropogenic changes in phosphorus bioavailability and limitation in mountain rivers. *Canadian Journal of Fisheries and Aquatic Sciences*, *62*(1), 174–184. https://doi.org/10.1139/f04-244

Bowman, M. F., Chambers, P. A., & Schindler, D. W. (2007). Constraints on benthic algal response to nutrient addition in oligotrophic mountain rivers. *River Research and Applications*, *23*(8), 858–876. https://doi.org/10.1002/rra.1025

Brown, G. H., Tranter, M., & Sharp, M. J. (1996). Experimental investigations of the weathering of suspended sediment bu alpine glacial meltwater. *Hydrological Processes*, *10*(4), 579–597. https://doi.org/10.1002/(SICI)1099-1085(199604)10:4<579::AID-HYP393>3.0.CO;2-D

Brown, G. H., Tranter, M., Sharp, M. J., Davies, T. D., & Tsiouris, S. (1994). Dissolved oxygen variations in alpine glacial meltwaters. *Earth Surface Processes and Landforms*, *19*(3), 247–253. https://doi.org/10.1002/esp.3290190305

Burke, A., Present, T. M., Paris, G., Rae, E. C. M., Sandilands, B. H., Gaillardet, J., Peucker-Ehrenbrink, B., Fischer, W. W., McClelland, J. W., Spencer, R. G. M., Voss, B. M., & Adkins, J. F. (2018). Sulfur isotopes in rivers: Insights into global weathering budgets, pyrite oxidation, and the modern sulfur cycle. *Earth and Planetary Science Letters*, *496*, 168–177. https://doi.org/10.1016/j.epsl.2018.05.022

Calmels, D., Gaillardet, J., Brenot, A., & France-Lanord, C. (2007). Sustained sulfide oxidation by physical erosion processes in the Mackenzie River basin: Climatic perspectives. *Geology*, *35*(11), 1003. https://doi.org/10.1130/G24132A.1

Comeau, L. E. L., Pietroniro, A., & Demuth, M. N. (2009). Glacier contribution to the North and South Saskatchewan rivers. *Hydrological Processes*, *23*(18), 2640–2653. https://doi.org/10.1002/hyp.7409

Comiti, F., Mao, L., Penna, D., Dell'Agnese, A., Engel, M., Rathburn, S., & Cavalli, M. (2019). Glacier melt runoff controls bedload transport in Alpine catchments. *Earth and Planetary Science Letters*, *520*, 77–86. https://doi.org/10.1016/j.epsl.2019.05.031

Demuth, M. N., & Horne, G. (2017). *Decadal-centenary glacier mass changes and their variability, Jasper National Park of Canada, Alberta, including the Columbia Icefield region* (8229; p. 25). https://doi.org/10.4095/304236

Demuth, M. N., & Pietroniro, A. (2003). *Mountain eastern slopes and implications for water resource-related adaptation in the Canadian Prairies: Phase I, Headwaters of the North Saskatchewan* (P55; p. 96). Prairie Adaptation Research Collaborative.

Deuerling, K. M., Martin, J. B., Martin, E. E., Abermann, J., Myreng, S. M., Petersen, D., & Rennermalm, Å. K. (2019). Chemical weathering across the western foreland of the Greenland Ice Sheet. *Geochimica et Cosmochimica Acta*, *245*, 426–440. https://doi.org/10.1016/j.gca.2018.11.025

Deuerling, K. M., Martin, J. B., Martin, E. E., & Scribner, C. A. (2018). Hydrologic exchange and chemical weathering in a proglacial watershed near Kangerlussuaq, west Greenland. *Journal of Hydrology*, *556*, 220–232. https://doi.org/10.1016/j.jhydrol.2017.11.002

Donnini, M., Frondini, F., Probst, J.-L., Probst, A., Cardellini, C., Marchesini, I., & Guzzetti, F. (2016). Chemical weathering and consumption of atmospheric carbon dioxide in the Alpine region. *Global and Planetary Change*, *136*, 65–81. https://doi.org/10.1016/j.gloplacha.2015.10.017

Drapeau, H. F., Tank, S. E., Cavaco, M., Serbu, J. A., St.Louis, V., & Bhatia, M. P. (2023). Shifts in organic matter character and microbial community structure from glacial headwaters to downstream reaches in Canadian Rocky Mountain rivers. *Biogeosciences Discussions*, *in review*. https://doi.org/10.5194/bg-2023-121

Gadd, B. (2009). *Handbook of the Canadian Rockies*. Corex Press.

Gaillardet, J., Dupré, B., Louvat, P., & Allègre, C. J. (1999). Global silicate weathering and CO2 consumption rates deduced from the chemistry of large rivers. *Chemical Geology*, *159*(1–4), 3–30. https://doi.org/10.1016/S0009-2541(99)00031-5

Geilhausen, M., Morche, D., Otto, J.-C., & Schrott, L. (2013). Sediment discharge from the proglacial zone of a retreating Alpine glacier. *Zeitschrift Für Geomorphologie, Supplementary Issues*, *57*(2), 29–53. https://doi.org/10.1127/0372-8854/2012/S-00122

Graly, J. A., Humphrey, N. F., Landowski, C. M., & Harper, J. T. (2014). Chemical weathering under the Greenland Ice Sheet. *Geology*, *42*(6), 551–554. https://doi.org/10.1130/G35370.1

Hall, R. O., & Ulseth, A. J. (2020). Gas exchange in streams and rivers. *WIREs Water*, *7*(1), e1391. https://doi.org/10.1002/wat2.1391

Hayashi, M. (2020). Alpine hydrogeology: The critical role of groundwater in sourcing the headwaters of the world. *Groundwater*, *58*(4), 498–510. https://doi.org/10.1111/gwat.12965

Hindshaw, R. S., Rickli, J., Leuthold, J., Wadham, J., & Bourdon, B. (2014). Identifying weathering sources and processes in an outlet glacier of the Greenland Ice Sheet using Ca and Sr isotope ratios. *Geochimica et Cosmochimica Acta*, *145*, 50–71. https://doi.org/10.1016/j.gca.2014.09.016

Hodson, A., Tranter, M., & Vatne, G. (2000). Contemporary rates of chemical denudation and atmospheric CO2 sequestration in glacier basins: An Arctic perspective. *Earth Surface Processes and Landforms*, *25*, 1447–1471.

Horgby, Å., Canadell, M. B., Ulseth, A. J., Vennemann, T. W., & Battin, T. J. (2019). High-resolution spatial sampling identifies groundwater as driver of CO2 dynamics in an alpine stream network. *Journal of Geophysical Research: Biogeosciences*, *124*(7), 1961–1976. https://doi.org/10.1029/2019JG005047

Ishikawa, N. F., Doi, H., & Finlay, J. C. (2012). Global meta-analysis for controlling factors on carbon stable isotope ratios of lotic periphyton. *Oecologia*, *170*(2), 541–549. https://doi.org/10.1007/s00442-012-2308-x

Isson, T. T., Planavsky, N. J., Coogan, L. A., Stewart, E. M., Ague, J. J., Bolton, E. W., Zhang, S., McKenzie, N. R., & Kump, L. R. (2020). Evolution of the global carbon cycle and climate regulation on Earth. *Global Biogeochemical Cycles*, *34*(2), e2018GB006061. https://doi.org/10.1029/2018GB006061

Jenckes, J., Muñoz, S., Ibarra, D. E., Boutt, D. F., & Munk, L. A. (2024). Geochemical weathering variability in high latitude watersheds of the Gulf of Alaska. *Journal of Geophysical Research: Earth Surface*, *129*(3), e2023JF007284. https://doi.org/10.1029/2023JF007284

Joint Task Group on Calcium Carbonate Saturation. (1990). Suggested methods for calculating and interpreting calcium carbonate saturation indexes. *American Water Works Association*, *82*(7), 71–77.

Kemeny, P. C., Torres, M. A., Lamb, M. P., Webb, S. M., Dalleska, N., Cole, T., Hou, Y., Marske, J., Adkins, J. F., & Fischer, W. W. (2021). Organic sulfur fluxes and geomorphic control of sulfur isotope ratios in rivers. *Earth and Planetary Science Letters*, *562*, 116838. https://doi.org/10.1016/j.epsl.2021.116838

Kempe, S. (1988). Freshwater Carbon and the Weathering Cycle. In A. Lerman & M. Meybeck (Eds.), *Physical and Chemical Weathering in Geochemical Cycles* (pp. 197–223). Springer Netherlands. https://doi.org/10.1007/978-94-009-3071-1_10

Khadka, M. B., Martin, J. B., & Jin, J. (2014). Transport of dissolved carbon and CO2 degassing from a river system in a mixed silicate and carbonate catchment. *Journal of Hydrology*, *513*, 391–402. https://doi.org/10.1016/j.jhydrol.2014.03.070

Li, S.-L., Calmels, D., Han, G., Gaillardet, J., & Liu, C.-Q. (2008). Sulfuric acid as an agent of carbonate weathering constrained by δ13CDIC: Examples from Southwest China. *Earth and Planetary Science Letters*, *270*(3–4), 189–199. https://doi.org/10.1016/j.epsl.2008.02.039

Li, X., Wang, N., Ding, Y., Hawkings, J. R., Yde, J. C., Raiswell, R., Liu, J., Zhang, S., Kang, S., Wang, R., Liu, Q., Liu, S., Bol, R., You, X., & Li, G. (2022). Globally elevated chemical weathering rates beneath glaciers. *Nature Communications*, *13*(1), 407. https://doi.org/10.1038/s41467-022-28032-1

Liu, Z., Dreybrodt, W., & Liu, H. (2011). Atmospheric CO_2 sink: Silicate weathering or carbonate weathering? *Applied Geochemistry*, *26*, S292–S294. https://doi.org/10.1016/j.apgeochem.2011.03.085

Mackenzie, F. T., & Garrels, R. M. . (1966). Chemical mass balance between rivers and oceans. *American Journal of Science*, *264*, 507–525.

Mancini, D., Dietze, M., Müller, T., Jenkin, M., Miesen, F., Roncoroni, M., Nicholas, A. P., & Lane, S. N. (2023). Filtering of the signal of sediment export from a glacier by its proglacial forefield. *Geophysical Research Letters*, *50*(21), e2023GL106082. https://doi.org/10.1029/2023GL106082

Marshall, S. J., & White, E. (2010). *Alberta glacier inventory and ice volume estimation* (Issue December, pp. 1–55). Crowfoot Ice Research and Consulting.

Marshall, S. J., White, E. C., Demuth, M. N., Bolch, T., Wheate, R., Menounos, B., Beedle, M. J., & Shea, J. M. (2011). Glacier water resources on the eastern slopes of the Canadian Rocky Mountains. *Canadian Water Resources Journal*, *36*(2), 109–134. https://doi.org/10.4296/cwrj3602823

Marwick, T. R., Tamooh, F., Teodoru, C. R., Borges, A. V., Darchambeau, F., & Bouillon, S. (2015). The age of river-transported carbon: A global perspective. *Global Biogeochemical Cycles*, *29*(2), 122–137. https://doi.org/10.1002/2014GB004911

Meybeck, M. (1993). Riverine transport of atmospheric carbon: Sources, global typology and budget. *Water, Air, & Soil Pollution*, *70*(1–4), 443–463.

Millot, R., Gaillardet, J., Dupré, B., & Allègre, C. J. (2002). The global control of silicate weathering rates and the coupling with physical erosion: New insights from rivers of the Canadian Shield. *Earth and Planetary Science Letters*, *196*(1–2), 83–98. https://doi.org/10.1016/S0012-821X(01)00599-4

Millot, R., Gaillardet, J. érôme, Dupré, B., & Allègre, C. J. (2003). Northern latitude chemical weathering rates: Clues from the Mackenzie River Basin, Canada. *Geochimica et Cosmochimica Acta*, *67*(7), 1305–1329. https://doi.org/10.1016/S0016-7037(02)01207-3

Mountjoy, E. W. (1962). *Mount Robson (southeast) map-area, Rocky Mountains of Alberta and British Columbia, 83E/SE* [Map]. Geological Survey of Canada. https://doi.org/10.4095/101251

Muñoz, S., Jenckes, J., Ramos, E. J., Munk, L. A., & Ibarra, D. E. (2024). Hydrologic and landscape controls on rock weathering along a glacial gradient in South Central Alaska, USA. *Journal of Geophysical Research: Earth Surface*, *129*(3), e2023JF007255. https://doi.org/10.1029/2023JF007255

Neal, C. (2002). Calcite saturation in eastern UK rivers. *Science of The Total Environment*, *282–283*, 311–326. https://doi.org/10.1016/S0048-9697(01)00921-4

Pana, D. I., & Elgr, R. (2013). *Geology of the Alberta Rocky Mountains and Foothills (Map No. 560)* [Map]. Alberta Geological Survey.

Paznekas, A., & Hayashi, M. (2016). Groundwater contribution to winter streamflow in the Canadian Rockies. *Canadian Water Resources Journal / Revue Canadienne Des Ressources Hydriques*, *41*(4), 484–499. https://doi.org/10.1080/07011784.2015.1060870

Price, R. A. (2000). *The Southern Canadian Rockies: Evolution of a Foreland Thrust and Fold Belt (Field Trip Guidebook)*. Canadian Society of Petroleum Geologists. DOI: 10.13140/2.1.2910.2887

Pryer, H. V., Hawkings, J. R., Wadham, J. L., Robinson, L. F., Hendry, K. R., Hatton, J. E., Kellerman, A. M., Bertrand, S., Gill-Olivas, B., Marshall, M. G., Brooker, R. A., Daneri, G., & Häussermann, V. (2020). The influence of glacial cover on riverine silicon and iron exports in Chilean Patagonia. *Global Biogeochemical Cycles*, *34*(12), e2020GB006611. https://doi.org/10.1029/2020GB006611

Raiswell, R. (1984). Chemical models of solute acquisition in glacial melt waters. *Journal of Glaciology*, *30*(104), 49–57. https://doi.org/10.3189/S0022143000008480

Relph, K. E., Stevenson, E. I., Turchyn, A. V., Antler, G., Bickle, M. J., Baronas, J. J., Darby, S. E., Parsons, D. R., & Tipper, E. T. (2021). Partitioning riverine sulfate sources using oxygen and sulfur isotopes: Implications for carbon budgets of large rivers. *Earth and Planetary Science Letters*, *567*, 116957. https://doi.org/10.1016/j.epsl.2021.116957

Robison, A. L., Deluigi, N., Rolland, C., Manetti, N., & Battin, T. (2023). Glacier loss and vegetation expansion alter organic and inorganic carbon dynamics in high-mountain streams. *Biogeosciences*, *20*(12), 2301–2316. https://doi.org/10.5194/bg-20-2301-2023

Rubey, W. W. (1951). Geologic history of sea water: An attempt to state the problem. *Bulletin of the Geological Society of America*, *62*, 1111–1148.

Serbu, J. A., St. Louis, V. L., Emmerton, C. A., Tank, S. E., Criscitiello, A. S., Silins, U., Bhatia, M. P., Cavaco, M. A., Christenson, C., Cooke, C. A., Drapeau, H. F., Enns, S. J. A., Flett, J. E., Holland, K. M., Lavallee-Whiffen, J., Ma, M., Muir, C. E., Poesch, M., & Shin, J. (2023). *Physicochemical, particulate matter, temperature, and hydrological datasets collected from climate-threatened glacial river headwaters on the eastern slopes of the Canadian Rocky Mountains (2019-2021)*.

Serbu, J. A., St. Louis, V. L., Emmerton, C. A., Tank, S. E., Criscitiello, A. S., Silins, U., Bhatia, M. P., Cavaco, M. A., Christenson, C., Cooke, C. A., Drapeau, H. F., Enns, S. J. A., Flett, J. E., Holland, K. M., Lavallee-Whiffen, J., Ma, M., Muir, C. E., Poesch, M., & Shin, J. (2024). A comprehensive biogeochemical assessment of climate-threatened glacial river headwaters on the eastern slopes of the Canadian Rocky Mountains. *Journal of Geophysical Research: Biogeosciences*, *129*(1), e2023JG007745. https://doi.org/10.1029/2023JG007745

Sharp, M., Tranter, M., Brown, G. H., & Skidmore, M. (1995). Rates of chemical denudation and CO_2 drawdown in a glacier-covered alpine catchment. *Geology*, *23*(1), 61. https://doi.org/10.1130/0091-7613(1995)023<0061:ROCDAC>2.3.CO;2

Skidmore, M., Sharp, M., & Tranter, M. (2004). Kinetic isotopic fractionation during carbonate dissolution in laboratory experiments: Implications for detection of microbial CO2 signatures using δ13C-DIC. *Geochimica et Cosmochimica Acta*, *68*(21), 4309–4317. https://doi.org/10.1016/j.gca.2003.09.024

St. Pierre, K. A., St. Louis, V. L., Schiff, S. L., Lehnherr, I., Dainard, P. G., Gardner, A. S., Aukes, P. J. K., & Sharp, M. J. (2019). Proglacial freshwaters are significant and previously unrecognized sinks of atmospheric CO $_2$. *Proceedings of the National Academy of Sciences*, *116*(36), 17690–17695. https://doi.org/10.1073/pnas.1904241116

Torres, M. A., Moosdorf, N., Hartmann, J., Adkins, J. F., & West, A. J. (2017). Glacial weathering, sulfide oxidation, and global carbon cycle feedbacks. *Proceedings of the National Academy of Sciences*, *114*(33), 8716–8721. https://doi.org/10.1073/pnas.1702953114

Tranter, M., Sharp, M. J., Lamb, H. R., Brown, G. H., Hubbard, B. P., & Willis, I. C. (2002). Geochemical weathering at the bed of Haut Glacier d'Arolla, Switzerland—A new model. *Hydrological Processes*, *16*(5), 959–993. https://doi.org/10.1002/hyp.309

Tranter, M., & Wadham, J. L. (2014). Geochemical Weathering in Glacial and Proglacial Environments. In *Treatise on Geochemistry* (pp. 157–173). Elsevier. https://doi.org/10.1016/B978-0-08-095975-7.00505-2

Ulseth, A. J., Hall, R. O., Boix Canadell, M., Madinger, H. L., Niayifar, A., & Battin, T. J. (2019). Distinct air–water gas exchange regimes in low- and high-energy streams. *Nature Geoscience*, *12*(4), 259–263. https://doi.org/10.1038/s41561-019-0324-8

Urey, H. C. (1952). On the early chemical history of the Earth and the origin of life. *Proceedings of the National Academy of Sciences*, *38*(4), 351–363. https://doi.org/10.1073/pnas.38.4.351

Urra, A., Wadham, J., Hawkings, J. R., Telling, J., Hatton, J. E., Yde, J. C., Hasholt, B., Van As, D., Bhatia, M. P., & Nienow, P. (2019). Weathering dynamics under contrasting Greenland Ice Sheet catchments. *Frontiers in Earth Science*, *7*, 299. https://doi.org/10.3389/feart.2019.00299

Vance, D., Teagle, D. A. H., & Foster, G. L. (2009). Variable Quaternary chemical weathering fluxes and imbalances in marine geochemical budgets. *Nature*, *458*(7237), 493–496. https://doi.org/10.1038/nature07828

Viers, J., Oliva, P., Dandurand, J.-L., Dupré, B., & Gaillardet, J. (2007). Chemical Weathering Rates, CO_2 Consumption, and Control Parameters Deduced from the Chemical Composition of Rivers. In *Treatise on Geochemistry* (2nd ed.).

Voss, B. M., Eglinton, T. I., Peucker-Ehrenbrink, B., Galy, V., Lang, S. Q., McIntyre, C., Spencer, R. G. M., Bulygina, E., Wang, Z. A., & Guay, K. A. (2023). Isotopic evidence for sources of dissolved carbon and the role of organic matter respiration in the Fraser River basin, Canada. *Biogeochemistry*, *164*(1), 207–228. https://doi.org/10.1007/s10533-022-00945-5

Wadham, J. L., Cooper, R. J., Tranter, M., & Hodgkins, R. (2001). Enhancement of glacial solute fluxes in the proglacial zone of a polythermal glacier. *Journal of Glaciology*, *47*(158), 378–386. https://doi.org/10.3189/172756501781832188

Wankiewicz, P. M. (1979). *Sedimentation in Sunwapta Lake, Jasper National Park, Alberta* [MSc]. University of Alberta.

Wanninkhof, R. (2014). Relationship between wind speed and gas exchange over the ocean revisited. *Limnology and Oceanography: Methods*, *12*(6), 351–362. https://doi.org/10.4319/lom.2014.12.351

Winnick, M. J., Carroll, R. W. H., Williams, K. H., Maxwell, R. M., Dong, W., & Maher, K. (2017). Snowmelt controls on concentration-discharge relationships and the balance of oxidative and acid-base weathering fluxes in an alpine catchment, East River, Colorado. *Water Resources Research*, *53*(3), 2507–2523. https://doi.org/10.1002/2016WR019724

Wojtowicz, J. A. (2001). The thermodynamic basis of the saturation index. *Journal of the Swimming Pool and Spa Industry*, *3*(1), 35–36.

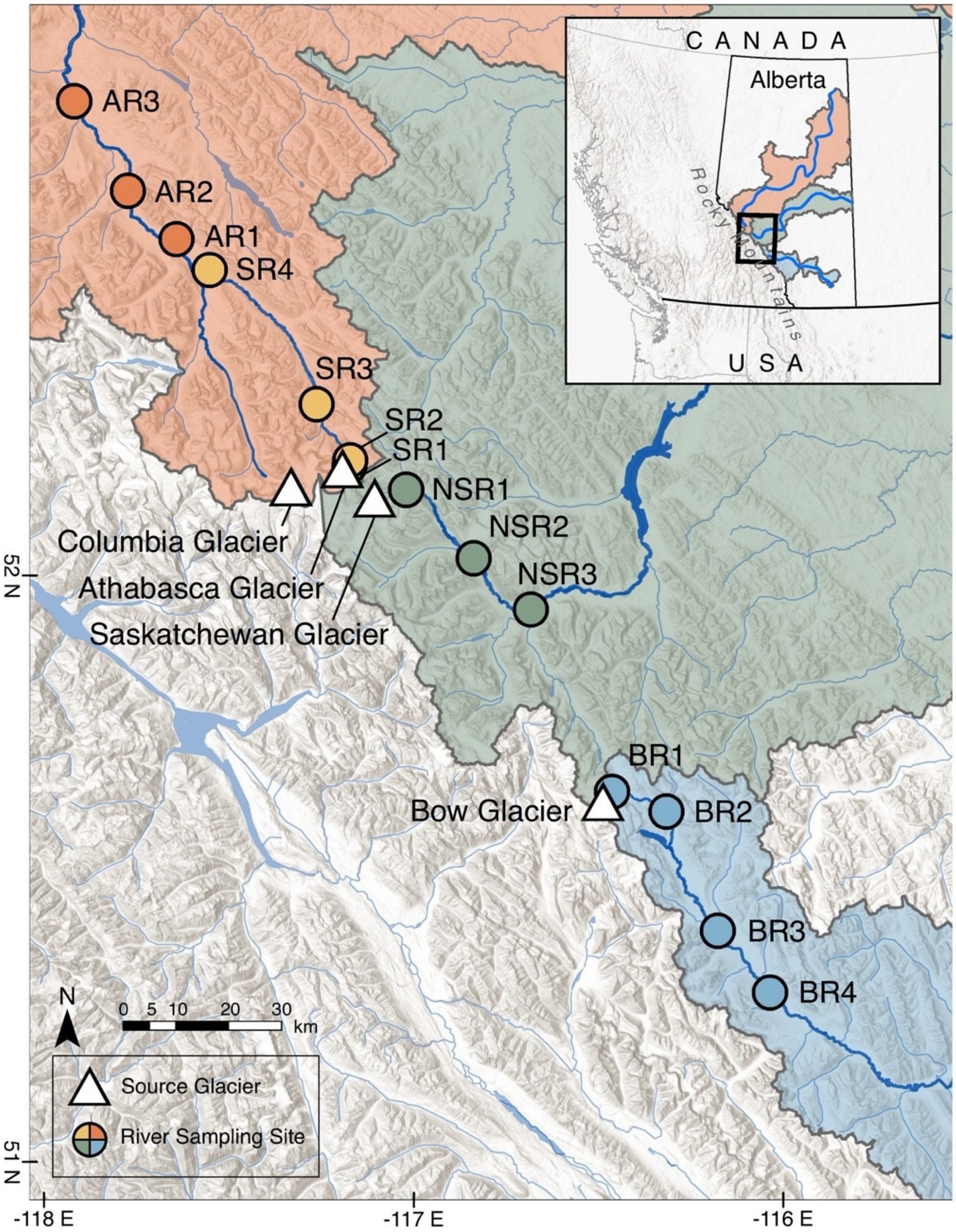

Figure 3.1. Map of source glaciers and our sampling sites on the Sunwapta (SR), Athabasca (AR), North Saskatchewan (NSR), and Bow (BR) rivers. Sampled watersheds are color-coded and match the watersheds depicted on the inset map of Alberta, Canada. All sampling was conducted in the headwaters of these major river systems in Jasper and Banff National Parks (Park boundaries not shown). Base map imagery from Esri, Government of Canada (Alberta Project NA1) 1983 Transverse Mercator. Modified from Serbu et al., 2024.

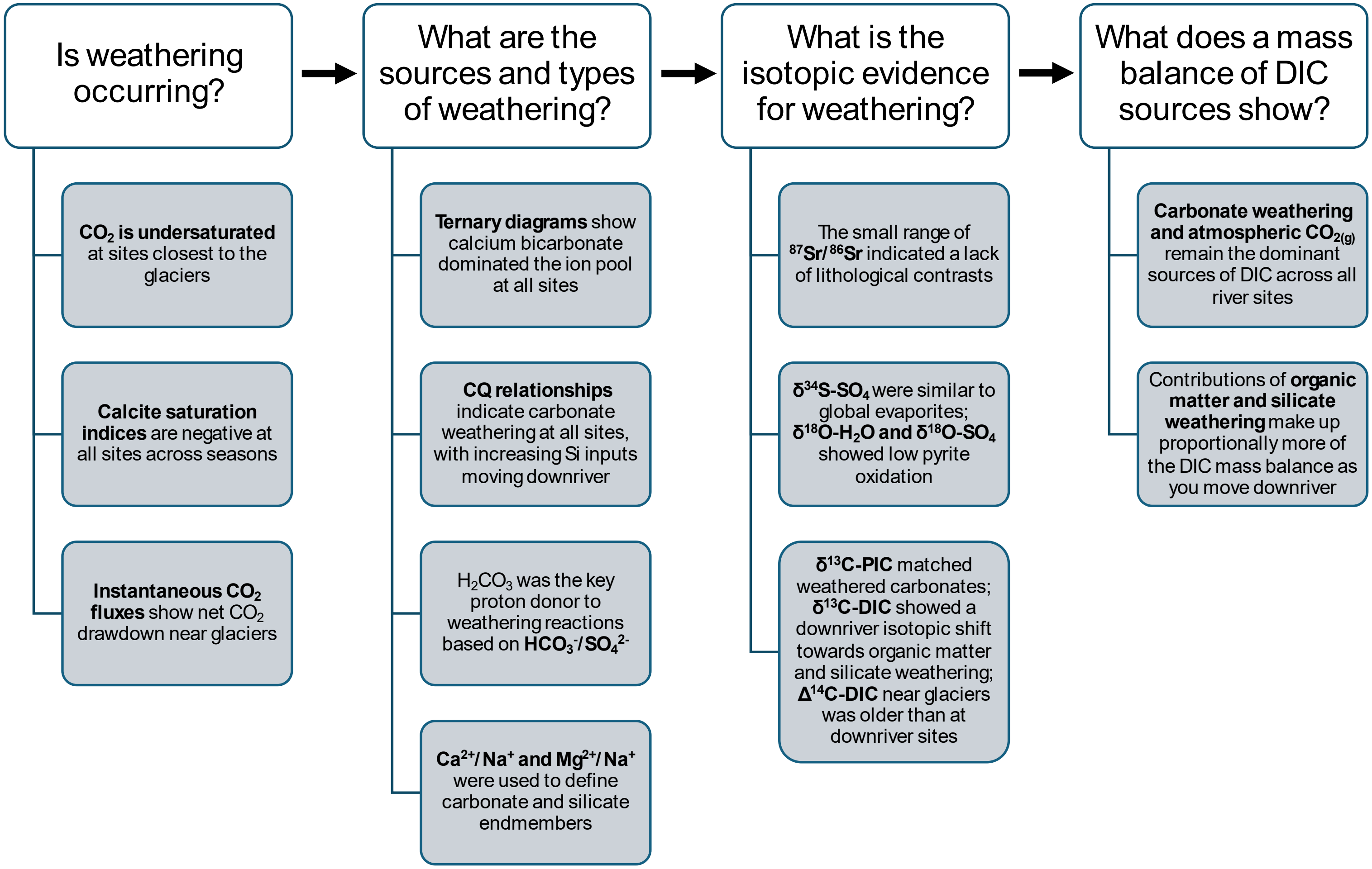

Figure 3.2. A conceptual model of our results and discussion, including the systematic questions and lines of evidence for weathering in our study rivers.

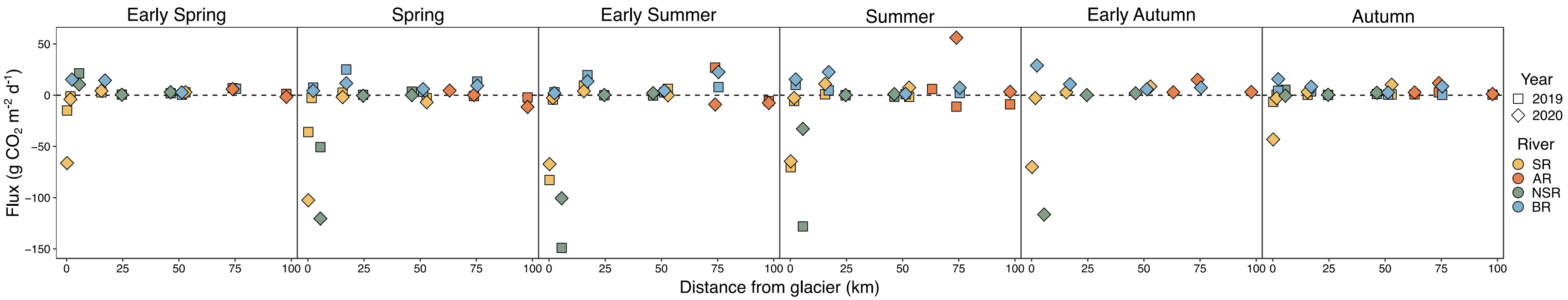

Figure 3.3. Modeled instantaneous CO$_2$ fluxes for riverine sampling sites at increasing downriver distance from source glaciers across the open water seasons in 2019 and 2020. Seasons are binned by sampling dates and are summarized in **Table A2.2**. Rivers are abbreviated as SR (Sunwapta River), AR (Athabasca River), NSR (North Saskatchewan River), and BR (Bow River).

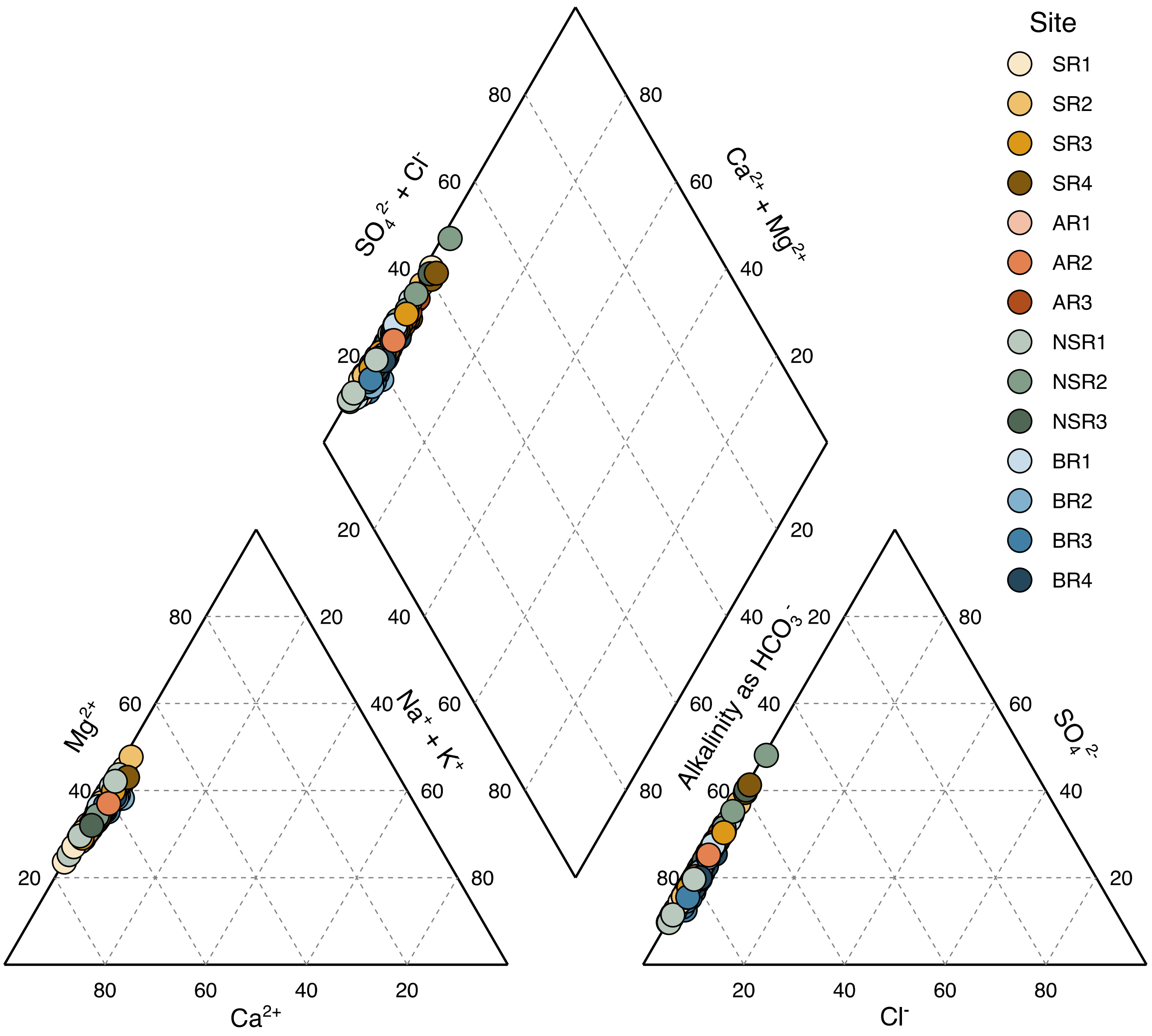

Figure 3.4. Ternary diagrams of all major cation and anion concentrations (in mEq L^{-1}) along our study rivers, color-coded by sampling site. Rivers are abbreviated as SR (Sunwapta River), AR (Athabasca River), NSR (North Saskatchewan River), and BR (Bow River).

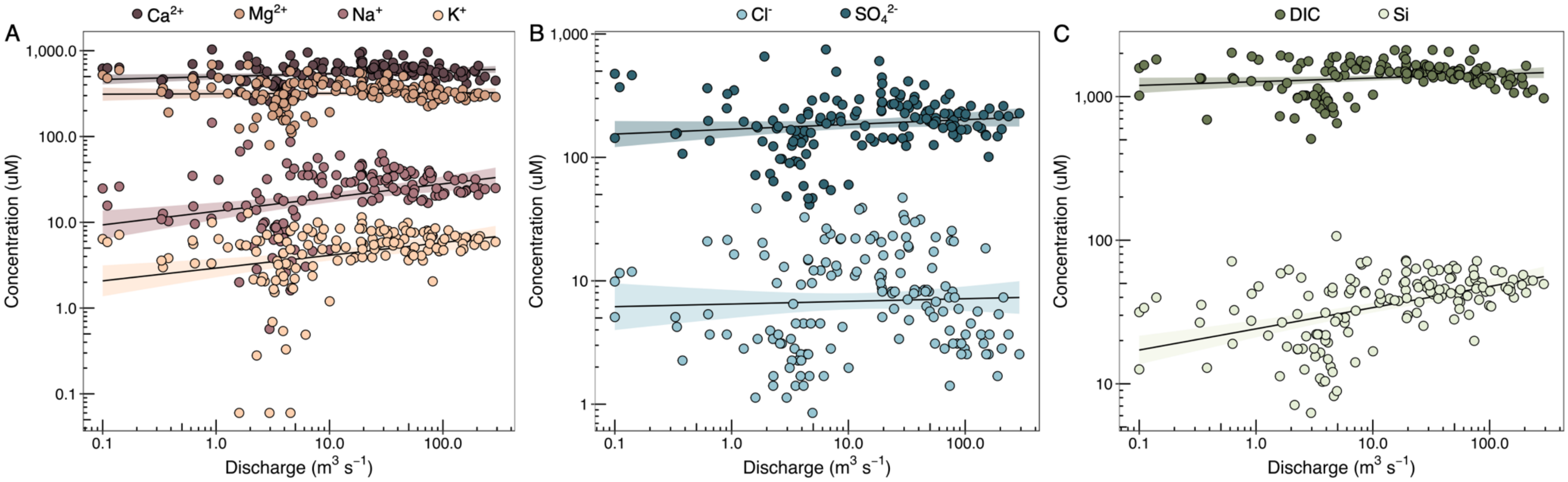

Figure 3.5. Log concentration-discharge (CQ) relationships for (a) cations (Ca^{2+}, Mg^{2+}, Na^{+}, K^{+}), (b) anions (Cl^{-}, SO_4^{2-}), and (c) DIC and Si. Also please note different y-axis scales. See **Table A2.4** for the numerical values of each regression.

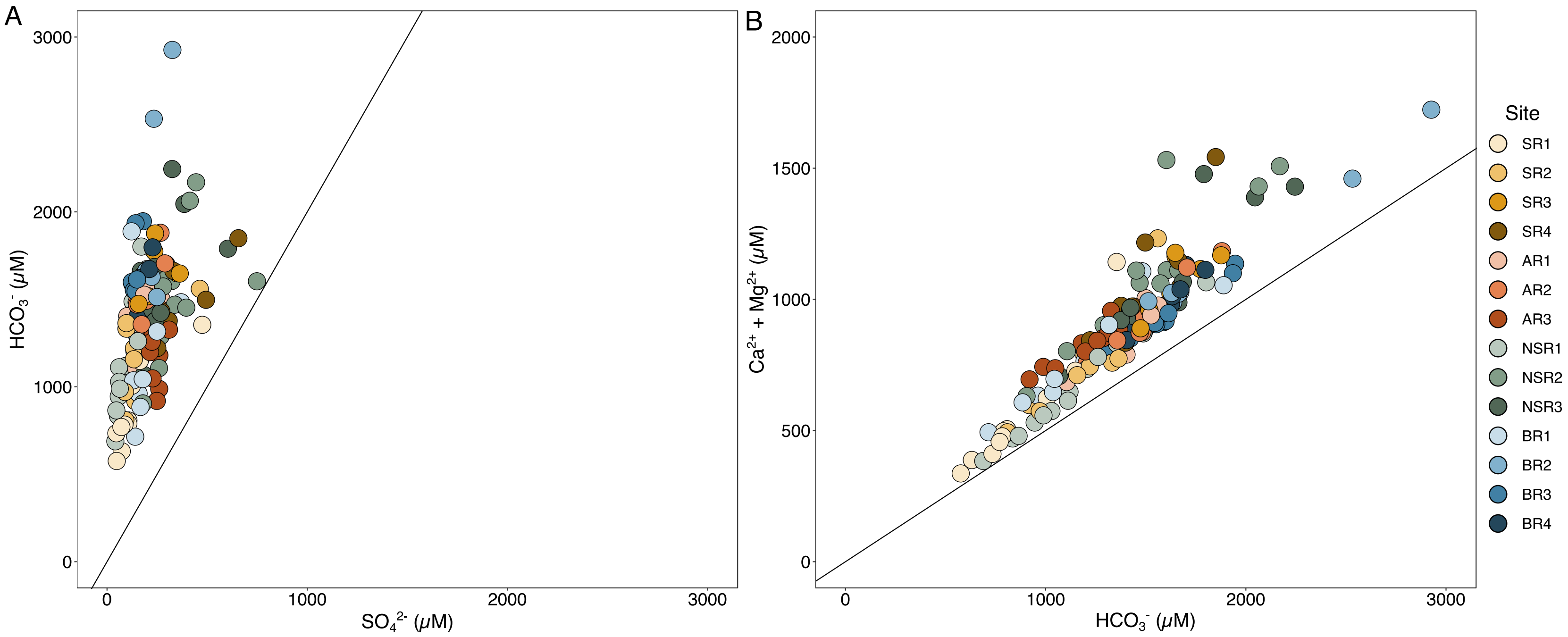

Figure 3.6. (A) Concentrations of SO_4^{2-} versus concentrations of HCO_3^- with a 2:1 line and (B) concentrations of HCO_3^- versus concentrations of Ca^{2+}+Mg^{2+} with a 0.5:1 line, color-coded by sampling sites for the Sunwapta (SR), Athabasca (AR), North Saskatchewan (NSR), and Bow (BR) rivers.

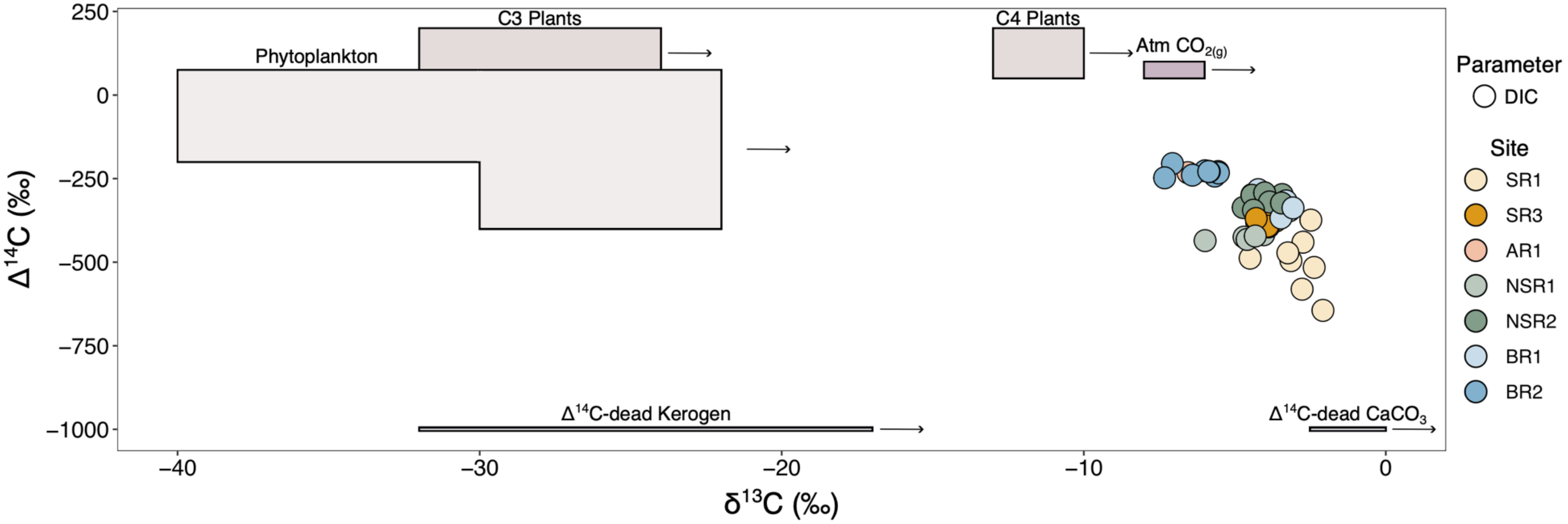

Figure 3.7. The $\delta^{13}C$ (‰) versus $\Delta^{14}C$ (‰) of dissolved inorganic carbon (DIC; circles) for sampling sites along the Sunwapta (SR), Athabasca (AR), North Saskatchewan (NSR), and Bow (BR) rivers. Arrows indicate a shift of $\delta^{13}C$ (‰) values due to natural fractionations associated with dissolution of carbon in aqueous solutions. Figure adapted from Voss et al. (2022) and Marwick et al. (2015) with global data from Marwick et al. (2015).

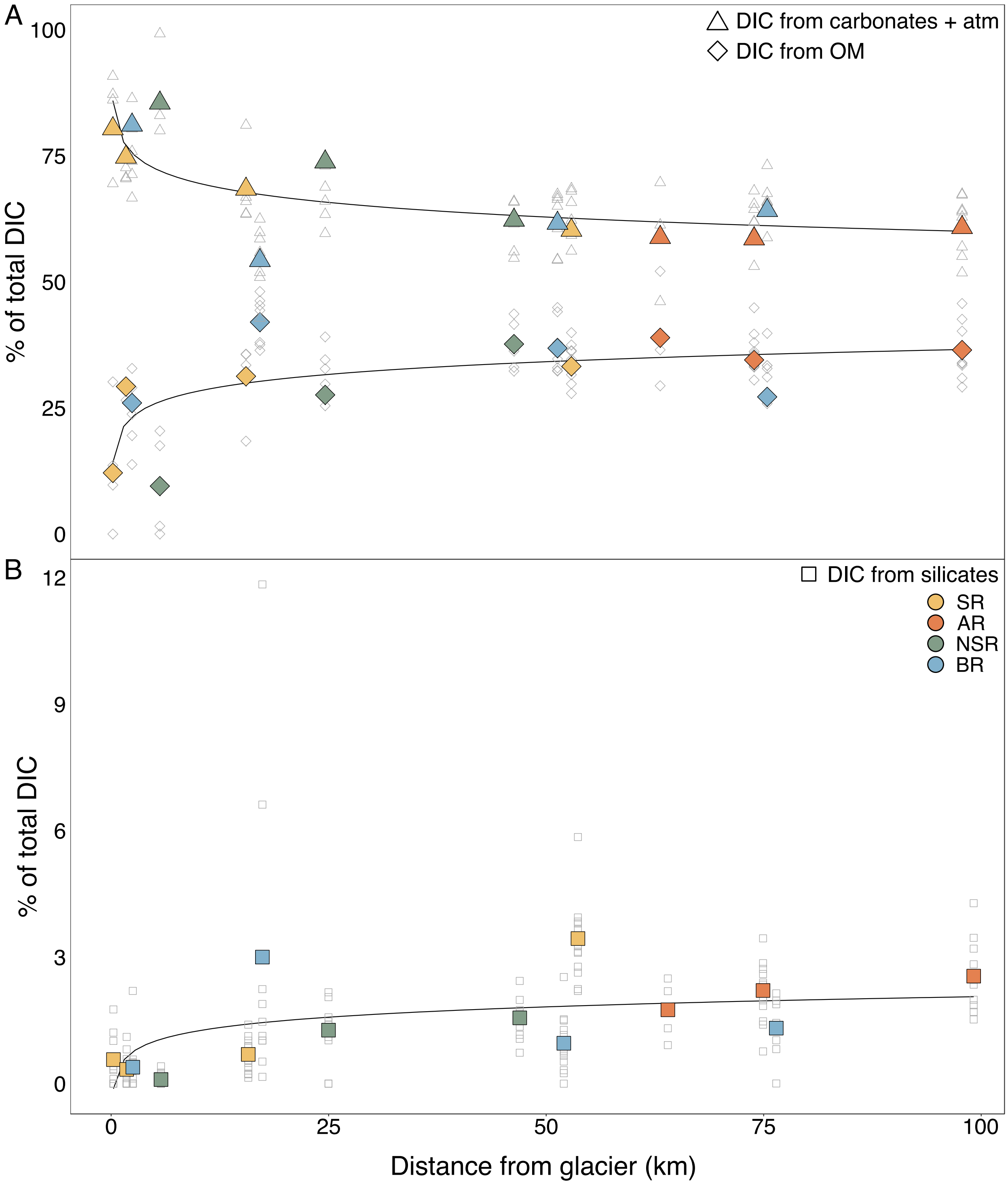

Figure 3.8. Percent of total dissolved inorganic carbon (DIC) derived from carbonates and the atmosphere, organic matter (OM), and silicate weathering with downriver distance from source glaciers (km) along the Sunwapta (SR), Athabasca (AR), North Saskatchewan (NSR), and Bow (BR) rivers. Colored symbols are means, while individual datapoints are seen outlined in grey.

Chapter 4: Removal of total and methyl mercury from North Saskatchewan River water during the production of municipal drinking water in Edmonton, Alberta, Canada

1 Introduction

Globally, access to clean drinking water is a basic human right. However, source freshwaters often contain numerous physical, chemical, and biological constituents that require treatment prior to water being safe for human consumption (P. Li & Wu, 2019). For example, sediments (Bortone, 2007), naturally occurring organic matter (Volk et al., 2005), contaminants such as toxic trace elements (Shah et al., 2023) or agriculturally derived pesticides (Syafrudin et al., 2021), and harmful microorganisms (Abkar et al., 2024) all require management and/or removal during the water treatment process to produce clean drinking water.

Mercury (Hg) is a ubiquitous freshwater contaminant of global concern. Human health Hg advisories generally focus on the consumption of predatory fish contaminated with the toxic and biomagnifiable methylated form of Hg (methylmercury; MeHg) since both inorganic Hg(II) and MeHg concentrations in water are typically not high enough to warrant consumption concerns. However, Hg in drinking water is still regulated to ensure overexposure does not occur (Thiem et al., 1976). For example, in Canada the maximum allowable Hg concentration in drinking water is 1 $\mu g\ L^{-1}$ (Health Canada, 1979, 2022). Limiting exposure may be especially important during periods of the year when, for example, water concentrations of both Hg(II) and MeHg may be high due to high runoff rates, or when accidental contamination of waterways with Hg has occurred (Thiem et al., 1976).

The EPCOR E.L. Smith Drinking Water Treatment Plant (DWTP) (**Figure A3.1**) in Edmonton, Alberta, Canada, produces municipal drinking water for over 1.4 million people (EPCOR, 2024), sourcing its water from the North Saskatchewan River (NSR), a newly designated Canadian Heritage River. In this study, we investigated at how efficiently the E.L. Smith DWTP removed total Hg (THg; all forms of Hg) and MeHg from NSR water and whether that efficiency changed depending on concentrations of Hg and other water quality properties (e.g., turbidity, color) in NSR water. As a potential measure of source watershed protection management, we also quantified how open water season (OWS; 1 May to 31 October) THg and MeHg concentrations, as well as THg yields, changed along sections of the NSR from its mountain source to where the E.L. Smith DWTP used it for drinking water production.

2 Methods

The NSR begins as a glacial melt river in Banff National Park on the eastern slopes of the Canadian Rocky Mountains (Anderson & Radić, 2020) before flowing through foothills, mixedwood, and parkland ecological subregions on its way to the large municipality of Edmonton (Government of Alberta, 2005). Upriver of Edmonton, the flow of the NSR is regulated by the Bighorn Dam (Nordegg, AB) on the NSR and the Brazeau Dam (Drayton Valley, AB) on Brazeau River, a high-output tributary of the NSR. Further, large swaths of land that line the NSR have been developed for agricultural purposes (Schindler & Donahue, 2006) (**Figure S1**).

2.1 Treatment of river water at the E.L. Smith DWTP

The process of drinking water production at the DWTP is schematized in **Figure 4.1**. Low lift pumps draw river water through intake screens from the deepest part of the NSR into the plant at low pressures but high volumes (260 – 360 million L d^{-1}). Aluminum sulphate ($Al_2(SO_4)_3 \cdot 14H_2O$; alum) and powdered activated carbon (PAC) are added in a mixing chamber downstream of the low lift pumps, while primary polymer is added further downstream near the clarifiers, using adjustable feed pumps and at doses proportional to river water conditions (e.g., turbidity and color). Alum is used mainly for removing bulk organics in river water during a coagulation process and works with primary polymer to remove turbidity and suspended solids via flocculation. PAC is used to enhance bulk organics removal when color is high during spring runoff and summer rainfall events, as well as remove organic precursors known to cause unwanted tastes and odors in finished water. Alum, primary polymer, and PAC complexes then settle out in clarifying chambers. Clear water is decanted from the surface of the clarifying chambers (Post-Clarification; PC) for further treatment, whereas sediments are drained back into the NSR downriver of the intakes after dechlorination. Sodium hypochlorite (0.8 % $NaClO$) is added post clarification for disinfection purposes, along with further amounts of alum and filter polymer. The water is then gravity filtered through layers of anthracite coal (~26 cm) and sand (~50 cm) (Post-Filtration; PF). Filters are regularly backwashed into the NSR after dechlorination. Post-filtration water passes through ultraviolet radiation (UV) channels for disinfection (Post-UV; PUV). Ammonia is then added, which combines with further NaClO additions, to form the long-lasting disinfectant monochloramine (NH_2Cl). Caustic soda is also added at this treatment stage to increase water pH to levels (7.8 ± 0.1) that minimizes corrosion in water distribution systems. Fluoride (F^-) is then added to the water prior to it being stored in on-site reservoirs until required by customers (EPCOR, 2024).

2.2 Sample collection

This study builds on a pilot study completed by Dr. Jennifer A. Graydon in 2003-2004 (**Table A3.1).** Water is regularly sampled in the E.L. Smith DWTP Operator's Laboratory for analyses of various chemical water quality parameters (EPCOR, 2024). A sampling portal was established where water is continually pumped from the main water line following each major treatment stage to constantly flowing taps in the laboratory. Samples (n = 348) were collected from the river (Raw), PC, PF, PUV and Reservoir taps for analyses of both THg and MeHg over a one year period (April 2020 to March 2021) (**Figure 4.2A**). Using the clean-hands, dirty-hands sampling protocol (U.S. EPA, 1996), samples were collected into new double Ziploc® bagged 125 ml (THg) and 250 ml (MeHg) pre-cleaned quality-certified Environmental Sampling Supply amber bottles with Teflon-lined lids that were rinsed three times with water from the relevant sample tap. We also collected additional Raw samples for analyses of dissolved THg and MeHg concentrations. These samples (FRaw) were filtered through acid-washed and milli-Q® water triple-rinsed 0.45-µm cellulose nitrate Nalgene™ Rapid-Flow Filter towers. The filtrate was then poured into new bottles. All samples were acidified with concentrated trace metal grade HCl equal to 0.2% (THg) or 0.4% (MeHg) of the sample volume. All sample processing was performed at the Canadian Association of Laboratory Accreditation (CALA)-certified Biogeochemical Analytical Service Laboratory (BASL; University of Alberta, Edmonton, AB) within a few hours of collection. Samples were then stored refrigerated in the dark at 4ºC until analyses, typically within two months.

2.3 Analysis of THg and MeHg

Samples were analysed for THg and MeHg in the BASL, following EPA methods 1631.E (U.S. EPA, 2002) and 1630 (U.S. EPA, 1998), respectively. Briefly, THg samples were brominated in their sample bottles using bromine monochloride (0.5% BrCl) ~24 hours prior to analysis, then neutralized just prior to analyses with hydroxylamine hydrochloride ($NH_2OH*HCl$). Stannous chloride ($SnCl_2$) was then added to samples to reduce oxidized Hg(II) to Hg(0) before analysis on an automated Tekran® 2600 Mercury Analyzer via cold vapor atomic fluorescence spectrometry (CVAFS). For MeHg analysis, ammonium 1-pyrrolidinecarbodithioate (APDC) and hydrochloric acid (HCl) were added to water samples for the elimination of interfering matrices, followed by the addition of 0.095 ng $Me^{201}Hg$ internal standard. Samples were then distilled using a Tekran® 2750 Methyl Mercury Distillation Unit. After distillation, ascorbic acid was added, then acetate buffer was used to adjust the pH to 4.9. Sodium tetraethyl borate (NaTEB) was added for ethylation and samples were analyzed on an automated Tekran® 2700 Methyl Mercury Analyzer coupled to an Agilent 7900 Inductively Coupled Plasma – Mass Spectrometer (ICP-MS). Concentrations were adjusted using $Me^{201}Hg$ isotope dilution corrections.

For both THg and MeHg analyses, quality control (QC) included method blanks, QC samples and duplicate samples. Method blanks were accepted if their concentrations did not exceed the reportable detection limit (RDL). QC samples were a secondary reference material used to monitor accuracy and instrument drift and were within a 100 ± 15% recovery range. Laboratory duplicate concentrations were also within a 100 ± 15% recovery range, while matrix spikes were used to monitor potential sample interference and were within a 100 ± 20% recovery range. Each QC was performed once per 25 samples. The RDL for THg and FTHg were 0.06 and 0.08 ng L^{-1}, respectively, and the RDL for MeHg and FMeHg were both 0.001 ng L^{-1}.

Block ANOVAs were used to compare Hg concentrations in river and water treatment process stages, accounting for the autocorrelation associated with date of sampling (**Table A3.2 & A3.3**). Tukey multiple comparisons of means were used to determine which pairs were significantly different. All statistics were performed in base R (R Core Team, 2022). Visualization of data was done using *ggplot2* (Wickham, 2016) and *ggbreak* (Xu et al., 2021).

2.4 Analysis of turbidity, color, and pH

Turbidity, color, and pH were analyzed following protocols outlined in the Standard Methods for the Examination of Water and Wastewater (24th ed.) (American Public Health Association et al., 2023a) under controlled conditions in the E.L. Smith DWTP Operator's Laboratory. Turbidity was analyzed by nephelometry via standard method 2130B (American Public Health Association et al., 2023b); color was analyzed by spectroscopy via standard method 2120C (American Public Health Association et al., 2023c); and pH was analyzed by potentiometry via standard method 4500H (American Public Health Association et al., 2023d).

2.5 Comparison of THg and MeHg concentrations and THg yields along the NSR

We compared 2020 OWS THg and MeHg concentrations and THg yields (g km^{-2}) along stretches of the NSR from its glacial headwaters in Banff National Park downriver to Edmonton to help understand the value in watershed management in protecting source water for the E.L. Smith DWTP. MeHg yields could not be similarly calculated because concentrations at the glacial headwater sites were consistently below the analytical RDL.

Concentrations and yields for three NSR headwater sampling sites (NSR1, NSR2, NSR3; **Figure A3.1**) were previously published by Serbu et al. (2024).

THg and MeHg samples from two additional sites from along the NSR (NSR4, NSR5; **Figure A3.1**) were collected in 2020 by water monitoring technologists from Alberta Environment and Protected Areas (AEPA) using the clean-hands, dirty-hands sampling method at a 30 cm subsurface river depth. All other sampling details and analysis were identical to those described above for the E.L. Smith DWTP sampling. AEPA data were subsequently recorded in an open access Water Quality Data Portal (Government of Alberta, 2024a). River discharge values required for Hg yield calculations at NSR4 and NSR5 were extrapolated using relationships developed at AEPA using archived gauged discharge from Water Survey of Canada (WSC) (Water Survey of Canada, 2021) and Alberta River Basins (Government of Alberta, 2024b). Daily discharge from a portion of the watershed area of NSR4 was directly measured at by hydrometric gauging stations (i.e., "NSR at Bighorn Dam" plus WSC's Ram River (station 05DC006)). Daily discharge from WSC's Ram River (station 05DC006) was then used to estimate discharge from the watershed area of NSR4 not covered by the other hydrometric gauging stations. Daily discharge for NSR5 was similarly obtained by using WSC's Ram River flow to fill in the ungauged shoulder seasons of WSC's NSR at Rocky Mountain House (station 05DC001), before subtracting flow from other hydrometric gauging stations (i.e., WSC's

Clearwater River at Dovercourt (station 05DB006) and WSC's Prairie at Rocky Mountain House (station 05DB006)) from it. Ultimately, catchment areas modeled this way were within ± 5% of the watershed areas delineated for NSR4 and NSR5. As modeled flow depended on watershed area, we can thus be reasonably certain of our estimates.

Mercury yields at the E.L. Smith DWTP NSR site were calculated using Raw NSR concentrations (**Table A3.4**) and mean daily river discharge quantified in Edmonton by a hydrometric gauging station maintained by WSC (station 05DF001) (Water Survey of Canada, 2021). Watershed areas for the Edmonton sampling site was obtained directly from WSC. From Hg concentrations and discharge, Hg loads were calculated using the *rloadest* package (Lorenz et al., 2017) for the U.S. Geological Survey's LOAD ESTimator (Runkel et al., 2004) in R. Models were selected based on the lowest Akaike Information Criterion (AIC), which indicated the best fit regression. We then ensured that the R^2 and percent bias (Bp) for the model was greater than 50 and lower than 25, respectively. All models with the lowest AIC met the statistical criteria and were used to calculate loads. Yields were then calculated by dividing load (g OWS^{-1}) by watershed area (km^2) for each sampling site.

3 Results & Discussion

3.2 Comparison of THg and MeHg concentrations between water treatment stages

At the E.L. Smith DWTP, Raw THg concentrations were generally highest during high spring and summer flows (> 500 $m^3 s^{-1}$) (**Figure 4.2B**) when waters were generally more turbid (**Figure A3.2A**) and colored (**Figure A3.2B**). However, the linear relationship between discharge and Raw THg concentration was poor ($R^2 = 0.20$) due to a high concentration outlier during the spring runoff period in 2020 (without the outlier, the linear relationship becomes moderate; $R^2 = 0.47$) (**Figure A3.3A**). There was a strong discharge-concentration linear relationship for Raw MeHg ($R^2 = 0.84$) (**Figure A3.3B**). In fact, the highest Raw MeHg concentration (0.93 ng L^{-1}) (**Figure 4.2C**) coincided with the highest mean daily discharge (1760 $m^3 s^{-1}$) (**Figure 4.2A**), turbidity (1100 NTU) (**Figure A3.2A**; **Figure A3.4A**), color (89.5 TCU) (**Figure A3.2B**; **Figure A3.4B**), and second lowest pH value (7.88) (**Figure A3.2C**; **Figure A3.4C**), suggesting that runoff from wetlands or other saturated soils, known sites of Hg methylation (St. Louis et al., 1996), in the watershed may have been an important contributor of MeHg to the NSR. Dissolved

THg (FRaw) concentrations represented 30.9 ± 18.8% (mean ± SD) of the Raw THg concentrations and were significantly lower than Raw THg concentrations (p_{adj}<0.001) (**Figure 4.3A**). Dissolved MeHg represented 40.1 ± 19.0 % of the total MeHg concentrations and were also significantly lower than Raw MeHg concentrations (p_{adj}<0.001) (**Figure 4.3B**). Additionally, though Hg concentrations in Raw river water varied temporally with discharge and other physicochemical factors, dissolved Hg concentrations were more stable across all conditions (**Figure 4.2**).

Concentrations of THg and MeHg were significantly lower following all stages of water treatment compared to concentrations in Raw NSR water (p_{adj} < 0.001; **Figure 4.3**). THg and MeHg concentrations were highest in Raw NSR water and significantly decreased after clarification, followed by further non-significant decreases after filtration and UV treatments, and finally a slight increase in on-site Reservoirs (**Figure 4.3**; **Table A3.4**). Interestingly, concentrations of both THg and MeHg decreased more following the clarification process than they did when Raw NSR water was filtered through 0.45 um filters (FTHg and FMeHg) to quantify the dissolved fraction (**Figure 4.2**, **Figure 4.3**). Specifically, clarification removed 74.6% of the THg and 66.0% of the MeHg compared to laboratory filtration which removed 69.1% of THg and 59.9% of the MeHg (**Figure 4.3**). The drop in THg and MeHg concentrations following the clarification stage suggests that the addition of chemicals along the water treatment process was key to binding and scavenging Hg from the water. Prior to the clarification stage, alum and primary polymers were added continually, while PAC was added seasonally in spring and summer when river flow and Hg concentrations were generally at their highest (**Figure 4.1**; **Figure 4.2**). Water treatment residuals are formed when these chemicals combine with suspended matter in river water, which then settle out in the clarification chambers (Sharma & Ahammed, 2023). Alum has been shown to remove Hg from aqueous solutions (Hovsepyan & Bonzongo, 2009) through sorption with the oxygen atoms of the alum (Quiñones et al., 2016). Primary polymer then acts as a binding agent to enhance the flocculation of alum (Bratby, 2016), which attracts silt, clay, and organic matter to form sludge. Adsorption of Hg by PAC can also remove both Hg(II) and MeHg from aqueous solutions (Abdel-Shafy et al., 1998; Thiem et al., 1976). As such, the conjunctive use of alum and PAC in the water treatment process can be highly effective in removing potentially high concentrations of Hg during periods of high turbidity in rivers (Ma et al., 1992). Even still, clarification did not proportionally remove as much MeHg as THg from NSR water (**Figure 4.3**). This may be because more of the overall THg pool (69 ± 19 %) was bound to particles than the MeHg portion (60 ± 19 %), as calculated by subtracting FRaw from Raw concentrations.

The clarification stage was so effective at stripping Hg from NSR water that there was little left to remove during the filtration stage, especially for THg (**Figure 4.2**, **Figure 4.3**). However, filtration still removed a further 9.8% THg and 31.8% MeHg post-clarification (**Figure 4.3**). Following filtration, water treated at the E.L. Smith DWTP undergoes the additional process of UV treatment. This step involves exposing water to a series of intense UV light bulbs which serve to further disinfect the water (EPCOR, 2024). UV radiation is known to photoreduce Hg(II) and MeHg to gaseous Hg(0) (Lehnherr & St. Louis, 2009; Rose et al., 2015) which can then be lost to the atmosphere (Lalonde et al., 2001). Yet, the UV process only marginally reduced concentrations of THg and MeHg by a further 1.5% and 0.8%, respectively, likely because Hg concentrations following clarification and filtration were so low that UV treatment did not have much Hg to liberate via photoreduction (**Figure 4.2**, **Figure 4.3**). THg and MeHg concentrations in reservoir water remained low but increased slightly by 5.1% and 4.3% following UV treatment (**Figure 4.2**, **Figure 4.3**). We suspect this slight increase in concentrations resulted from impurities in one of the four chemicals added following UV treatment (**Figure 4.1**). Regardless, the final THg concentrations in the fully treated water were an order of magnitude below Canada’s maximum allowable concentration for drinking water (Health Canada, 1979, 2022).

Ultimately, sludge-bound Hg and treatment residuals associated with both the clarification and filtration processes were flushed back into the NSR downriver of the plant (**Figure 4.1**), resulting in low net removal of Hg from the NSR. However, it is likely that the released sludge-bound Hg initially settled to the bottom of the river instead of being suspended.

3.3 Watershed protection of source waters

Source water quality and treatment infrastructure are the two most important determinants of drinking water quality (Scheili et al., 2016). Here we examine how Hg concentrations and yields changed along the NSR, from its headwaters to Edmonton, during the OWS when NSR discharge was at its highest.

In 2020, mean OWS concentrations of Raw and FRaw THg at sampling sites NSR1 through NSR5 ranged between 0.48 to 2.19 ng L^{-1} and 0.09 to 0.36 ng L^{-1}, respectively (**Table 4.1**). Mean concentrations of Raw and FRaw THg increased to 6.53 ng L^{-1} and 1.11 ng L^{-1}, respectively, by the time the NSR reached Edmonton (**Table 4.1**). The NSR's many tributaries, and the diverse landscapes they flow through, may have a large impact on Hg concentrations at the initial convergence of waterways; however, Hg concentrations tend to become more similar across landscape types in major rivers (Emmerton et al., 2023).

Although Hg concentrations are important to quantify for water quality and bioaccumulation studies, they only represent sample-specific masses in a given volume of water, thus reducing their discussion to specific sampling sites and times. Hence, to determine how loads of Hg in the NSR changed as water moved downriver, we calculated yields for the 2020 OWS. THg yields varied greatly at the mountain headwater and mid-river sites, ranging from 0.127 to 1.29 g OWS^{-1} km^{-2} (**Table 4.1**). The site with the highest yields, NSR2, is a glacial outwash floodplain site where sediment exchange between the floodplain and river water can be great during periods of high discharge (Serbu et al., 2024). However, THg yields were highest at 1.89 g OWS^{-1} km^{-2} for the NSR site at Edmonton, 534 kms downstream from its glacial headwaters. Additionally, though the FTHg yields were low in source water regions (0.042 - 0.146 g OWS^{-1} km^{-2}), they were more than doubled at the Edmonton site (0.324 g OWS^{-1} km^{-2}). This indicates that between the headwaters/mid-river sites and Edmonton, there were elevated watershed inputs of total and dissolved Hg into the NSR.

Broad landscape characteristics are known to influence Hg concentrations in landscape runoff (Emmerton et al., 2023; Hurley et al., 1995). For instance, Burns et al., (2012) found that landscape characteristics such as mountain and riparian area could explain up to 90% of the variation in THg and MeHg concentrations in the Hudson River watershed, while Fink-Mercier et al., (2022) found that water and wetland area drove variation in THg and MeHg concentrations and yields in boreal rivers. The NSR begins at the Saskatchewan Glacier and meanders through the relatively pristine Canadian Rocky Mountains (Serbu et al., 2024) before reaching Abraham Lake (a reservoir) behind the Bighorn Dam in the foothills (**Figure A3.1**). The yields in THg decreased between NSR3 and NSR4 (**Table 4.1**), suggesting that the Bighorn Dam acted as a sink for particulate-bound Hg.

Overall, mean THg and MeHg concentrations in the NSR at Edmonton (**Table A3.4**) fell within the range of other major global rivers as summarized in Emmerton et al., 2023 (0.9-21.4 ng L^{-1} and 0.05-0.30 ng L^{-1}, respectively). Similarly, full annual THg and MeHg yields, calculated for 2020 at the Edmonton site only, were 2.19 g yr^{-1} km^{-2} and 0.059 g yr^{-1} km^{-2}, respectively, compared to a range of 0.1 to 10.2 g yr^{-1} km^{-2} for THg and 0.01 to 0.86 g yr^{-1} km^{-2} for MeHg in other major global rivers (Emmerton et al., 2023).

Though the Hg exposure risk in Edmonton was low given the low Hg concentrations in both the NSR and drinking water leaving the E.L. Smith DWTP for distribution to the municipality (**Table A3.4**), this may not be the case everywhere. Some regions with particularly high source water Hg concentrations or less effective DWTP infrastructure could be at risk for Hg overexposure. To mitigate some of the costs associated with treatment, protection of source waters via the preservation of watersheds and their inherent ecosystem services, is therefore essential (Price & Heberling, 2018). New York City, for instance, famously began protecting its surrounding watersheds in 1997 to avoid building an expensive and energy-consuming water filtration plant (Bennett et al., 2014). Yet, climate change is altering land-river connectivity through changing frequencies of droughts and floods (L. Li et al., 2024), which subsequently influences watershed runoff and Hg yields. NSR headwaters are initially sourced from mountain glaciers and snowpacks along the eastern slopes of the Canadian Rocky Mountains, a region vulnerable to climate change (Tennant et al., 2012). At the broader scale, the Saskatchewan-Nelson watershed has some of the highest demand of any mountain-stemming watershed in North America, despite only a moderate supply of mountain waters (Immerzeel et al., 2020). Thus, with decreases in water quantity, producing water of consumption quality may strain our local DWTPs and cement water insecurity as the leading issue of the coming decades.

References

Abdel-Shafy, H. I., Abdel-Sabour, M. F., & Aly, R. O. (1998). Adsorption of nickel and mercury from drinking water simulant by activated carbon. *Environmental Management and Health*, *9*(4), 170–175. https://doi.org/10.1108/09566169810228999

Abkar, L., Moghaddam, H. S., & Fowler, S. J. (2024). Microbial ecology of drinking water from source to tap. *Science of The Total Environment*, *908*, 168077. https://doi.org/10.1016/j.scitotenv.2023.168077

American Public Health Association, American Water Works Association, & Water Environment Federation. (2023a). Method 2120C-Colour. In W. C. Lipps, T. E. Baxter, & E. Braun-Howland (Eds.), *Standard Methods For the Examination of Water and Wastewater* (24th ed.). APHA Press. https://doi.org/10.2105/smww.2882.048

American Public Health Association, American Water Works Association, & Water Environment Federation. (2023b). Method 2130B-Turbidity. In W. C. Lipps, T. E. Baxter, & E. Braun-Howland (Eds.), *Standard Methods For the Examination of Water and Wastewater* (24th ed.). APHA Press. https://doi.org/10.2105/smww.2882.048

American Public Health Association, American Water Works Association, & Water Environment Federation. (2023c). Method 4500-H-pH for Water. In W. C. Lipps, T. E. Baxter, & E. Braun-Howland (Eds.), *Standard Methods For the Examination of Water and Wastewater* (24th ed.). APHA Press. https://doi.org/10.2105/smww.2882.048

American Public Health Association, American Water Works Association, & Water Environment Federation. (2023d). *Standard Methods for the Examination of Water and Wastewater* (W. C. Lipps, T. E. Baxter, & E. Braun-Howland, Eds.; 24th ed.). APHA Press. https://doi.org/10.2105/smww.2882.048

Anderson, S., & Radić, V. (2020). Identification of local water resource vulnerability to rapid deglaciation in Alberta. *Nature Climate Change*, *10*(10), 933–938. https://doi.org/10.1038/s41558-020-0863-4

Bennett, D. E., Gosnell, H., Lurie, S., & Duncan, S. (2014). Utility engagement with payments for watershed services in the United States. *Ecosystem Services*, *8*, 56–64. https://doi.org/10.1016/j.ecoser.2014.02.001

Bortone, G. (2007). Sediment Treatment—A General Introduction. In *Sustainable Management of Sediment Resources* (Vol. 2, pp. 1–10). Elsevier. https://doi.org/10.1016/S1872-1990(07)80013-4

Bratby, J. (2016). Chapter 3. Coagulants. In *Coagulation and Flocculation in Water and Wastewater Treatment* (3rd ed.). IWA Publishing.

Burns, D. A., Riva-Murray, K., Bradley, P. M., Aiken, G. R., & Brigham, M. E. (2012). Landscape controls on total and methyl Hg in the upper Hudson River basin, New York, USA. *Journal of Geophysical Research: Biogeosciences*, *117*(G1), 2011JG001812. https://doi.org/10.1029/2011JG001812

Emmerton, C. A., Drevnick, P. E., Serbu, J. A., Cooke, C. A., Graydon, J. A., Reichert, M., Evans, M. S., & McMaster, M. E. (2023). Downstream modification of mercury in diverse river systems underscores the role of local conditions in fish bioaccumulation. *Ecosystems*, *26*(1), 114–133. https://doi.org/10.1007/s10021-022-00745-w

EPCOR. (2024). *E.L. Smith Water Treatment Plant*. https://www.epcor.com/about/who-we-are-what-we-do/about-our-company/where-we-operate/edmonton/Pages/el-smith-water-treatment-plant.aspx

Fink-Mercier, C., Lapierre, J., Amyot, M., & Del Giorgio, P. A. (2022). Concentrations and yields of total Hg and MeHg in large boreal rivers linked to water and wetland coverage in the watersheds. *Journal of Geophysical Research: Biogeosciences*, *127*(5), e2022JG006892. https://doi.org/10.1029/2022JG006892

Government of Alberta. (2005). *2005 Natural Regions and Subregions of Alberta* [Map]. Government of Alberta.

Government of Alberta. (2024a). *Alberta River Basins*. Alberta River Basins. https://rivers.alberta.ca

Government of Alberta. (2024b). *Water Quality Data Portal*. Water Quality Data Portal. https://environment.extranet.gov.ab.ca/apps/WaterQuality/dataportal/

Health Canada. (1979). *Guidelines for Canadian Drinking Water Quality: Guideline Technical Document—Mercury*. Water and Air Quality Bureau, Healthy Environments and Consumer Safety Branch, Health Canada.

Health Canada. (2022). *Guidelines for Canadian Drinking Water Quality—Summary Tables*. Water and Air Quality Bureau, Healthy Environments and Consumer Safety Branch, Health Canada.

Hovsepyan, A., & Bonzongo, J.-C. J. (2009). Aluminum drinking water treatment residuals (Al-WTRs) as sorbent for mercury: Implications for soil remediation. *Journal of Hazardous Materials*, *164*(1), 73–80. https://doi.org/10.1016/j.jhazmat.2008.07.121

Hurley, J. P., Benoit, J. M., Babiarz, C. L., Shafer, M. M., Andren, A. W., Sullivan, J. R., Hammond, Richard., & Webb, D. A. (1995). Influences of watershed characteristics on mercury levels in Wisconsin rivers. *Environmental Science & Technology*, *29*(7), 1867–1875. https://doi.org/10.1021/es00007a026

Immerzeel, W. W., Lutz, A. F., Andrade, M., Bahl, A., Biemans, H., Bolch, T., Hyde, S., Brumby, S., Davies, B. J., Elmore, A. C., Emmer, A., Feng, M., Fernández, A., Haritashya, U., Kargel, J. S., Koppes, M., Kraaijenbrink, P. D. A., Kulkarni, A. V., Mayewski, P. A., … Baillie, J. E. M. (2020). Importance and vulnerability of the world's water towers. *Nature*, *577*(7790), 364–369. https://doi.org/10.1038/s41586-019-1822-y

Lalonde, J. D., Amyot, M., Kraepiel, A. M. L., & Morel, F. M. M. (2001). Photooxidation of Hg(0) in artificial and natural waters. *Environmental Science & Technology*, *35*(7), 1367–1372. https://doi.org/10.1021/es001408z

Lehnherr, I., & St. Louis, V. L. (2009). Importance of ultraviolet radiation in the photodemethylation of methylmercury in freshwater ecosystems. *Environmental Science & Technology*, *43*(15), 5692–5698. https://doi.org/10.1021/es9002923

Li, L., Knapp, J. L. A., Lintern, A., Ng, G.-H. C., Perdrial, J., Sullivan, P. L., & Zhi, W. (2024). River water quality shaped by land–river connectivity in a changing climate. *Nature Climate Change*, *14*(3), 225–237. https://doi.org/10.1038/s41558-023-01923-x

Li, P., & Wu, J. (2019). Drinking water quality and public health. *Exposure and Health*, *11*(2), 73–79. https://doi.org/10.1007/s12403-019-00299-8

Lorenz, D., Runkel, R., De Cicco, L., Watkins, D., & Stachelek, J. (2017). *rloadest: River load estimation, version 0.4.5*.

Ma, X., Subramanian, K. S., Chakrabarti, C. L., Guo, R., Cheng, J., Lu, Y., & Pickering, W. F. (1992). Removal of trace mercury(II) from drinking water: Sorption by granular activated carbon. *Journal of Environmental Science and Health . Part A: Environmental Science and*

Engineering and Toxicology, *27*(6), 1389–1404. https://doi.org/10.1080/10934529209375802

Price, J. I., & Heberling, M. T. (2018). The effects of source water quality on drinking water treatment costs: A review and synthesis of empirical literature. *Ecological Economics*, *151*, 195–209. https://doi.org/10.1016/j.ecolecon.2018.04.014

Quiñones, K., Hovsepyan, A., Oppong-Anane, A., & Bonzongo, J.-C. J. (2016). Insights into the mechanisms of mercury sorption onto aluminum based drinking water treatment residuals. *Journal of Hazardous Materials*, *307*, 184–192. https://doi.org/10.1016/j.jhazmat.2016.01.001

R Core Team. (2022). *R: A language and environment for statistical computing*. https://www.R-project.org/

Rose, C. H., Ghosh, S., Blum, J. D., & Bergquist, B. A. (2015). Effects of ultraviolet radiation on mercury isotope fractionation during photo-reduction for inorganic and organic mercury species. *Chemical Geology*, *405*, 102–111. https://doi.org/10.1016/j.chemgeo.2015.02.025

Runkel, B. R. L., Crawford, C. G., & Cohn, T. A. (2004). Load Estimator (LOADEST): A FORTRAN program for estimating constituent loads in streams and rivers. In *Techniques and Methods Book 4*.

Scheili, A., Delpla, I., Sadiq, R., & Rodriguez, M. J. (2016). Impact of raw water quality and climate factors on the variability of drinking water quality in small systems. *Water Resources Management*, *30*(8), 2703–2718. https://doi.org/10.1007/s11269-016-1312-z

Schindler, D. W., & Donahue, W. F. (2006). An impending water crisis in Canada's western prairie provinces. *Proceedings of the National Academy of Sciences*, *103*(19), 7210–7216. https://doi.org/10.1073/pnas.0601568103

Serbu, J. A., St. Louis, V. L., Emmerton, C. A., Tank, S. E., Criscitiello, A. S., Silins, U., Bhatia, M. P., Cavaco, M. A., Christenson, C., Cooke, C. A., Drapeau, H. F., Enns, S. J. A., Flett, J. E., Holland, K. M., Lavallee-Whiffen, J., Ma, M., Muir, C. E., Poesch, M., & Shin, J. (2024). A comprehensive biogeochemical assessment of climate-threatened glacial river headwaters on the eastern slopes of the Canadian Rocky Mountains. *Journal of Geophysical Research: Biogeosciences*, *129*(1), e2023JG007745. https://doi.org/10.1029/2023JG007745

Shah, A., Arjunan, A., Baroutaji, A., & Zakharova, J. (2023). A review of physicochemical and biological contaminants in drinking water and their impacts on human health. *Water Science and Engineering*, *16*(4), 333–344. https://doi.org/10.1016/j.wse.2023.04.003

Sharma, S., & Ahammed, M. M. (2023). Application of modified water treatment residuals in water and wastewater treatment: A review. *Heliyon*, *9*(5), e15796. https://doi.org/10.1016/j.heliyon.2023.e15796

St. Louis, V. L., Rudd, J. W. M., Kelly, C. A., Beaty, K. G., Flett, R. J., & Roulet, N. T. (1996). Production and loss of Mmthylmercury and loss of total mercury from boreal forest catchments containing different types of wetlands. *Environmental Science & Technology*, *30*(9), 2719–2729. https://doi.org/10.1021/es950856h

Syafrudin, M., Kristanti, R. A., Yuniarto, A., Hadibarata, T., Rhee, J., Al-onazi, W. A., Algarni, T. S., Almarri, A. H., & Al-Mohaimeed, A. M. (2021). Pesticides in drinking water—A review. *International Journal of Environmental Research and Public Health*, *18*(2), 468. https://doi.org/10.3390/ijerph18020468

Tennant, C., Menounos, B., Wheate, R., & Clague, J. J. (2012). Area change of glaciers in the Canadian Rocky Mountains, 1919 to 2006. *The Cryosphere*, *6*(6), 1541–1552. https://doi.org/10.5194/tc-6-1541-2012

Thiem, L., Badorek, D., & O'Connor, J. T. (1976). Removal of mercury from drinking water using activated carbon. *Journal American Water Works Association*, *68*(8), 447–451. https://doi.org/10.1002/j.1551-8833.1976.tb02454.x

U.S. EPA. (1996). *Method 1669: Sampling ambient water for trace metals at EPA water quality criteria levels*.

U.S. EPA. (1998). *Method 1630: Methyl mercury in water by distillation, aqueous ethylation, purge and trap, and cold vapor atomic fluorescence spectrometry*.

U.S. EPA. (2002). *Method 1631, Revision E: Mercury in water by oxidation, purge and trap, and cold vapor atomic fluorescence spectrometry*.

Volk, C., Kaplan, L. A., Robinson, J., Johnson, B., Wood, L., Zhu, H. W., & LeChevallier, M. (2005). Fluctuations of dissolved organic matter in river used for drinking water and impacts on conventional treatment plant performance. *Environmental Science & Technology*, *39*(11), 4258–4264. https://doi.org/10.1021/es040480k

Water Survey of Canada. (2021). *National Water Data Archive: HYDAT*. https://www.canada.ca/en/environment-climate-change/services/water-overview/quantity/monitoring/survey/data-products-services/national-archive-hydat.html

Wickham, H. (2016). *ggplot2: Elegant graphics for data analysis*.

Xu, S., Chen, M., Feng, T., Zhan, L., Zhou, L., & Yu, G. (2021). Use ggbreak to effectively utilize plotting space to deal with large datasets and outliers. *Frontiers in Genetics*, *12*, 774846. https://doi.org/10.3389/fgene.2021.774846

Table 4.1. Sampling site coordinates, mean (± standard deviation) 2020 total mercury (THg; Raw and filtered Raw [FRaw]) concentrations during the open water season (OWS; 1 May to 31 October), water discharge volumes and THg yields at three North Saskatchewan River (NSR) mountain headwater sites (NSR1, NSR2, NSR3) (Serbu et al., 2024), two sites further downriver of the headwater sites (NSR4, NSR5) and near the intake location for the E.L. Smith Drinking Water Treatment Plant in the City of Edmonton.

Site	Coordinates (DD)		Raw THg	FRaw THg	Discharge	THg	FTHg
	Latitude	Longitude	Concentration (ng L^{-1})		Total OWS km^3	Yield (g OWS^{-1} km^{-2})	
NSR1	52.169472N	-117.076361W	0.35 ± 0.17	0.09 ± 0.04	0.071	0.559	NA
NSR2	52.069194N	-116.915250W	2.19 ± 3.78	0.20 ± 0.23	0.448	1.29	0.146
NSR3	51.970556N	-116.721111W	1.33 ± 1.44	0.15 ± 0.03	1.15	0.987	0.145
NSR4	52.45381N	-115.75947W	0.48 ± 0.25	0.17 ± 0.07	2.13	0.210	0.070
NSR5	52.34808N	-114.98176W	1.24 ± 0.95	0.36 ± 0.42	2.26	0.127	0.042
Edmonton	53.472118N	-113.615505W	6.53 ± 8.36	1.11 ± 0.71	6.57	1.89	0.324

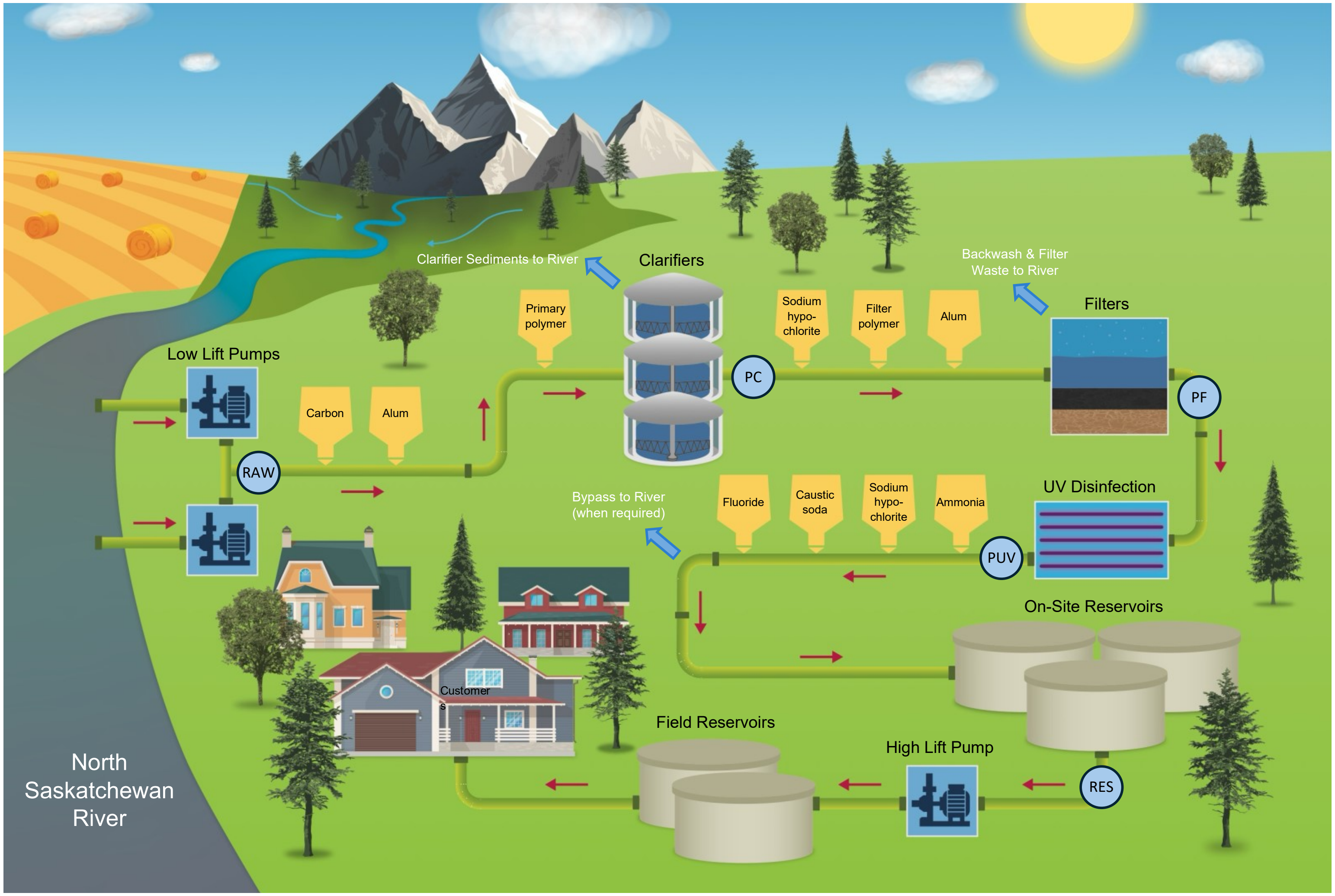

Figure 4.1. Schematic of the water treatment process and infrastructure at the E.L. Smith Water Treatment Plant in Edmonton, Alberta, Canada. Raw river water, as well as processed water following major stages in the treatment process (post-clarification (PC), post-filtration (PF) and post-ultraviolet (PUV)) and in on-site holding reservoirs (RES) was collected for analyses of total mercury and methylmercury.

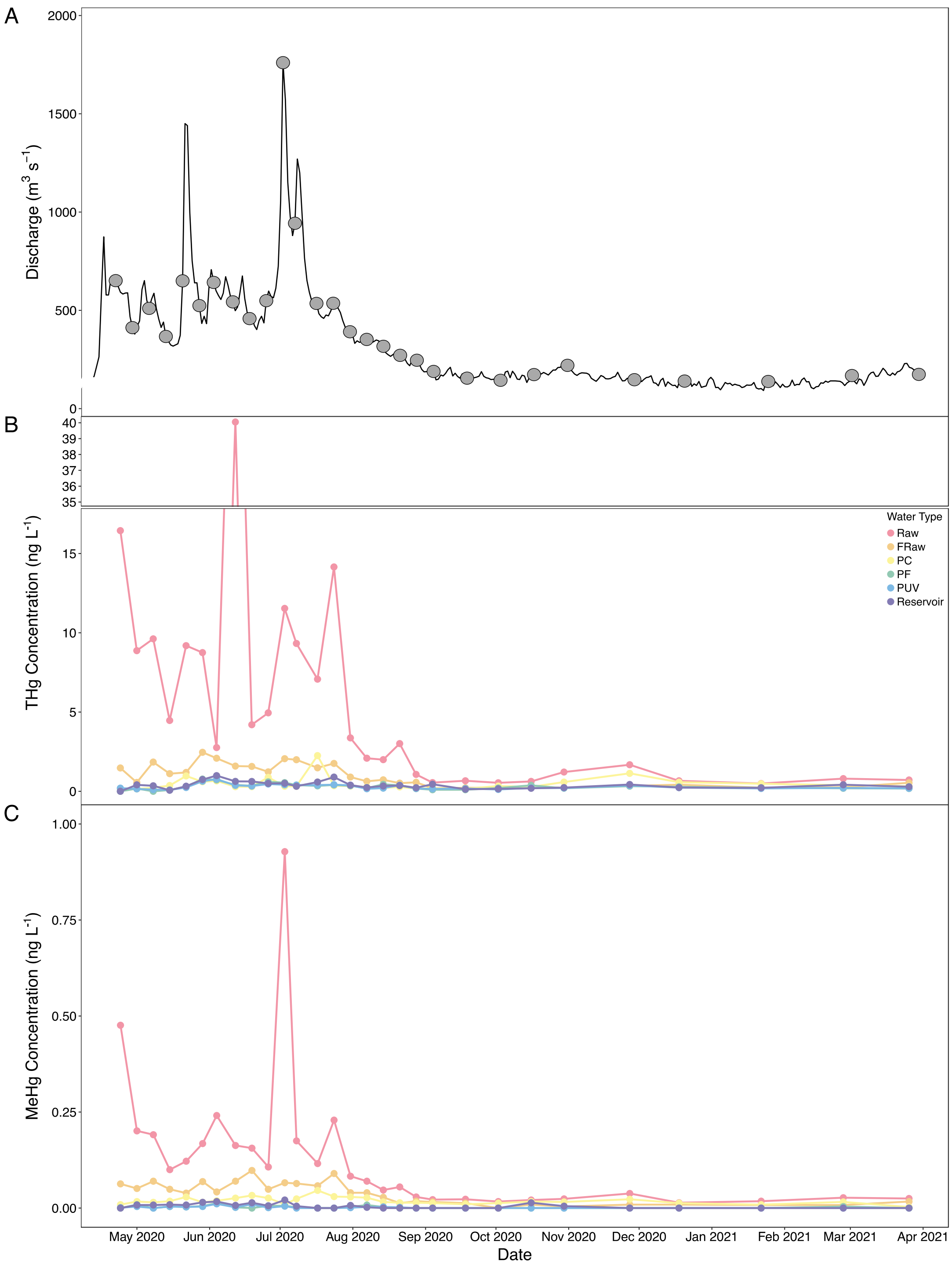

Figure 4.2. (A) River discharge (Q) at Water Survey of Canada's North Saskatchewan River-Edmonton hydrometric gauging station (05DF001). Sampling dates are represented by grey dots. (B) Total mercury and (C) methylmercury concentrations in river water (Raw), filtered river water (FRaw), as well as processed water following major stages in the treatment process (post-clarification (PC), post-filtration (PF) and post-ultraviolet (PUV)) and in on-site holding reservoirs (Reservoir).

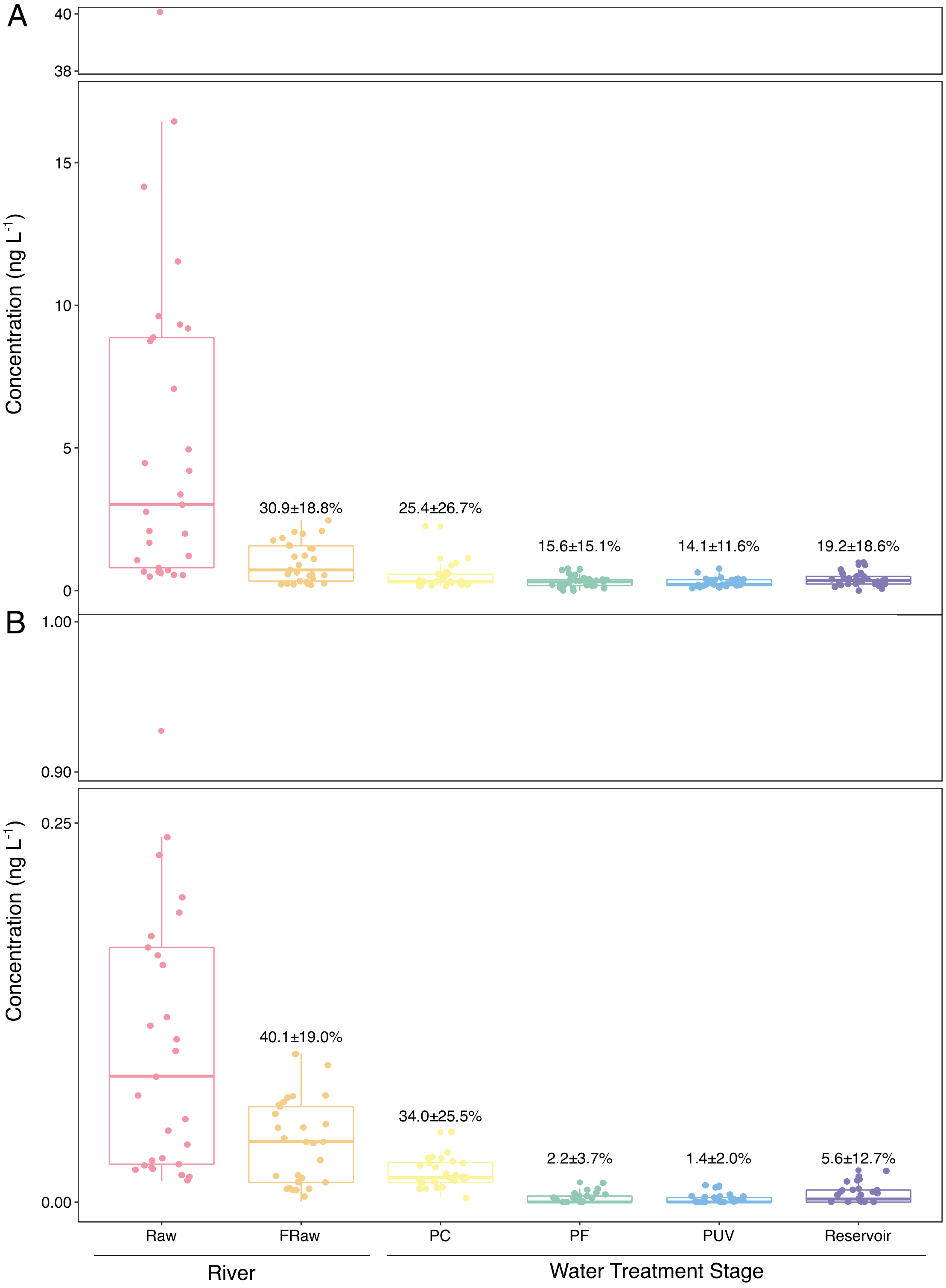

Figure 4.3. Boxplots of (A) total mercury and (B) methylmercury concentrations in river water (Raw), filtered river water (FRaw), as well as Post-Clarification (PC), Post-Filtration (PF) and Post-Ultraviolet (PUV) treatments and in the on-site holding reservoir (Reservoir). Mean ± standard deviation above boxplots denotes percent of Raw Hg.

Chapter 5: General conclusions

Mountains are considered global water towers, supplying freshwater from glacier and snow melt to ecologically and socioeconomically diverse downriver regions (Immerzeel et al., 2020). Yet, climate change is accelerating the mass loss of glaciers worldwide and leaving receiving regions at risk of water insecurity (Bliss et al., 2014). So far, studies have generally focused on the loss of glaciers themselves (e.g., Gardner et al., 2013; Rounce et al., 2023; Tennant & Menounos, 2013), with few studies focused on the biogeochemical impacts that rapidly melting glaciers may have on downriver environments (Milner et al., 2017). To address this gap in the literature, we conducted three distinct biogeochemical studies on rivers stemming from the eastern slopes of the Canadian Rocky Mountains from 2019-2021. These three rivers – the Sunwapta-Athabasca, North Saskatchewan, and Bow – have their headwaters in the world-famous Jasper and Banff National Parks. They then flow eastward and become main rivers supplying clean freshwater to small communities and large municipalities, agriculture, industry, and recreation across the Province of Alberta and beyond (S. Anderson & Radić, 2020; Schindler & Donahue, 2006).

A water quality investigation of a large (200+ parameters, 260,000+ datapoints) biogeochemical dataset was presented in Chapter 2. Using river, precipitation (rain and snow), and glacial ice water isotope signatures, we were able to create the first known Local Meteoric Water Line (LMWL) for our study region. In an ideal scientific world, we would have been able to use those same water isotope signatures to create an endmember model and quantify the proportion of river water that came from each source, but variation in isotope signatures in precipitation and glacier ice was too great to do so. The next step would therefore be to collect glacier terminus ice and groundwater for water isotope analyses in the hopes that they represent a more defined endmember for river water source apportionment modeling. We next determined that distance from glacier explained more data variability in river physicochemical measures than other spatiotemporal factors such as season, year, or river. The size of the glacier was not directly quantified and considered in this endeavor, though could possibly explain additional variation. A larger glacier size could theoretically produce more communited sediment and discharge, altering the concentrations of chemical species and an analysis of their variation. We then determined open water season (OWS) chemical yields for 25 of the parameters along our river continuums. Knowing what we know now about how different landscape characteristics impacted the fate of particulate, total, and dissolved parameters, an amendment to our sampling design would be to add more sampling sites along each of our transects to further enhance this understanding. For example, sampling immediately upstream and downstream of proglacial lakes or glacial outwash flood plains would have been of interest to better constrain their roles as chemical sinks and sources. However, given the logistical, time, and monetary constraints of our research program, the fact that we were able to get seasonal – including winter – data from 14 sampling sites over multiple years was a large achievement in itself.

Spatiotemporal patterns in carbon dioxide (CO_2) cycling linked to geochemical weathering were presented in Chapter 3. Key to the novelty of this study was the fact that our glacial headwater river transects spanned glacierized, alpine, subalpine, and montane altitudinal life zones. Teasing out geochemical weathering from other factors that impact the inorganic carbon cycle (such as metabolism) in ecologically complex environments proved scientifically challenging. Ultimately, we decided to implement eight strategies for determining: if geochemical weathering was occurring in our study rivers ((1) CO_2 saturation, (2) calcite saturation indices, and (3) instantaneous CO_2 fluxes); what the sources and types of weathering were in our study rivers ((4) ternary diagrams, (5) chemical concentration-discharge relationships, (6) molar ratios); (7) what the isotopic evidence was for weathering in our study rivers ($^{87}Sr/^{86}Sr$, $\delta^{34}S\text{-}SO_4$, $\delta^{18}O\text{-}SO_4$, $\delta^{13}C$-PIC, $\delta^{13}C$-DIC, $\Delta^{14}C$-DIC); and (8) what a mass balance of DIC sources in our study rivers showed. As suggested elsewhere (e.g., St.Pierre, 2018), continuous monitoring of in situ CO_2 and other parameters (such as ions and isotopes) would be a natural extension of the work done here. Additionally, a study on the diel metabolism at each downstream study site would be particularly valuable. In fact, I have already completed the field and laboratory work for such a study, which is expected to be written into manuscript format in fall 2024. This study would provide us with an estimation of net in situ CO_2 consumption due to aquatic metabolism as opposed to geochemical weathering and allow for more broad conclusions regarding inorganic carbon cycling in our study system.

Lastly, we selected the North Saskatchewan River to look at impacts of contaminant cycling beyond the glacial headwaters. We first assessed total mercury and methylmercury (THg and MeHg, respectively) removal along different drinking water treatment stages at the E.L. Smith Drinking Water Plant in Edmonton, Alberta. There we found that the first stage – chemical additions and clarification – removed the majority of the Hg from raw river water. An experiment would allow us to test which chemical or combination of chemicals (alum, primary polymer, powdered activated carbon) best allowed for the flocculation of Hg during the clarification stage, particularly under simulated high river turbidity and Hg concentration conditions. We also examined how OWS THg yields changed from the North Saskatchewan River glacial headwaters (from Chapter 2) and mid-river sites to where water was removed for drinking water production in Edmonton. One obvious addition would be to collect both THg and MeHg at more sites along the NSR. Similar to Chapter 2, adding more sampling sites along each transect would likely provide more definitive answers about whether certain landscape (e.g., wetlands, lakes) or anthropogenic (e.g., reservoirs, dams) features acted as mediators of Hg and other chemical yields, which in turn could help with watershed protection for securing clean water sources for processing. Additionally, although we were limited to THg yields due to MeHg, the more toxic form of Hg, often being below the analytical detection limit at headwater sites, modeling OWS MeHg yields at additional sites could provide us with more information regarding how that faction of the Hg budget changes downriver.

Overall, these three studies present the most comprehensive analysis and discussion of the largest dataset of biogeochemistry ever gathered for the headwaters and immediate downriver environment of our three study rivers. This body of work is thus foundational and can be used as a contemporary baseline which future work in this region can be compared against. Comparisons will become especially important as climate change continues to wreak havoc on mountain environments through glacier mass loss and changes in temperature and precipitation regimes, impacting downstream biogeochemistry in currently unimaginable ways.

References

Anderson, S., & Radić, V. (2020). Identification of local water resource vulnerability to rapid deglaciation in Alberta. *Nature Climate Change*, *10*(10), 933–938. https://doi.org/10.1038/s41558-020-0863-4

Bliss, A., Hock, R., & Radić, V. (2014). Global response of glacier runoff to twenty-first century climate change. *Journal of Geophysical Research: Earth Surface*, *119*(4), 717–730. https://doi.org/10.1002/2013JF002931

Gardner, A. S., Moholdt, G., Cogley, J. G., Wouters, B., Arendt, A. A., Wahr, J., Berthier, E., Hock, R., Pfeffer, W. T., Kaser, G., Ligtenberg, S. R. M., Bolch, T., Sharp, M. J., Hagen, J. O., Van Den Broeke, M. R., & Paul, F. (2013). A reconciled estimate of glacier contributions to sea level rise: 2003 to 2009. *Science*, *340*(6134), 852–857. https://doi.org/10.1126/science.1234532

Immerzeel, W. W., Lutz, A. F., Andrade, M., Bahl, A., Biemans, H., Bolch, T., Hyde, S., Brumby, S., Davies, B. J., Elmore, A. C., Emmer, A., Feng, M., Fernández, A., Haritashya, U., Kargel, J. S., Koppes, M., Kraaijenbrink, P. D. A., Kulkarni, A. V., Mayewski, P. A., … Baillie, J. E. M. (2020). Importance and vulnerability of the world's water towers. *Nature*, *577*(7790), 364–369. https://doi.org/10.1038/s41586-019-1822-y

Milner, A. M., Khamis, K., Battin, T. J., Brittain, J. E., Barrand, N. E., Füreder, L., Cauvy-Fraunié, S., Gíslason, G. M., Jacobsen, D., Hannah, D. M., Hodson, A. J., Hood, E., Lencioni, V., Ólafsson, J. S., Robinson, C. T., Tranter, M., & Brown, L. E. (2017). Glacier shrinkage driving global changes in downstream systems. *Proceedings of the National Academy of Sciences*, *114*(37), 9770–9778. https://doi.org/10.1073/pnas.1619807114

Rounce, D. R., Hock, R., Maussion, F., Hugonnet, R., Kochtitzky, W., Huss, M., Berthier, E., Brinkerhoff, D., Compagno, L., Copland, L., Farinotti, D., Menounos, B., & McNabb, R. W. (2023). Global glacier change in the 21st century: Every increase in temperature matters. *Science*, *379*(6627), 78–83. https://doi.org/10.1126/science.abo1324

Schindler, D. W., & Donahue, W. F. (2006). An impending water crisis in Canada's western prairie provinces. *Proceedings of the National Academy of Sciences*, *103*(19), 7210–7216. https://doi.org/10.1073/pnas.0601568103

St.Pierre, K. (2018). *Biogeochemical impacts of glacial meltwaters across a High Arctic watershed (Lake Hazen, Nunavut, Canada)* [PhD]. University of Alberta.

Tennant, C., & Menounos, B. (2013). Glacier change of the Columbia Icefield, Canadian Rocky Mountains, 1919–2009. *Journal of Glaciology*, *59*(216), 671–686. https://doi.org/10.3189/2013JoG12J135

Full Bibliography

Abdel-Shafy, H. I., Abdel-Sabour, M. F., & Aly, R. O. (1998). Adsorption of nickel and mercury from drinking water simulant by activated carbon. *Environmental Management and Health*, *9*(4), 170–175. https://doi.org/10.1108/09566169810228999

Abkar, L., Moghaddam, H. S., & Fowler, S. J. (2024). Microbial ecology of drinking water from source to tap. *Science of The Total Environment*, *908*, 168077. https://doi.org/10.1016/j.scitotenv.2023.168077

Alberta Biodiversity Monitoring Institute. (2010). ABMI Wall-to-Wall Land Cover Inventory. [Dataset]. https://abmi.ca/home/data-analytics/da-top/da-product-overview/Data-Archive/Land-Cover.html. Retrieved March 2023.

Alberta Biodiversity Monitoring Institute. (2021). ABMI Wetland Inventory. [Dataset]. https://abmi.ca/home/data-analytics/da-top/da-product-overview/Advanced-Landcover-Prediction-and-Habitat-Assessment--ALPHA--Products/ABMI-Wetland-Inventory.html. Retrieved March 2023.

Alberta Environment and Parks. (2018). Alberta ArcHydro Phase 2 Data. [Dataset]. Government of Alberta. https://open.alberta.ca/opendata/gda-d22f5906-358e-47b9-9259-02702932a7a0#summary. Retrieved February 2023.

Alberta Environment and Parks. (2019a). *Water supply outlook for Alberta*. Edmonton, AB: Government of Alberta. https://rivers.alberta.ca. Retrieved April 2023.

Alberta Environment and Parks. (2019b). Winter precipitation percent of normal. Edmonton, AB: Government of Alberta.

Alberta Environment and Parks. (2020a). *Water supply outlook for Alberta*. Edmonton, AB: Government of Alberta. https://rivers.alberta.ca. Retrieved April 2023.

Alberta Environment and Parks. (2020b). Winter precipitation percent of normal. Edmonton, AB: Government of Alberta.

American Public Health Association, American Water Works Association, & Water Environment Federation. (2023a). Method 2120C-Colour. In W. C. Lipps, T. E. Baxter, & E. Braun-Howland (Eds.), *Standard Methods For the Examination of Water and Wastewater* (24th ed.). APHA Press. https://doi.org/10.2105/smww.2882.048

American Public Health Association, American Water Works Association, & Water Environment Federation. (2023b). Method 2130B-Turbidity. In W. C. Lipps, T. E. Baxter,

& E. Braun-Howland (Eds.), *Standard Methods For the Examination of Water and Wastewater* (24th ed.). APHA Press. https://doi.org/10.2105/smww.2882.048

American Public Health Association, American Water Works Association, & Water Environment Federation. (2023c). Method 4500-H-pH for Water. In W. C. Lipps, T. E. Baxter, & E. Braun-Howland (Eds.), *Standard Methods For the Examination of Water and Wastewater* (24th ed.). APHA Press. https://doi.org/10.2105/smww.2882.048

American Public Health Association, American Water Works Association, & Water Environment Federation. (2023d). *Standard Methods for the Examination of Water and Wastewater* (W. C. Lipps, T. E. Baxter, & E. Braun-Howland, Eds.; 24th ed.). APHA Press. https://doi.org/10.2105/smww.2882.048

Anderson, S. P. (2005). Glaciers show direct linkage between erosion rate and chemical weathering fluxes. *Geomorphology*, *67*(1-2 SPEC. ISS.), 147–157. https://doi.org/10.1016/j.geomorph.2004.07.010

Anderson, S. P. (2007). Biogeochemistry of glacial landscape systems. *Annual Review of Earth and Planetary Sciences*, *35*, 375–399. https://doi.org/10.1146/annurev.earth.35.031306.140033

Anderson, S. P., Drever, J. I., Frost, C. D., & Holden, P. (2000). Chemical weathering in the foreland of a retreating glacier. *Geochimica et Cosmochimica Acta*, *64*(7), 1173–1189. https://doi.org/10.1016/S0016-7037(99)00358-0

Anderson, S. P., Drever, J. I., & Humphrey, N. F. (1997). Chemical weathering in glacial environments. *Geology*, *25*(5), 399–402.

Anderson, S. P., Drever, J. I., & Humphrey, N. F. (1997). Chemical weathering in glacial environments. *Geology*, *25*(5), 399–402.

Anderson, S., & Radić, V. (2020). Identification of local water resource vulnerability to rapid deglaciation in Alberta. *Nature Climate Change*, *10*(10), 933–938. https://doi.org/10.1038/s41558-020-0863-4

Antweiler, R. C., & Taylor, H. E. (2008). Evaluation of statistical treatments of left-censored environmental data using coincident uncensored data sets: I. Summary statistics. *Environmental Science and Technology*, *42*(10), 3732–3738. https://doi.org/10.1021/acs.est.5b02385

Appling, A. P., Leon, M. C., & McDowell, W. H. (2015). Reducing bias and quantifying uncertainty in watershed flux estimates: The R package loadflex. *Ecosphere*, *6*(12). https://doi.org/10.1890/ES14-00517.1

Arendt, C. A., Aciego, S. M., & Hetland, E. A. (2015). An open source Bayesian Monte Carlo isotope mixing model with applications in Earth surface processes. *Geochemistry, Geophysics, Geosystems*, *16*(5), 1274–1292. https://doi.org/10.1002/2014GC005683

Arendt, C. A., Stevenson, E. I., & Aciego, S. M. (2016). Hydrologic controls on radiogenic Sr in meltwater from an alpine glacier system: Athabasca Glacier, Canada. *Applied Geochemistry*, *69*, 42–49. https://doi.org/10.1016/j.apgeochem.2016.04.002

Ashbaugh, L. L., Malm, W. C., & Sadehs, W. Z. (1985). A residence time probability analysis of sulfur concentrations at Grand Canyon National Park. *Atmospheric Environment*, *19*(8), 1263–1270.

Aucour, A.-M., Sheppard, S. M. F., Guyomar, O., & Wattelet, J. (1999). Use of 13C to trace origin and cycling of inorganic carbon in the Rhone river system. *Chemical Geology*, *159*, 87–105.

Bade, D. L. (2009). Gas Exchange at the Air–Water Interface. In *Encyclopedia of Inland Waters* (pp. 70–78). Elsevier. https://doi.org/10.1016/B978-012370626-3.00213-1

Barker, J. D., Sharp, M. J., Fitzsimons, S. J., & Turner, R. J. (2006). Abundance and dynamics of dissolved organic carbon in glacier systems. *Arctic, Antarctic, and Alpine Research*, *38*(2), 163–172. https://doi.org/10.1657/1523-0430(2006)38[163:AADODO]2.0.CO;2

Bagshaw, E. A., Wadham, J. L., Tranter, M., Beaton, A. D., Hawkings, J. R., Lamarche-Gagnon, G., & Mowlem, M. C. (2021). Measuring pH in low ionic strength glacial meltwaters using ion selective field effect transistor (ISFET) technology. *Limnology and Oceanography: Methods*, *19*(3), 222–233. https://doi.org/10.1002/lom3.10416

Beal, S. A., Osterberg, E. C., Zdanowicz, C. M., & Fisher, D. A. (2015). Ice core perspective on mercury pollution during the past 600 years. *Environmental Science and Technology*, *49*(13), 7641–7647. https://doi.org/10.1021/acs.est.5b01033

Beniston, M. (2003). Climatic change in mountain regions: A review of possible impacts. *Climatic Change*, *59*, 5–31. https://doi.org/10.1007/978-94-015-1252-7_2

Bennet, M. R., & Glasser, N. F. (2009). Glacial geology: Ice sheets and landforms. In *Glacial Geology: Ice Sheets and Landforms* (2nd ed.). Wiley-Blackwell.

Bennett, D. E., Gosnell, H., Lurie, S., & Duncan, S. (2014). Utility engagement with payments for watershed services in the United States. *Ecosystem Services*, *8*, 56–64. https://doi.org/10.1016/j.ecoser.2014.02.001

Beria, H., Larsen, J. R., Ceperley, N. C., Michelon, A., Vennemann, T., & Schaefli, B. (2018). Understanding snow hydrological processes through the lens of stable water isotopes. *Wiley Interdisciplinary Reviews: Water*, *5*(6), 1–23. https://doi.org/10.1002/wat2.1311

Berner, R. A. (1992). Weathering, plants, and the long-term carbon cycle. *Geochimica et Cosmochimica Acta*, *56*(8), 3225–3231. https://doi.org/10.1016/0016-7037(92)90300-8

Bershaw, J., Hansen, D. D., & Schauer, A. J. (2020). Deuterium excess and 17O-excess variability in meteoric water across the Pacific Northwest, USA. *Tellus B: Chemical and Physical Meteorology*, *72*(1), 1–17. https://doi.org/10.1080/16000889.2020.1773722

Bhatia, M. P., Das, S. B., Kujawinski, E. B., Henderson, P., Burke, A., & Charette, M. A. (2011). Seasonal evolution of water contributions to discharge from a Greenland outlet glacier: Insight from a new isotope-mixing model. *Journal of Glaciology*, *57*(205), 929–941. https://doi.org/10.3189/002214311798043861

Blais, J. M., Schindler, D. W., G Muir, D. C., Sharp, M., Donald, D., Lafrenière, M., Braekevelt, E., & J Strachan, W. M. (2001). Melting glaciers: A major source of persistent organochlorines to subalpine Bow Lake in Banff National Park, Canada. *Ambio*, *30*(7), 410–415.

Bliss, A., Hock, R., & Radić, V. (2014). Global response of glacier runoff to twenty-first century climate change. *Journal of Geophysical Research: Earth Surface*, *119*(4), 717–730. https://doi.org/10.1002/2013JF002931

Blum, J. D., Gazis, C. A., Jacobson, A. D., & Page Chamberlain, C. (1998). Carbonate versus silicate weathering in the Raikhot watershed within the High Himalayan Crystalline Series. *Geology*, *26*(5), 411. https://doi.org/10.1130/0091-7613(1998)026<0411:CVSWIT>2.3.CO;2

Bogen, J., Xu, M., & Kennie, P. (2015). The impact of pro-glacial lakes on downstream sediment delivery in Norway. *Earth Surface Processes and Landforms*, *40*(7), 942–952. https://doi.org/10.1002/esp.3669

Bortone, G. (2007). Sediment Treatment—A General Introduction. In *Sustainable Management of Sediment Resources* (Vol. 2, pp. 1–10). Elsevier. https://doi.org/10.1016/S1872-1990(07)80013-4

Boutron, C. F. (1995). Historical reconstruction of the earth's past atmospheric environment from Greenland and Antarctic snow and ice cores. *Environmental Reviews*, *3*(1), 1–28. https://doi.org/10.1139/a95-001

Bowman, M. F., Chambers, P. A., & Schindler, D. W. (2005). Epilithic algal abundance in relation to anthropogenic changes in phosphorus bioavailability and limitation in mountain rivers. *Canadian Journal of Fisheries and Aquatic Sciences*, *62*(1), 174–184. https://doi.org/10.1139/f04-244

Bowman, M. F., Chambers, P. A., & Schindler, D. W. (2007). Constraints on benthic algal response to nutrient addition in oligotrophic mountain rivers. *River Research and Applications*, *23*(8), 858–876. https://doi.org/10.1002/rra.1025

Bratby, J. (2016). Chapter 3. Coagulants. In *Coagulation and Flocculation in Water and Wastewater Treatment* (3rd ed.). IWA Publishing.

Brown, G. H., Tranter, M., & Sharp, M. J. (1996). Experimental investigations of the weathering of suspended sediment by alpine glacial meltwater. *Hydrological Processes*, *10*(4), 579–597. https://doi.org/10.1002/(SICI)1099-1085(199604)10:4<579::AID-HYP393>3.0.CO;2-D

Brown, G. H., Tranter, M., Sharp, M. J., Davies, T. D., & Tsiouris, S. (1994). Dissolved oxygen variations in alpine glacial meltwaters. *Earth Surface Processes and Landforms*, *19*(3), 247–253. https://doi.org/10.1002/esp.3290190305

Burke, A., Present, T. M., Paris, G., Rae, E. C. M., Sandilands, B. H., Gaillardet, J., Peucker-Ehrenbrink, B., Fischer, W. W., McClelland, J. W., Spencer, R. G. M., Voss, B. M., & Adkins, J. F. (2018). Sulfur isotopes in rivers: Insights into global weathering budgets, pyrite oxidation, and the modern sulfur cycle. *Earth and Planetary Science Letters*, *496*, 168–177. https://doi.org/10.1016/j.epsl.2018.05.022

Burns, D. A., Riva-Murray, K., Bradley, P. M., Aiken, G. R., & Brigham, M. E. (2012). Landscape controls on total and methyl Hg in the upper Hudson River basin, New York, USA. *Journal of Geophysical Research: Biogeosciences*, *117*(G1), 2011JG001812. https://doi.org/10.1029/2011JG001812

Calmels, D., Gaillardet, J., Brenot, A., & France-Lanord, C. (2007). Sustained sulfide oxidation by physical erosion processes in the Mackenzie River basin: Climatic perspectives. *Geology*, *35*(11), 1003. https://doi.org/10.1130/G24132A.1

Campbell, É. M. S., & Ryan, M. C. (2021). Nested recharge systems in mountain block hydrology: High-elevation snowpack generates low-elevation overwinter baseflow in a Rocky Mountain river. *Water (Switzerland)*, *13*(16). https://doi.org/10.3390/w13162249

Carroll, R. W. H., Deems, J., Maxwell, R., Sprenger, M., Brown, W., Newman, A., Beutler, C., Bill, M., Hubbard, S. S., & Williams, K. H. (2022). Variability in observed stable water isotopes in snowpack across a mountainous watershed in Colorado. *Hydrological Processes*, *36*(8). https://doi.org/10.1002/hyp.14653

Carroll, R. W. H., Deems, J., Sprenger, M., Maxwell, R., Brown, W., Newman, A., Beutler, C., & Williams, K. H. (2022). Modeling snow dynamics and stable water isotopes across mountain landscapes. *Geophysical Research Letters*, *49*(20). https://doi.org/10.1029/2022GL098780

Carrivick, J. L., & Tweed, F. S. (2013). Proglacial lakes: Character, behaviour and geological importance. *Quaternary Science Reviews*, *78*, 34–52. https://doi.org/10.1016/j.quascirev.2013.07.028

Cauvy-Fraunié, S., & Dangles, O. (2019). A global synthesis of biodiversity responses to glacier retreat. *Nature Ecology & Evolution*, *3*(12), 1675–1685. https://doi.org/10.1038/s41559-019-1042-8

Clark, L. M. (1949). Geology of Rocky Mountain front ranges near Bow River, Alberta. *Bulletin of the American Association of Petroleum Geologists*, *33*(4), 614–633. https://doi.org/10.1306/sv15347c2

Clarke, G. K. C., Jarosch, A. H., Anslow, F. S., Radić, V., & Menounos, B. (2015). Projected deglaciation of western Canada in the twenty-first century. *Nature Geoscience*, *8*(5), 372–377. https://doi.org/10.1038/ngeo2407

Comeau, L. E. L., Pietroniro, A., & Demuth, M. N. (2009). Glacier contribution to the North and South Saskatchewan rivers. *Hydrological Processes*, *23*, 2640–2653. https://doi.org/10.1002/hyp.7409

Comiti, F., Mao, L., Penna, D., Dell'Agnese, A., Engel, M., Rathburn, S., & Cavalli, M. (2019). Glacier melt runoff controls bedload transport in Alpine catchments. *Earth and Planetary Science Letters*, *520*, 77–86. https://doi.org/10.1016/j.epsl.2019.05.031

Copernicus. (2024). *Global Climate Highlights 2023*. https://climate.copernicus.eu/copernicus-2023-hottest-year-record

Criscitiello, A. S., Marshall, S. J., Evans, M. J., Kinnard, C., Norman, A. L., & Sharp, M. J. (2016). Marine aerosol source regions to prince of Wales Icefield, Ellesmere Island, and influence from the tropical Pacific, 1979-2001. *Journal of Geophysical Research*, *121*(16), 9492–9507. https://doi.org/10.1002/2015JD024457

Crutzen, P. J., & Stoermer, E. F. (2000). The "Anthropocene." *Global Change Newsletter*, *41*, 17–18.

Dansgaard, W. (1964). Stable isotopes in precipitation. *Tellus*, *16*(4), 436–468. https://doi.org/10.1111/j.2153-3490.1964.tb00181.x

Demuth, M. N., & Horne, G. (2017). *Decadal-centenary glacier mass changes and their variability, Jasper National Park of Canada, Alberta, including the Columbia Icefield region* (Issue December). https://doi.org/10.4095/302705

Demuth, M. N., & Pietroniro, A. (2003). *The impact of climate change on the glaciers of the Canadian Rocky Mountain eastern slopes and implications for water resource-related adaptation in the Canadian prairies 'Phase I'- Headwaters of the North Saskatchewan River Basin*.

Deuerling, K. M., Martin, J. B., Martin, E. E., Abermann, J., Myreng, S. M., Petersen, D., & Rennermalm, Å. K. (2019). Chemical weathering across the western foreland of the Greenland Ice Sheet. *Geochimica et Cosmochimica Acta*, *245*, 426–440. https://doi.org/10.1016/j.gca.2018.11.025

Deuerling, K. M., Martin, J. B., Martin, E. E., & Scribner, C. A. (2018). Hydrologic exchange and chemical weathering in a proglacial watershed near Kangerlussuaq, west Greenland. *Journal of Hydrology*, *556*, 220–232. https://doi.org/10.1016/j.jhydrol.2017.11.002

Dixon, J. C., & Thorn, C. E. (2005). Chemical weathering and landscape development in mid-latitude alpine environments. *Geomorphology*, *67*(1-2 SPEC. ISS.), 127–145. https://doi.org/10.1016/j.geomorph.2004.07.009

Dodds, W. K., & Whiles, M. R. (2020). Freshwater Ecology. *Aquatic Ecology* (3rd Edition). Cambridge, MA: Academic Press.

Donnini, M., Frondini, F., Probst, J.-L., Probst, A., Cardellini, C., Marchesini, I., & Guzzetti, F. (2016). Chemical weathering and consumption of atmospheric carbon dioxide in the Alpine region. *Global and Planetary Change*, *136*, 65–81. https://doi.org/10.1016/j.gloplacha.2015.10.017

Drapeau, H. F., Tank, S. E., Cavaco, M., Serbu, J. A., St.Louis, V., & Bhatia, M. P. (2023). Shifts in organic matter character and microbial community structure from glacial headwaters to downstream reaches in Canadian Rocky Mountain rivers. *Biogeosciences Discussions*, *in review*. https://doi.org/10.5194/bg-2023-121

Dubnick, A., Kazemi, S., Sharp, M., Wadham, J., Hawkings, J., Beaton, A., & Lanoil, B. (2017). Hydrological controls on glacially exported microbial assemblages. *Journal of Geophysical Research: Biogeosciences*, *122*(5), 1049–1061. https://doi.org/10.1002/2016JG003685

Emmerton, C. A., Drevnick, P. E., Serbu, J. A., Cooke, C. A., Graydon, J. A., Reichert, M., Evans, M. S., & McMaster, M. E. (2023). Downstream modification of mercury in diverse river systems underscores the role of local conditions in fish bioaccumulation. *Ecosystems*, *26*(1), 114–133. https://doi.org/10.1007/s10021-022-00745-w

Environment and Climate Change Canada. (2019). Monthly climate summaries Alberta [Dataset]. https://climate.weather.gc.ca/prods_servs/cdn_climate_summary_e.html. Retrieved April 2023.

Environment and Climate Change Canada. (2020). Monthly climate summaries Alberta [Dataset]. https://climate.weather.gc.ca/prods_servs/cdn_climate_summary_e.html. Retrieved April 2023.

EPCOR. (2024). *E.L. Smith Water Treatment Plant*. https://www.epcor.com/about/who-we-are-what-we-do/about-our-company/where-we-operate/edmonton/Pages/el-smith-water-treatment-plant.aspx

Felden, J., Möller, L., Schindler, U., Huber, R., Schumacher, S., Koppe, R., Diepenbroek, M., & Glöckner, F. O. (2023). PANGAEA - Data Publisher for Earth & Environmental Science. *Scientific Data*, *10*(1), 347. https://doi.org/10.1038/s41597-023-02269-x

Fernández, P., Carrera, G., Grimalt, J. O., Ventura, M., Camarero, L., Catalan, J., Nickus, U., Thies, H., & Psenner, R. (2003). Factors governing the atmospheric deposition of polycyclic aromatic hydrocarbons to remote areas. *Environmental Science and Technology*, *37*(15), 3261–3267. https://doi.org/10.1021/es020137k

Fink-Mercier, C., Lapierre, J., Amyot, M., & Del Giorgio, P. A. (2022). Concentrations and yields of total Hg and MeHg in large boreal rivers linked to water and wetland coverage in the watersheds. *Journal of Geophysical Research: Biogeosciences*, *127*(5), e2022JG006892. https://doi.org/10.1029/2022JG006892

Gadd, B. (2009). *Handbook of the Canadian Rockies*. Corex Press.

Gaillardet, J., Dupré, B., Louvat, P., & Allègre, C. J. (1999). Global silicate weathering and CO2 consumption rates deduced from the chemistry of large rivers. *Chemical Geology*, *159*(1–4), 3–30. https://doi.org/10.1016/S0009-2541(99)00031-5

Gardner, A. S., Moholdt, G., Cogley, J. G., Wouters, B., Arendt, A. A., Wahr, J., Berthier, E., Hock, R., Pfeffer, W. T., Kaser, G., Ligtenberg, S. R. M., Bolch, T., Sharp, M. J., Hagen, J. O., Van Den Broeke, M. R., & Paul, F. (2013). A reconciled estimate of glacier contributions to sea level rise: 2003 to 2009. *Science*, *340*(6134), 852–857. https://doi.org/10.1126/science.1234532

Geilhausen, M., Morche, D., Otto, J.-C., & Schrott, L. (2013). Sediment discharge from the proglacial zone of a retreating Alpine glacier. *Zeitschrift Für Geomorphologie, Supplementary Issues*, *57*(2), 29–53. https://doi.org/10.1127/0372-8854/2012/s-00122

Gibson, J. J., Holmes, T., Stadnyk, T. A., Birks, S. J., Eby, P., & Pietroniro, A. (2020). 18O and 2H in streamflow across Canada. In *Journal of Hydrology: Regional Studies* (Vol. 32). Elsevier B.V. https://doi.org/10.1016/j.ejrh.2020.100754

Gilbert, R., & Shaw, J. (1981). Sedimentation in proglacial Sunwapta Lake, Alberta. *Canadian Journal of Earth Sciences*, *18*(1), 81–93. https://doi.org/10.1139/e81-007

Goff, J. R., & Ashmore, P. (1994). Gravel transport and morphological change in braided Sunwapta River, Alberta, Canada. *Earth Surface Processes and Landforms*, *19*(3), 195–212. https://doi.org/10.1002/esp.3290190302

Government of Alberta. (2005). *2005 Natural Regions and Subregions of Alberta* [Map]. Government of Alberta.

Government of Alberta. (2024a). *Alberta River Basins*. Alberta River Basins. https://rivers.alberta.ca

Government of Alberta. (2024b). *Water Quality Data Portal*. Water Quality Data Portal. https://environment.extranet.gov.ab.ca/apps/WaterQuality/dataportal/

Graly, J. A., Humphrey, N. F., Landowski, C. M., & Harper, J. T. (2014). Chemical weathering under the Greenland Ice Sheet. *Geology*, *42*(6), 551–554. https://doi.org/10.1130/G35370.1

Habibullah, M. S., Din, B. H., Tan, S.-H., & Zahid, H. (2022). Impact of climate change on biodiversity loss: Global evidence. *Environmental Science and Pollution Research*, *29*(1), 1073–1086. https://doi.org/10.1007/s11356-021-15702-8

Hall, R. O., & Ulseth, A. J. (2020). Gas exchange in streams and rivers. *WIREs Water*, *7*(1), e1391. https://doi.org/10.1002/wat2.1391

Halofsky, J. E., Peterson, D. L., & Harvey, B. J. (2020). Changing wildfire, changing forests: The effects of climate change on fire regimes and vegetation in the Pacific Northwest, USA. *Fire Ecology*, *16*(1), 4. https://doi.org/10.1186/s42408-019-0062-8

Hawkings, J. R., Benning, L. G., Raiswell, R., Kaulich, B., Araki, T., Abyaneh, M., Stockdale, A., Koch-Müller, M., Wadham, J. L., & Tranter, M. (2018). Biolabile ferrous iron bearing nanoparticles in glacial sediments. *Earth and Planetary Science Letters*, *493*, 92–101. https://doi.org/10.1016/j.epsl.2018.04.022

Hawkings, J. R., Skidmore, M. L., Wadham, J. L., Priscu, J. C., Morton, P. L., & Hatton, J. E. (2020). Enhanced trace element mobilization by Earth's ice sheets. *Proceedings of the National Academy of Sciences of the United States of America*, 1–12. https://doi.org/10.1073/pnas.2014378117

Hayashi, M. (2020). Alpine hydrogeology: The critical role of groundwater in sourcing the headwaters of the world. *Groundwater*, *58*(4), 498–510. https://doi.org/10.1111/gwat.12965

Health Canada. (1979). *Guidelines for Canadian Drinking Water Quality: Guideline Technical Document—Mercury*. Water and Air Quality Bureau, Healthy Environments and Consumer Safety Branch, Health Canada.

Health Canada. (2022). *Guidelines for Canadian Drinking Water Quality—Summary Tables*. Water and Air Quality Bureau, Healthy Environments and Consumer Safety Branch, Health Canada.

Helsel, D. R. (1990). Less than obvious: Statistical treatment of data below the detection limit. *Environmental Science & Technology*, *24*(12), 1766–1774.

Heusser, C. J. (1956). Postglacial environments in the Canadian Rocky Mountains. *Ecological Monographs*, *26*(4), 263–302. https://doi.org/10.2307/1948543

Higgs, E. S. (2023). *Mountain Legacy Project*. University of Victoria, Canada. Retrieved 28 June 2023, from https://explore.mountainlegacy.ca

Hindshaw, R. S., Rickli, J., Leuthold, J., Wadham, J., & Bourdon, B. (2014). Identifying weathering sources and processes in an outlet glacier of the Greenland Ice Sheet using Ca and Sr isotope ratios. *Geochimica et Cosmochimica Acta*, *145*, 50–71. https://doi.org/10.1016/j.gca.2014.09.016

Hodson, A., Tranter, M., & Vatne, G. (2000). Contemporary rates of chemical denudation and atmospheric CO2 sequestration in glacier basins: An Arctic perspective. *Earth Surface Processes and Landforms*, *25*, 1447–1471.

Hoegh-Guldberg, O., Jacob, D., Taylor, M., Guillén Bolaños, T., Bindi, M., Brown, S., Camilloni, I. A., Diedhiou, A., Djalante, R., Ebi, K., Engelbrecht, F., Guiot, J., Hijioka, Y., Mehrotra, S., Hope, C. W., Payne, A. J., Pörtner, H.-O., Seneviratne, S. I., Thomas, A., … Zhou, G. (2019). The human imperative of stabilizing global climate change at 1.5°C. *Science*, *365*(6459), eaaw6974. https://doi.org/10.1126/science.aaw6974

Holdsworth, G., Fogarasi, S., & Krouse, H. R. (1991). Variation of the stable isotopes of water with altitude in the Saint Elias Mountains of Canada. *Journal of Geophysical Research*, *96*(D4), 7483–7494. https://doi.org/10.1029/91JD00048

Hood, E., Battin, T. J., Fellman, J., O'neel, S., & Spencer, R. G. M. (2015). Storage and release of organic carbon from glaciers and ice sheets. *Nature Geoscience*, *8*(2), 91–96. https://doi.org/10.1038/ngeo2331

Hood, E., & Scott, D. (2008). Riverine organic matter and nutrients insoutheast Alaska affected by glacial coverage. *Nature Geoscience*, *1*(9), 583–587. https://doi.org/10.1038/ngeo280

Hopwood, M. J., Statham, P. J., Tranter, M., & Wadham, J. L. (2014). Glacial flours as a potential source of Fe(II) and Fe(III) to polar waters. *Biogeochemistry*, *118*(1–3), 443–452. https://doi.org/10.1007/s10533-013-9945-y

Horgby, Å., Canadell, M. B., Ulseth, A. J., Vennemann, T. W., & Battin, T. J. (2019). High-resolution spatial sampling identifies groundwater as driver of CO2 dynamics in an alpine stream network. *Journal of Geophysical Research: Biogeosciences*, *124*(7), 1961–1976. https://doi.org/10.1029/2019JG005047

Hovsepyan, A., & Bonzongo, J.-C. J. (2009). Aluminum drinking water treatment residuals (Al-WTRs) as sorbent for mercury: Implications for soil remediation. *Journal of Hazardous Materials*, *164*(1), 73–80. https://doi.org/10.1016/j.jhazmat.2008.07.121

Houghton, R. A., & Woodwell, G. M. (1989). Global climatic change. *Scientific American*.

Hu, J., Yan, Y., Yeung, L. Y., & Dee, S. G. (2022). Sublimation origin of negative deuterium excess observed in snow and ice samples from McMurdo Dry Valleys and Allan Hills blue ice areas, East Antarctica. *Journal of Geophysical Research: Atmospheres*, *127*(11). https://doi.org/10.1029/2021JD035950

Hurley, J. P., Benoit, J. M., Babiarz, C. L., Shafer, M. M., Andren, A. W., Sullivan, J. R., Hammond, Richard., & Webb, D. A. (1995). Influences of watershed characteristics on mercury levels in Wisconsin rivers. *Environmental Science & Technology*, *29*(7), 1867–1875. https://doi.org/10.1021/es00007a026

Huss, M., Bookhagen, B., Huggel, C., Jacobsen, D., Bradley, R. S., Clague, J. J., Vuille, M., Buytaert, W., Cayan, D. R., Greenwood, G., Mark, B. G., Milner, A. M., Weingartner, R., & Winder, M. (2017). Toward mountains without permanent snow and ice. *Earth's Future*, *5*(5), 418–435. https://doi.org/10.1002/2016EF000514

Huss, M., & Hock, R. (2018). Global-scale hydrological response to future glacier mass loss. *Nature Climate Change*, *8*(2), 135–140. https://doi.org/10.1038/s41558-017-0049-x

Immerzeel, W. W., Lutz, A. F., Andrade, M., Bahl, A., Biemans, H., Bolch, T., Hyde, S., Brumby, S., Davies, B. J., Elmore, A. C., Emmer, A., Feng, M., Fernández, A., Haritashya, U., Kargel, J. S., Koppes, M., Kraaijenbrink, P. D. A., Kulkarni, A. V., Mayewski, P. A., … Baillie, J. E. M. (2020). Importance and vulnerability of the world's water towers. *Nature*, *577*(7790), 364–369. https://doi.org/10.1038/s41586-019-1822-y

International Atomic Energy Agency. (2009). Laser spectroscopic analysis of liquid water samples for stable hydrogen and oxygen isotopes. In IAEA, *Training Course Series No. 35*.

IPCC. (2023). *Climate Change 2023: Synthesis Report. Contribution of Working Groups I, II, and III to the Sixth Assessment Report of the Intergovernmental Panel on Climate Change*.

Ishikawa, N. F., Doi, H., & Finlay, J. C. (2012). Global meta-analysis for controlling factors on carbon stable isotope ratios of lotic periphyton. *Oecologia*, *170*(2), 541–549. https://doi.org/10.1007/s00442-012-2308-x

Isson, T. T., Planavsky, N. J., Coogan, L. A., Stewart, E. M., Ague, J. J., Bolton, E. W., Zhang, S., McKenzie, N. R., & Kump, L. R. (2020). Evolution of the global carbon cycle and climate regulation on Earth. *Global Biogeochemical Cycles*, *34*(2), e2018GB006061. https://doi.org/10.1029/2018GB006061

Jansson, P., Hock, R., & Schneider, T. (2003). The concept of glacier storage: A review. *Journal of Hydrology*, *282*(1–4), 116–129. https://doi.org/10.1016/S0022-1694(03)00258-0

Jenckes, J., Muñoz, S., Ibarra, D. E., Boutt, D. F., & Munk, L. A. (2024). Geochemical weathering variability in high latitude watersheds of the Gulf of Alaska. *Journal of Geophysical Research: Earth Surface*, *129*(3), e2023JF007284. https://doi.org/10.1029/2023JF007284

Joint Task Group on Calcium Carbonate Saturation. (1990). Suggested methods for calculating and interpreting calcium carbonate saturation indexes. *American Water Works Association*, *82*(7), 71–77.

Kalnay, E., Kanamitsu, M., Kistler, R., Collins, W., Deaven, D., Gandin, L., Iredell, M., Saha, S., White, G., Woollen, J., Zhu, Y., Chelliah, M., Ebisuzaki, + W, Higgins, + W, Janowiak, + J, Mo, + K C, Ropelewski, + C, Wang, + J, Leetmaa, + A, … Joseph, D. (1996). The NCEP/NCAR 40-Year Reanalysis Project. *Bulletin of the American Meteorological Society*, *77*(3), 437–471.

Karl, T. R., & Trenberth, K. E. (2003). Modern global climate change. *Science*, *302*(5651), 1719–1723. https://doi.org/10.1126/science.1090228

Kassambara, A., & Mundt, F. (2020). *factoextra: Extract and visualize the results of multivariate data analyses*. R package version 1.0.7, https://CRAN.R-project.org/package=factoextra

Keeling, C. D. (1960). The concentration and isotopic abundances of carbon dioxide in the atmosphere. *Tellus*, *12*(2), 200–203. https://doi.org/10.1111/j.2153-3490.1960.tb01300.x

Kemeny, P. C., Torres, M. A., Lamb, M. P., Webb, S. M., Dalleska, N., Cole, T., Hou, Y., Marske, J., Adkins, J. F., & Fischer, W. W. (2021). Organic sulfur fluxes and geomorphic control of sulfur isotope ratios in rivers. *Earth and Planetary Science Letters*, *562*, 116838. https://doi.org/10.1016/j.epsl.2021.116838

Kempe, S. (1988). Freshwater Carbon and the Weathering Cycle. In A. Lerman & M. Meybeck (Eds.), *Physical and Chemical Weathering in Geochemical Cycles* (pp. 197–223). Springer Netherlands. https://doi.org/10.1007/978-94-009-3071-1_10

Khadka, M. B., Martin, J. B., & Jin, J. (2014). Transport of dissolved carbon and CO2 degassing from a river system in a mixed silicate and carbonate catchment. *Journal of Hydrology*, *513*, 391–402. https://doi.org/10.1016/j.jhydrol.2014.03.070

Knight, J. (2022). Scientists' warning of the impacts of climate change on mountains. *PeerJ*, *10*, e14253. https://doi.org/10.7717/peerj.14253

Kohler, T. J., Fodelianakis, S., Michoud, G., Ezzat, L., Bourquin, M., Peter, H., Busi, S. B., Pramateftaki, P., Deluigi, N., Styllas, M., Tolosano, M., de Staercke, V., Schön, M., Brandani, J., Marasco, R., Daffonchio, D., Wilmes, P., & Battin, T. J. (2022). Glacier shrinkage will accelerate downstream decomposition of organic matter and alters microbiome structure and function. *Global Change Biology*, *28*(12), 3846–3859. https://doi.org/10.1111/gcb.16169

Lafrenière, M. J., & Sharp, M. J. (2004). The concentration and fluorescence of dissolved organic carbon (DOC) in glacial and nonglacial catchments: Interpreting hydrological flow routing and DOC sources. *Arctic, Antarctic, and Alpine Research*, *36*(2), 156–165. https://doi.org/10.1657/1523-0430(2004)036[0156:TCAFOD]2.0.CO;2

Lafrenière, M. J., & Sharp, M. J. (2005). A comparison of solute fluxes and sources from glacial and non-glacial catchments over contrasting melt seasons. *Hydrological Processes*, *19*(15), 2991–3012. https://doi.org/10.1002/hyp.5812

Lafrenière, M. J., & Sinclair, K. E. (2011). Snowpack and precipitation chemistry at a high altitude site in the Canadian Rocky Mountains. *Journal of Hydrology*, *409*(3–4), 737–748. https://doi.org/10.1016/j.jhydrol.2011.09.007

Lalonde, J. D., Amyot, M., Kraepiel, A. M. L., & Morel, F. M. M. (2001). Photooxidation of Hg(0) in artificial and natural waters. *Environmental Science & Technology*, *35*(7), 1367–1372. https://doi.org/10.1021/es001408z

Lê, S., Josse, J., & Husson, F. (2008). FactoMineR: An R package for multivariate analysis. *Journal of Statistical Software*, *25*(1), 1–18. https://doi.org/10.18637/jss.v025.i01

Lehnherr, I., & St. Louis, V. L. (2009). Importance of ultraviolet radiation in the photodemethylation of methylmercury in freshwater ecosystems. *Environmental Science & Technology*, *43*(15), 5692–5698. https://doi.org/10.1021/es9002923

Li, L., Knapp, J. L. A., Lintern, A., Ng, G.-H. C., Perdrial, J., Sullivan, P. L., & Zhi, W. (2024). River water quality shaped by land–river connectivity in a changing climate. *Nature Climate Change*, *14*(3), 225–237. https://doi.org/10.1038/s41558-023-01923-x

Li, P., & Wu, J. (2019). Drinking water quality and public health. *Exposure and Health*, *11*(2), 73–79. https://doi.org/10.1007/s12403-019-00299-8

Li, S.-L., Calmels, D., Han, G., Gaillardet, J., & Liu, C.-Q. (2008). Sulfuric acid as an agent of carbonate weathering constrained by δ13CDIC: Examples from Southwest China. *Earth and Planetary Science Letters*, *270*(3–4), 189–199. https://doi.org/10.1016/j.epsl.2008.02.039

Li, X., Wang, N., Ding, Y., Hawkings, J. R., Yde, J. C., Raiswell, R., Liu, J., Zhang, S., Kang, S., Wang, R., Liu, Q., Liu, S., Bol, R., You, X., & Li, G. (2022). Globally elevated chemical weathering rates beneath glaciers. *Nature Communications*, *13*(1), 407. https://doi.org/10.1038/s41467-022-28032-1

Liu, Z., Dreybrodt, W., & Liu, H. (2011). Atmospheric CO_2 sink: Silicate weathering or carbonate weathering? *Applied Geochemistry*, *26*, S292–S294. https://doi.org/10.1016/j.apgeochem.2011.03.085

Lorenz, D., Runkel, R., De Cicco, L., Watkins, D., & Stachelek, J. (2017). *rloadest: River load estimation, version 0.4.5*. U.S. Geological Survey.

Ma, X., Subramanian, K. S., Chakrabarti, C. L., Guo, R., Cheng, J., Lu, Y., & Pickering, W. F. (1992). Removal of trace mercury(II) from drinking water: Sorption by granular activated carbon. *Journal of Environmental Science and Health . Part A: Environmental Science and Engineering and Toxicology*, *27*(6), 1389–1404. https://doi.org/10.1080/10934529209375802

Mackenzie, F. T., & Garrels, R. M. (1966). Chemical mass balance between rivers and oceans. *American Journal of Science*, *264*, 507–525.

Madakumbura, G. D., Kim, H., Utsumi, N., Shiogama, H., Fischer, E. M., Seland, Ø., Scinocca, J. F., Mitchell, D. M., Hirabayashi, Y., & Oki, T. (2019). Event-to-event intensification of the hydrologic cycle from 1.5°C to a 2°C warmer world. *Scientific Reports*, *9*(1), 3483. https://doi.org/10.1038/s41598-019-39936-2

Mahindawansha, A., Jost, M., & Gassmann, M. (2022). Spatial and temporal variations of stable isotopes in precipitation in the mountainous region, North Hesse. *Water (Switzerland)*, *14*(23). https://doi.org/10.3390/w14233910

Malard, F., Uehlinger, U., Zah, R., & Tockner, K. (2006). Flood-pulse and riverscape dynamics in a braided glacial river. *Ecology*, *87*(3), 704–716. https://doi.org/10.1890/04-0889

Malhi, Y. (2017). The concept of the Anthropocene. *Annual Review of Environment and Resources*, *42*, 77–104. https://doi.org/10.1146/annurev- environ102016- 060854

Mancini, D., Dietze, M., Müller, T., Jenkin, M., Miesen, F., Roncoroni, M., Nicholas, A. P., & Lane, S. N. (2023). Filtering of the signal of sediment export from a glacier by its proglacial forefield. *Geophysical Research Letters*, *50*(21), e2023GL106082. https://doi.org/10.1029/2023GL106082

Mansilha, C., Carvalho, A., Guimarães, P., & Marques, J. E. (2014). Water quality concerns due to forest fires: Polycyclic aromatic hydrocarbons (PAH) contamination of groundwater from mountain areas. *Journal of Toxicology and Environmental Health - Part A: Current Issues*, *77*(14–16), 806–815. https://doi.org/10.1080/15287394.2014.909301

Marshall, S. J. (2014). Meltwater run-off from Haig Glacier, Canadian Rocky Mountains, 2002-2013. *Hydrology and Earth System Sciences*, *18*(12), 5181–5200. https://doi.org/10.5194/hess-18-5181-2014

Marshall, S. J., White, E. C., Demuth, M. N., Bolch, T., Wheate, R., Menounos, B., Beedle, M. J., & Shea, J. M. (2011). Glacier water resources on the eastern slopes of the Canadian Rocky Mountains. *Canadian Water Resources Journal*, *36*(2), 109–134. https://doi.org/10.4296/cwrj3602823

Marshall, S., & White, E. (2010). *Alberta glacier inventory and ice volume estimation* (Issue December).

Marvin, C. H., Berthiaume, A., Burniston, D. A., Chibwe, L., Dove, A., Evans, M., Hewitt, L. M., Hodson, P. V., Muir, D. C. G., Parrott, J., Thomas, P. J., & Tomy, G. T. (2021). Polycyclic aromatic compounds in the Canadian Environment: Aquatic and terrestrial environments. In *Environmental Pollution* (Vol. 285). Elsevier Ltd. https://doi.org/10.1016/j.envpol.2021.117442

Marwick, T. R., Tamooh, F., Teodoru, C. R., Borges, A. V., Darchambeau, F., & Bouillon, S. (2015). The age of river-transported carbon: A global perspective. *Global Biogeochemical Cycles*, *29*(2), 122–137. https://doi.org/10.1002/2014GB004911

Menounos, B., Hugonnet, R., Shean, D., Gardner, A., Howat, I., Berthier, E., Pelto, B., Tennant, C., Shea, J., Noh, M. J., Brun, F., & Dehecq, A. (2019). Heterogeneous changes in western North American glaciers linked to decadal variability in zonal wind strength. *Geophysical Research Letters*, *46*(1), 200–209. https://doi.org/10.1029/2018GL080942

Meybeck, M. (1993). Riverine transport of atmospheric carbon: Sources, global typology and budget. *Water, Air, & Soil Pollution*, *70*(1–4), 443–463.

Miller, J. E., Kahl, J. D. W., Heller, F., & Harris, J. M. (2002). A three-dimensional residence-time analysis of potential summertime atmospheric transport to Summit, Greenland. *Annals of Glaciology*, *35*. https://www.cambridge.org/core.

Millot, R., Gaillardet, J., Dupré, B., & Allègre, C. J. (2002). The global control of silicate weathering rates and the coupling with physical erosion: New insights from rivers of the Canadian Shield. *Earth and Planetary Science Letters*, *196*(1–2), 83–98. https://doi.org/10.1016/S0012-821X(01)00599-4

Millot, R., Gaillardet, J., Dupré, B., & Allègre, C. J. (2003). Northern latitude chemical weathering rates: Clues from the Mackenzie River Basin, Canada. *Geochimica et Cosmochimica Acta*, *67*(7), 1305–1329. https://doi.org/10.1016/S0016-7037(02)01207-3

Milner, A. M., Khamis, K., Battin, T. J., Brittain, J. E., Barrand, N. E., Füreder, L., Cauvy-Fraunié, S., Gíslason, G. M., Jacobsen, D., Hannah, D. M., Hodson, A. J., Hood, E., Lencioni, V., Ólafsson, J. S., Robinson, C. T., Tranter, M., & Brown, L. E. (2017). Glacier shrinkage driving global changes in downstream systems. *Proceedings of the National Academy of Sciences of the United States of America*, *114*(37), 9770–9778. https://doi.org/10.1073/pnas.1619807114

Mountjoy, E. W. (1962). *Mount Robson (southeast) map-area, Rocky Mountains of Alberta and British Columbia, 83E/SE* [Map]. Geological Survey of Canada. https://doi.org/10.4095/101251

Muñoz, S., Jenckes, J., Ramos, E. J., Munk, L. A., & Ibarra, D. E. (2024). Hydrologic and landscape controls on rock weathering along a glacial gradient in South Central Alaska, USA. *Journal of Geophysical Research: Earth Surface*, *129*(3), e2023JF007255. https://doi.org/10.1029/2023JF007255

Neal, C. (2002). Calcite saturation in eastern UK rivers. *Science of The Total Environment*, *282–283*, 311–326. https://doi.org/10.1016/S0048-9697(01)00921-4

Nicholls, R. (2011). Planning for the impacts of sea level rise. *Oceanography*, *24*(2), 144–157. https://doi.org/10.5670/oceanog.2011.34

Niu, Y., Castro, M. C., Hall, C. M., Aciego, S. M., & Arendt, C. A. (2017). Characterizing glacial meltwater sources in the Athabasca Glacier, Canada, using noble gases as tracers. *Applied Geochemistry*, *76*, 136–147. https://doi.org/10.1016/j.apgeochem.2016.11.015

Ommanney, C. S. L. (2002). Glaciers of the Canadian Rockies. In *Glaciers of North America*.

Pana, D. I., & Elgr, R. (2013). Geology of the Alberta Rocky Mountains and Foothills (Map No. 560). Edmonton, AB: Alberta Geological Survey.

Pasteris, D. R., McConnell, J. R., Das, S. B., Criscitiello, A. S., Evans, M. J., Maselli, O. J., Sigl, M., & Layman, L. (2014). Seasonally resolved ice core records from West Antarctica indicate a sea ice source of sea-salt aerosol and a biomass burning source of ammonium. *JGR: Atmospheres*, *119*(14), 9168–9182. https://doi.org/10.1002/2013JD020720

Paznekas, A., & Hayashi, M. (2016). Groundwater contribution to winter streamflow in the Canadian Rockies. *Canadian Water Resources Journal*, *41*(4), 484–499. https://doi.org/10.1080/07011784.2015.1060870

Pepin, N. C., Arnone, E., Gobiet, A., Haslinger, K., Kotlarski, S., Notarnicola, C., Palazzi, E., Seibert, P., Serafin, S., Schöner, W., Terzago, S., Thornton, J. M., Vuille, M., & Adler, C. (2022). Climate changes and their elevational patterns in the mountains of the world. *Reviews of Geophysics*, *60*(1), e2020RG000730. https://doi.org/10.1029/2020RG000730

Penn, K., Marshall, S. J., & Sinclair, K. E. (2023). Seasonal enrichment of heavy isotopes in meltwater runoff from Haig Glacier, Canadian Rocky Mountains. *Frontiers in Earth Science*, *11*. https://doi.org/10.3389/feart.2023.1125877

Pfahl, S., & Sodemann, H. (2014). What controls deuterium excess in global precipitation? *Climate of the Past*, *10*(2), 771–781. https://doi.org/10.5194/cp-10-771-2014

Price, M. F. (2015). Mountains: A very short introduction. In *Mountains: A Very Short Introduction*. Oxford University Press.

Price, R. A. (2000). *The Southern Canadian Rockies: Evolution of a Foreland Thrust and Fold Belt (Field Trip Guidebook)*. Canadian Society of Petroleum Geologists. DOI: 10.13140/2.1.2910.2887

Price, J. I., & Heberling, M. T. (2018). The effects of source water quality on drinking water treatment costs: A review and synthesis of empirical literature. *Ecological Economics*, *151*, 195–209. https://doi.org/10.1016/j.ecolecon.2018.04.014

Pryer, H. V., Hawkings, J. R., Wadham, J. L., Robinson, L. F., Hendry, K. R., Hatton, J. E., Kellerman, A. M., Bertrand, S., Gill‐Olivas, B., Marshall, M. G., Brooker, R. A., Daneri, G., & Häussermann, V. (2020). The influence of glacial cover on riverine silicon and iron exports in Chilean Patagonia. *Global Biogeochemical Cycles*, *34*(12). https://doi.org/10.1029/2020GB006611

Quiñones, K., Hovsepyan, A., Oppong-Anane, A., & Bonzongo, J.-C. J. (2016). Insights into the mechanisms of mercury sorption onto aluminum based drinking water treatment residuals. *Journal of Hazardous Materials*, *307*, 184–192. https://doi.org/10.1016/j.jhazmat.2016.01.001

R Core Team. (2022). *R: A language and environment for statistical computing*. R Foundation for Statistical Computing. https://www.R-project.org/

Race, D., Gentle, P., & Mathew, S. (2023). Living on the margins: Climate change impacts and adaptation by remote communities living in the Pacific Islands, the Himalaya and desert Australia. *Climate Risk Management*, *40*, 100503. https://doi.org/10.1016/j.crm.2023.100503

Radić, V., Bliss, A., Beedlow, A. C., Hock, R., Miles, E., & Cogley, J. G. (2014). Regional and global projections of twenty-first century glacier mass changes in response to climate scenarios from global climate models. *Climate Dynamics*, *42*(1–2), 37–58. https://doi.org/10.1007/s00382-013-1719-7

Raiswell, R. (1984). Chemical models of solute acquisition in glacial melt waters. *Journal of Glaciology*, *30*(104), 49–57. https://doi.org/10.3189/S0022143000008480

Relph, K. E., Stevenson, E. I., Turchyn, A. V., Antler, G., Bickle, M. J., Baronas, J. J., Darby, S. E., Parsons, D. R., & Tipper, E. T. (2021). Partitioning riverine sulfate sources using oxygen and sulfur isotopes: Implications for carbon budgets of large rivers. *Earth and Planetary Science Letters*, *567*, 116957. https://doi.org/10.1016/j.epsl.2021.116957

Rippin, D. M., Sharp, M., Van Wychen, W., & Zubot, D. (2020). 'Detachment' of icefield outlet glaciers: Catastrophic thinning and retreat of the Columbia Glacier (Canada). *Earth Surface Processes and Landforms*, *45*(2), 459–472. https://doi.org/10.1002/esp.4746

Robison, A. L., Deluigi, N., Rolland, C., Manetti, N., & Battin, T. (2023). Glacier loss and vegetation expansion alter organic and inorganic carbon dynamics in high-mountain streams. *Biogeosciences*, *20*(12), 2301–2316. https://doi.org/10.5194/bg-20-2301-2023

Rose, C. H., Ghosh, S., Blum, J. D., & Bergquist, B. A. (2015). Effects of ultraviolet radiation on mercury isotope fractionation during photo-reduction for inorganic and organic mercury species. *Chemical Geology*, *405*, 102–111. https://doi.org/10.1016/j.chemgeo.2015.02.025

Rounce, D. R., Hock, R., Maussion, F., Hugonnet, R., Kochtitzky, W., Huss, M., Berthier, E., Brinkerhoff, D., Compagno, L., Copland, L., Farinotti, D., Menounos, B., & Mcnabb, R. W. (2023). Global glacier change in the 21st century: Every increase in temperature matters. In *Science* (Vol. 379). https://www.science.org

Rubey, W. W. (1951). Geologic history of sea water: An attempt to state the problem. *Bulletin of the Geological Society of America*, *62*, 1111–1148.

Runkel, B. R. L., Crawford, C. G., & Cohn, T. A. (2004). Load Estimator (LOADEST): A FORTRAN program for estimating constituent loads in streams and rivers. In *Techniques and Methods Book 4*.

Scheili, A., Delpla, I., Sadiq, R., & Rodriguez, M. J. (2016). Impact of raw water quality and climate factors on the variability of drinking water quality in small systems. *Water Resources Management*, *30*(8), 2703–2718. https://doi.org/10.1007/s11269-016-1312-z

Schindler, D. W., & Donahue, W. F. (2006). An impending water crisis in Canada's western prairie provinces. *Proceedings of the National Academy of Sciences of the United States of America*, *103*(19), 7210–7216. https://doi.org/10.1073/pnas.0601568103

Schroth, A. W., Crusius, J., Chever, F., Bostick, B. C., & Rouxel, O. J. (2011). Glacial influence on the geochemistry of riverine iron fluxes to the Gulf of Alaska and effects of deglaciation. *Geophysical Research Letters*, *38*(16), n/a-n/a. https://doi.org/10.1029/2011GL048367

Schuster, J. K., Harner, T., Su, K., Mihele, C., & Eng, A. (2015). First results from the oil sands passive air monitoring network for polycyclic aromatic compounds. *Environmental Science and Technology*, *49*(5), 2991–2998. https://doi.org/10.1021/es505684e

Serbu, J. A., St.Louis, V. L., Emmerton, C. A., Tank, S. E., Criscitiello, A. S., Silins, U, Bhatia, M. P., Cavaco, M. A., Christenson, C., Cooke, C. A., Drapeau, H. F., Enns, S. J. A., Flett, J. E., Holland, K. M., Lavallee-Whiffen, J., Ma, M., Muir, C. E., Poesch, M., & Shin, J. Physicochemical, particulate matter, temperature, and hydrological datasets collected from climate-threatened glacial river headwaters on the eastern slopes of the Canadian Rocky Mountains (2019-2021). PANGAEA. https://doi.org/10.1594/PANGAEA.963863

Serbu, J. A., St. Louis, V. L., Emmerton, C. A., Tank, S. E., Criscitiello, A. S., Silins, U., Bhatia, M. P., Cavaco, M. A., Christenson, C., Cooke, C. A., Drapeau, H. F., Enns, S. J. A., Flett, J. E., Holland, K. M., Lavallee-Whiffen, J., Ma, M., Muir, C. E., Poesch, M., & Shin, J. (2024). A comprehensive biogeochemical assessment of climate-threatened glacial river headwaters on the eastern slopes of the Canadian Rocky Mountains. *Journal of Geophysical Research: Biogeosciences*, *129*(1), e2023JG007745. https://doi.org/10.1029/2023JG007745

Shah, A., Arjunan, A., Baroutaji, A., & Zakharova, J. (2023). A review of physicochemical and biological contaminants in drinking water and their impacts on human health. *Water Science and Engineering*, *16*(4), 333–344. https://doi.org/10.1016/j.wse.2023.04.003

Sharma, S., & Ahammed, M. M. (2023). Application of modified water treatment residuals in water and wastewater treatment: A review. *Heliyon*, *9*(5), e15796. https://doi.org/10.1016/j.heliyon.2023.e15796

Sharma, B. M., Nizzetto, L., Bharat, G. K., Tayal, S., Melymuk, L., Sáňka, O., Přibylová, P., Audy, O., & Larssen, T. (2015). Melting Himalayan glaciers contaminated by legacy atmospheric depositions are important sources of PCBs and high-molecular-weight PAHs for the Ganges floodplain during dry periods. *Environmental Pollution*, *206*, 588–596. https://doi.org/10.1016/j.envpol.2015.08.012

Sharp, M., Tranter, M., Brown, G. H., & Skidmore, M. (1995). Rates of chemical denudation and CO_2 drawdown in a glacier-covered alpine catchment. *Geology*, *23*(1), 61. https://doi.org/10.1130/0091-7613(1995)023<0061:ROCDAC>2.3.CO;2

Sinclair, K. E., & Marshall, S. J. (2008). Post-depositional modification of stable water isotopes in winter snowpacks in the Canadian Rocky Mountains. *Annals of Glaciology*, *49*, 96–106. https://doi.org/10.3189/172756408787814979

Sinclair, K. E., & Marshall, S. J. (2009). Temperature and vapour-trajectory controls on the stable-isotope signal in Canadian Rocky Mountain snowpacks. *Journal of Glaciology*, *55*(191), 485–498. https://doi.org/10.3189/002214309788816687

Skidmore, M., Sharp, M., & Tranter, M. (2004). Kinetic isotopic fractionation during carbonate dissolution in laboratory experiments: Implications for detection of microbial CO2 signatures using δ13C-DIC. *Geochimica et Cosmochimica Acta*, *68*(21), 4309–4317. https://doi.org/10.1016/j.gca.2003.09.024

Somers, L. D., & McKenzie, J. M. (2020). A review of groundwater in high mountain environments. In *Wiley Interdisciplinary Reviews: Water* (Vol. 7, Issue 6). John Wiley and Sons Inc. https://doi.org/10.1002/wat2.1475

Standard Methods Committee of the American Public Health Association, American Water Works Association, & Water Environment Federation. (a). Method 3125: Metals by Inductively Coupled Plasma-Mass Spectrometry (ICP-MS). In W. C. Lipps, T. E. Baxter, & E. Braun-Howland (Eds.), *Standard Methods for the Examination of Water and Wastewater*. APHA Press. https://doi.org/10.2105/smww.2882.048

Standard Methods Committee of the American Public Health Association, American Water Works Association, & Water Environment Federation. (b). Method 4500-NH3 (Ammonia). In W. C. Lipps, T. E. Baxter, & E. Braun-Howland (Eds.), *Standard Methods for the Examination of Water and Wastewater*. APHA Press. https://doi.org/10.2105/SMWW.2882.087

Standard Methods Committee of the American Public Health Association, American Water Works Association, & Water Environment Federation. (c). Method 4500-P (Phosphorus). In W. C. Lipps, T. E. Baxter, & E. Braun-Howland (Eds.), *Standard Methods for the Examination of Water and Wastewater*. APHA Press.

Standard Methods Committee of the American Public Health Association, American Water Works Association, & Water Environment Federation. (d). Method 4500-SiO2 (Silica). In W. C. Lipps, T. E. Baxter, & E. Braun-Howland (Eds.), *Standard Methods for the Examination of Water and Wastewater*. APHA Press. https://doi.org/10.2105/SMWW.2882.095

Standard Methods Committee of the American Public Health Association, American Water Works Association, & Water Environment Federation. (e). Method 5310 - TOC (Total organic carbon). In W. C. Lipps, T. E. Baxter, & E. Braun-Howland (Eds.), *Standard Methods for the Examination of Water and Wastewater*. APHA Press. https://doi.org/10.2105/SMWW.2882.104

St. Louis, V. L., Rudd, J. W. M., Kelly, C. A., Beaty, K. G., Flett, R. J., & Roulet, N. T. (1996). Production and loss of Mmthylmercury and loss of total mercury from boreal forest catchments containing different types of wetlands. *Environmental Science & Technology*, *30*(9), 2719–2729. https://doi.org/10.1021/es950856h

St.Pierre, K. (2018). *Biogeochemical impacts of glacial meltwaters across a High Arctic watershed (Lake Hazen, Nunavut, Canada)* [PhD]. University of Alberta.

St. Pierre, K. A., St. Louis, V. L., Schiff, S. L., Lehnherr, I., Dainard, P. G., Gardner, A. S., Aukes, P. J. K., & Sharp, M. J. (2019). Proglacial freshwaters are significant and previously unrecognized sinks of atmospheric CO2. *Proceedings of the National Academy of Sciences of the United States of America*, *116*(36), 17690–17695. https://doi.org/10.1073/pnas.1904241116

Staniszewska, K. J., Cooke, C. A., & Reyes, A. V. (2020). Quantifying meltwater sources and contaminant fluxes from the Athabasca Glacier, Canada. *ACS Earth and Space Chemistry*. https://doi.org/10.1021/acsearthspacechem.0c00256

Steffen, W., Broadgate, W., Deutsch, L., Gaffney, O., & Ludwig, C. (2015). The trajectory of the Anthropocene: The Great Acceleration. *The Anthropocene Review*, *2*(1), 81–98. https://doi.org/10.1177/2053019614564785

Stein, A. F., Draxler, R. R., Rolph, G. D., Stunder, B. J. B., Cohen, M. D., & Ngan, F. (2015). NOAA's HYSPLIT atmospheric transport and dispersion modeling system. In *Bulletin of the American Meteorological Society* (Vol. 96, Issue 12, pp. 2059–2077). American Meteorological Society. https://doi.org/10.1175/BAMS-D-14-00110.1

Syafrudin, M., Kristanti, R. A., Yuniarto, A., Hadibarata, T., Rhee, J., Al-onazi, W. A., Algarni, T. S., Almarri, A. H., & Al-Mohaimeed, A. M. (2021). Pesticides in drinking water—A review. *International Journal of Environmental Research and Public Health*, *18*(2), 468. https://doi.org/10.3390/ijerph18020468

Tennant, C., & Menounos, B. (2013). Glacier change of the Columbia Icefield, Canadian Rocky Mountains, 1919-2009. *Journal of Glaciology*, *59*(216), 671–686. https://doi.org/10.3189/2013JoG12J135

Tennant, C., Menounos, B., Wheate, R., & Clague, J. J. (2012). Area change of glaciers in the Canadian Rocky Mountains, 1919 to 2006. *Cryosphere*, *6*(6), 1541–1552. https://doi.org/10.5194/tc-6-1541-2012

Thiem, L., Badorek, D., & O'Connor, J. T. (1976). Removal of mercury from drinking water using activated carbon. *Journal American Water Works Association*, *68*(8), 447–451. https://doi.org/10.1002/j.1551-8833.1976.tb02454.x

Torres, M. A., Moosdorf, N., Hartmann, J., Adkins, J. F., & West, A. J. (2017). Glacial weathering, sulfide oxidation, and global carbon cycle feedbacks. *Proceedings of the National Academy of Sciences*, *114*(33), 8716–8721. https://doi.org/10.1073/pnas.1702953114

Trail to Peak. (2024). *Iceberg Lake + Bow Glacier's Big Toe* [Blog]. Trail to Peak: The Adventurous Path. https://trailtopeaktheadventurouspath.wordpress.com/2019/09/04/iceberg-lake-bow-glaciers-big-toe/

Tranter, M., Sharp, M. J., Lamb, H. R., Brown, G. H., Hubbard, B. P., & Willis, I. C. (2002). Geochemical weathering at the bed of Haut Glacier d'Arolla, Switzerland—A new model. *Hydrological Processes*, *16*(5), 959–993. https://doi.org/10.1002/hyp.309

Tranter, M., & Wadham, J. L. (2013). Geochemical weathering in glacial and proglacial environments. In *Treatise on Geochemistry: Second Edition* (2nd ed., Vol. 7, pp. 157–173). Elsevier Ltd. https://doi.org/10.1016/B978-0-08-095975-7.00505-2

Ulseth, A. J., Hall, R. O., Boix Canadell, M., Madinger, H. L., Niayifar, A., & Battin, T. J. (2019). Distinct air–water gas exchange regimes in low- and high-energy streams. *Nature Geoscience*, *12*(4), 259–263. https://doi.org/10.1038/s41561-019-0324-8

Urey, H. C. (1952). On the early chemical history of the Earth and the origin of life. *Proceedings of the National Academy of Sciences*, *38*(4), 351–363. https://doi.org/10.1073/pnas.38.4.351

Urra, A., Wadham, J., Hawkings, J. R., Telling, J., Hatton, J. E., Yde, J. C., Hasholt, B., Van As, D., Bhatia, M. P., & Nienow, P. (2019). Weathering dynamics under contrasting Greenland Ice Sheet catchments. *Frontiers in Earth Science*, *7*, 299. https://doi.org/10.3389/feart.2019.00299

U.S. EPA. (1989). Method 1625C: Semivolatile organic compounds by isotope dilution GCMS. U.S. EPA Federal Registry.

U.S. EPA. (1971a). Method 160.1: Total dissolved solids. In *Methods for Chemical Analysis of Water and Wastes (EPA 600/4-79-020)*. U.S. EPA Federal Registry.

U.S. EPA. (1971b). Method 160.2: Non-filterable residue and total suspended solids. In *Methods for Chemical Analysis of Water and Wastes (EPA 600/4-79-020)*. U.S. EPA Federal Registry.

U.S. EPA. (1993a). Method 300.1: Determination of anions in drinking water by ion chromatography. In *Methods for the Determination of Organic and Inorganic Compounds in Drinking Water (EPA 815/R-00-014)*. U.S. EPA Federal Registry.

U.S. EPA. (1993b). Method 353.2: Determination of nitrate-nitrite nitrogen by automated colorimetry. In *Methods for Chemical Analysis of Water and Wastes (EPA 600/4-79-020)*. U.S. EPA Federal Registry.

U.S. EPA. (1994). *Method 200.7, Revision 4.4: Determination of metals and trace elements in water and wastes by Inductively Coupled Plasma-Atomic Emission Spectrometry (ICP-AES)*. U.S. EPA Federal Registry.

U.S. EPA. (1996). *Method 1669: Sampling ambient water for trace metals at EPA water quality criteria levels*. U.S. EPA Federal Registry.

U.S. EPA. (1997). Method 440.0: Carbon and nitrogen in sediments and particulates. In *Methods for the Determination of Chemical Substances in Estuarine Environmental Matrices (EPA 600/R-97-072)*. U.S. EPA Federal Registry.

U.S. EPA. (1998). *Method 1630: Methyl mercury in water by distillation, aqueous ethylation, purge and trap, and cold vapor atomic fluorescence spectrometry*. U.S. EPA Federal Registry.

U.S. EPA. (2002). *Method 1631, Revision E: Mercury in water by oxidation, purge and trap, and cold vapor atomic fluorescence spectrometry*. U.S. EPA Federal Registry.

U.S. EPA. (2014). Method 8270E (SW-846): Semivolatile organic compounds by Gas Chromatography/Mass Spectrometry (GC/MS). U.S. EPA Federal Registry.

Vance, D., Teagle, D. A. H., & Foster, G. L. (2009). Variable Quaternary chemical weathering fluxes and imbalances in marine geochemical budgets. *Nature*, *458*(7237), 493–496. https://doi.org/10.1038/nature07828

Viers, J., Oliva, P., Dandurand, J.-L., Dupré, B., & Gaillardet, J. (2007). Chemical Weathering Rates, CO_2 Consumption, and Control Parameters Deduced from the Chemical Composition of Rivers. In *Treatise on Geochemistry* (2nd ed.).

Viviroli, D., Archer, D. R., Buytaert, W., Fowler, H. J., Greenwood, G. B., Hamlet, A. F., Huang, Y., Koboltschnig, G., Litaor, M. I., López-Moreno, J. I., Lorentz, S., Schädler, B., Schreier, H., Schwaiger, K., Vuille, M., & Woods, R. (2011). Climate change and mountain water resources: Overview and recommendations for research, management and policy. *Hydrology and Earth System Sciences*, *15*(2), 471–504. https://doi.org/10.5194/hess-15-471-2011

Volk, C., Kaplan, L. A., Robinson, J., Johnson, B., Wood, L., Zhu, H. W., & LeChevallier, M. (2005). Fluctuations of dissolved organic matter in river used for drinking water and impacts on conventional treatment plant performance. *Environmental Science & Technology*, *39*(11), 4258–4264. https://doi.org/10.1021/es040480k

Vorobyeva, S. S., Trunova, V. A., Stepanova, O. G., Zvereva, V. V., Petrovskii, S. K., Melgunov, M. S., Zheleznyakova, T. O., Chechetkina, L. G., & Fedotov, A. P. (2015). Impact of glacier changes on ecosystem of proglacial lakes in high mountain regions of East Siberia (Russia). *Environmental Earth Sciences*, *74*(3), 2055–2063. https://doi.org/10.1007/s12665-015-4164-6

Voss, B. M., Eglinton, T. I., Peucker-Ehrenbrink, B., Galy, V., Lang, S. Q., McIntyre, C., Spencer, R. G. M., Bulygina, E., Wang, Z. A., & Guay, K. A. (2023). Isotopic evidence for sources of dissolved carbon and the role of organic matter respiration in the Fraser River basin, Canada. *Biogeochemistry*, *164*(1), 207–228. https://doi.org/10.1007/s10533-022-00945-5

Wadham, J. L., Cooper, R. J., Tranter, M., & Hodgkins, R. (2001). Enhancement of glacial solute fluxes in the proglacial zone of a polythermal glacier. *Journal of Glaciology*, *47*(158), 378–386. https://doi.org/10.3189/172756501781832188

Wang, Z. A., Lawson, G. L., Pilskaln, C. H., & Maas, A. E. (2017). Seasonal controls of aragonite saturation states in the Gulf of Maine. *Journal of Geophysical Research: Oceans*, *122*(1), 372–389. https://doi.org/10.1002/2016JC012373

Wankiewicz, P. M. (1979). *Sedimentation in Sunwapta Lake, Jasper National Park, Alberta* (Master's thesis). Edmonton, AB: University of Alberta.

Warner, K. A., Saros, J. E., & Simon, K. S. (2017). Nitrogen subsidies in glacial meltwater: Implications for high elevation aquatic chains. *Water Resources Research*, *53*(11), 9791–9806. https://doi.org/10.1002/2016WR020096

Water Survey of Canada. (2021). National Water Data Archive: HYDAT [Dataset]. Environment and Climate Change Canada, Government of Canada. https://www.canada.ca/en/environment-climate-change/services/water-overview/quantity/monitoring/survey/data-products-services/national-archive-hydat.html. Retrieved January 2021.

Wickham, H. (2016). *ggplot2: Elegant graphics for data analysis*. Springer-Verlag.

Winnick, M. J., Carroll, R. W. H., Williams, K. H., Maxwell, R. M., Dong, W., & Maher, K. (2017). Snowmelt controls on concentration-discharge relationships and the balance of oxidative and acid-base weathering fluxes in an alpine catchment, East River, Colorado. *Water Resources Research*, *53*(3), 2507–2523. https://doi.org/10.1002/2016WR019724

Witze, A. (2024). Geologists reject the Anthropocene as Easth’s new epoch—After 15 years of debate. *Nature*, *627*, 249–250. https://doi.org/10.1038/d41586-024-00675-8

Wojtowicz, J. A. (2001). The thermodynamic basis of the saturation index. *Journal of the Swimming Pool and Spa Industry*, *3*(1), 35–36.

Xu, S., Chen, M., Feng, T., Zhan, L., Zhou, L., & Yu, G. (2021). Use ggbreak to effectively utilize plotting space to deal with large datasets and outliers. *Frontiers in Genetics*, *12*, 774846. https://doi.org/10.3389/fgene.2021.774846

Zalasiewicz, J., Waters, C., & Williams, M. (2020). The Anthropocene. In *Geologic Time Scale 2020* (pp. 1257–1280). Elsevier. https://doi.org/10.1016/B978-0-12-824360-2.00031-0

Zalasiewicz, J., Williams, M., Steffen, W., & Crutzen, P. (2010). The new world of the Anthropocene. *Environmental Science & Technology*, *44*(7), 2228–2231. https://doi.org/10.1021/es903118j

Zhou, Y., Wang, X., Chen, M., Fu, J., Zhu, T., Wang, C., Gong, P., Wang, L., & Ren, J. (2024). Proglacial river sediments are a substantial sink of perfluoroalkyl substances released by glacial meltwater. *Communications Earth & Environment*, *5*(1), 68. https://doi.org/10.1038/s43247-024-01223-y

Zhu, T., Wang, X., Lin, H., Ren, J., Wang, C., & Gong, P. (2020). Accumulation of pollutants in proglacial lake sediments: Impacts of glacial meltwater and anthropogenic activities.

Environmental Science & Technology, *54*(13), 7901–7910. https://doi.org/10.1021/acs.est.0c01849

Appendix 1: Supporting information for Chapter 2 "A comprehensive biogeochemical assessment of climate-threatened glacial river headwaters on the eastern Slopes of the Canadian Rocky Mountains"

3 Results & Discussion

3.2 Water sources

The wide range of $\delta^{18}O$, $\delta^{2}H$, and d-excess signatures in precipitation and glacial ice can be partially and broadly attributed to the sources of rain and snow to our study region (Sinclair & Marshall, 2009). The analysis of air mass back trajectory residence time densities showed a mix of air mass sources that contributed to the eastern slopes of the Canadian Rocky Mountains during our sampling years (**Figure A1.6**). From 2019 to 2021, air masses were tracked from western North America, circumpolar Arctic, and the North Pacific Ocean, but the highest residence time densities were found on the coastal southwest margin of Canada. Winter air mass ranges were at their most latitudinally diverse, but the greatest residence time densities extended down coastal North America. In spring, moderate residence time densities were found as far east as Hudson Bay yet were primarily centered around coastal southwest Canada. Summer displayed the broadest area of moderate to high residence time densities which extended west from the coast into the Gulf of Alaska. The area with moderate to high residence time densities shrunk in the autumn to a small local region in coastal southwest Canada before low residence time densities began to spread to their winter range (**Figure A1.6**). Precipitation that fell in our study region would have been brought by these diverse air masses, with atmospheric transport routes and any associated isotopic transformations greatly impacting their water isotope signatures. As the air masses with the greatest residence time densities traveled to and across the Rocky Mountain Range from the west coast, the high topographic relief would have prompted the onset of orographic precipitation, resulting in isotopic fractionations occurring across elevational and associated temperature gradients (Beria et al., 2018; Sinclair & Marshall, 2009). After the deposition of snow, elevation-dependent processes such as snowpack sublimination or rain-on-snow events cause further fractionations (Carroll, Deems, Maxwell, et al., 2022; Carroll, Deems, Sprenger, et al., 2022). Indeed, a positive and significant correlation with elevation was observed for $\delta^{18}O$ ($r_{Pearson} = 0.64$, $p < 0.05$, **Figure A1.7a**), $\delta^{2}H$ ($r_{Pearson} = 0.70$, $p < 0.05$, **Figure A1.7c**) and d-excess ($r_{Pearson} = 0.57$, $p < 0.05$, **Figure A1.7e**) signatures of our combined snow samples.

Though snow isotope signatures demonstrated a strong relationship with elevation (Holdsworth et al., 1991; Mahindawansha et al., 2022), the influence of elevation was less apparent in the riverine water isotope signatures. Overall, riverine δ^{18}O signatures were not correlated with elevation ($r_{Spearman} = 0.09$, $p > 0.05$, **Figure A1.7b**), while riverine δ^{2}H signatures were weakly correlated ($r_{Spearman} = 0.18$, $p < 0.05$, **Figure A1.7d**), and d-excess signatures were strongly correlated ($r_{Spearman} = 0.46$, $p < 0.05$, **Figure A1.7f**), with elevation. When δ^{18}O and δ^{2}H were binned for season, no elevational correlations were significant ($p > 0.05$). However, riverine d-excess signatures were significantly correlated to elevation in spring ($r_{Spearman} = 0.58$, $p < 0.05$) and summer ($r_{Spearman} = 0.44$, $p < 0.05$), but not in autumn ($r_{Pearson} = 0.32$, $p > 0.05$) or winter ($r_{Pearson} = 0.46$, $p > 0.05$). In this case, the riverine d-excess signatures likely reflected variability in water source contributions to the rivers during the high discharge spring and summer periods. The d-excess signatures of snowmelt inputs into our rivers during spring freshet would predominantly reflect the elevation of the snowpacks providing these meltwaters. During summer, the d-excess signatures of glacier meltwater would likely be most reflected in river waters closest to their source glacier (where they are essentially single-source river waters), but progressively less so with movement downriver as a mix of water sources are introduced. For instance, it has been shown that groundwater can contribute a large proportion of river water in mountain landscapes (see winter samples in **Figure 2.5a**) and that this groundwater's isotopic signature is dependent on the original source, route, and residence time of the water through the larger system (Hayashi, 2020; Paznekas & Hayashi, 2016; Somers & McKenzie, 2020). Additionally, interflow is also known to play a large role in mountain river recharge and may be especially important in seasons when the infiltration of new precipitation into the landscape acts as a catalyst for input into downstream segments of the rivers (Campbell & Ryan, 2021).

3.3 Measures and patterns in physicochemical parameters

Certain physicochemical parameters measured in rivers were excluded from PCAs as they did not meet the criteria described in *Section 2.5*. As such, some interpretations of the PCAs presented in this study should be viewed through a critical lens. For example, TDP was excluded from analyses because over 25% of concentrations were below the DL, whereas SRP was excluded because concentrations were also largely below the DL and only collected in 2020. The elimination of dissolved phosphorus species from PCA analysis was anticipated given that productivity in these rivers is phosphorus limited, so any bioavailable phosphorus was likely rapidly used (Bowman et al., 2005). Additionally, of the 49 PAH congeners analyzed, only 18 had less than 25% of their concentrations below the DL, and the sum of PAHs was low when compared with other Canadian riverine systems (Marvin et al., 2021). Contaminants such as Hg and PAHs can be atmospherically transported from anthropogenically active emission areas to high-altitude regions and deposited onto snow and ice (Beal et al., 2015; Mansilha et al., 2014). Meltwaters stemming from snow and icepacks have been documented to contain elevated contaminant signatures (Sharma et al., 2015). Yet, because our measured contaminant concentrations were low (see also Staniszewska et al., 2020), we could only include THg in the main physicochemical PCA, indicating that either the cryospheric components that feed our rivers are not the depositional grounds of air-borne contaminants or that pollutants historically archived in glacial ice were not released into our rivers during our study years. These results are supported by X-Ray Diffraction analysis in that the underlying bedrock of our study system does not include Hg-containing minerals and is thus not a source of Hg (please see dataset in *Data Availability*). Another noteworthy absence, specifically from the trace element PCA, is non-PTL Fe. Across 2019 and 2020, PTL Fe concentrations were lowest at NSR2 in August 2019 (0.13 ug L^{-1}) and highest at NSR2 in June 2020 (15.00 ug L^{-1}; $median_{PTL}$ = 0.72 ug L^{-1}). Dissolved Fe concentrations were lowest at AR1 in October (0.93 ug L^{-1}) and highest at SR1 in June (36.05 ug L^{-1}) in the 2019 data ($median_{dissolved}$ = 4.20 ug L^{-1}) but 2020 data were disregarded due to analytical issues. Trends in Fe across spatiotemporal factors would have been of interest given reports of elevated PTL Fe concentrations coming from glacial environments and its potential bioavailability (Hawkings et al., 2018; Hopwood et al., 2014).

Table A1.1. Distance from glacier, watershed area, elevation, coordinates, and description of our 14 sampling sites along the study rivers in Jasper and Banff National Parks. Asterisked (*) sampling sites are those that have Water Survey of Canada (WSC) hydrometric gauging stations.

Site ID	Distance from glacier (km)	Watershed area (km^2)	Elevation (m)	Coordinates (DD)		Site description
				Latitude	Longitude	
			Sunwapta River (SR)[1]			
SR1	0.2	22.7	2063	52.206739	-117.234767	Near Athabasca Glacier terminus
SR2*	1.7	29.3	1951	52.216950	-117.234069	Outflow of proglacial Sunwapta Lake; WSC station ID 07AA007
SR3	15.5	197.5	1580	52.310583	-117.332583	Glacial outwash plain
SR4	52.9	730.8	1396	52.532972	-117.644222	Upstream of Sunwapta Falls
			Athabasca River (AR)[1]			
AR1	63.1	1635.1	1240	52.594869	-117.805439	Mt. Christie Picnic Area
AR2	73.9	1955.8	1184	52.662917	-117.881028	Upstream of Athabasca Falls
AR3	97.8	3019.9	1060	52.812056	-118.042556	At Mile Five Bridge
			North Saskatchewan River (NSR)[2]			
NSR1	5.6	76.2	1682	52.169472	-117.076361	At Highway 93 bend
NSR2	24.6	616.3	1440	52.069194	-116.915250	Glacial outwash plain
NSR3	46.3	1550.7	1400	51.970556	-116.721111	At North Saskatchewan Crossing
			Bow River (BR)[2]			
BR1	2.4	21.4	1996	51.661750	-116.486939	Inflow of subalpine Bow Lake
BR2	17.1	104.7	1840	51.631500	-116.335167	Outflow of wetland at Mosquito Creek Campground
BR3*	51.3	422.0	1560	51.428667	-116.189000	In Lake Louise Township; WSC station ID 05BA001
BR4	75.4	1103.9	1480	51.284950	-115.983500	Upstream of Castle Junction

[1] Jasper National Park, Alberta

[2] Banff National Park, Alberta

Table A1.2. Relative percent watershed area of each sampling site covered by major and minor land cover classes. Land cover data was obtained using the Alberta Biodiversity Monitoring Institute (ABMI) Wall-to-Wall Land Cover Inventory (Alberta Biodiversity Monitoring Institute, 2010).

Site ID	Water[1]	Snow and ice	Rock and rubble	Exposed land	Shrubland	Grassland	Coniferous forest	Broadleaf forest	Mixed forest	Developed	Total
	%	%	%	%	%	%	%	%	%	%	%
SR1	1.1	50.7	46.8	0.0	0.0	0.0	0.0	0.0	0.0	0.0	98.6
SR2	1.5	41.8	54.2	0.0	0.2	0.1	0.3	0.0	0.0	0.8	98.9
SR3	1.0	19.1	55.3	0.0	5.7	4.7	12.8	0.2	0.1	1.1	99.8
SR4	1.5	6.6	50.2	0.0	8.4	6.8	25.1	0.4	0.1	0.8	100.0
AR1	1.9	12.2	43.2	0.1	7.6	6.4	27.3	0.6	0.2	0.4	99.9
AR2	1.9	10.8	42.8	0.0	7.7	6.4	29.0	0.7	0.3	0.4	99.9
AR3	1.9	8.4	41.2	0.0	7.4	7.4	32.0	0.8	0.3	0.5	99.9
NSR1	0.6	54.7	35.3	0.2	1.7	3.7	3.6	0.2	0.0	0.0	100.0
NSR2	1.6	19.1	40.8	0.1	7.4	5.6	24.4	0.2	0.1	0.5	99.8
NSR3	2.1	18.8	37.4	0.1	6.9	4.0	29.7	0.1	0.0	0.5	99.7
BR1	2.0	41.5	47.7	0.0	2.4	1.4	4.8	0.0	0.0	0.0	99.9
BR2	4.3	11.1	42.0	0.0	8.4	1.3	31.4	0.0	0.0	1.5	100.0
BR3	3.6	9.6	35.7	0.0	6.7	1.8	41.0	0.0	0.0	1.4	99.8
BR4	2.4	5.6	38.1	0.0	8.7	2.5	41.3	0.0	0.0	1.3	99.9

[1] Relative percent wetland cover (fen + bog + marsh + swap) was quantified separately using the ABMI Wetland Inventory (Alberta Biodiversity Monitoring Institute, 2021) and likely overlapped with the water land cover class in the ABMI Wall-to-Wall Land Cover Inventory. Watershed area covered by wetland at our study sites ranged from 0.0-2.1%. Wetland cover exceeding 1.0% were found at BR2 (2.1%), BR3 (1.9%), and BR4 (1.6%).

Table A1.3. Water Survey of Canada (WSC) hydrometric gauging station information, including station name, station ID, watershed, watershed area, and whether discharge data was continuous or seasonal (May - October), for the nine WSC stations that were used to model discharge for our hydrometrically ungauged sampling sites (Water Survey of Canada, 2021). Five of the gauging stations were then used to calibrate our modeled discharge (**Figure A1.5**).

WSC station name (Site ID in brackets, if relevant)	Station ID	Watershed	Watershed area (km^2)	Continuous or seasonal data	Calibration site
Sunwapta River at Athabasca Glacier (SR2)	07AA007	Sunwapta/Athabasca	29.3	Seasonal	Yes
Miette River near Jasper	07AA001	Athabasca	629.0	Continuous	No
Athabasca River near Jasper	07AA002	Athabasca	3870.0	Continuous	Yes
Silverhorn Creek near the Mouth	05DA010	North Saskatchewan	21.0	Continuous	No
Mistaya River near Saskatchewan Crossing	05DA007	North Saskatchewan	248.0	Continuous	No
North Saskatchewan River at Whirlpool Point	05DA009	North Saskatchewan	1920.0	Continuous	Yes
Pipestone River near Lake Louise	05BA002	Bow	306.0	Continuous	No
Bow River at Lake Louise (BR3)	05BA001	Bow	422.0	Seasonal	Yes
Bow River at Banff	05BB001	Bow	2210.0	Continuous	Yes

Table A1.4. Field sampling methodology, sample preservation, and instrument of analysis for each parameter sampled in this study. All samples were stored at 4° Celsius until analysis unless otherwise noted. For parameter abbreviations, please see *Section 2.3* in the main text.

Parameter		Sampling methodology and preservation	Instrument of analysis	Laboratory	Reference method
TSS		Collected by passing a known volume of water through a pre-weighed 47mm 0.45 µm cellulose acetate filter within 24h of sampling	Analysis by weight	BASL[a]	EPA 160.2 (U.S. EPA, 1971b)
TDS		Filtered through a pre-weighed 47mm 0.45 µm cellulose acetate filter in a pre-cleaned filtration tower within 24h of sampling	Analysis by weight	BASL	EPA 160.1 (U.S. EPA, 1971a)
Temp, pH, ODO, Cond, Turb		In situ continuous river measurements	YSI EXO2 multiparameter sonde	NA	NA
Nutrients	TP, TN	Raw water, digested prior to analysis	Lachet QuickChem QC8500 FIA Automated Ion Analyzer	BASL	EPA 353.2 (U.S. EPA, 1993b), SM 4500-NH_3 (SM-APHAb), SM 4500-P (SM-APHAc), SM 4500-SiO_2 (APHAd)
	TDP, SRP, TDN, NH_4, NO_2^-+NO_3^-, Si	Filtered onsite through a 0.45 µm Sartorius™ Minisart™ cellulose acetate syringe filter, SRP, NH_4, NO_2^-+NO_3^- frozen			
Ca^{2+}, K^+, Mg^{2+}, Na^+		Filtered onsite through a 0.45 µm Whatman™ polyethersulfone (PES) syringe filter, preserved with trace metal grade nitric acid until pH < 2	Thermo Scientific iCAP 6300 Inductively Coupled Plasma – Optical Emissions Spectrometer (ICP-OES)	BASL	EPA 200.7 (U.S. EPA, 1994), SM 3125 (SM-APHAa)
Cl^-, SO_4^{2-}		Filtered onsite through a 47mm 0.45 µm cellulose acetate filter in a pre-cleaned filtration tower	Dionex DX-600 Ion Chromatography	BASL	EPA 300.1 (U.S. EPA, 1993a)
Trace elements		Filtered onsite through a 0.45 µm Whatman™ polyethersulfone (PES) syringe filter, preserved with trace metal grade nitric acid until pH < 2	Thermo Scientific iCAP Q ICP-MS & Agilent 7900 ICP-MS	CCIM[b] & BASL	EPA 200.7, SM 3125 (SM-APHAa)
Water isotopes		Filtered onsite through a 0.45 µm Sartorius™ Minisart™ cellulose acetate syringe filter	Picarro L2130-i	Academic	IAEA-TCS-35 (International Atomic Energy Agency, 2009)
PC and PN		Collected by passing a known volume of water through a pre-combusted 25mm 0.7 µm glass fiber filter within 24h of sampling	Exeter Analytical Inc. CE-440 Elemental Analyzer	BASL	EPA 440.0 (U.S. EPA, 1997)
DIC		Filtered onsite through a 0.45 µm Sartorius™ Minisart™ cellulose acetate syringe filter	Apollo SciTech AS-C3 DIC analyzer interfaced with a LI-COR LI-7000 infrared CO_2 analyzer	Academic	St Pierre et al., 2019 (sampling), Wang et al., 2017 (analysis)
DOC		Filtered onsite through a 0.45 µm Basix™ PES filter and preserved with trace metal grade HCl to 0.1% of its volume	Shimadzu TOC-V analyzer	Academic	SM 5310-TOC (SM-APHAe)
THg	THg	Preserved with trace metal grade HCl to 0.2% of their volume within 24h of sampling	Tekran 2600 mercury analyzer	BASL	EPA 1631.E (U.S. EPA, 2002)
	FHg	0.45µm pre-acid washed Nalgene filter towers and preserved with trace metal grade HCl to 0.2% of their volume within 24h of sampling			
MeHg	MeHg	Preserved with trace metal grade HCl to 0.4% of their volume within 24h of sampling	Tekran 2750 methyl mercury distillation unit and Tekran 2700 methyl mercury analyzer coupled to an Agilent 7900 ICP-MS	BASL	EPA 1630 (U.S. EPA, 1998)
	FMeHg	0.45µm pre-acid washed Nalgene filter towers and preserved with trace metal grade HCl to 0.4% of their volume within 24h of sampling within 24h of sampling			
PAHs		Raw water collected in certified clean glass bottles and preserved with 50 mg sodium azide per 1L within 24h of sampling	Gas chromatography – mass spectrometry with selected ion monitoring	SGS AXYS[c]	EPA 1625C (U.S. EPA, 1989), EPA 8270E (SW-846) (U.S. EPA, 2014)
Cation_PTL and Trace element_PTL		Filtered onsite through an acid-washed 102mm 0.45 µm polyethersulfone (PES) filter and frozen, rinsed from filter and freeze dried prior to analysis	CEM MARS 6 iWave Microwave Digestion System and Agilent 7900 ICP-MS	BASL	EPA 200.7 (U.S. EPA, 1994), SM 3125 (SM-APHAa)

[a] Biogeochemical Analytical Service Laboratory (BASL, University of Alberta); CALA-accredited

[b] The Canadian Centre for Isotopic Microanalysis (CCIM, University of Alberta)

[c] SGS AXYS Analytical Services Ltd. Laboratory (Sidney, British Columbia); NELAC-, CALA-, and U.S. DoD ELAP-accredited

Table A1.5. Condensed results from USGS loadflex models considered for this study (Appling et al., 2015). For each parameter (column 1) and site (column 2) investigated, total summed load results from each model (rectangular interpolation, linear regression, LOADEST regression, and composite) are reported. Mean ± standard deviation (SD) and relative standard deviation (RSD) were calculated on the total summed load to estimate difference between models.

Parameter	Site ID	Total summed 2019 & 2020 load (kg OWS^{-1})				Statistics	
		Rectangular Interpolation	Linear Regression	LOADEST Regression	Composite	Mean ± SD	RSD (%)
DIC	SR1	641,435	661,163	652,406	623,879	644,721 ± 16,068	2.5
DIC	SR3	4,596,191	4,591,145	4,591,219	4,591,041	4,592,399 ± 2,529	0.06
NO_2^-+NO_3^-	SR1	3,565	3,760	3,472	3,328	3,531 ± 181	5.1
NO_2^-+NO_3^-	SR3	21,928	21,951	21,722	22,038	21,910 ± 134	0.6

Table A1.6. Summary of LOADEST models eliminated for each parameter and site, if relevant (Runkel et al., 2004). Model elimination was based on bias percent (Bp > 25%) and coefficient of determination ($R^2 < 50$) statistics, not a number (NaN) erroneous model output, or poor model fit as shown via quality control (QC) graphs. Rivers are abbreviated as SR (Sunwapta River), AR (Athabasca River), NSR (North Saskatchewan River), and BR (Bow River). For site abbreviations please see **Table A1.1** and for parameter abbreviations please see *Section 2.3* in the main text.

Parameter	Site ID	Reason for LOADEST model elimination
NFR	SR3	Bp > 25%
	AR2	Best model NaN error produced = second best model accepted
	AR3	Best model NaN error produced; Second best model NaN error produced; Third best model Bp > 25%
PN	SR2	Best Model NaN error produced = next best model accepted
	SR3	Bp > 25%
	AR2	Best model NaN error produced = next best model accepted
	AR3	Best model NaN error produced = next best model accepted
PC	SR3	Bp > 25%
	AR3	Best model NaN error produced = next best model accepted
DOC	SR2	Best model NaN error produced = second best model accepted
TP	SR2	Best model NaN error produced = second best model accepted
	SR3	Bp > 25%
	NSR3	Bp > 25%
TN	SR2	Best model NaN error produced; Second best model Bp > 25%
TDN	SR2	Best model NaN error produced = second best model accepted
$NO_2^-+NO_3^-$	SR2	Best model NaN error produced = second best model accepted
K	SR2	Best model NaN error produced = second best model accepted
	NSR1	Best model NaN error produced; Second best model Bp > 25%
Ba	SR2	Best model NaN error produced = second best model accepted
	NSR1	Bp > 25%
Cr	AR2	Best model NaN error produced; Second best model NaN error produced; Third best model $R^2 < 50$
	AR3	Best model NaN error produced; Second best model NaN error produced; Third best model $R^2 < 50$
Mn	NSR1	Bp > 25%
	BR1	Best model NaN error produced = second best model accepted
Mo	SR2	$R^2 < 50$
	AR3	$R^2 < 50$
FHg	SR3	$R^2 < 50$
	NSR1	Bp > 25% and $R^2 < 50$

Table A1.7. LOADEST model chosen, and correlation coefficient (R^2) and percent bias (Bp; %) statistics for (a) basic chemical parameters, (b) nutrients, (c) ions, (d) trace elements, and (e) contaminants. Rivers are abbreviated as SR (Sunwapta River), AR (Athabasca River), NSR (North Saskatchewan River), and BR (Bow River). For site abbreviations please see **Table A1.1** and for parameter abbreviations please see *Section 2.3* in the main text.

a.	TSS			TDS			PN			PC			DIC			DOC		
Site ID	Model	R^2	Bp	Model	R^2	Bp	Model	R^2	Bp	Model	R^2	Bp	Model	R^2	Bp	Model	R^2	Bp
SR1	1	88.14	-6.80	2	85.15	3.15	1	86.88	-10.00	1	84.94	-22.98	2	97.17	0.79	1	82.43	-6.36
SR2	2	96.34	3.82	4	96.45	-0.05	2	97.59	-1.01	1	92.56	12.79	1	99.34	0.16	6	71.03	-6.76
SR3				6	97.93	0.08							6	99.54	0.05	4	90.76	-3.26
SR4	1	85.98	11.79	4	95.20	-0.36	1	75.03	-21.05	1	67.37	-23.09	4	99.67	-0.13	4	74.49	-0.50
AR2	4	86.57	24.06	1	80.16	-0.59	4	91.14	-1.68	4	85.61	14.05	6	99.80	0.00	4	94.99	1.85
AR3				1	92.22	-0.40	4	82.62	19.86	4	74.41	17.42	1	98.66	-0.04	4	93.15	2.61
NSR1	4	94.82	-17.04	4	91.90	0.27	6	91.48	8.17	4	94.46	0.51	4	98.71	-0.47	6	89.51	0.51
NSR2	2	88.57	-19.26	4	90.16	-0.09	2	81.95	-17.96	2	86.57	-24.88	6	98.90	0.02	4	97.76	2.31
NSR3	1	86.58	14.89	6	89.17	-0.16	2	89.41	-16.29	1	83.22	-15.82	6	98.58	0.03	4	97.84	-0.49
BR1	4	93.87	-2.44	6	97.97	0.49	1	94.34	-0.21	1	77.73	-12.94	4	98.94	-0.39	1	93.11	-0.60
BR2	6	98.72	-1.07	6	97.99	-0.02	6	95.31	-4.57	1	87.60	0.32	1	99.28	0.18	6	99.69	0.24
BR3	1	91.92	-10.21	6	98.28	0.04	2	92.17	-7.79	1	89.63	-11.56	1	97.73	0.20	6	99.00	0.23
BR4	4	91.14	-4.00	6	97.98	0.22	1	86.30	-12.89	1	88.30	-0.39	1	99.96	-0.02	6	99.33	-0.14

b.	TP			TN			TDN			NO_2^-+NO_3^-			Si		
Site ID	Model	R^2	Bp	Model	R^2	Bp	Model	R^2	Bp	Model	R^2	Bp	Model	R^2	Bp
SR1	1	92.14	-22.96	2	72.58	2.92	4	91.67	-4.12	2	92.36	-1.27	1	90.20	-1.41
SR2	1	82.75	16.50				4	78.17	0.00	4	94.63	-0.96	1	90.86	-1.10
SR3				6	99.33	-0.10	6	97.65	-0.79	4	98.49	-0.61	4	96.07	-1.14
SR4	2	84.24	-17.63	1	64.91	-4.99	6	93.88	-0.83	6	95.09	0.44	6	97.21	0.17
AR2	1	71.49	7.69	6	98.35	0.63	6	92.42	0.15	6	98.70	0.04	6	98.39	-0.07
AR3	4	82.12	7.16	6	97.11	1.24	4	91.09	-0.54	4	94.08	-0.08	6	99.22	0.04
NSR1	6	95.77	3.13	6	89.45	-1.34	6	95.34	2.58	6	90.88	-0.63	4	89.80	-0.18
NSR2	2	79.76	-19.95	6	97.43	-2.68	4	85.49	-1.57	4	94.60	0.37	4	96.53	-0.22
NSR3				6	98.14	-1.44	4	94.04	-0.08	4	94.15	0.63	6	98.82	0.48
BR1	6	96.20	3.84	6	98.68	0.27	6	98.12	0.81	4	95.97	0.50	4	96.29	-0.66
BR2	2	82.15	1.62	4	92.39	1.13	6	92.24	1.80	4	97.38	-0.09	1	96.09	0.34
BR3	6	93.67	3.24	4	98.29	0.24	4	97.02	-0.24	4	96.52	-0.34	4	98.67	-0.09
BR4	2	94.14	3.01	6	98.34	-0.03	6	97.59	0.52	1	86.88	-0.22	4	99.36	-0.15

c.	Ca^{2+}			K^+			Mg^{2+}			Na^+			Cl^-			SO_4^{2-}		
Site ID	Model	R^2	Bp	Model	R^2	Bp	Model	R^2	Bp	Model	R^2	Bp	Model	R^2	Bp	Model	R^2	Bp
SR1	2	97.73	0.62	6	77.81	19.81	2	88.66	-0.08	6	68.78	12.84	1	75.50	-1.81	1	82.42	-0.66
SR2	1	98.85	0.42	4	88.75	-0.59	4	97.27	0.27	4	94.93	0.20	1	52.59	-3.32	1	89.27	-0.99
SR3	1	98.60	-0.74	6	96.36	1.24	4	98.80	-0.45	4	98.03	-1.25	6	91.37	-0.20	4	97.81	-0.59
SR4	1	97.51	-0.10	4	94.86	-0.24	6	99.71	0.02	6	98.45	0.13	4	68.18	-1.24	4	94.74	0.07
AR2	1	98.14	-0.19	4	93.83	-0.22	6	99.64	0.00	6	98.67	-0.05	6	59.33	-0.19	1	96.59	-0.08
AR3	1	96.64	0.07	4	94.22	-0.17	6	99.91	0.00	6	99.56	0.07	1	53.51	-0.90	1	96.50	-0.41
NSR1	4	97.76	-0.25				6	98.11	-0.07	6	94.22	0.24	4	78.40	-4.44	6	96.83	-0.21
NSR2	6	94.00	-0.09	6	85.03	-0.03	4	93.75	0.17	6	79.49	-0.14	6	82.47	-0.24	4	87.09	-0.01
NSR3	6	95.70	-0.06	6	96.14	0.74	6	96.41	0.17	6	96.65	0.33	6	62.38	0.12	6	93.82	0.11
BR1	4	96.47	0.53	4	91.59	-0.25	4	99.05	0.06	4	92.93	0.32	1	75.56	-0.07	1	96.76	0.39
BR2	6	95.91	-0.19	1	91.62	-0.06	6	98.54	-0.11	6	83.73	-0.34	4	96.92	-0.05	6	99.69	-0.01
BR3	1	97.49	-0.40	4	93.58	1.03	4	99.82	0.13	4	96.17	-0.30	4	90.41	-1.07	1	98.82	-0.12
BR4	1	98.62	0.12	1	94.17	0.11	4	99.89	-0.01	6	99.79	-0.01	1	96.71	0.26	4	98.88	-0.17

d.	Al			Ba			Cr			Mn			Mo			Sr		
Site ID	Model	R^2	Bp	Model	R^2	Bp	Model	R^2	Bp	Model	R^2	Bp	Model	R^2	Bp	Model	R^2	Bp
SR1	6	89.05	3.64	2	75.10	4.56	2	78.38	-2.00	2	83.15	-2.22	1	77.05	-1.52	2	91.42	0.01
SR2	4	96.32	1.96	1	63.19	-3.37	1	61.98	5.69	4	86.99	7.51				4	96.71	0.47
SR3	2	91.79	-2.10	2	86.92	3.07	2	68.42	-3.61	6	93.13	-0.26	4	96.99	-0.58	4	99.02	-0.03
SR4	6	98.52	0.04	6	96.52	0.15	2	65.34	-5.25	6	91.57	0.83	1	86.30	0.34	1	96.50	-0.04
AR2	6	98.53	0.52	6	93.35	-0.35				4	86.08	1.74	2	96.38	-0.05	6	99.50	-0.03
AR3	4	95.97	2.67	2	89.05	-1.86				2	91.11	4.78				1	97.97	-0.07
NSR1	1	92.00	3.11				1	61.63	3.08				4	61.22	8.91	6	97.82	-0.06
NSR2	2	63.76	-15.24	1	68.74	0.41	6	85.58	-1.06	1	80.37	11.05	2	84.34	-0.22	4	92.87	-0.17
NSR3	4	93.63	10.80	6	90.44	0.09	1	51.16	1.24	1	87.60	-4.24	6	98.46	0.29	6	91.94	0.06
BR1	1	73.21	-7.76	1	80.27	-0.14	2	96.45	-0.13	4	91.68	14.81	4	99.15	-0.02	1	97.85	0.47
BR2	4	90.98	14.99	2	91.60	-1.47	2	80.92	-0.70	2	82.20	6.18	6	99.44	0.01	4	97.69	-0.36
BR3	1	79.71	0.87	1	81.55	-1.10	2	78.94	0.64	6	97.29	0.33	1	98.15	0.50	6	99.96	-0.01
BR4	4	93.47	6.38	2	90.16	-3.26	2	80.87	-4.70	6	96.80	-0.25	6	95.39	-0.51	6	99.94	-0.01

e.	THg			FHg		
Site ID	Model	R^2	Bp	Model	R^2	Bp
SR1	6	96.29	2.42	1	74.97	-5.91
SR2	4	98.42	1.43	1	87.33	7.08
SR3	4	91.77	-16.59			
SR4	4	96.13	-3.66	4	93.63	3.73
AR2	6	90.03	2.72	4	84.29	11.35
AR3	4	87.24	11.95	4	76.38	24.06
NSR1	1	85.38	1.60			
NSR2	2	83.82	-21.61	4	50.01	7.32
NSR3	1	91.29	-15.59	4	77.02	0.89
BR1	6	96.73	-4.85	6	93.97	-4.84
BR2	6	99.29	0.32	4	94.76	6.37
BR3	1	85.56	5.09	4	85.75	5.85
BR4	4	94.96	4.92	6	97.62	2.24

Table A1.8. Monthly mean temperatures for Jasper (Station: Jasper Warden, 52.926N -118.030E) and Banff (Station: Banff CS, 51.193N -115.552E), and their mean ± standard deviation (SD) for 2019 and 2020 (Environment and Climate Change Canada, 2019, 2020).

	January	February	March	April	May	June	July	August	September	October	November	December
2019												
Jasper	-6.8	-19.1	-2.8	2.9	9.4	12.2	14.2	13.7	10.2	1.8	-3.3	-8.1
Banff	-6.2	-17.6	-2.8	3.1	7.3	11.5	13.3	14.1	9.0	0.6	-5.1	-7.3
Mean ± SD	-6.5 ± 0.4	-18.4 ± 1.1	-2.8 ± 0.0	3.0 ± 0.1	8.4 ± 1.5	11.9 ± 0.5	13.8 ± 0.6	13.9 ± 0.3	9.6 ± 0.8	1.2 ± 0.8	-4.2 ± 1.3	-7.7 ± 0.6
2020												
Jasper	-11.0	-4.4	-5.4	1.0	8.3	11.9	15.2	14.4	12.2	1.8	-2.4	-4.7
Banff	-9.3	-5.6	-5.2	0.3	6.7	11.6	14.6	14.8	11.4	1.5	-2.3	-5.5
Mean ± SD	-10.2 ± 1.2	-5.0 ± 0.8	-5.3 ± 0.1	0.7 ± 0.5	7.5 ± 1.0	11.8 ± 0.2	14.9 ± 0.4	14.6 ± 0.3	11.8 ± 0.6	1.7 ± 0.2	-2.4 ± 0.1	-5.1 ± 0.6

Table A1.9. Mean (± standard deviation) 2019 and 2020 main physicochemical measures for (a) in situ parameters, (b) basic chemical parameters, (c) nutrients, (d) ions, (e) trace elements, and (f) contaminants. January 2021 data was added to 2020. Rivers are abbreviated as SR (Sunwapta River), AR (Athabasca River), NSR (North Saskatchewan River), and BR (Bow River). For site abbreviations please see **Table A1.1** and for parameter abbreviations please see *Section 2.3* in the main text.

a.	Temperature °C		pH		Turbidity FNU		Conductivity uS cm^{-1}		ODO % saturation (corrected)		ODO mg L^{-1}	
Site ID	2019	2020	2019	2020	2019	2020	2019	2020	2019	2020	2019	2020
SR1	0.3 ± 0.3	0.4 ± 0.2	8.3 ± 0.4	8.5 ± 0.3	74.8 ± 33.9	141.2 ± 161.1	75.3 ± 35.1	54.9 ± 16.4	96.3 ± 6.7	100.9 ± 4.0	11.1 ± 0.8	11.5 ± 0.5
SR2	2.7 ± 1.6	2.9 ± 1.0	8.1 ± 0.4	8.3 ± 0.1	39.3 ± 17.3	61.6 ± 24.3	100.2 ± 29.6	80.0 ± 8.4	104.9 ± 3.1	100.9 ± 2.5	11.4 ± 0.7	10.8 ± 0.2
SR3	7.0 ± 3.3	6.1 ± 2.6	8.2 ± 0.1	7.9 ± 0.4	10.8 ± 16.8	77.7 ± 141.2	130.0 ± 40.9	116.2 ± 54.4	104.2 ± 4.5	99.3 ± 3.8	10.6 ± 0.9	10.2 ± 0.4
SR4	6.0 ± 3.4	5.8 ± 2.8	8.1 ± 0.2	8.0 ± 0.1	16.2 ± 6.8	28.2 ± 29.3	136.1 ± 9.7	122.6 ± 19.8	103.8 ± 4.5	99.6 ± 1.6	11.1 ± 1.1	10.5 ± 0.8
AR1	4.3 ± 4.5	7.2 ± 1.3	7.6 ± 0.1	8.0 ± 0.1	NA	20.9 ± 8.7	112.8 ± 10.6	115.1 ± 24.5	99.9 ± 2.0	101.8 ± 1.2	11.3 ± 1.6	10.6 ± 0.4
AR2	6.3 ± 4.5	6.9 ± 3.4	8.0 ± 0.4	8.0 ± 0.1	20.8 ± 21.7	29.9 ± 21.3	125.0 ± 9.4	121.3 ± 13.3	102.1 ± 5.9	100.8 ± 1.8	11.1 ± 1.1	10.7 ± 1.0
AR3	7.6 ± 3.7	8.4 ± 1.9	8.1 ± 0.3	8.0 ± 0.1	26.0 ± 7.6	26.3 ± 14.4	121.7 ± 7.6	112.3 ± 14.8	105.1 ± 2.6	102.8 ± 2.1	11.2 ± 1.1	10.6 ± 0.5
NSR1	3.7 ± 2.4	3.8 ± 1.9	8.2 ± 0.3	7.9 ± 0.1	6.5 ± 8.0	9.8 ± 7.7	83.5 ± 25.7	76.1 ± 15.4	104.6 ± 2.1	106.8 ± 3.8	11.3 ± 0.5	11.5 ± 0.8
NSR2	5.8 ± 2.5	5.8 ± 1.4	8.1 ± 0.3	8.0 ± 0.1	19.0 ± 5.6	135.1 ± 211.5	157.4 ± 31.0	142.9 ± 19.2	101.9 ± 1.6	100.1 ± 1.2	10.7 ± 0.6	10.5 ± 0.3
NSR3	6.3 ± 2.6	6.4 ± 1.7	8.2 ± 0.2	7.9 ± 0.1	28.9 ± 10.8	68.2 ± 118.8	149.6 ± 30.5	135.7 ± 17.8	106.0 ± 2.8	104.3 ± 1.0	11.1 ± 0.6	10.9 ± 0.4
BR1	4.6 ± 2.6	4.6 ± 1.2	8.1 ± 0.4	7.9 ± 0.1	9.1 ± 5.2	6.2 ± 5.5	96.8 ± 23.6	92.7 ± 17.1	104.6 ± 3.0	105.3 ± 2.3	10.7 ± 0.6	10.7 ± 0.3
BR2	9.7 ± 4.1	8.7 ± 2.3	8.2 ± 0.4	7.9 ± 0.1	2.4 ± 0.6	2.7 ± 2.0	143.5 ± 3.5	139.8 ± 8.3	100.0 ± 1.1	99.3 ± 1.3	9.2 ± 0.8	9.3 ± 0.4
BR3	7.9 ± 5.4	9.8 ± 2.2	8.2 ± 0.4	8.0 ± 0.1	8.2 ± 8.4	7.1 ± 6.9	128.5 ± 10.8	131.4 ± 5.9	102.5 ± 3.7	100.6 ± 0.9	10.2 ± 1.4	9.5 ± 0.5
BR4	8.4 ± 3.5	8.6 ± 2.4	8.3 ± 0.5	8.1 ± 0.2	7.5 ± 4.4	6.7 ± 8.2	139.0 ± 7.6	138.6 ± 11.7	103.9 ± 4.5	100.7 ± 1.6	10.3 ± 1.1	9.9 ± 0.6

b.	TSS mg L^{-1}		TDS mg L^{-1}		PN ug L^{-1}		PC mg L^{-1}		DIC mg L^{-1}		DOC mg L^{-1}	
Site ID	2019	2020	2019	2020	2019	2020	2019	2020	2019	2020	2019	2020
SR1	61.4 ± 44.3	168.2 ± 193.8	76.8 ± 43.9	44.8 ± 28.5	22.9 ± 20	98.9 ± 123.4	3.19 ± 0.24	11.45 ± 15.75	11.5 ± 4.5	9.4 ± 2.6	0.4 ± 0.2	0.2 ± 0.2
SR2	37.8 ± 23.2	66.4 ± 23	86.8 ± 41.2	69.4 ± 21.7	22.1 ± 13.3	45.4 ± 16.8	2.02 ± 1.30	3.87 ± 1.64	14.8 ± 4.5	13.1 ± 1.2	0.4 ± 0.3	0.1 ± 0
SR3	16.7 ± 14.3	116.2 ± 183	116.6 ± 22.5	103.4 ± 26.4	8.5 ± 9.2	79 ± 140.9	0.94 ± 0.89	8.30 ± 15.68	19.5 ± 2.1	19.6 ± 2.6	0.4 ± 0.3	0.3 ± 0.2
SR4	12.2 ± 9.1	46.3 ± 53.6	120 ± 23.5	110.4 ± 37	15.8 ± 11.7	41.8 ± 57.8	0.69 ±0. 51	2.46 ± 3.18	18.1 ± 2.2	17.7 ± 2.4	1.1 ± 0.9	0.7 ± 0.5
AR1	10.4 ± 12	31.5 ± 16.1	103.5 ± 30.4	89 ± 17.8	8.7 ± 10.1	49.5 ± 29.1	0.61 ± 0.58	2.98 ± 1.76	18.2 ± 2.9	16.6 ± 1.2	0.4 ± 0.1	0.4 ± 0.2
AR2	16 ± 17.2	43.1 ± 30.3	103.5 ± 20.6	116.1 ± 39.4	12.7 ± 12.3	35.8 ± 26.8	0.84 ± 0.83	1.97 ± 1.40	18 ± 2.3	17.5 ± 2.4	0.9 ± 0.8	0.6 ± 0.4
AR3	17.3 ± 11.8	42.2 ± 27.4	105 ± 15.4	99.7 ± 21	18.7 ± 12.1	41.6 ± 22.3	0.94 ± 0.62	2.58 ± 1.95	14.8 ± 2.6	14.1 ± 1.4	1.2 ± 0.9	0.7 ± 0.5
NSR1	5 ± 5.6	18.4 ± 23.5	73 ± 29.5	58.1 ± 17.7	3.9 ± 2.8	11 ± 10.4	0.32 ± 0.33	0.95 ± 0.90	14.2 ± 4.2	12.8 ± 2.5	0.3 ± 0.4	0.2 ± 0.1
NSR2	10.6 ± 7	184.4 ± 375.6	138.6 ± 46.8	111.2 ± 33.6	7.7 ± 4	110.3 ± 203	0.76 ± 0.44	9.52 ± 17.93	20 ± 4.2	19 ± 3.3	0.5 ± 0.5	0.3 ± 0.2
NSR3	21.2 ± 14.4	53.7 ± 63.6	127.4 ± 45	110.5 ± 33.4	16.1 ± 8.1	58.1 ± 91.9	1.18 ± 0.72	3.33 ± 4.71	20 ± 4.3	19 ± 3.6	0.5 ± 0.4	0.4 ± 0.3
BR1	4.2 ± 2.9	9.3 ± 10.5	85.3 ± 33.3	70.3 ± 13.9	8.2 ± 5.6	15.7 ± 10.7	0.31 ± 0.20	1.24 ± 1.79	13.7 ± 4.4	13.5 ± 3	0.2 ± 0	0.2 ± 0.1
BR2	2.5 ± 2.9	3.7 ± 3.6	103.3 ± 33.3	105.2 ± 17	10 ± 5.6	17 ± 11.2	0.43 ± 0.20	0.45 ± 0.32	20 ± 4.4	20 ± 1.8	0.5 ± 0	0.8 ± 0.4
BR3	5.8 ± 4.9	10.1 ± 13.6	94.7 ± 14.8	91.8 ± 12	10.3 ± 4.6	15.9 ± 12.4	0.37 ± 0.30	0.53 ± 0.55	19.4 ± 2.1	19.5 ± 2.9	1 ± 0.9	0.6 ± 0.2
BR4	6.2 ± 4.1	6.4 ± 9.1	112.8 ± 17.2	109.2 ± 35.9	11.1 ± 5.3	16.3 ± 14.6	0.29 ± 0.17	0.43± 0.39	19 ± 2	18.6 ± 1.1	1.2 ± 1.2	0.6 ± 0.3

c.	TP ug L^{-1}		TN ug L^{-1}		TDN ug L^{-1}		NO$_2^-$+NO$_3^-$ ug L^{-1}		Si mg L^{-1}	
Site ID	2019	2020	2019	2020	2019	2020	2019	2020	2019	2020
SR1	22 ± 14.1	81.2 ± 99.1	8.3 ± 0.4	8.5 ± 0.3	89.8 ± 41.4	58.8 ± 33.7	81 ± 37.7	52.4 ± 24.7	0.4 ± 0.3	0.4 ± 0.2
SR2	23 ± 19.8	36 ± 17.3	8.1 ± 0.4	8.3 ± 0.1	92.8 ± 39	58.2 ± 32.3	83.4 ± 35.8	55.5 ± 16.8	0.6 ± 0.3	0.5 ± 0.1
SR3	7.6 ± 6.3	46.6 ± 70.3	8.2 ± 0.1	7.9 ± 0.4	119.4 ± 34.2	101.7 ± 37.3	110.4 ± 30	93.1 ± 44	1.2 ± 0.4	1.1 ± 0.4
SR4	6 ± 1.6	20.1 ± 25.6	8.1 ± 0.2	8.0 ± 0.1	104 ± 38.5	89 ± 36.1	75.5 ± 44.2	71.7 ± 43.5	1.6 ± 0.4	1.5 ± 0.2
AR1	34 ± 41	22.7 ± 8.4	7.6 ± 0.1	8.0 ± 0.1	75.5 ± 31.8	71.7 ± 12	59 ± 29.7	55.9 ± 3.8	1.6 ± 0.2	1.2 ± 0.2
AR2	15.2 ± 10.8	26 ± 14.4	8.0 ± 0.4	8.0 ± 0.1	107 ± 42.7	83.6 ± 37.6	86.3 ± 40.6	70.3 ± 45.2	1.6 ± 0.4	1.6 ± 0.7
AR3	15.8 ± 10.4	23.3 ± 11.5	8.1 ± 0.3	8.0 ± 0.1	98.6 ± 49.6	73 ± 35.1	68.3 ± 34.3	47.6 ± 7.1	1.6 ± 0.3	1.4 ± 0.1
NSR1	3.7 ± 2.3	5.5 ± 4.1	8.2 ± 0.3	7.9 ± 0.1	76 ± 30	52 ± 37.4	76.2 ± 41.9	55 ± 27.5	0.8 ± 0.5	0.6 ± 0.2
NSR2	9 ± 3	106.7 ± 205.3	8.1 ± 0.3	8.0 ± 0.1	92.2 ± 41.9	90 ± 44	91.4 ± 44.7	61.6 ± 22.7	1.4 ± 0.5	1.1 ± 0.3
NSR3	20.4 ± 11.9	73.8 ± 104.1	8.2 ± 0.2	7.9 ± 0.1	100.2 ± 37.6	83.3 ± 25.6	90.2 ± 33.1	65.2 ± 14	1.2 ± 0.5	1.1 ± 0.3
BR1	5.5 ± 3.7	4.1 ± 2.2	8.1 ± 0.4	7.9 ± 0.1	89 ± 17.8	72.3 ± 24.6	90.8 ± 42.2	65.6 ± 23.8	0.6 ± 0.3	0.6 ± 0.2
BR2	4.3 ± 3.7	2.3 ± 0.5	8.2 ± 0.4	7.9 ± 0.1	68 ± 17.8	56.5 ± 22	44.6 ± 42.2	35 ± 6.5	1.2 ± 0.3	1.2 ± 0.1
BR3	4.4 ± 2.3	5.3 ± 3.4	8.2 ± 0.4	8.0 ± 0.1	91.7 ± 27.1	78.5 ± 15.1	62.9 ± 17	49.7 ± 11.9	1.3 ± 0.3	1.2 ± 0.1
BR4	4.4 ± 1.1	6 ± 5.3	8.3 ± 0.5	8.1 ± 0.2	105.4 ± 33.6	72.6 ± 11.3	78.4 ± 14.6	52.3 ± 5.7	1.5 ± 0.3	1.3 ± 0

d.	Ca^{2+} mg L^{-1}		K^{+} mg L^{-1}		Mg^{2+} mg L^{-1}		Na^{+} mg L^{-1}		Cl^{-} mg L^{-1}		SO_4^{2-} mg L^{-1}	
Site ID	2019	2020	2019	2020	2019	2020	2019	2020	2019	2020	2019	2020
SR1	15.2 ± 6.5	13.4 ± 2.6	0.2 ± 0.1	0.1 ± 0.1	6.2 ± 4.4	4.2 ± 2	0.3 ± 0.2	0.2 ± 0.2	0.2 ± 0.1	0.1 ± 0	17.4 ± 16	8.7 ± 4.4
SR2	18.5 ± 4.9	17.7 ± 1.1	0.2 ± 0.1	0.1 ± 0.1	8.2 ± 4	6.6 ± 1.3	0.3 ± 0.2	0.2 ± 0.1	0.2 ± 0.1	0.2 ± 0.3	20.9 ± 13.8	10.6 ± 2.1
SR3	24.4 ± 3.2	27 ± 1.8	0.2 ± 0	0.1 ± 0.1	9.5 ± 2.1	8.8 ± 1.9	0.6 ± 0.2	0.5 ± 0.2	0.5 ± 0.2	0.4 ± 0.2	26.2 ± 6	21.4 ± 6.9
SR4	23.8 ± 3.8	26.3 ± 4.5	0.4 ± 0.1	0.3 ± 0.1	9.5 ± 1.6	9.6 ± 3.2	1 ± 0.2	0.9 ± 0.4	0.4 ± 0.2	0.3 ± 0.2	29.3 ± 10.6	28.7 ± 16.1
AR1	20.6 ± 4.9	24.6 ± 3.1	0.3 ± 0	0.2 ± 0.1	8 ± 2.5	7 ± 0.6	0.7 ± 0.3	0.5 ± 0.1	0.2 ± 0.1	0.2 ± 0.1	20.1 ± 8.7	15.8 ± 5.3
AR2	23.3 ± 3.6	24.7 ± 1.6	0.3 ± 0	0.2 ± 0.1	8.3 ± 1.6	7.5 ± 1.3	0.7 ± 0.2	0.6 ± 0.2	0.2 ± 0.1	0.2 ± 0.1	20.8 ± 4.3	17.9 ± 4.6
AR3	19.5 ± 3.1	21.3 ± 1.9	0.3 ± 0	0.2 ± 0	7.8 ± 0.9	7.3 ± 0.3	0.7 ± 0.1	0.6 ± 0.1	0.2 ± 0.1	0.1 ± 0	24.8 ± 3.5	21.4 ± 0.5
NSR1	16.8 ± 4.8	16.9 ± 2.7	0.1 ± 0.1	0 ± 0.1	6.5 ± 3.1	5 ± 2	0.2 ± 0.1	0.1 ± 0.1	0.1 ± 0.1	0.1 ± 0.1	10.5 ± 5.2	7.9 ± 4
NSR2	29.8 ± 8.4	28.1 ± 6.6	0.3 ± 0.1	0.2 ± 0.1	10.4 ± 3.1	8.9 ± 2.4	0.8 ± 0.3	0.5 ± 0.3	0.3 ± 0.1	0.3 ± 0.2	39.3 ± 19.6	30.4 ± 8.3
NSR3	28.6 ± 7.7	28.6 ± 5	0.3 ± 0.1	0.2 ± 0.1	9.6 ± 3.4	8.2 ± 1.7	0.7 ± 0.3	0.5 ± 0.1	0.2 ± 0.1	0.1 ± 0	32.3 ± 16.2	23.5 ± 4.9
BR1	17.5 ± 5.6	20.7 ± 5.7	0.2 ± 0	0.1 ± 0.1	7.6 ± 3	7.4 ± 1.9	0.3 ± 0.1	0.3 ± 0.1	0.2 ± 0.2	0.1 ± 0	20.3 ± 10.3	16.8 ± 4.5
BR2	25.9 ± 5.6	25.6 ± 4.8	0.3 ± 0	0.2 ± 0.1	11.6 ± 3	10.7 ± 1.6	1.4 ± 0.1	0.9 ± 0.5	0.7 ± 0.2	0.6 ± 0.2	22.8 ± 10.3	20.3 ± 2.7
BR3	21.7 ± 3.4	23.4 ± 2.3	0.2 ± 0	0.2 ± 0	9.2 ± 1.2	8.8 ± 0.6	0.9 ± 0.4	0.8 ± 0.3	1 ± 0.4	0.9 ± 0.4	14.4 ± 1.8	13.1 ± 1
BR4	22 ± 3.5	24.1 ± 2.7	0.3 ± 0	0.2 ± 0	9.4 ± 1.1	9.6 ± 0.8	1 ± 0.3	1 ± 0.2	1 ± 0.3	1 ± 0.2	20.4 ± 4.6	18.7 ± 2.9

e.	Al ug L^{-1}		Ba ug L^{-1}		Cr ug L^{-1}		Mn ug L^{-1}		Mo ug L^{-1}		Sr ug L^{-1}	
Site ID	2019	2020	2019	2020	2019	2020	2019	2020	2019	2020	2019	2020
SR1	9.3 ± 8.8	5 ± 2.7	2.5 ± 1.6	8.6 ± 6.2	0.2 ± 0.1	0.1 ± 0	0.6 ± 0.5	0.6 ± 0.6	0.1 ± 0	0.1 ± 0	83.6 ± 55.2	57.4 ± 24.3
SR2	5.7 ± 2.6	4.3 ± 1.1	3.3 ± 1.5	7.9 ± 4.7	0.1 ± 0.1	0.1 ± 0	1.2 ± 0.9	1 ± 0.8	0.1 ± 0.1	0.1 ± 0	99.4 ± 51.3	75.2 ± 14.1
SR3	4.3 ± 2.4	3.7 ± 1.9	7 ± 2.9	9.8 ± 4.7	0.2 ± 0.1	0.1 ± 0	0.3 ± 0.2	0.5 ± 0.5	0.1 ± 0	0.1 ± 0	146.5 ± 34.8	140.1 ± 29.8
SR4	15.3 ± 4.1	12.4 ± 2.2	35.2 ± 6.2	38 ± 9.2	0.2 ± 0.1	0.1 ± 0	1.3 ± 0.5	1.1 ± 0.3	0.1 ± 0	0.1 ± 0	257.3 ± 93.4	281.2 ± 165
AR1	5.1 ± 0.7	7 ± 1.3	51.2 ± 0.1	42.4 ± 20	0.1 ± 0.1	0.1 ± 0	0.8 ± 0	0.8 ± 0.1	0.1 ± 0.1	0.1 ± 0	168.5 ± 91.9	166 ± 41.6
AR2	12.5 ± 7.5	8.8 ± 2.9	43.7 ± 16.1	41.5 ± 13.1	0.1 ± 0.1	0.1 ± 0	1 ± 0.7	0.8 ± 0.3	0.1 ± 0	0.1 ± 0	201 ± 51.9	181 ± 44.1
AR3	20.5 ± 10.4	18.6 ± 10.2	33 ± 10.1	37.3 ± 11.3	0.1 ± 0.1	0.1 ± 0	2.2 ± 0.9	2 ± 1	0.1 ± 0	0.1 ± 0	152.7 ± 43.9	139.1 ± 19
NSR1	6.1 ± 3.4	5.3 ± 1.5	5 ± 3.8	13.3 ± 18.3	0.1 ± 0.1	0.1 ± 0	0.2 ± 0.2	0.3 ± 0.2	0.1 ± 0	0.1 ± 0	94.8 ± 43.6	76.8 ± 26.3
NSR2	13.2 ± 18	3.5 ± 0.6	20.2 ± 6.5	24.1 ± 11.5	0.2 ± 0.1	0.1 ± 0	0.5 ± 0.3	0.5 ± 0.3	0.3 ± 0.1	0.2 ± 0.1	644 ± 273	569.6 ± 111.2
NSR3	5.8 ± 3	19.2 ± 25.1	19.1 ± 6.6	21.2 ± 7	0.2 ± 0.1	0.1 ± 0	0.7 ± 0.2	0.9 ± 0.4	0.2 ± 0	0.2 ± 0	589.1 ± 289.7	493.8 ± 88.6
BR1	4.7 ± 2.5	8.4 ± 14.3	7.8 ± 1.9	15.7 ± 9.5	0.1 ± 0.1	0.1 ± 0	0.5 ± 0.5	0.5 ± 0.6	0.1 ± 0	0.1 ± 0	426.9 ± 158.2	447.9 ± 62.8
BR2	5.2 ± 2.5	3.3 ± 1.9	13.3 ± 1.9	16.8 ± 5.5	0.2 ± 0.1	0.1 ± 0	0.4 ± 0.5	0.9 ± 0.9	0.1 ± 0	0.1 ± 0	264 ± 158.2	267.8 ± 41.9
BR3	4.9 ± 4	2.7 ± 0.7	10.2 ± 1.2	15.4 ± 6.5	0.1 ± 0.1	0.1 ± 0	0.3 ± 0.2	0.5 ± 0.3	0.1 ± 0	0.1 ± 0	162.4 ± 10.4	160.5 ± 17.4
BR4	6 ± 4.7	2.9 ± 2.1	10.1 ± 1	16.1 ± 6	0.2 ± 0.1	0.1 ± 0	0.4 ± 0.2	0.6 ± 0.4	0.1 ± 0	0.1 ± 0	108.4 ± 13	115.3 ± 17.5

f.	THg ng L^{-1}		FHg ng L^{-1}	
Site ID	2019	2020	2019	2020
SR1	2 ± 1.1	2.9 ± 2.2	0.6 ± 0.6	0.2 ± 0.1
SR2	1.6 ± 1	1.7 ± 0.2	0.3 ± 0.2	0.2 ± 0.1
SR3	0.7 ± 0.7	1.8 ± 2.4	0.8 ± 1.1	0.1 ± 0.1
SR4	1.3 ± 0.9	1.7 ± 1.6	0.6 ± 0.5	0.4 ± 0.3
AR1	0.6 ± 0.5	1.2 ± 0.8	0.2 ± 0.1	0.2 ± 0.1
AR2	1.1 ± 1	1.4 ± 0.8	0.6 ± 0.7	0.3 ± 0.2
AR3	1 ± 0.6	1.4 ± 0.8	0.7 ± 0.6	0.5 ± 0.3
NSR1	0.5 ± 0.7	0.3 ± 0.2	0.5 ± 0.7	0.1 ± 0
NSR2	0.4 ± 0.2	2.2 ± 3.8	0.3 ± 0.3	0.2 ± 0.2
NSR3	0.7 ± 0.3	1.3 ± 1.4	0.3 ± 0.2	0.2 ± 0
BR1	0.8 ± 0.6	0.7 ± 0.5	0.2 ± 0.1	0.3 ± 0.2
BR2	0.5 ± 0.6	0.6 ± 0.3	0.3 ± 0.1	0.4 ± 0.2
BR3	0.6 ± 0.3	0.7 ± 0.4	0.4 ± 0.3	0.3 ± 0.1
BR4	0.8 ± 0.5	0.5 ± 0.4	0.5 ± 0.4	0.3 ± 0.2

Table A1.10. Principal Component (PC) loading matrices for (a) the main physicochemical parameters, relating to **Figure 2.6**, (b) cations, relating to **Figure A1.9**, and (c) trace elements, relating to **Figure A1.10**. For parameter abbreviations, please see *Section 2.3* in the main text.

a.	PC1	PC2	PC3	PC4	PC5	PC6	PC7	PC8	PC9	PC10	PC11	PC12	PC13	PC14	PC15	PC16	PC17	PC18	PC19	PC20	PC21	PC22	PC23
Temp	0.28	0.31	25.02	7.82	3.99	5.15	3.36	0.58	0.93	0.10	0.01	0.09	3.41	4.58	9.84	0.02	14.21	1.36	0.49	7.69	8.91	1.70	0.16
pH	0.57	0.03	0.15	1.03	67.71	9.06	11.04	3.74	0.33	0.28	2.32	0.19	0.91	0.03	0.57	0.21	0.90	0.00	0.40	0.06	0.24	0.21	0.00
Cond	7.77	0.26	5.00	0.67	0.24	2.78	3.61	5.87	3.70	0.81	0.08	3.15	10.90	4.14	8.04	0.53	34.33	0.16	5.35	1.06	0.07	1.35	0.15
ODO	0.02	0.68	28.79	2.10	1.13	0.05	12.71	4.86	6.16	0.22	0.03	1.93	0.63	3.76	15.69	1.70	1.18	2.69	1.62	5.48	7.86	0.72	0.00
TSS	2.50	16.11	0.99	0.81	0.03	0.11	0.00	0.03	0.02	0.02	0.87	0.13	0.05	0.11	0.00	1.04	0.37	0.91	10.51	0.98	14.39	37.46	12.53
TDS	8.00	0.26	0.11	2.35	0.32	5.60	0.01	1.80	15.05	0.00	8.80	10.46	32.41	4.58	3.45	4.29	0.22	0.37	0.00	0.89	0.83	0.11	0.09
TP	1.92	16.19	1.08	0.93	0.12	0.00	0.03	0.30	0.24	0.74	0.16	2.21	0.11	0.63	6.47	8.87	9.30	26.22	0.89	12.22	0.01	1.35	10.01
TN	2.10	7.68	3.76	3.01	1.47	0.25	9.34	4.30	1.56	57.22	4.05	0.00	0.37	0.25	0.67	1.41	0.01	2.17	0.15	0.01	0.02	0.00	0.20
TDN	4.41	3.49	7.15	2.68	0.13	0.87	10.33	0.33	0.50	10.12	3.30	19.87	2.41	14.52	13.68	2.11	0.31	1.33	2.34	0.00	0.07	0.07	0.00
NO_2^-+NO_3^-	3.20	1.55	13.63	0.26	0.91	0.52	18.94	0.52	15.80	6.49	3.30	8.29	0.02	20.41	2.74	0.21	1.19	0.49	1.30	0.00	0.01	0.08	0.14
Si	7.71	1.44	0.01	1.51	0.90	0.83	5.58	16.98	0.00	3.36	2.36	11.61	5.40	7.97	6.41	20.40	0.10	1.51	0.19	1.69	2.49	0.97	0.58
Ca^{2+}	8.02	0.56	0.61	3.95	0.69	0.12	1.59	6.41	2.41	2.48	32.75	0.63	0.15	3.19	1.10	2.68	0.93	3.01	14.70	7.84	0.22	5.96	0.02
K^+	8.08	0.91	0.00	0.91	1.55	3.75	4.64	3.44	21.94	0.94	4.43	1.40	0.10	2.80	3.83	12.03	0.06	12.60	6.53	1.90	6.50	1.42	0.24
Mg^{2+}	9.58	0.27	0.29	2.92	0.63	0.88	0.00	4.04	1.47	0.85	0.05	0.19	3.28	2.22	8.11	6.47	0.61	1.04	19.27	3.67	26.98	6.02	1.18
Na^+	6.99	0.17	2.19	0.10	7.26	3.83	12.05	0.85	15.25	3.77	5.99	0.00	6.36	7.24	0.70	1.84	1.21	10.41	4.67	3.22	0.70	5.21	0.01
Cl^-	3.65	0.01	4.08	1.48	8.86	45.64	0.51	0.23	5.34	0.02	16.33	0.08	0.39	0.48	2.92	1.65	0.13	0.61	6.14	0.33	0.47	0.66	0.00
SO_4^{2-}	6.41	0.37	0.39	9.16	0.03	11.83	0.18	4.47	0.03	2.81	9.27	2.82	17.97	0.48	0.69	15.67	5.36	1.94	1.22	7.27	0.03	1.61	0.00
PN	2.14	16.62	1.93	0.51	0.01	0.02	0.22	0.00	0.10	0.24	0.01	0.02	0.08	0.17	0.21	0.04	0.33	3.71	0.31	1.84	8.53	20.76	42.20
PC	2.59	15.10	1.19	1.10	0.19	0.09	0.14	0.41	0.08	3.02	0.36	0.15	0.11	1.04	0.47	4.44	0.00	25.88	5.26	0.02	3.54	5.32	29.51
DIC	8.88	1.00	1.35	1.53	0.06	2.28	0.89	0.00	3.48	1.43	2.72	9.48	0.02	12.79	2.22	12.06	1.58	0.19	0.34	29.78	5.07	2.83	0.03
DOC	2.27	1.64	0.28	25.53	0.66	0.08	3.93	4.66	3.29	4.50	1.84	9.23	14.79	7.51	9.46	1.23	5.72	1.25	0.37	0.03	0.99	0.73	0.02
THg	2.71	14.92	0.23	1.15	0.14	0.60	0.43	1.98	0.45	0.22	0.01	1.58	0.03	0.16	1.56	1.11	21.54	1.93	16.45	13.18	11.83	5.05	2.75
FHg	0.22	0.43	1.79	28.49	2.99	5.67	0.47	34.21	1.89	0.37	0.98	16.46	0.09	0.94	1.18	0.00	0.41	0.22	1.51	0.83	0.23	0.43	0.17

b.	PC1	PC2	PC3	PC4	PC5	PC6	PC7	PC8
Ca^{2+}	8.05	14.33	46.26	3.19	27.65	0.46	0.03	0.02
K^{+}	11.38	11.45	33.23	0.02	5.38	36.73	1.69	0.13
Mg^{2+}	10.77	16.91	6.45	0.66	62.44	2.22	0.36	0.19
Na^{+}	12.44	13.50	13.21	1.91	0.48	57.98	0.41	0.08
Ca^{2+}_PTL	16.03	9.53	0.77	6.45	0.12	1.64	61.17	4.29
K^{+}_PTL	13.98	13.47	0.00	11.25	0.43	0.35	15.80	44.71
Mg^{2+}_PTL	11.83	15.73	0.00	26.55	0.44	0.62	0.05	44.78
Na^{+}_PTL	15.52	5.08	0.08	49.96	3.05	0.00	20.50	5.80

c.	PC1	PC2	PC3	PC4	PC5	PC6	PC7	PC8	PC9	PC10	PC11	PC12	PC13	PC14	PC15	PC16	PC17	PC18	PC19
Al	0.03	10.69	21.82	18.43	11.02	25.17	1.56	8.83	0.29	0.99	0.34	0.29	0.07	0.03	0.38	0.05	0.01	0.00	0.00
Ba	0.11	9.96	21.79	8.56	53.74	2.33	1.37	1.01	0.29	0.50	0.19	0.00	0.07	0.04	0.04	0.01	0.00	0.00	0.00
Cr	0.50	9.60	0.32	61.17	23.79	0.30	0.01	1.07	3.16	0.02	0.02	0.00	0.00	0.03	0.00	0.00	0.00	0.00	0.00
Mn	0.10	25.46	6.98	6.59	3.05	39.21	5.16	12.51	0.77	0.02	0.01	0.03	0.01	0.02	0.05	0.04	0.00	0.00	0.00
Mo	0.16	26.51	18.22	0.08	2.88	0.35	1.29	11.00	35.68	2.25	1.17	0.24	0.00	0.03	0.12	0.00	0.00	0.01	0.00
Sr	0.02	16.82	29.19	4.02	1.23	6.27	1.48	0.78	37.77	1.27	0.66	0.09	0.01	0.01	0.38	0.00	0.01	0.01	0.01
Ag_PTL	7.64	0.12	0.00	0.45	1.30	1.73	0.18	1.50	2.65	45.38	31.81	5.79	1.33	0.00	0.00	0.06	0.00	0.03	0.03
Al_PTL	7.91	0.00	0.01	0.00	0.00	0.38	0.40	2.55	0.05	0.10	0.14	39.95	8.56	2.86	0.00	25.37	5.78	5.88	0.06
Ba_PTL	7.74	0.15	0.03	0.01	0.02	0.80	1.40	1.98	5.45	16.50	50.89	1.23	11.75	0.80	0.10	0.48	0.08	0.37	0.21
Co_PTL	7.76	0.01	0.05	0.00	0.03	2.49	1.66	5.83	0.47	4.58	1.00	3.57	13.59	10.58	0.27	3.91	7.84	20.43	15.92
Cr_PTL	7.94	0.02	0.02	0.01	0.03	0.12	1.34	0.05	0.03	0.00	0.26	8.68	6.52	1.80	0.01	9.81	2.33	52.29	8.73
Cu_PTL	6.52	0.21	0.09	0.00	0.21	4.41	60.14	1.38	0.88	1.57	1.08	1.26	0.15	9.75	11.88	0.15	0.21	0.10	0.00
Fe_PTL	7.86	0.00	0.00	0.00	0.02	1.23	1.80	2.09	0.00	6.73	0.03	2.90	5.88	0.01	0.72	0.29	2.73	1.28	66.42
Mn_PTL	7.79	0.04	0.47	0.04	0.33	0.01	2.61	2.73	0.75	4.51	0.05	25.02	0.00	22.01	13.44	11.08	1.83	0.23	7.07
Ni_PTL	7.95	0.01	0.01	0.06	0.02	0.20	0.77	0.05	0.15	3.09	0.37	0.57	0.02	17.36	0.01	4.35	64.04	0.98	0.00
Pb_PTL	7.39	0.19	0.24	0.19	1.72	4.34	2.76	16.26	8.06	0.01	0.42	0.70	0.11	8.12	32.30	12.79	3.61	0.80	0.01
Sr_PTL	7.61	0.01	0.08	0.02	0.00	3.95	1.49	11.31	0.02	9.09	11.31	2.57	48.88	0.59	1.24	0.08	1.34	0.05	0.36
V_PTL	7.51	0.20	0.58	0.16	0.60	1.80	2.47	14.85	3.40	3.34	0.10	3.23	0.69	11.71	0.00	30.51	0.11	17.54	1.18
Zn_PTL	7.47	0.01	0.10	0.20	0.00	4.91	12.11	4.21	0.12	0.04	0.15	3.88	2.36	14.28	39.06	1.02	10.07	0.00	0.00

Table A1.11. Open water season (OWS; May 1 to October 31) 2019 and 2020 chemical yields for (a) basic chemical parameters, (b) nutrients, (c) ions, (d) trace elements, and (e) contaminants and water. Yields were calculated using the U.S. Geological Survey LOAD Estimator (LOADEST; Runkel et al., 2004), modeled OWS daily chemical loads (see *Section 2.6* in the main text) and site-specific watershed area (km^2; **Table A1.1**). Gaps in the table are when a chemical yield could not be calculated for a sampling site (i.e., gaps in **Table A1.9** for reasons summarized in **Table A1.6**). Rivers are abbreviated as SR (Sunwapta River), AR (Athabasca River), NSR (North Saskatchewan River), and BR (Bow River). For site abbreviations please see **Table A1.1** and for parameter abbreviations please see *Section 2.3* in the main text.

a.	TSS		TDS		PN		PC		DIC		DOC	
	Mg OWS^{-1} km^{-2}		Mg OWS^{-1} km^{-2}		kg OWS^{-1} km^{-2}		Mg OWS^{-1} km^{-2}		Mg OWS^{-1} km^{-2}		kg OWS^{-1} km^{-2}	
Site ID	2019	2020	2019	2020	2019	2020	2019	2020	2019	2020	2019	2020
SR1	211	300	69.2	99.0	116	167	11.7	16.2	12.8	17.4	351	455
SR2	73.1	78.9	83.7	89.9	41.9	45.0	5.76	6.94	15.4	17.2	303	341
SR3			60.4	69.0					10.6	12.7	214	244
SR4	26.6	45.0	67.8	71.8	23.1	31.5	1.26	1.66	11.0	12.2	559	617
AR2	27.1	48.0	71.2	78.2	19.1	34.3	1.30	2.10	11.1	12.4	545	578
AR3			67.0	73.1	24.0	34.2	1.30	1.89	9.40	10.2	638	680
NSR1	10.0	20.2	45.0	49.6	7.74	15.9	0.677	1.28	9.18	10.9	123	151
NSR2	39.1	95.9	76.5	79.6	27.6	60.6	2.47	5.16	12.3	13.8	259	278
NSR3	32.3	51.0	77.0	81.9	21.9	37.9	1.66	2.48	12.8	14.1	305	320
BR1	11.3	15.0	102	134	22.7	33.1	1.30	1.88	16.9	21.8	271	353
BR2	2.22	3.52	73.2	84.8	8.85	14.4	0.310	0.445	13.8	16.4	590	653
BR3	5.62	8.93	62.9	70.3	9.13	12.6	0.324	0.459	12.5	14.7	526	579
BR4	4.94	6.18	74.8	78.5	9.27	11.4	0.251	0.333	12.2	13.5	655	705

b.	TP kg OWS^{-1} km^{-2}		TN kg OWS^{-1} km^{-2}		TDN kg OWS^{-1} km^{-2}		NO_2^-+NO_3^- kg OWS^{-1} km^{-2}		Si kg OWS^{-1} km^{-2}	
Site ID	2019	2020	2019	2020	2019	2020	2019	2020	2019	2020
SR1	84.2	119	68.6	95.2	75.3	92.0	72.8	96.7	460	589
SR2	47.7	55.3			75.3	80.7	68.3	74.1	601	667
SR3			56.4	65.0	62.4	71.5	52.1	57.9	621	706
SR4	9.92	16.0	75.6	86.3	58.6	64.1	38.8	41.4	973	1090
AR2	17.8	22.3	59.1	67.6	58.6	64.2	40.3	42.1	931	1020
AR3	14.4	18.9	55.5	62.8	53.0	57.0	35.3	37.4	985	1080
NSR1	3.44	5.27	66.1	75.5	50.4	58.4	43.7	50.2	421	471
NSR2	24.1	54.9	71.3	88.2	58.9	63.2	45.8	50.1	780	851
NSR3			66.4	77.4	59.3	63.7	48.9	53.2	771	847
BR1	9.51	15.6	107	144	119	174	91.3	115	750	956
BR2	2.07	2.59	45.4	55.1	44.2	52.9	27.6	31.7	830	1000
BR3	3.36	4.78	50.3	58.4	54.8	62.9	34.8	40.5	800	932
BR4	3.09	4.40	64.6	69.8	60.9	65.8	42.4	47.0	917	1010

c.	Ca^{2+} Mg OWS^{-1} km^{-2}		K^+ kg OWS^{-1} km^{-2}		Mg^{2+} Mg OWS^{-1} km^{-2}		Na^+ kg OWS^{-1} km^{-2}		Cl^- kg OWS^{-1} km^{-2}		SO_4^{2-} Mg OWS^{-1} km^{-2}	
Site ID	2019	2020	2019	2020	2019	2020	2019	2020	2019	2020	2019	2020
SR1	17.8	23.8	148	183	5.83	7.94	232	272	108	134	12.3	15.3
SR2	20.7	23.1	132	136	7.50	8.11	253	266	205	226	13.9	15.1
SR3	14.4	17.4	106	119	5.29	5.96	347	382	248	282	12.4	13.7
SR4	15.3	17.0	190	204	5.58	6.13	564	616	198	203	15.5	16.4
AR2	15.4	17.1	161	170	4.87	5.37	398	432	100	102	11.4	12.3
AR3	13.7	15.0	165	177	5.02	5.51	425	457	114	121	15.2	16.7
NSR1	11.9	14.5			3.63	4.17	111	118	86.3	98.2	5.47	6.10
NSR2	17.5	18.5	143	146	5.90	6.30	373	376	220	235	20.2	21.3
NSR3	18.5	20.4	154	168	5.72	6.19	391	417	110	114	17.1	17.8
BR1	24.4	30.9	183	215	9.05	11.5	312	373	133	161	21.5	27.0
BR2	17.7	20.1	177	205	7.64	8.74	792	769	516	564	14.3	16.8
BR3	14.6	17.3	136	159	5.83	6.87	590	650	599	661	8.80	10.3
BR4	15.0	16.5	177	195	6.09	6.79	636	688	604	651	12.3	13.5

d.	Al		Ba		Cr		Mn		Mo		Sr	
	kg OWS^{-1} km^{-2}		kg OWS^{-1} km^{-2}		g OWS^{-1} km^{-2}		kg OWS^{-1} km^{-2}		g OWS^{-1} km^{-2}		kg OWS^{-1} km^{-2}	
Site ID	2019	2020	2019	2020	2019	2020	2019	2020	2019	2020	2019	2020
SR1	8.34	8.83	10.5	16.5	110	135	0.645	0.794	104	131	79.9	108
SR2	7.16	7.83	6.86	7.68	126	140	1.55	1.84			86.5	93.6
SR3	2.21	2.72	4.60	6.48	86.3	82.1	0.211	0.310	67.1	76.0	79.6	90.2
SR4	8.95	9.59	23.2	26.9	87.6	81.7	0.786	0.920	63.3	69.4	142	152
AR2	7.45	7.60	24.8	27.1			0.643	0.706	61.8	65.1	112	122
AR3	14.5	17.1	23.8	28.5			1.46	2.14			93.9	101
NSR1	4.98	6.57			71.5	87.7			47.5	54.3	54.0	63.2
NSR2	4.45	4.46	13.9	15.4	85.3	87.0	0.351	0.445	151	158	362	391
NSR3	8.04	12.7	13.8	15.8	98.9	108	0.553	0.650	128	145	341	365
BR1	9.55	13.0	17.3	22.6	117	144	0.926	1.01	176	224	558	714
BR2	3.04	4.22	10.3	13.4	88.6	99.5	0.533	0.576	68.0	80.5	178	218
BR3	2.55	3.24	8.70	10.4	69.6	73.2	0.268	0.391	55.5	65.9	102	122
BR4	4.11	4.39	8.50	10.3	77.2	83.2	0.310	0.411	86.7	87.6	69.1	78.0

e.	THg		FHg		Water	
	g OWS^{-1} km^{-2}		g OWS^{-1} km^{-2}		m^3 OWS^{-1} km^{-2} x10^{-6}	
Site ID	2019	2020	2019	2020	2019	2020
SR1	3.82	4.36	0.518	0.684	1.34	1.76
SR2	3.00	3.41	0.403	0.470	1.27	1.85
SR3	0.765	1.34			0.55	0.67
SR4	1.16	1.47	0.347	0.384	0.65	0.73
AR2	1.03	1.14	0.279	0.295	0.67	0.74
AR3	0.936	1.21	0.444	0.505	0.67	0.75
NSR1	0.375	0.559			0.75	0.93
NSR2	0.695	1.29	0.146	0.146	0.64	0.73
NSR3	0.736	0.987	0.135	0.145	0.66	0.74
BR1	1.66	2.95	0.640	1.35	1.40	1.84
BR2	0.437	0.532	0.270	0.335	0.70	0.84
BR3	0.484	0.639	0.225	0.265	0.66	0.78
BR4	0.503	0.577	0.292	0.303	0.66	0.74

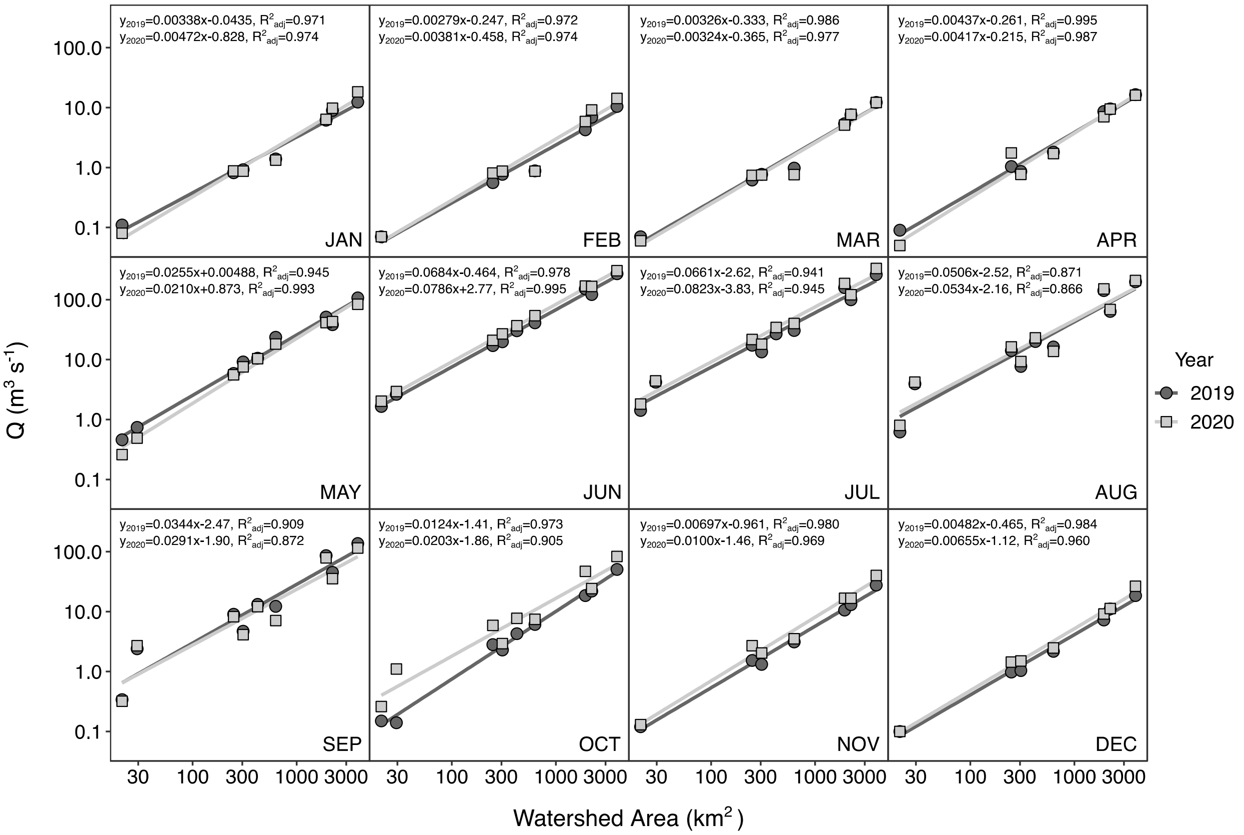

Figure A1.1. For visualization purposes only, log-log regression relationships between watershed area (km^2) and mean monthly discharge (Q; $m^3\ s^{-1}$) in 2019 and 2020 for the nine Water Survey of Canada hydrometric gauging stations described in **Table A1.3**. Linear regression equations and coefficients of determination (R^2) for monthly relationships are shown in the top left of each graph. In this study, regression relationships between watershed area and mean *daily* discharge in 2019 and 2020 for the nine WSC hydrometric gauging stations were applied to the watershed areas of our 12 non-gauged sampling sites to calculate continuous Q from January 01, 2019 to January 01, 2021 (see **Figure 2.4**).

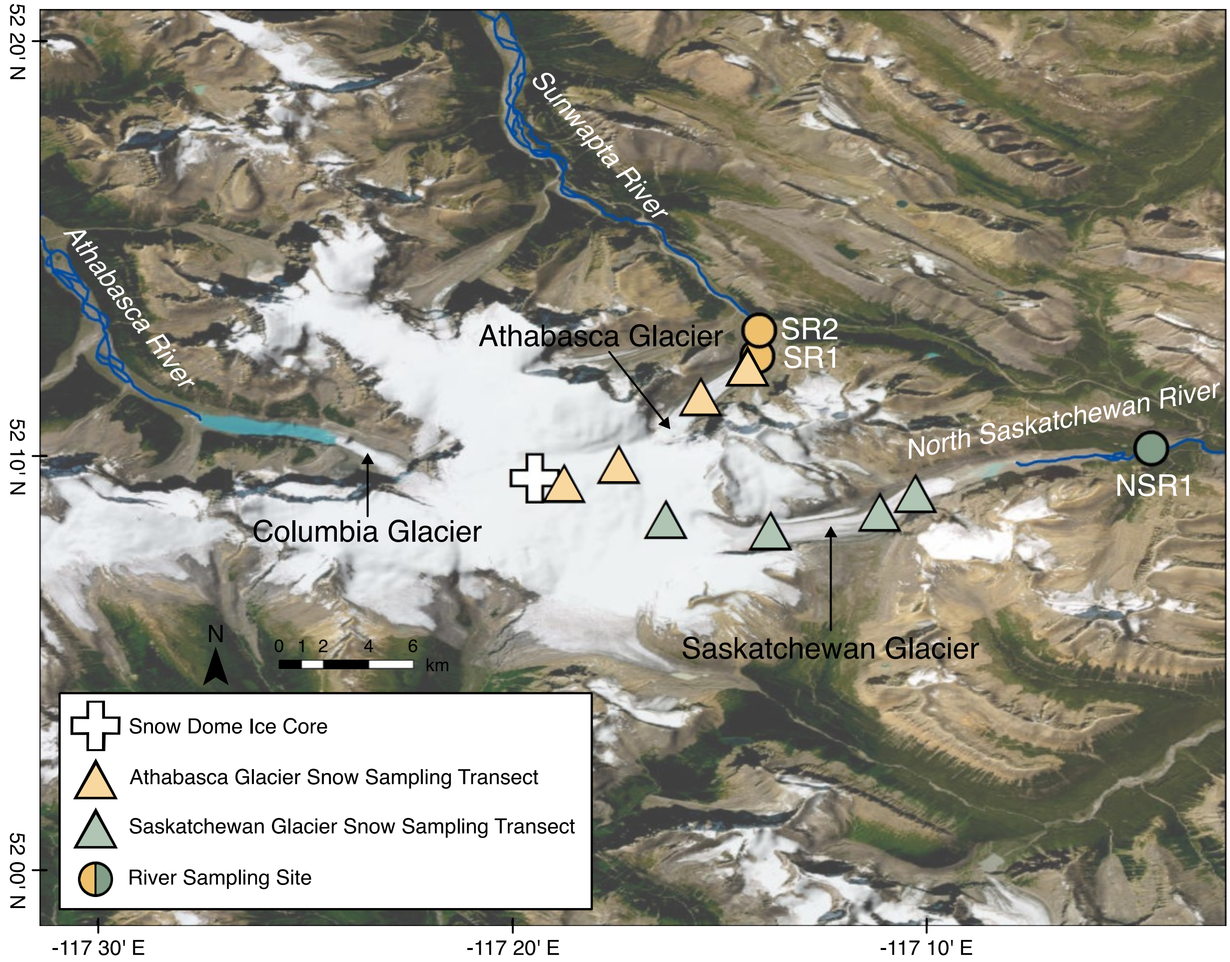

Figure A1.2. Map of the Columbia Icefield in Jasper National Park labeled with the Mt. Snow Dome ice core extraction site, Athabasca and Saskatchewan glacier snow sampling transect sites, and water sampling sites immediately downstream of the source glaciers. Base map imagery from Esri, Maxar, GeoEye, Earthstar Geographics, CNES/Airbus DS, USDA, USGS, AeroGRID, IGN, and the GIS User Community. For site abbreviations, please see **Table A1.1**.

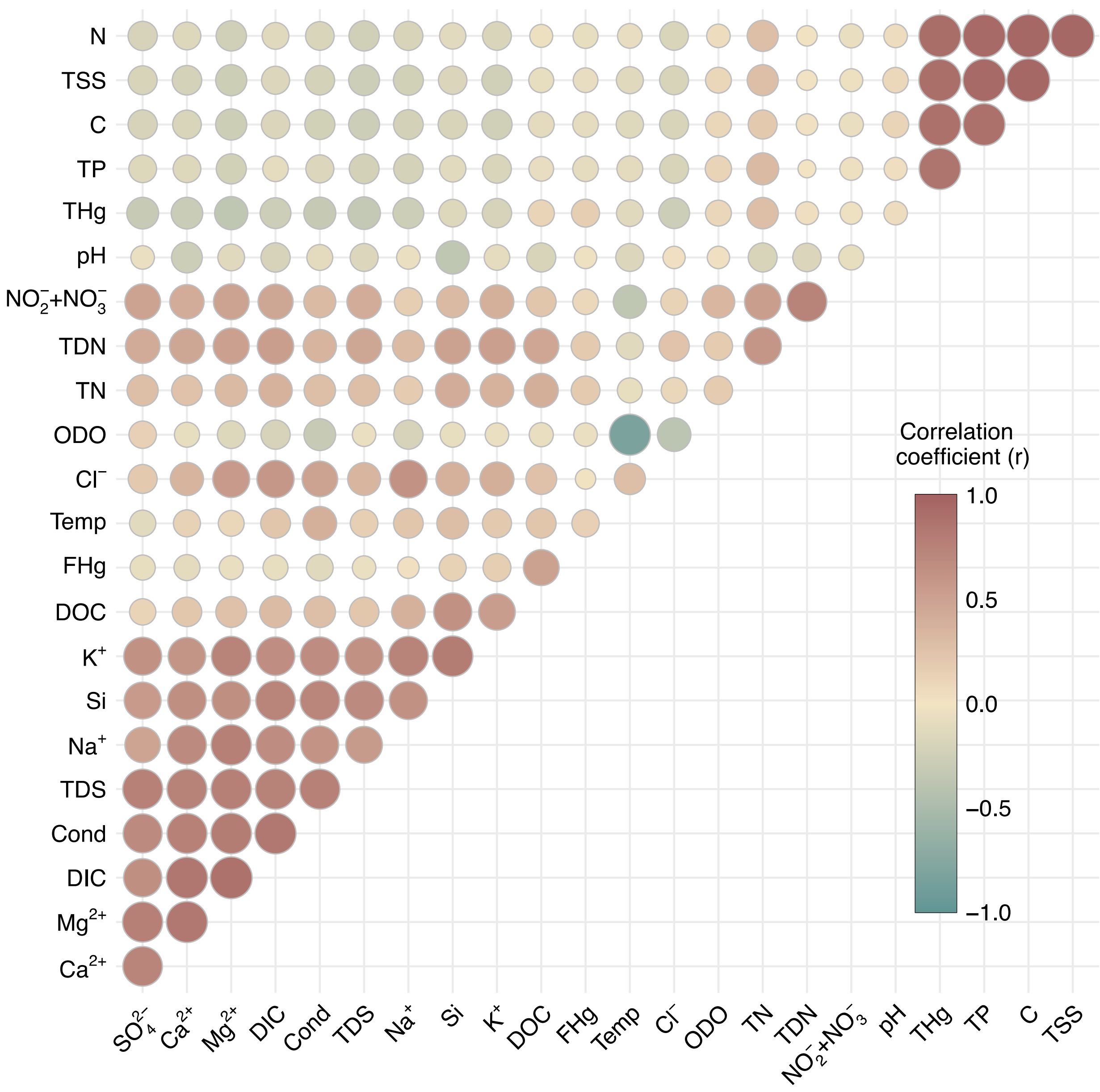

Figure A1.3. Correlation matrix of some physicochemical parameters in this study. An increase in size of bubble symbolizes a stronger correlation between two parameters, whereas the boldness of the color of bubble distinguishes whether the correlation is more positive (pink) or negative (green). For parameter abbreviations, please see *Section 2.3* in the main text.

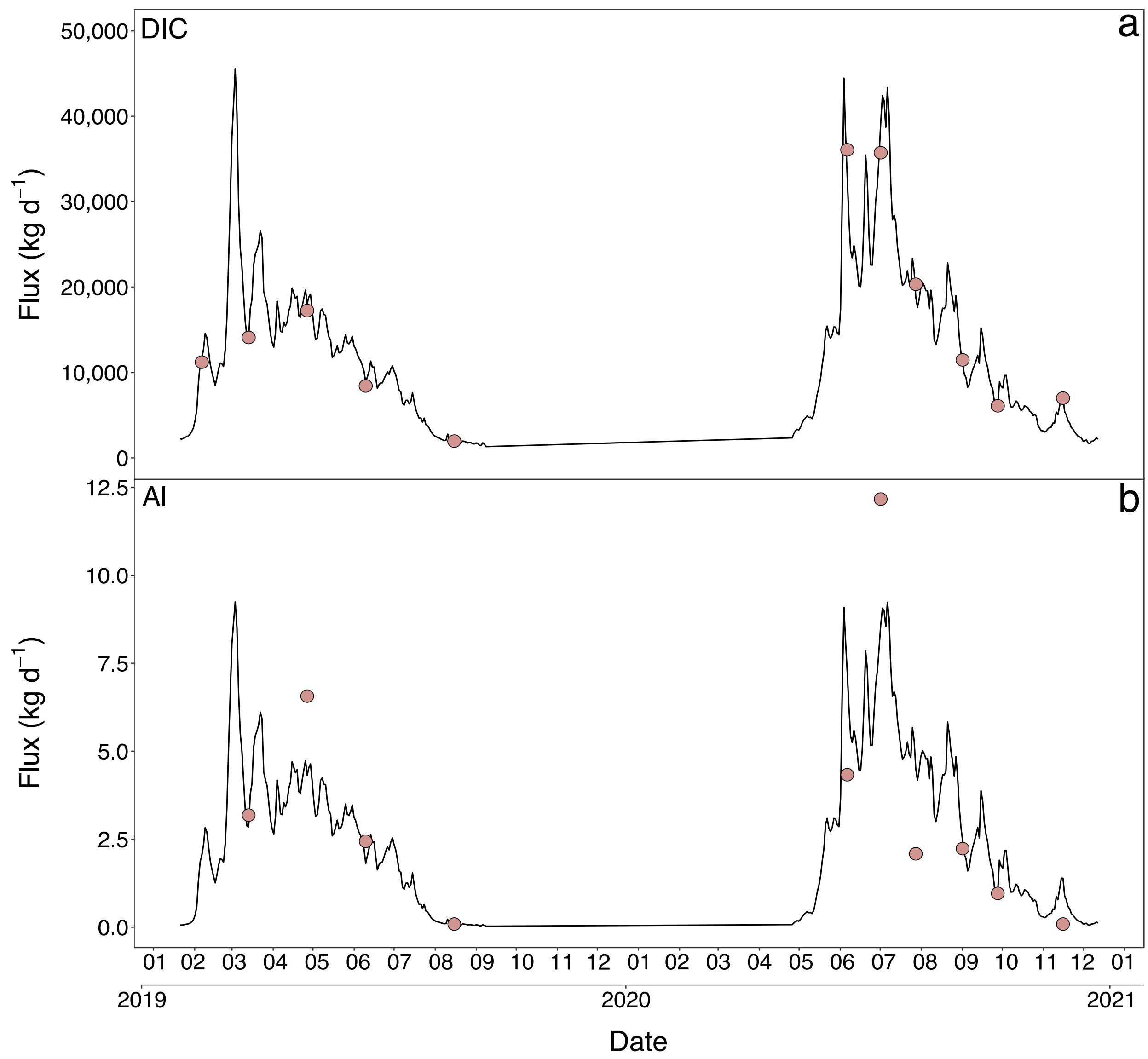

Figure A1.4. Examples of load (kg d^{-1}) quality control (QC) graphs for (a) dissolved inorganic carbon (DIC) and (b) aluminum (Al) at a mid-river site SR3 (Sunwapta River) for 2019 and 2020. Modeled loads produced with the U.S. Geological Survey LOADEST program are shown as the black line while manually calculated loads for biogeochemistry sampling dates are pink dots. The alignment of modeled and manually calculated loads are representative of a good and moderate model fit for DIC and Al, respectively. Quality control graphs were created for all parameter and site combinations to support model eliminations (i.e., **Table A1.6**) or acceptance (i.e., **Table A1.7**).

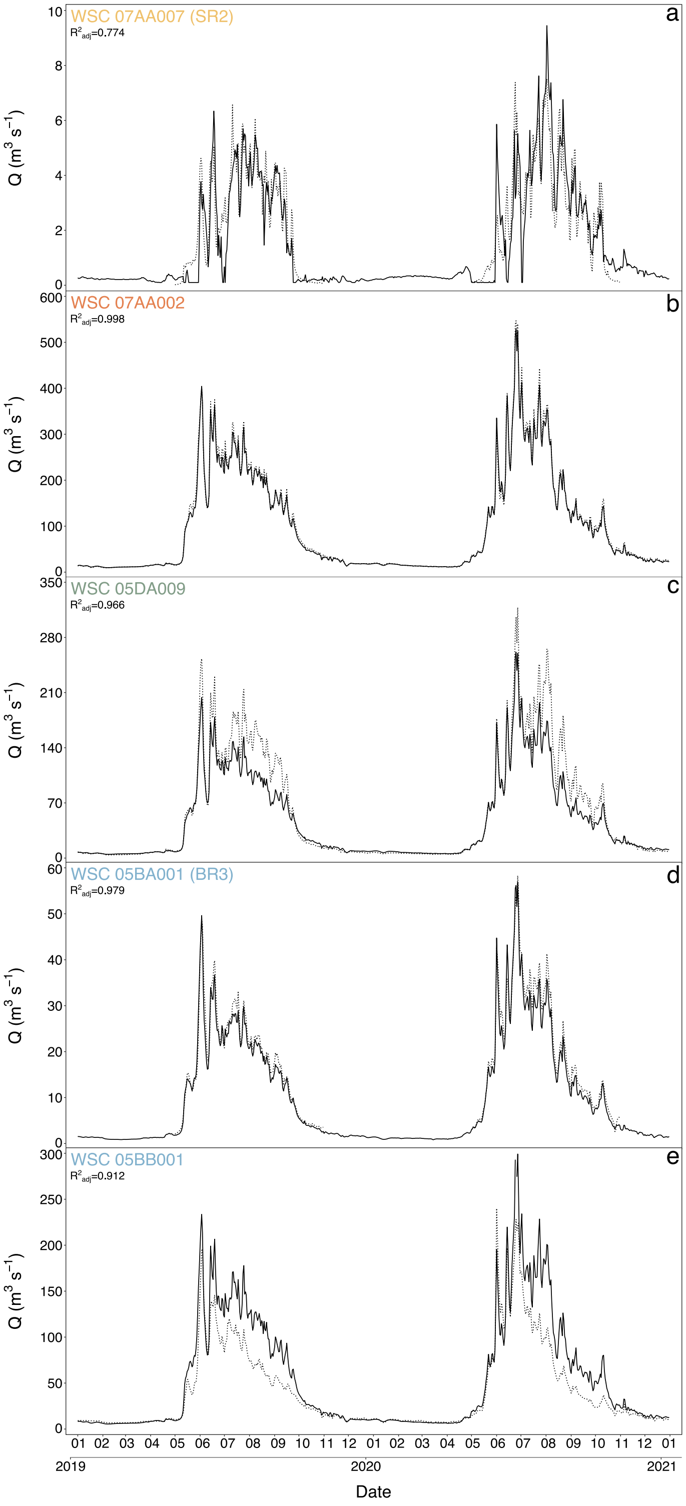

Figure A1.5 (a-e). Relationship between modeled (solid line) and measured Water Survey of Canada (WSC; dotted line) discharge (Q; m^3 s^{-1}) at five hydrometrically gauged sites within the study watersheds (see Calibration Sites in **Table A1.3**) for 2019 and 2020. Adjusted coefficients of determination (R^2) for each relationship are shown in the top left of each graph under the WSC station ID (site ID in brackets, if relevant). Please note different y-axis scales.

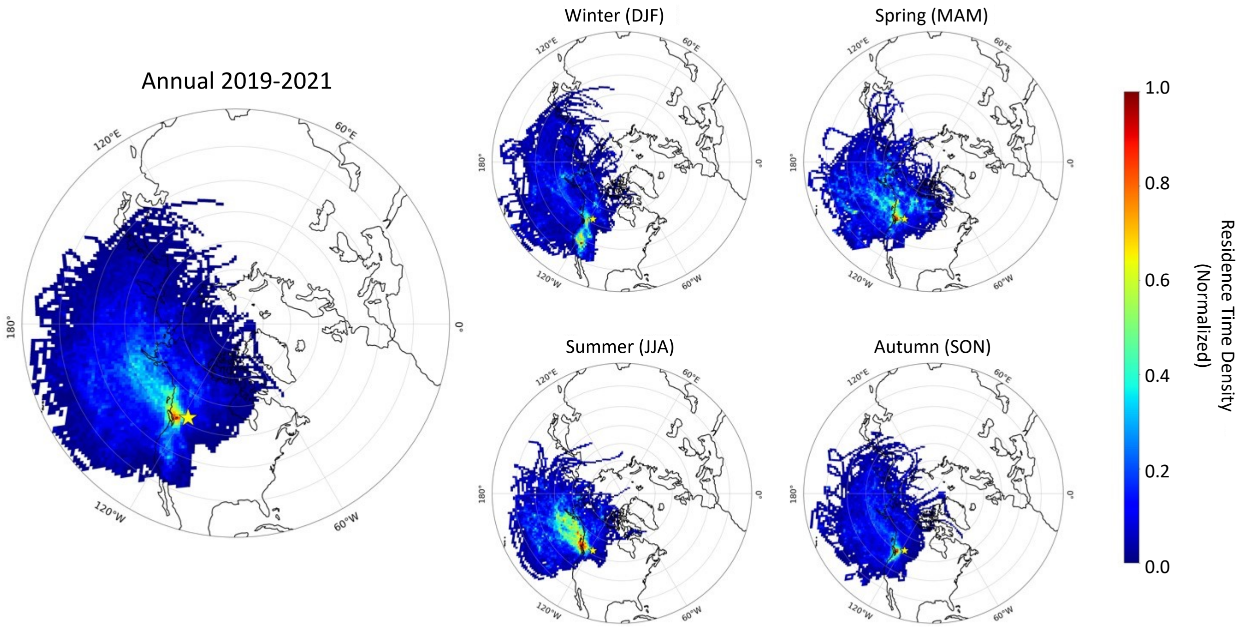

Figure A1.6. Residence time density plots (normalized) for air masses reaching Mt. Snow Dome for 2019-2021 annually and by season. Seasons include Winter (December, January, February), Spring (March, April, May), Summer (June, July, August), and Autumn (September, October, November). The back trajectory starting point was set to the Columbia Icefield apex, Mt. Snow Dome (star symbol). Residence time density was calculated from 10-day back trajectories, and detrended for concentric patterning caused by central tendency.

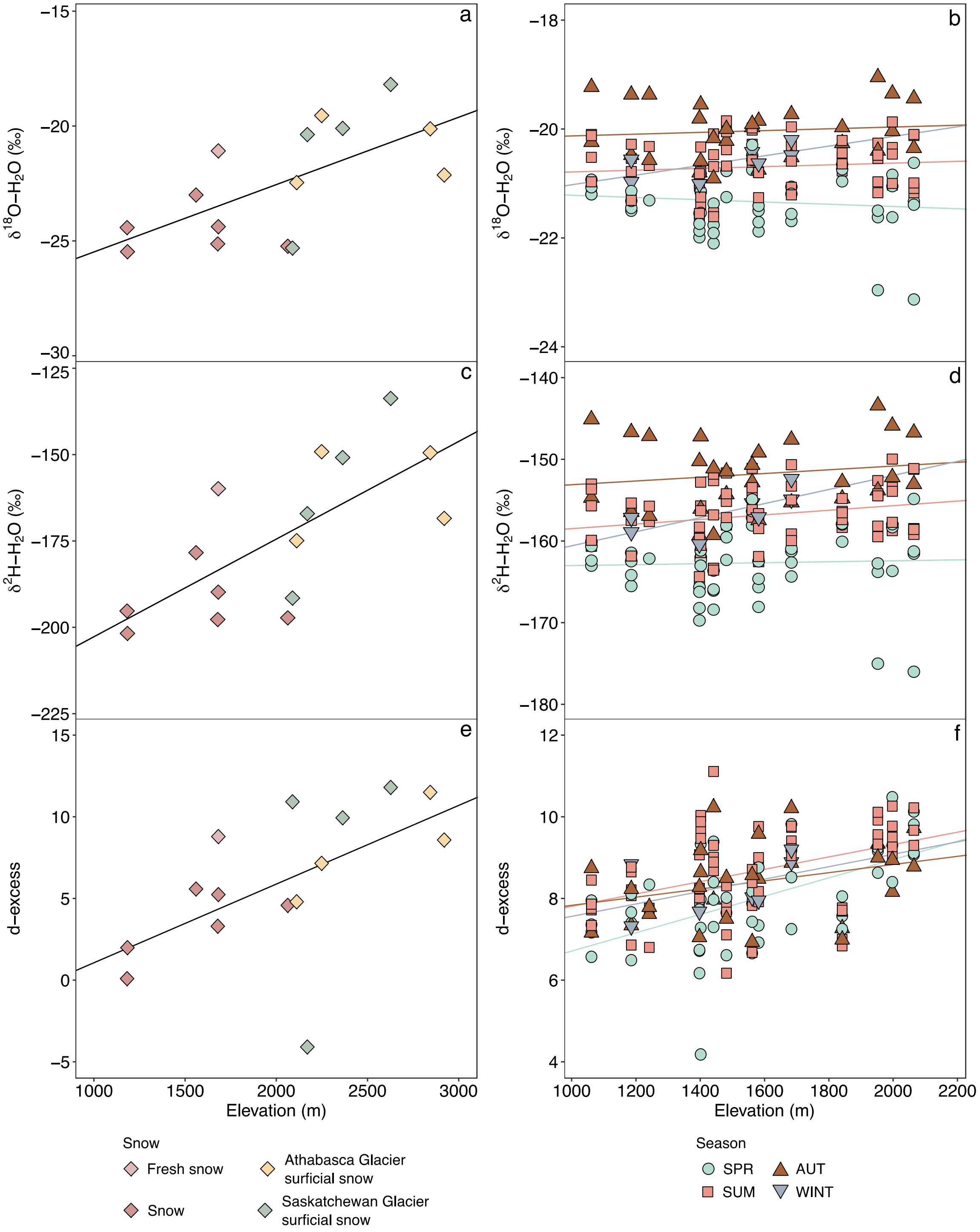

Figure A1.7. Elevation and $\delta^{18}O$ (a, b), $\delta^{2}H$ (c, d), and d-excess (e, f) of precipitation (left column) and river (right column) samples. Water source for precipitation samples is color-coded (with back lines of best fit), while river samples are color-coded and shaped by season (with matching-colored lines of best fit). Seasons are abbreviated as SPR (spring; May 14 – June 25), SUM (summer; July 14 – September 3), AUT (autumn; October 9 – 14), and WINT (winter; December 20 – January 29).

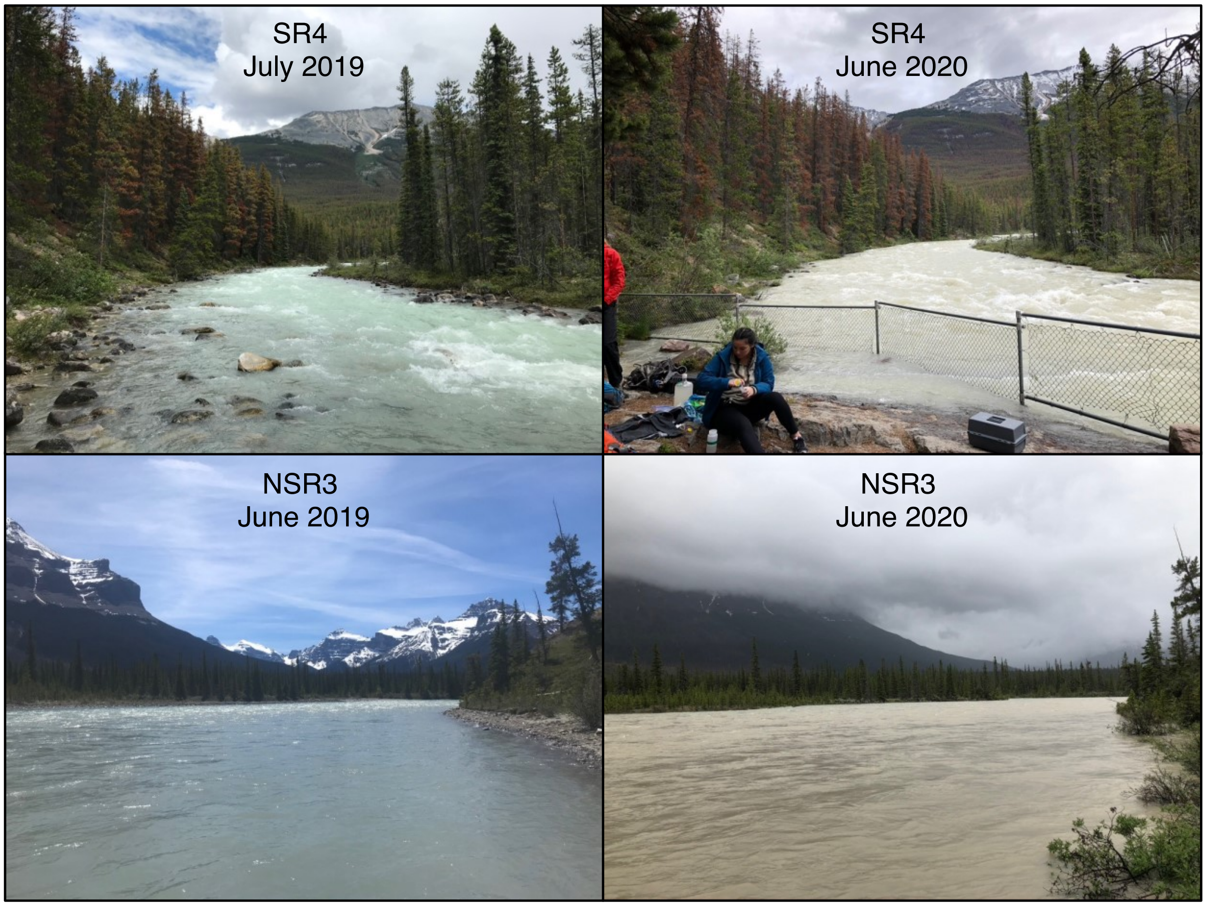

Figure A1.8. Sampling sites SR4 (top row) and NSR3 (bottom row) in 2019 and late June 2020. Photographs from 2019 show the typical spring and summer flow conditions during our sampling years and photographs from June 2020 show the impact of a large precipitation event and resultant overland flow. When comparing photographs from the same site, please note the color/turbidity of river water and water level along the riverbanks.

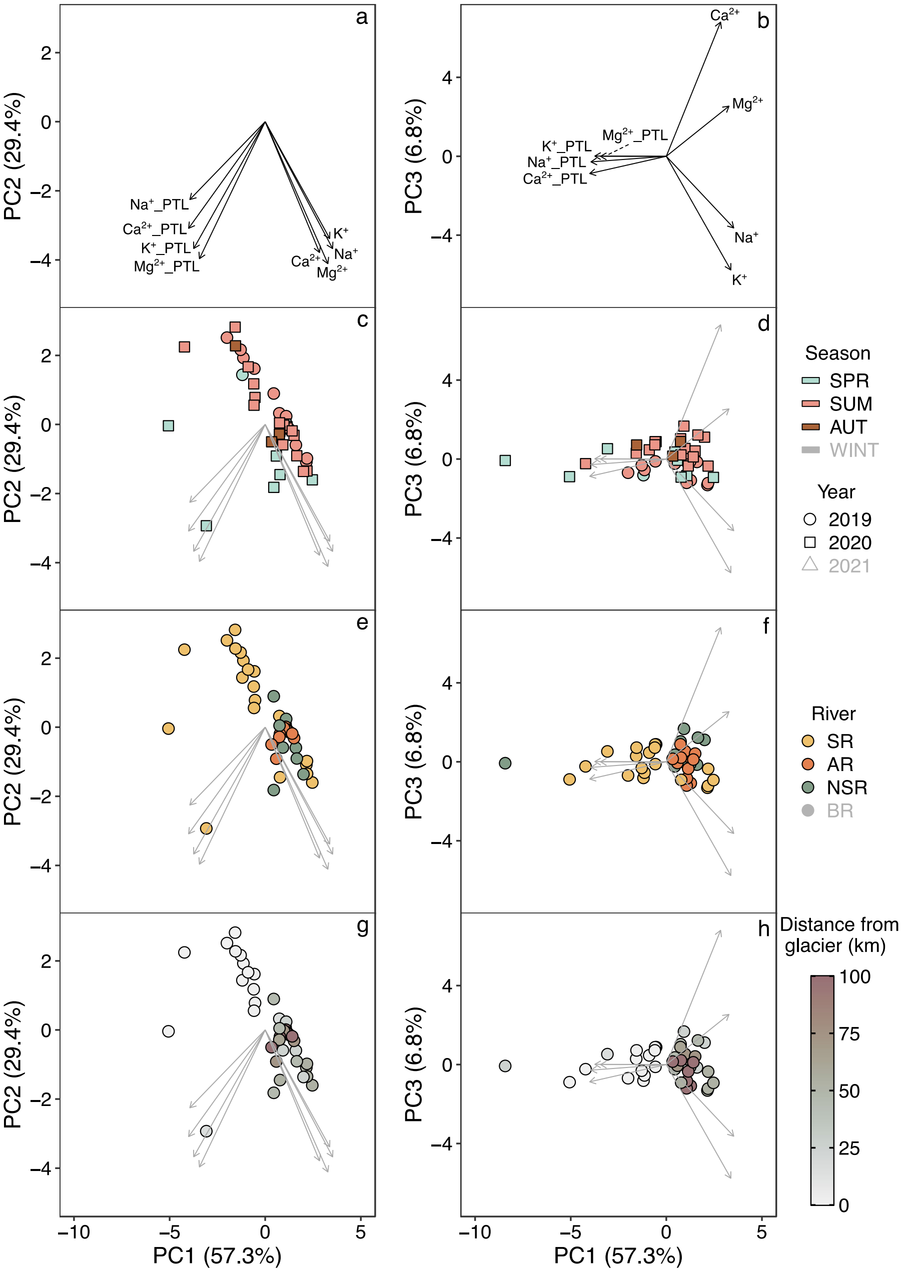

Figure A1.9. Principal Component Analyses (PCA) of total recoverable particulate (PTL) and dissolved cation concentrations collected at the river sampling sites. Shown are biplots of PC1 versus PC2 (left column) and PC1 versus PC3 (right column), with parameters and scaled vectors (**a-b**), and sampling sites color-coded spatiotemporally by season and year (**c-d**), river (**e-f**), and distance from glacier (km; **g-h**) for visual comparison. Grey symbology in the legend denotes factors that are missing from the PCA. The first three PCs account for 93.5% of the variation in particulate and dissolved ion concentrations. Seasons are abbreviated as SPR (spring; May 14 – June 25), SUM (summer; July 14 – September 3), AUT (autumn; October 9 – 14), and WINT (winter; December 20 – January 29). Rivers are abbreviated as SR (Sunwapta River), AR (Athabasca River), NSR (North Saskatchewan River), and BR (Bow River). For parameter abbreviations, please see *Section 2.3* in the main text.

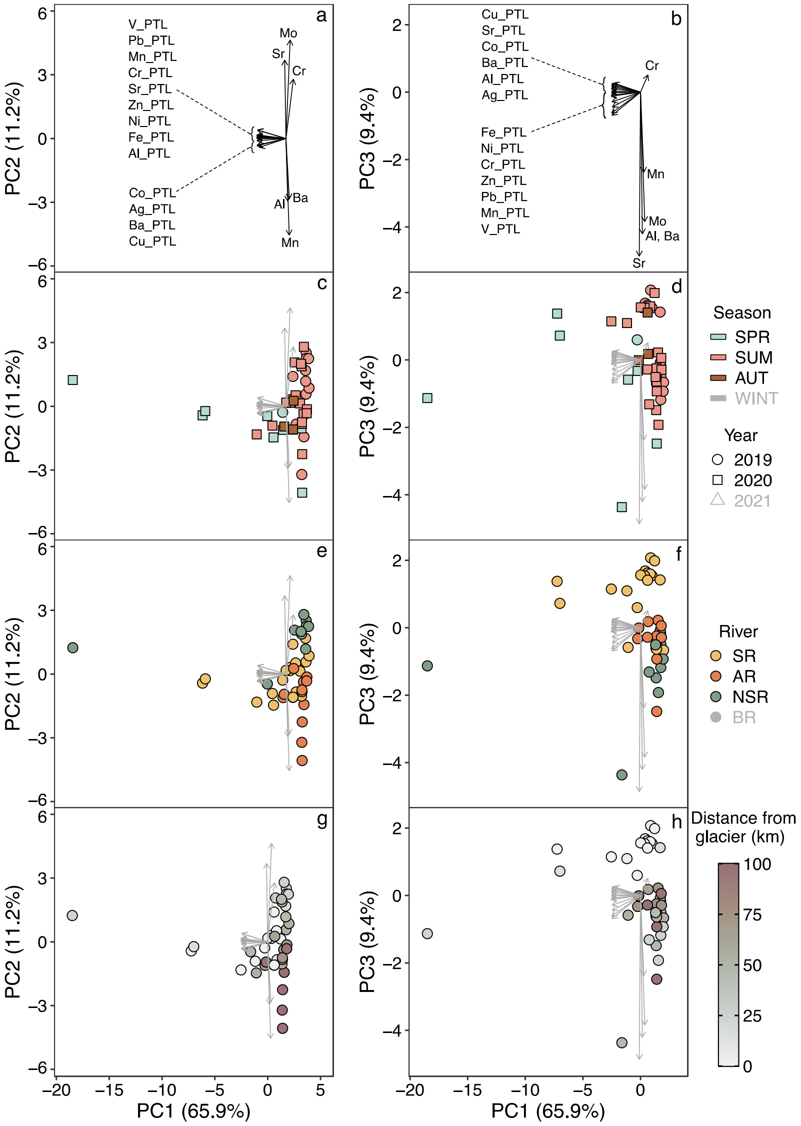

Figure A1.10. Principal Component Analyses (PCA) of total recoverable particulate (PTL) and dissolved trace element concentrations collected at the river sampling sites. Shown are biplots of PC1 versus PC2 (left column) and PC1 versus PC3 (right column), with parameters and scaled vectors (**a-b**), and sampling sites color-coded spatiotemporally by season and year (**c-d**), river (**e-f**), and distance from glacier (km; **g-h**) for visual comparison. Grey symbology in the legend denotes factors that are missing from the PCA. The first three PCs account for 87.2% of the variation in particulate and dissolved trace element concentrations. Seasons are abbreviated as SPR (spring; May 14 – June 25), SUM (summer; July 14 – September 3), AUT (autumn; October 9 – 14), and WINT (winter; December 20 – January 29). Rivers are abbreviated as SR (Sunwapta River), AR (Athabasca River), NSR (North Saskatchewan River), and BR (Bow River). For parameter abbreviations, please see *Section 2.3* in the main text.

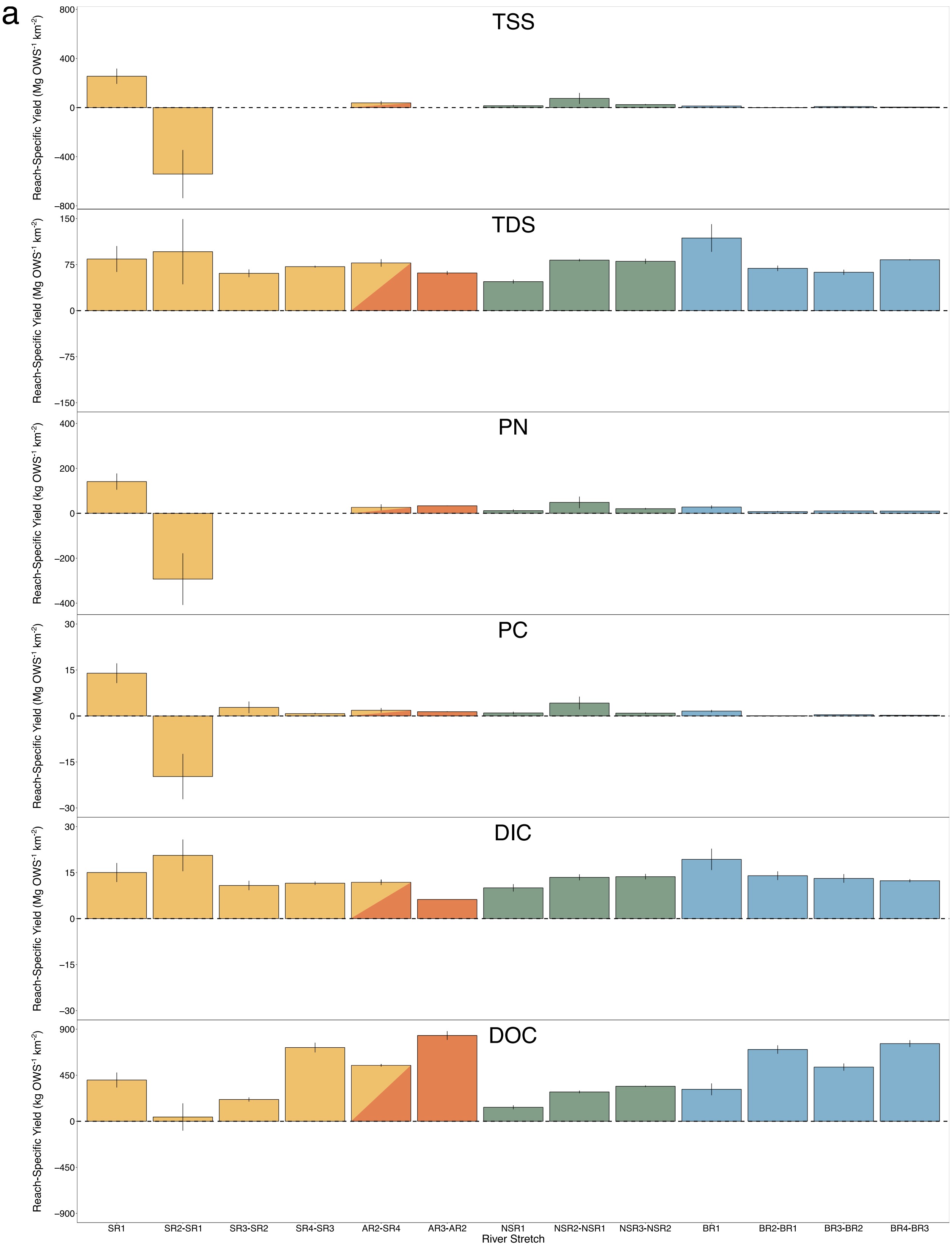
a
TSS
TDS
PN
PC
DIC
DOC
Reach-Specific Yield (Mg OWS⁻¹ km⁻²)
Reach-Specific Yield (kg OWS⁻¹ km⁻²)
800
400
0
−400
−800
150
75
−75
−150
200
−200
−400
30
15
−15
−30
900
450
−450
−900
SR1
SR2-SR1
SR3-SR2
SR4-SR3
AR2-SR4
AR3-AR2
NSR1
NSR2-NSR1
NSR3-NSR2
BR1
BR2-BR1
BR3-BR2
BR4-BR3
River Stretch

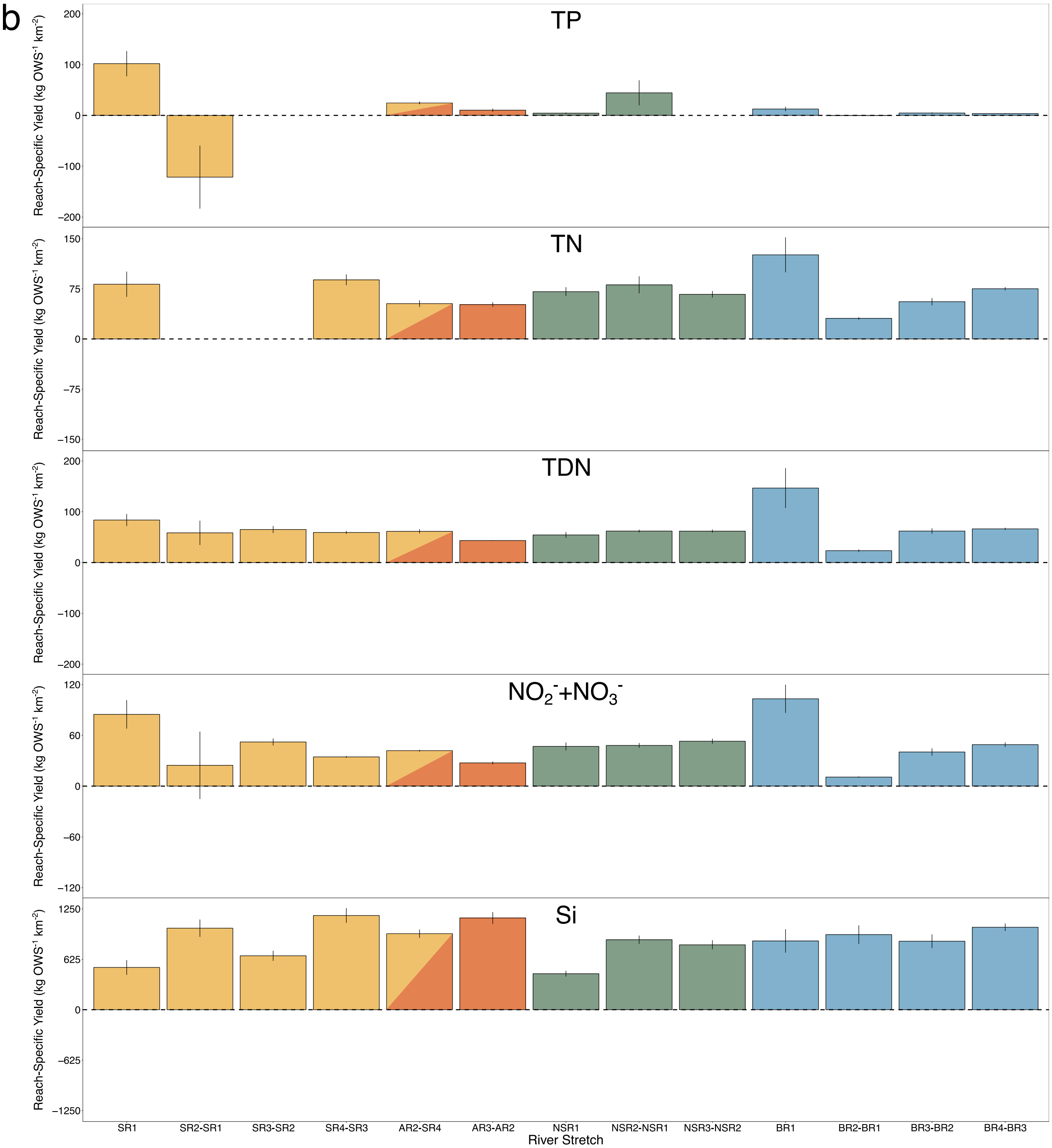
b
TP
TN
TDN
$NO_2^-+NO_3^-$
Si
Reach-Specific Yield (kg OWS⁻¹ km⁻²)
200
100
0
−100
−200
150
75
−75
−150
120
60
−60
−120
1250
625
−625
−1250
SR1
SR2-SR1
SR3-SR2
SR4-SR3
AR2-SR4
AR3-AR2
NSR1
NSR2-NSR1
NSR3-NSR2
BR1
BR2-BR1
BR3-BR2
BR4-BR3
River Stretch

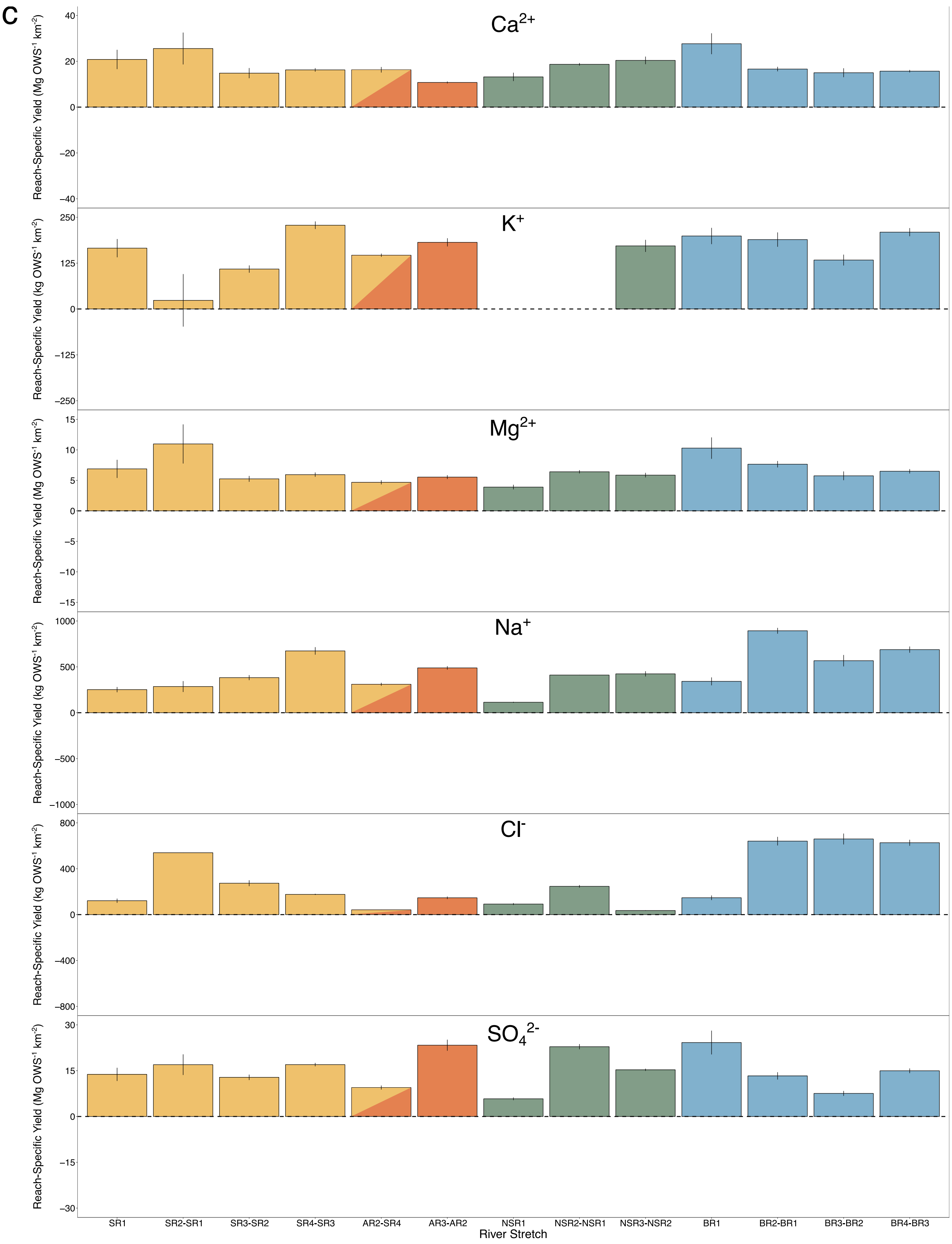c
Ca^{2+}
K^{+}
Mg^{2+}
Na^{+}
Cl^{-}
SO$_4^{2-}$
Reach-Specific Yield (Mg OWS^{-1} km^{-2})
Reach-Specific Yield (kg OWS^{-1} km^{-2})
40
20
0
−20
−40
250
125
0
−125
−250
15
10
5
0
−5
−10
−15
1000
500
0
−500
−1000
800
400
0
−400
−800
30
15
0
−15
−30
SR1
SR2-SR1
SR3-SR2
SR4-SR3
AR2-SR4
AR3-AR2
NSR1
NSR2-NSR1
NSR3-NSR2
BR1
BR2-BR1
BR3-BR2
BR4-BR3
River Stretch

d

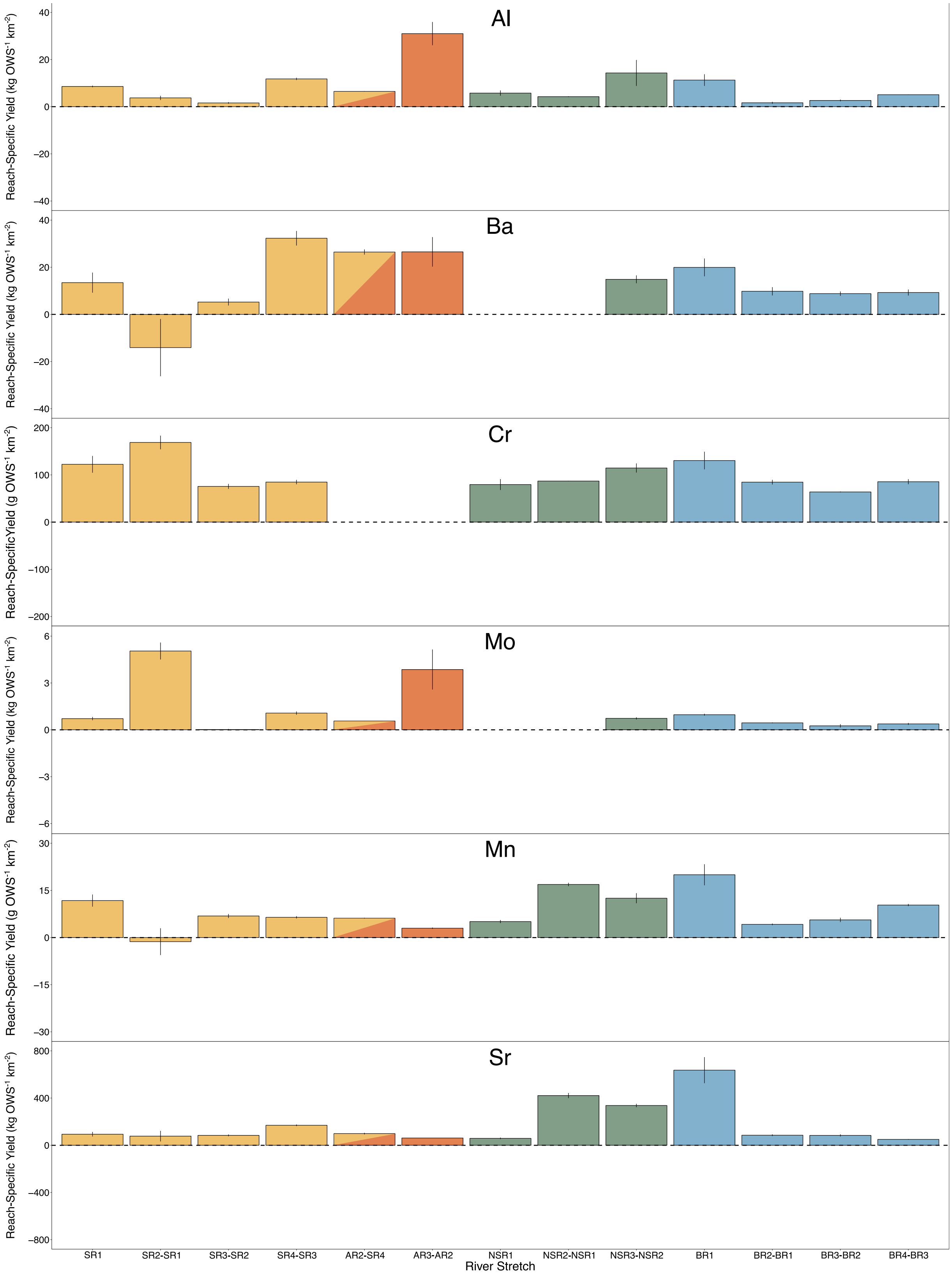
Al
Reach-Specific Yield (kg OWS⁻¹ km⁻²)
40
20
0
−20
−40
Ba
Reach-Specific Yield (kg OWS⁻¹ km⁻²)
40
20
0
−20
−40
Cr
Reach-SpecificYield (g OWS⁻¹ km⁻²)
200
100
0
−100
−200
Mo
Reach-Specific Yield (kg OWS⁻¹ km⁻²)
6
3
0
−3
−6
Mn
Reach-Specific Yield (g OWS⁻¹ km⁻²)
30
15
0
−15
−30
Sr
Reach-Specific Yield (kg OWS⁻¹ km⁻²)
800
400
0
−400
−800
SR1
SR2-SR1
SR3-SR2
SR4-SR3
AR2-SR4
AR3-AR2
NSR1
NSR2-NSR1
NSR3-NSR2
BR1
BR2-BR1
BR3-BR2
BR4-BR3
River Stretch

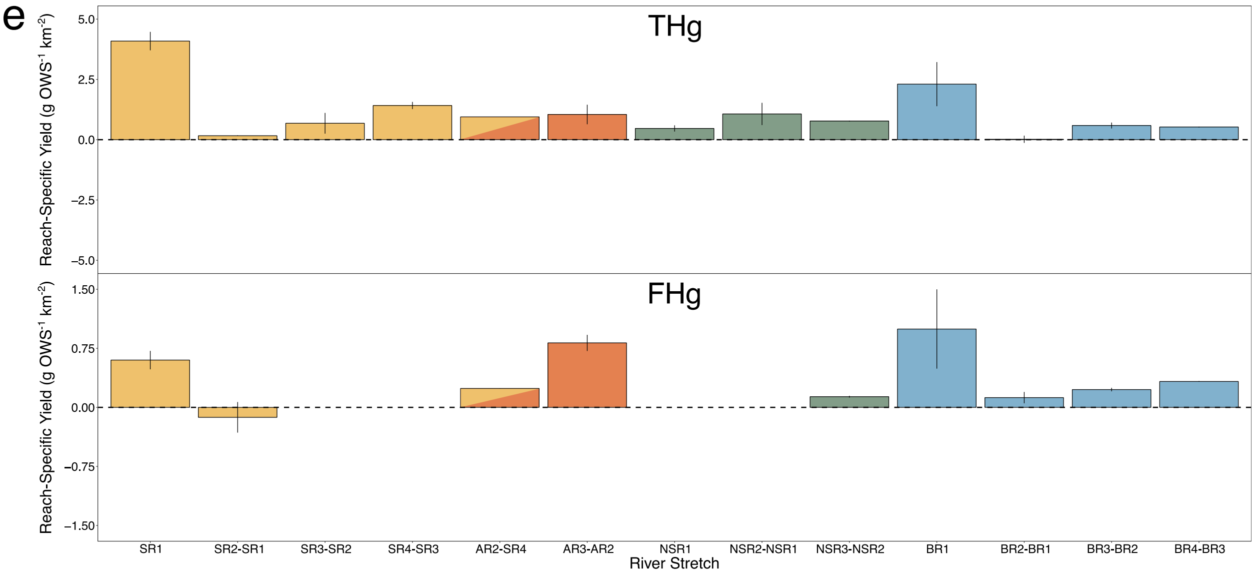

Figure A1.11. Mean 2019 and 2020 (± standard deviation) open water season (OWS; May 1 to October 31) river reach-specific chemical yields for (a) basic chemical parameters, (b) nutrients, (c) ions, (d) trace elements, and (e) contaminants. The black dashed line set to zero signifies no change in yield. When a chemical yield could not be calculated for a sampling site (i.e., gaps in **Table A1.10** for reasons summarized in **Table A1.5**), it was necessarily omitted from the river stretch calculations. Rivers are abbreviated as SR (Sunwapta River), AR (Athabasca River), NSR (North Saskatchewan River), and BR (Bow River). For parameter abbreviations, please see *Section 2.3* in the main text.

Appendix 2: Supporting information for Chapter 3 “Spatiotemporal patterns of geochemical weathering along rivers spanning glacierized to montane altitudinal life zones”

2 Methods

2.1 Sampling site descriptions and underlying geology

The Athabasca Glacier, a valley glacier of the Columbia Icefield, is the point of origin for the Sunwapta River (SR) (Ommanney, 2002). The SR passes through a proglacial lake prior to braiding through a sparsely vegetated glacial outwash plain. The braids converge into one channel and further downriver goes over two waterfalls (Sunwapta Falls). The SR then merges into the Athabasca River (AR), which originates upriver of this juncture at the Columbia Glacier in the northwest margin of the Columbia Icefield (Ommanney, 2002). The large AR flows over a large waterfall (Athabasca Falls) northeast towards our most northern sampling site 97.8 km downriver, upriver of Jasper Township (Serbu et al. 2024).

The North Saskatchewan River (NSR) originates at the Saskatchewan Glacier on the southern edge of the Columbia Icefield (Ommanney, 2002). Meltwaters from the Saskatchewan Glacier, the largest outlet glacier of the Columbia Icefield, initially enter a large proglacial lake before flowing downriver through a short narrow canyon. From there, the NSR meanders through a prominent glacial floodplain area vegetated with low-lying shrubs and grasses before forming a single large channel that flows through montane forest until our last sampling site 46.3 km downriver (Serbu et al. 2024).

The Bow River (BR) begins at the cirque Bow Glacier in the Wapta Icefield (Ommanney, 2002), flowing from proglacial Iceberg Lake, over a large waterfall, and into a braided forefield. The BR then feeds a large subalpine lake surrounded by subalpine forest (Bow Lake), after which it passes through a forested wetland area. Dense montane forest lined the remainder of the headwaters of the BR towards our most southern sampling site 75.4 km downriver, upriver of Banff Township (Serbu et al. 2024).

2.2 Sample collection and analyses

2.2.1 Collection of samples for analyses of basic chemistry and stable and radiogenic isotopes

Sondes were factory serviced annually prior to spring fieldwork, and sensors calibrated prior to each sampling campaign except for ODO, which was calibrated for at each sampling site and time. Low ionic strength standards were not used for the calibration of pH or conductivity, and as a result, possible measurement biases may have occurred in our low ionic glacial meltwaters (Bagshaw et al., 2021). However, we calibrated often, opted for spot sampling over long term deployments, and eliminated the first five minutes of data at each site ensuring *in situ* equilibrium was reached, all of which help to reduce bias (Bagshaw et al., 2021).

All CO_2 probes underwent certified factory calibration annually, but were also checked inhouse against Praxair 47.9, 347 and 910 ppm certified CO_2 standards both before and after field seasons. Temperature (T) (air T for $CO_{2(g)}$ and water T for $CO_{2(aq)}$ readings) and true barometric pressure (non-sea level corrected) were input into the Vaisala meter at each sampling site and time. Atmospheric $CO_{2(g)}$ concentrations were measured by suspending the probe ~1 meter above ground in a clearing back from the edge of the river. CO_2 probes used to quantify dissolved $CO_{2(aq)}$ concentrations were encased within a tight fitting waterproofing polytetrafluoroethylene (PTFE) sleeve permeable to gas exchange (Johnson et al., 2010). These probes were then deployed into the main current of the river just below the surface. To further assess the accuracy of these $CO_{2(aq)}$ measurements, we on one occasion tested them against $CO_{2(aq)}$ concentrations measured using a gas displacement technique and a PP Systems EGM-5 Portable CO_2 Gas Analyzer as described by Zolkos et al., 2018; all measurements from the two methods were within ± 10 ppm.

Water samples for major cation (Ca^{2+}, K^+, Mg^{2+}, Na^+) and trace element analyses were filtered onsite with all-plastic syringes and 0.45 µm Whatman™ polyethersulfone (PES) syringe filters into high density polyethylene (HDPE) scintillation vials, then preserved with trace metal grade HNO_3 until $pH < 2$ in our field laboratory within 12 hours of collection. All syringes and scintillation vials used for cation and trace element sampling and storage were first soaked in 0.01% CITRANOX® acid detergent overnight, followed by a 10 % HCl bath overnight, and rinsed thoroughly with Millipore Milli-Q™ water. Water collected for dissolved silica (Si) analyses was filtered onsite through a 0.45 µm Sartorius™ Minisart™ cellulose acetate syringe filters.

Water samples collected for analyses of dissolved inorganic carbon (DIC), δ^{13}C-DIC, and Δ^{14}C-DIC analyses were processed at each sampling site using the same filter, then stored without headspace in pre-washed and muffled glass Labco Exetainers® (DIC and δ^{13}C-DIC) or Wheaton bottles (Δ^{14}C-DIC) with rubber-lined caps. A known volume of water collected for particulate inorganic carbon (PIC) and δ^{13}C-PIC analyses was passed through a muffled and pre-weighed 25 mm 0.7 µm Whatman™ glass fiber filter (GF/F) within 12 hours of collection in our field laboratory, then frozen. Sampling protocols for particulate and dissolved organic carbon (POC and DOC, respectively) and their respective isotopes were detailed in Drapeau, 2023. Briefly, water samples for DOC and δ^{13}C-DOC analyses were filtered onsite through a pre-washed 0.45 µm Basix™ PES filter into acid-washed and muffled amber glass receivers, while water samples for organic radiocarbon were transported back to the field laboratory and processed in glass filter towers cleaned the same way. Muffled and pre-weighed Whatman™ 0.7 µm GF/F filters were used to capture δ^{13}C-POC and Δ^{14}C-POC samples, and the filtrate from the latter was kept for analyses of Δ^{14}C-DOC. All DOC samples were preserved with trace metal grade HCl to 0.1 % of its volume, while POC filters were frozen in our field laboratory.

Water samples for analyses of anions (Cl^-, SO_4^{2-}), sulfate isotopes (δ^{34}S-SO_4, δ^{18}O-SO_4), and radiogenic strontium ($^{87}Sr/^{86}Sr$) analyses were filtered through a 47 mm 0.45 µm cellulose acetate filter in a pre-cleaned filtration tower in the field laboratory.

All samples were stored in the dark at 4 ºC until analysis unless frozen.

2.2.2 Analyses of basic chemistry samples

Major cations, trace elements, anions, and Si were analyzed in the Canadian Association of Laboratory Accreditation (CALA)-accredited Biogeochemical Analytical Service Laboratory (BASL, University of Alberta). Major cations were analyzed on a Thermo Scientific iCAP 6300 Inductively Coupled Plasma – Optical Emissions Spectrometer (ICP-OES) and trace elements were analyzed on an Agilent 7900 ICP – Mass Spectrometer (MS) using reference methods EPA 200.7 and SM 3125 (Standard Methods Committee of the APHA-a; U.S. EPA, 1994). Anions were analyzed on a Dionex DX-600 Ion Chromatography System following reference method EPA 300.1 (U.S. EPA, 1993), whereas Si was analyzed on a Lachat Instruments QuikChem® QC8500 FIA Automated Ion Analyzer using reference method SM 4500-SiO_2 (Standard Methods Committee of the APHA-b). Bicarbonate (HCO_3^-) was calculated via the charge balance of major (Ca^{2+}, K^+, Mg^{2+}, Na^+) and anions (Cl^-, SO_4^{2-}) (in mEq L^{-1}) (Schlesinger & Bernhardt, 2013). Minor anions like organic acids and halogens other than Cl^- were assumed to be negligible in our study system and were thus ignored in the calculation (e.g., Hodson et al., 2000). Charge balance-derived HCO_3^- was then checked by interpreting the linear relationship between it and Ca^{2+} ($R^2_{adj} = 0.84$, $p < 0.001$). An Apollo SciTech AS-C3 DIC Analyzer interfaced with a LI-COR Biosciences LI-7000 infrared CO_2 Analyzer was used to quantify DIC concentrations (Wang et al., 2017) whereas a Shimadzu Total Organic Carbon (TOC)-V Analyzer was used to quantify DOC concentrations (Drapeau, 2023; Standard Methods Committee of the APHA-c).

All data from four sampling times at site AR1 were eliminated from statistical analyses when inputs from an upriver tributary disproportionately influenced the biogeochemical signal (please see Serbu et al., 2024 for more information). Concentration data that fell below analytical detection limits (DL) were modified to half DL values for statistical purposes (Antweiler & Taylor, 2008; Helsel, 1990). Non-sea salt concentrations (denoted by Parameter_{nss}) were calculated via Cl^- corrected ratios. Sea salt ratios originally published by Gaillardet et al., 1999 and used by Voss et al., 2023 included $Ca^{2+}/Cl^- = 0.017$, $Mg^{2+}/Cl^- = 0.0019$, $Na^+/Cl^- = 0.870$, and $HCO_3^-/Cl^- = 0.000008$ (where DIC was substituted for HCO_3^-), while $K^+/Cl^- = 0.019$ came from Deuerling et al., 2019. In three cases, sea salt corrected Na^+ resulted in marginally negative values (-0.42, -0.60, -2.00 µM) so these sites were removed from molar ratios involving Na^+.

2.2.3 Analyses of isotope samples

δ^{13}C-DIC ($2\sigma = 0.3$ ‰ VPDB) samples were first processed by converting all inorganic carbon to CO_2, followed by analysis on a Thermo Scientific Gasbench coupled to a Thermo Scientific DELTA V Plus Isotope Ratio (IR)-MS at the Environment Isotope Laboratory (EIL; University of Waterloo, Canada). Stable isotopes of SO_4^{2-} were also processed and quantified at the EIL, with prepared precipitations of δ^{34}S-SO_4 ($2\sigma = 0.3$ ‰ VCDT) analyzed on a Costech Analytical Elemental Combustion System 4010 coupled to an Elementar isoprime presION IRMS and δ^{18}O-

SO_4 (2σ = 0.3 ‰ VSMOW) analyzed via an Elementar vario PYRO Cube® Elemental Analyzer paired with a GV Instruments IsoPrime™ IRMS. δ^{13}C-PIC (2σ = 0.05 ‰ VPDB) was quantified at the Ján Veizer Stable Isotope Laboratory (University of Ottawa, Canada) by converting samples to CO_2, then analyzing them in dual-inlet mode on a Thermo Scientific DELTA V Plus IRMS. Approximately 600 ng Sr was extracted and purified via Sr Spec ion chromatography column chemistry in a PicoTrace Laboratory at the Woods Hole Oceanographic Institution (WHOI; USA) and a Thermo Fisher Neptune Multicollector-ICP-MS in the WHOI Plasma Facility was then used to quantify $^{87}Sr/^{86}Sr$ after correcting for Rb interferences and instrumental mass bias. Analytical blanks were insignificant. Isotope values are normalized to standard reference material NBS 987 $^{87}Sr/^{86}Sr$=0.710240. Δ^{14}C-DIC samples were submitted to the André E. Lalonde Accelerator Mass Spectrometry (AMS) Laboratory (University of Ottawa, Canada) where they were purified into CO_2, then analyzed on a 3 MV tandem AMS (Murseli et al., 2019). Method analysis of stable- and radio-organic carbon isotopes (δ^{13}C-DOC, δ^{13}C-POC, Δ^{14}C-DOC, Δ^{14}C-POC) are described in detail in Drapeau, 2023.

3 Results & Discussion

3.1 Determining weathering feasibility with CO_2 saturation, calcite saturation indices, and instantaneous CO_2 fluxes

Saturation indices (SIs) were calculated in the Python (Van Rossum & Drake, 2009) package *AqEquil* (Boyer et al., 2023) using EQ3/6 software (Wolery, 2013) in the open-source Water-Organic-Rock-Microbe (WORM) Portal (Boyer & Shock, 2023) for each sampling site and time where full data was available (n=146). Measured or calculated physicochemical inputs included temperature, pH, HCO_3^-, O_2, SiO_2, $NO_2^- + NO_3^-$, CH_4, Ca^{2+}, Mg^{2+}, K^+, Na^+, Cl^-, and SO_4^{2-}. Concentrations of NH_4^+, PO_4^{3-}, Li^+, and Fe^{2+} were set to half DL, either because they were predominantly <DL or because analytical methods changed between the two study years.

3.1.1 Instantaneous CO_2 flux estimations

The water-atmosphere CO_2 flux estimates in this study were limited by our ability to quantify gas exchange velocity (k_{600}) at our sampling sites. Gross primary productivity (GPP) was low across all sampling sites, preventing us from using dissolved O_2 concentration time series to estimate k_{600} (Hall & Ulseth, 2020). Sampling sites with few white rapids and moderately sized waterfalls (i.e., SR3 and AR1) were explored for changes in k_{600} across river discontinuities (Hall & Ulseth, 2020) but all efforts failed, either due to a non-effect on k_{600} or sampling inaccessibility. While working in Canadian National Parks afforded us relatively pristine sampling conditions, the addition of tracer gases to measure gas exchange velocities was forbidden. Given the riverscapes of our three watersheds, and the desire to be methodologically consistent across all sampling sites, empirical equations and models were instead used to estimate k_{600} (Hall & Ulseth, 2020). Therefore, instantaneous CO_2 fluxes at our sites during sampling times (except winter) were estimated using the modeled slope and calculations outlined by various foundational contributions.

Energy dissipation rate (eD) and k_{600} were determined by the model defined in Ulseth et al., 2019. eD relies on gravitational acceleration (9.81 m s^{-2}) and two unknowns, river slope (unitless) and water velocity (m s^{-1}). Slope was appraised using the Alberta Provincial DEM which was downloaded and used in ArcGIS (Alberta Environment and Parks, 2017; ESRI, 2023). Due to the 25 m resolution of the Alberta Provincial DEM, if a sampling site had a steeper slope, we were able to measure its slope within a smaller distance (e.g., within 250 m of site), but if the sampling site slope was gentle, we sometimes had to quantify longer river sections (e.g., within 4000 m of the site).

Measured and modeled Qs for each sampling site were previously documented by Serbu et al., 2024 (**Figure A2.1**). A power relationship was then applied to Q to determine V for each of our sampling sites and times (**Figure A2.5**). This power relationship was derived using Q and V measured at four hydrometric gauging stations (**Table A2.3**) along our rivers by Water Survey of Canada (WSC) from 2019 to 2021 (**Figure A2.5**). The four gauging stations, including those at our sampling sites SR2 and BR3, were selected because they (a) were all along the SR, AR, NSR, and BR study rivers, (b) had watershed areas (km^2) similar to those of our sampling sites, and (c) were operational during our sampling years of 2019 and 2020. The power relationship determined for the 56 Q and V point samples was $V=0.30Q^{0.35}$ ($R^2 = 0.72$).

Table A2.1. Relative percent watershed area of each sampling site covered by major and minor land cover classes. Originally published in Serbu et al., 2024.

Site ID	Water[1]	Snow and ice	Rock and rubble	Exposed land	Shrubland	Grassland	Coniferous forest	Broadleaf forest	Mixed forest	Developed	Total
	%	%	%	%	%	%	%	%	%	%	%
SR1	1.1	50.7	46.8	0.0	0.0	0.0	0.0	0.0	0.0	0.0	98.6
SR2	1.5	41.8	54.2	0.0	0.2	0.1	0.3	0.0	0.0	0.8	98.9
SR3	1.0	19.1	55.3	0.0	5.7	4.7	12.8	0.2	0.1	1.1	99.8
SR4	1.5	6.6	50.2	0.0	8.4	6.8	25.1	0.4	0.1	0.8	100.0
AR1	1.9	12.2	43.2	0.1	7.6	6.4	27.3	0.6	0.2	0.4	99.9
AR2	1.9	10.8	42.8	0.0	7.7	6.4	29.0	0.7	0.3	0.4	99.9
AR3	1.9	8.4	41.2	0.0	7.4	7.4	32.0	0.8	0.3	0.5	99.9
NSR1	0.6	54.7	35.3	0.2	1.7	3.7	3.6	0.2	0.0	0.0	100.0
NSR2	1.6	19.1	40.8	0.1	7.4	5.6	24.4	0.2	0.1	0.5	99.8
NSR3	2.1	18.8	37.4	0.1	6.9	4.0	29.7	0.1	0.0	0.5	99.7
BR1	2.0	41.5	47.7	0.0	2.4	1.4	4.8	0.0	0.0	0.0	99.9
BR2	4.3	11.1	42.0	0.0	8.4	1.3	31.4	0.0	0.0	1.5	100.0
BR3	3.6	9.6	35.7	0.0	6.7	1.8	41.0	0.0	0.0	1.4	99.8
BR4	2.4	5.6	38.1	0.0	8.7	2.5	41.3	0.0	0.0	1.3	99.9

[1] Relative percent wetland cover (fen + bog + marsh + swap) was quantified separately and likely overlapped with the water land cover class. Watershed area covered by wetland at our study sites ranged from 0.0-2.1 %. Wetland cover exceeding 1.0 % were found at BR2 (2.1 %), BR3 (1.9 %), and BR4 (1.6 %).

Table A2.2. Dates (2019 – 2021) of river sampling trips binned into seasons for data analysis and interpretation.

Season	Sampling Dates	
	2019	2020/2021
Early Spring	May 14-16	June 3-5
Spring	June 11-13	June 22-25
Early Summer	July 15-18	July 13-16
Summer	August 19-22	August 10-13
Early Autumn	NA	August 31-September 3
Autumn	October 11-14	October 9-12
Winter	December 20-22	January 28-29 (2021)

Table A2.3. Water Survey of Canada (WSC) hydrometric gauging station information, including station name, station ID, watershed, and watershed area for the four WSC stations that were used to determine a relationship between measured discharge (Q) and water velocity (V) in **Figure A2.5** (Water Survey of Canada, 2021).

WSC station name	Station ID	Watershed	Watershed area (km^2)
Sunwapta River at Athabasca Glacier	07AA007	Sunwapta/Athabasca	29.3
Athabasca River near Jasper	07AA002	Athabasca	3870.0
North Saskatchewan River at Whirlpool Point	05DA009	North Saskatchewan	1920.0
Bow River at Lake Louise	05BA001	Bow	422.0

Table A2.4. Numerical values of the log concentration-discharge (CQ) regressions from **Figure 3.5**.

Parameter	Regression formula	p-value	Residuals (min, median, max)	Residual standard error
Ca^{2+}	C=564Q+0.02	0.93	-307, 2.4, 470	151
Mg^{2+}	C=347Q-0.2	0.19	-267, 4.9, 342	108
Na^{+}	C=26Q+0.01	0.69	-25, -2.7, 119	18.3
K^{+}	C=5.0Q+0.009	0.014	-4.9, 0.07, 7.8	2.4
Cl^{-}	C=11Q-0.03	0.030	-10, -2.2, 37	9.2
SO_4^{2-}	C=213Q-0.02	0.89	-171, -15, 537	111
DIC	C=1412Q-0.4	0.49	-904, 26, 742	334
Si	C=36Q-0.1	0.00010	-30, -0.35, 71	17

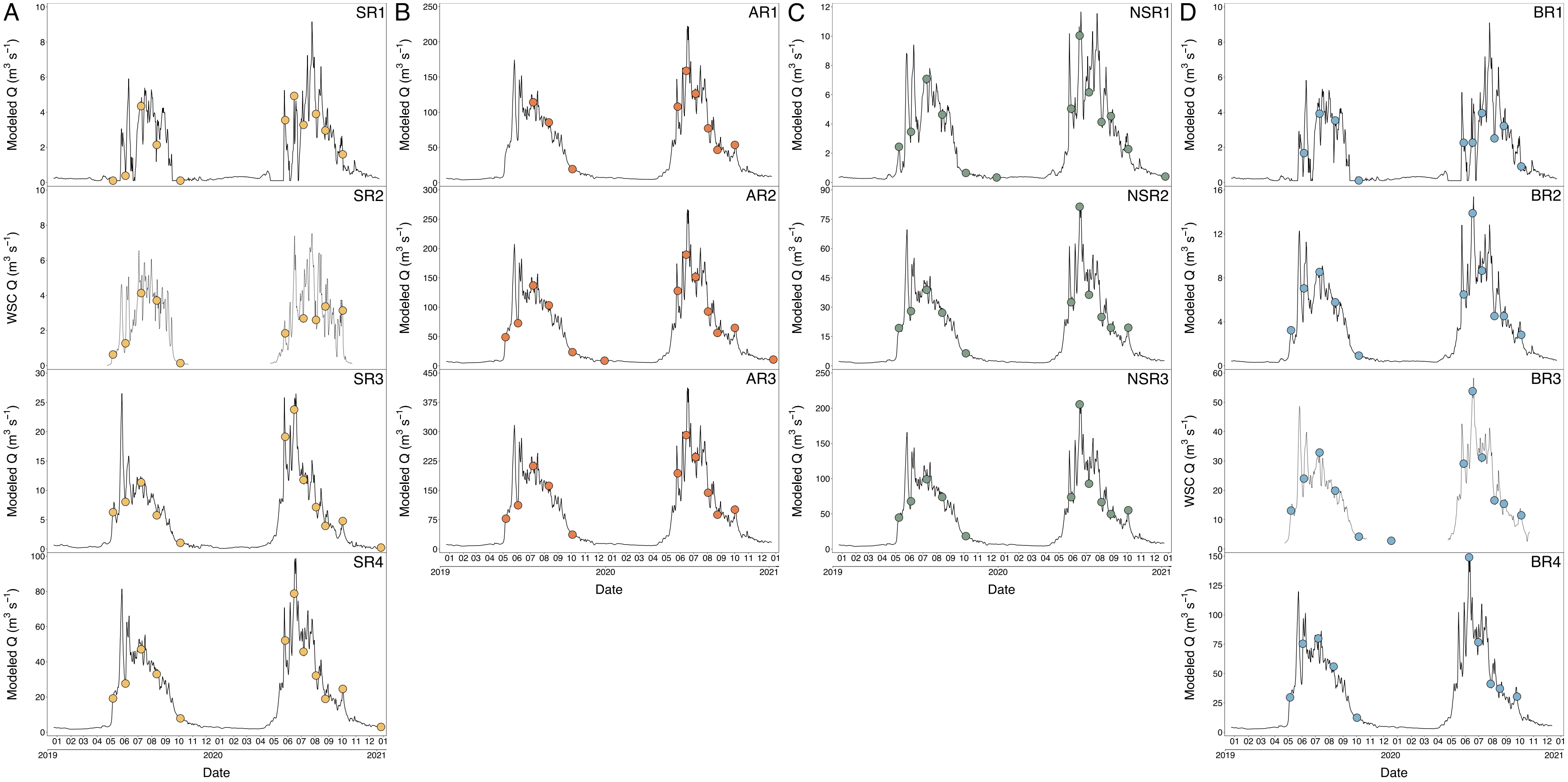

Figure A2.1. Modeled (solid line) and measured Water Survey of Canada (WSC; dotted line) discharge (Q; m^3 s^{-1}) and physicochemical sampling dates (colored circles) at the 14 sampling sites along the (a) Sunwapta (SR), (b) Athabasca (AR), (c) North Saskatchewan (NSR), and (d) Bow (BR) rivers for 2019 through early 2021. Stars in the orange circles for AR1 symbolize sampling dates where dissolved concentration data was eliminated from all data analyses. Please note different y-axis scales. Originally published in Serbu et al., 2024. Mean daily Q for each sampling site was either measured or modeled as previously detailed in Serbu et al., 2024.

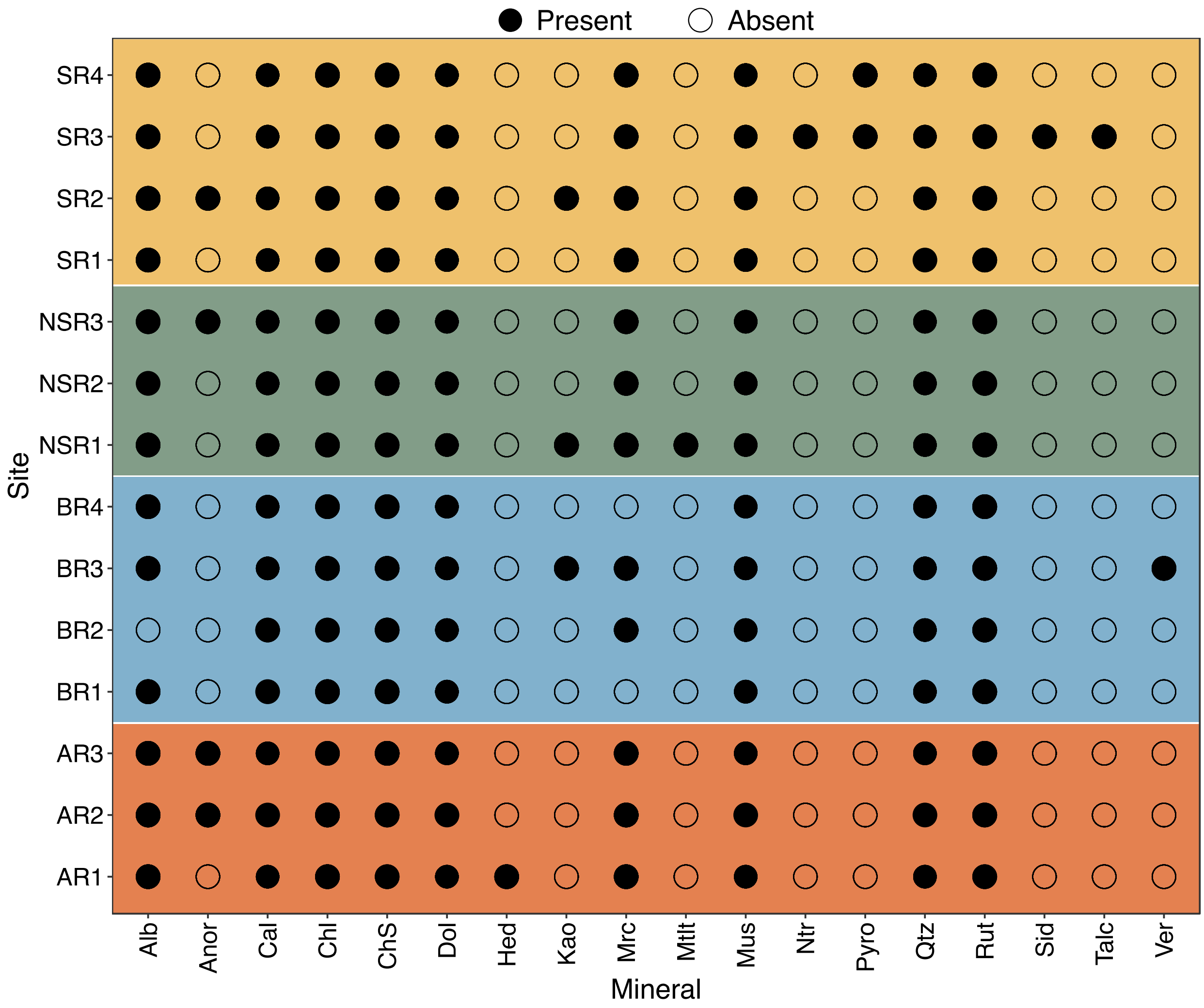

Figure A2.2. X-Ray Diffraction (XRD) minerology present/absent results from sampling sites along the Sunwapta (SR), Athabasca (AR), North Saskatchewan (NSR), and Bow (BR) rivers, with background colors relating to rivers. All data were combined for this figure, meaning if a mineral showed up only once at a site, it was marked as "present". Alb = Albite, Anor = Anorthite, Cal = Calcite, Chl = Clinochlore, ChS = Chlorite-Serpentine, Dol = Dolomite, Hed = Hedenbergite, Kao = Kaolinite, Mrc = Microcline, Mtlt = Montmorillonite, Mus = Muscovite, Ntr = Nontronite, Pyro = Pyrophyllite, Qtz = Quartz, Rut = Rutile, Sid = Siderotil, Talc = Talc, Ver = Vermiculite.

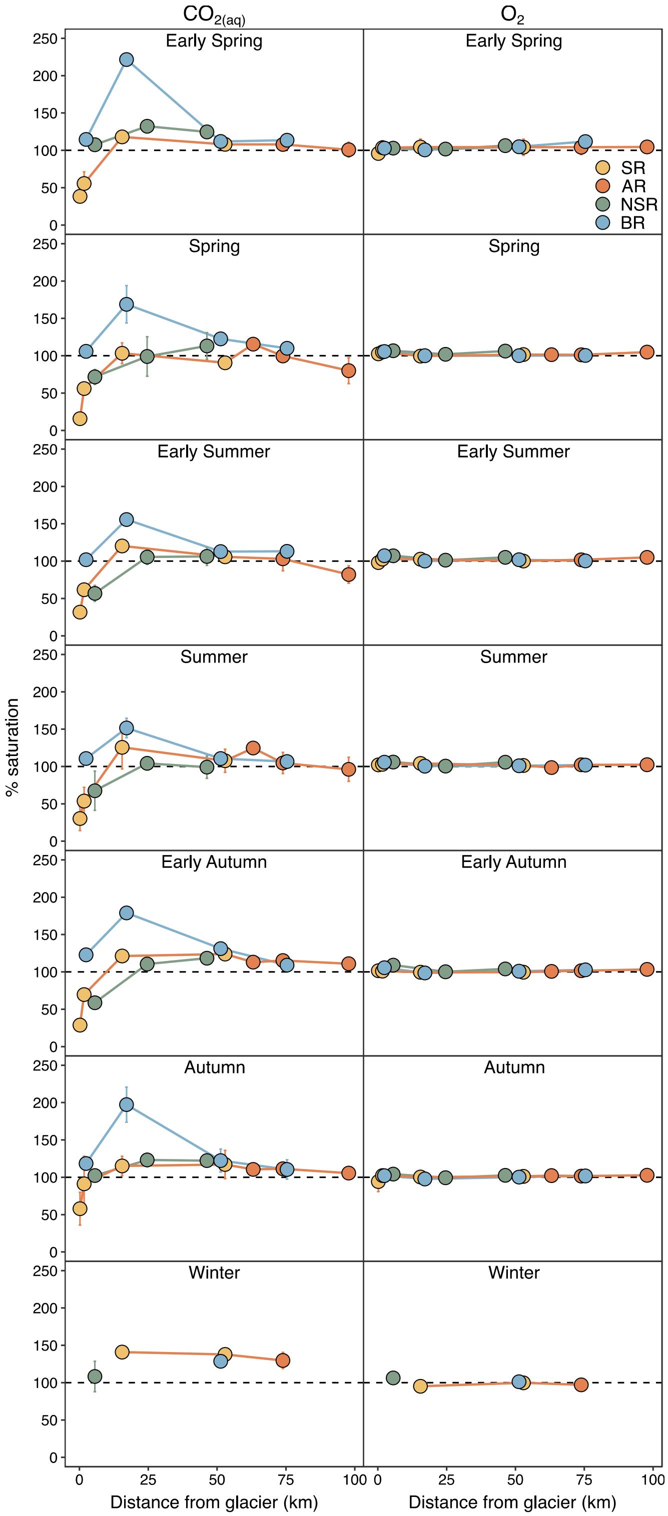

Figure A2.3. Mean (± SD) 2019 and 2020 seasonal dissolved CO₂ (CO₂(aq); left column) and O₂; right column) % saturation for riverine sampling sites at increasing downriver distance from source glaciers. Sampling dates in each season bin are summarized in **Table A2.2**. Rivers are abbreviated as SR (Sunwapta River), AR (Athabasca River), NSR (North Saskatchewan River), and BR (Bow River).

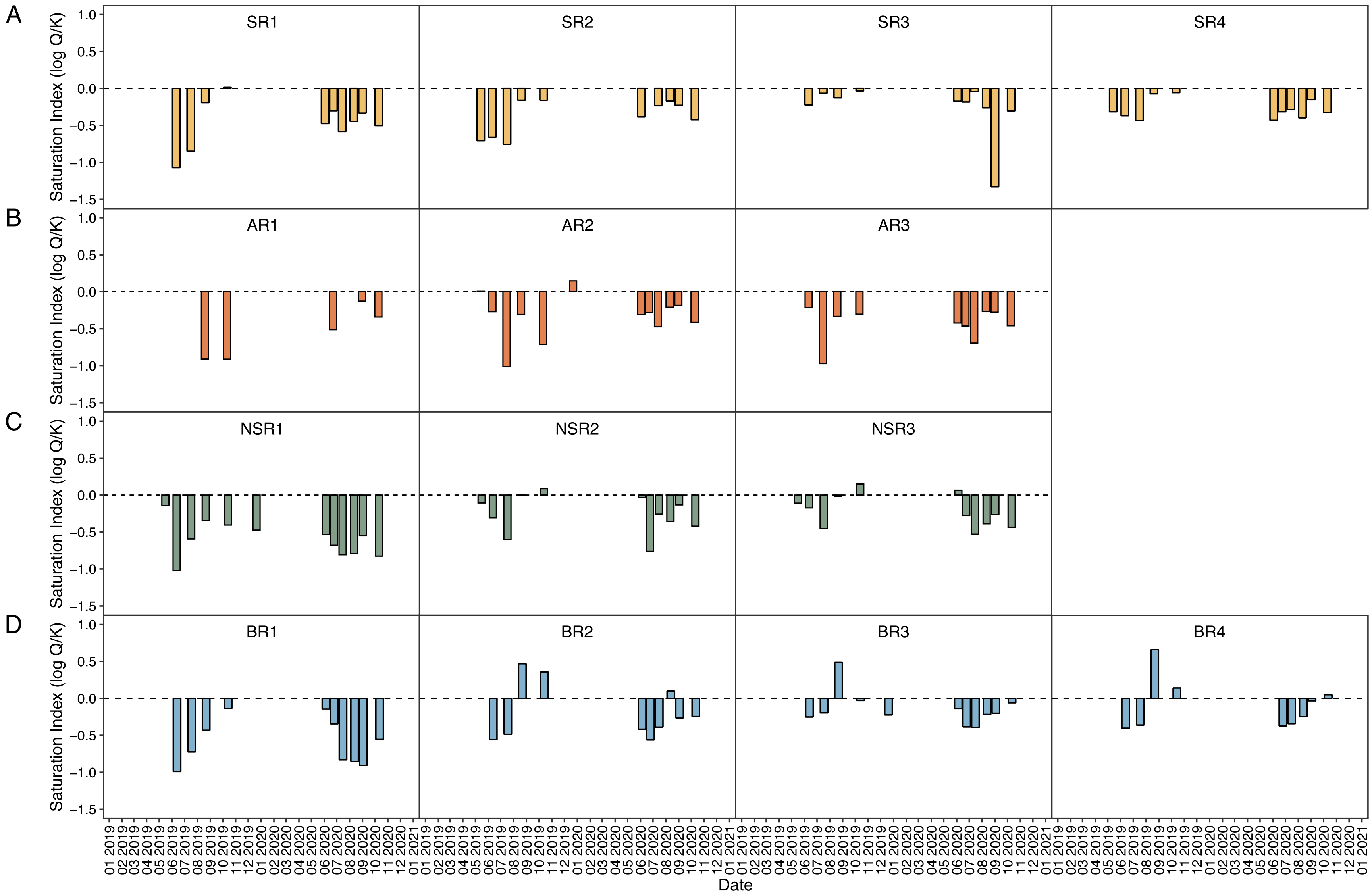

Figure A2.4. Calcite saturation indices at sampling sites along the (A) Sunwapta (SR), (B) Athabasca (AR), (C) North Saskatchewan (NSR), and (D) Bow (BR) rivers. Equilibrium for calcite saturation index is represented by the dashed black line.

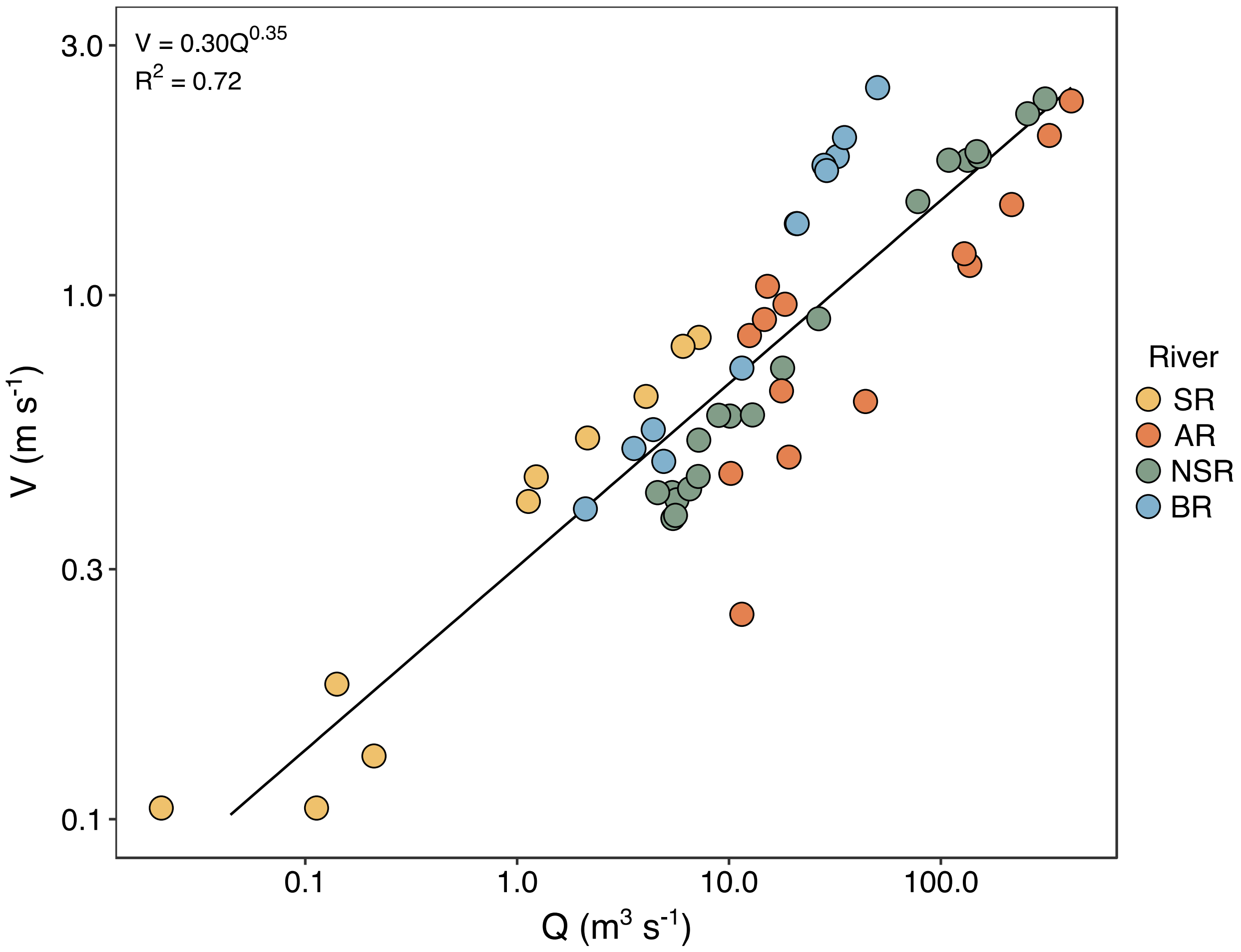

Figure A2.5. The power relationship between discharge (Q) and velocity (V). Q and V were measured by the Water Survey of Canada from 2019 to 2021 at four hydrometric gauging stations along our study rivers (the Sunwapta (SR), Athabasca (AR), North Saskatchewan (NSR), and Bow (BR) rivers), described in **Table A2.3**. The power regression equation and coefficient of determination (R^2) for the Q-V relationship is shown in the top left of the graph.

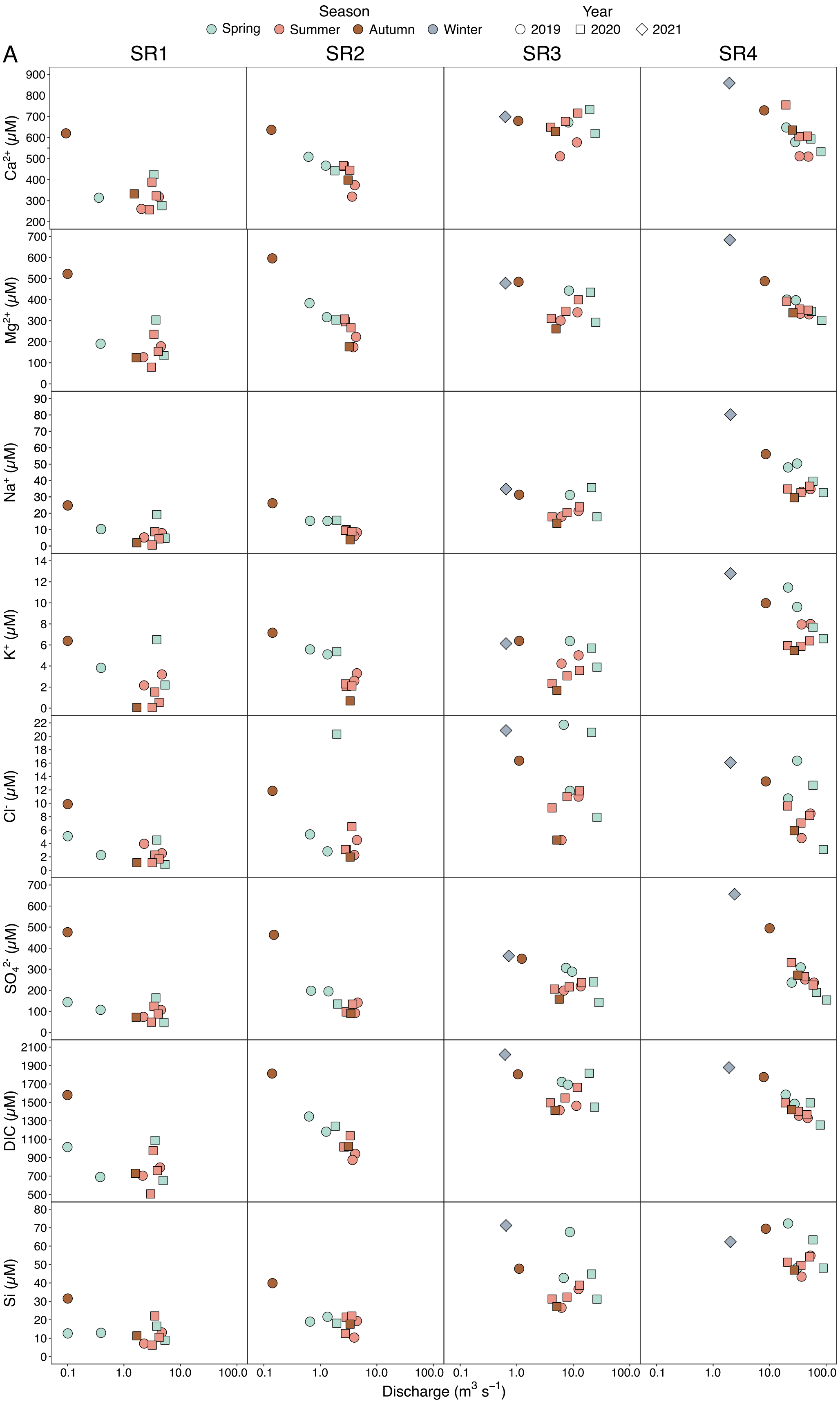
Season
Spring
Summer
Autumn
Winter
Year
2019
2020
2021
A
SR1
SR2
SR3
SR4
Ca2+ (μM)
Mg2+ (μM)
Na+ (μM)
K+ (μM)
Cl- (μM)
SO42- (μM)
DIC (μM)
Si (μM)
0.1
1.0
10.0
100.0
Discharge (m3 s−1)

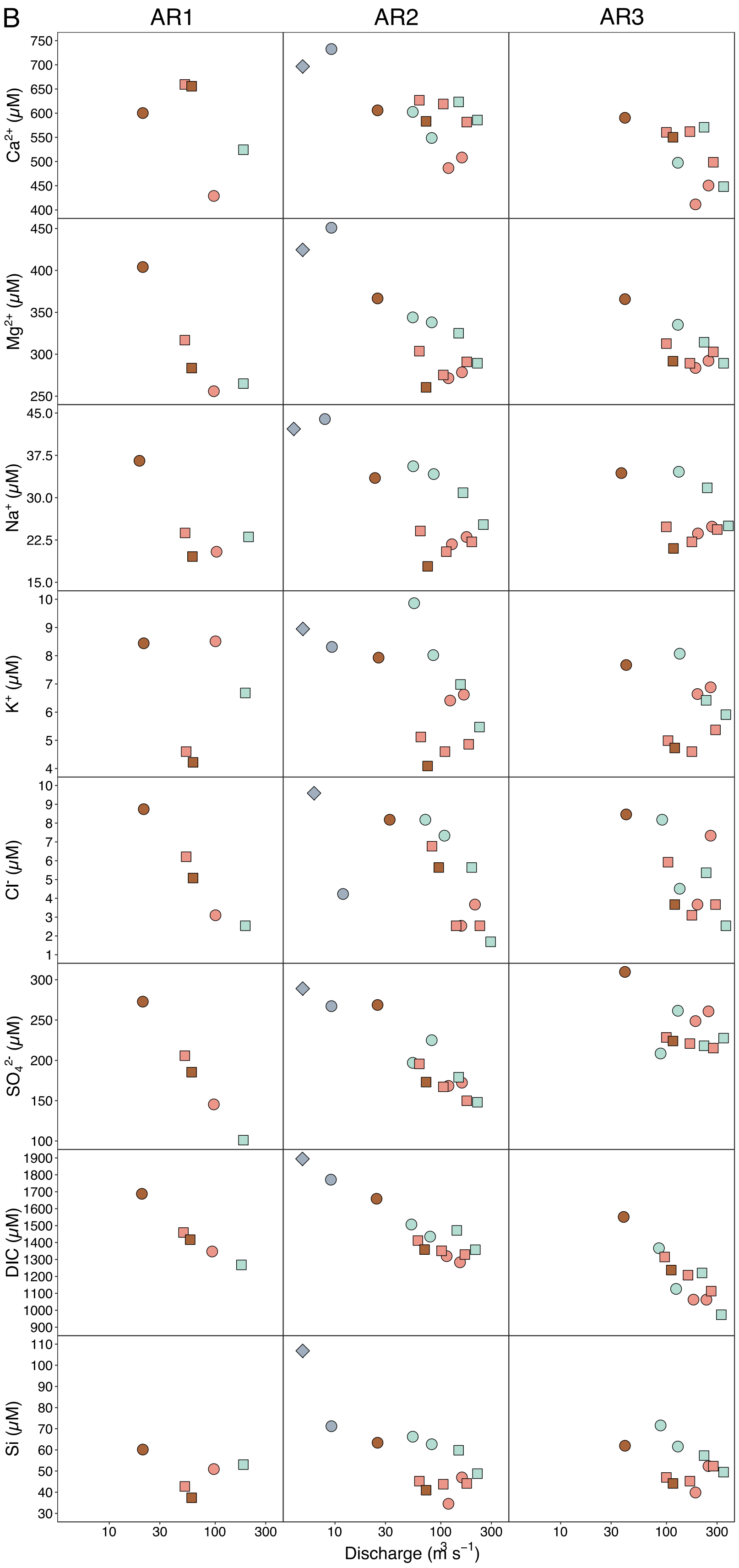
B
AR1
AR2
AR3
Ca²⁺ (μM)
750
700
650
600
550
500
450
400
Mg²⁺ (μM)
450
400
350
300
250
Na⁺ (μM)
45.0
37.5
30.0
22.5
15.0
K⁺ (μM)
10
9
8
7
6
5
4
Cl⁻ (μM)
10
9
8
7
6
5
4
3
2
1
SO₄²⁻ (μM)
300
250
200
150
100
DIC (μM)
1900
1800
1700
1600
1500
1400
1300
1200
1100
1000
900
Si (μM)
110
100
90
80
70
60
50
40
30
10
30
100
300
Discharge (m³ s⁻¹)

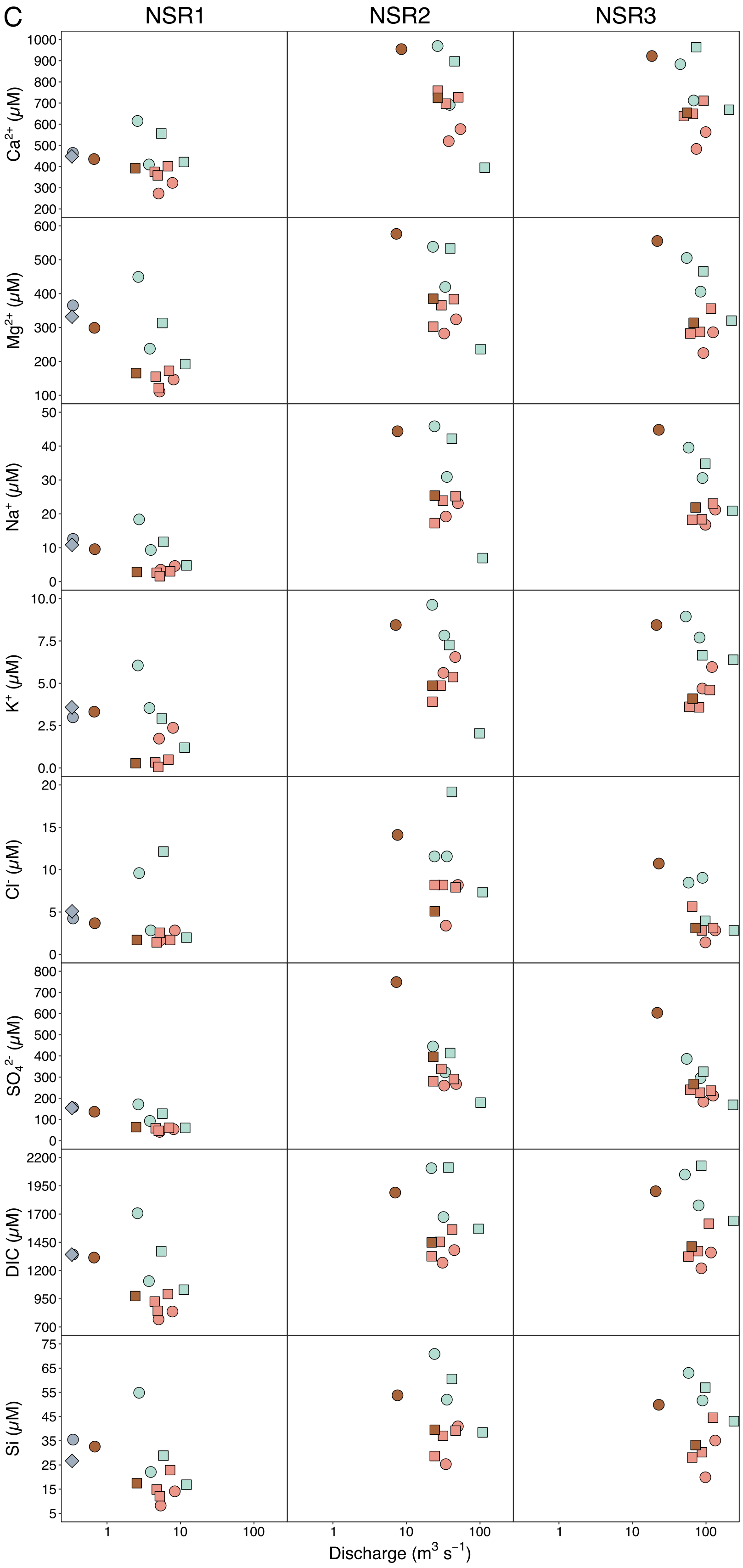
C
NSR1
NSR2
NSR3
Ca2+ (μM)
1000
900
800
700
600
500
400
300
200
Mg2+ (μM)
600
500
400
300
200
100
Na+ (μM)
50
40
30
20
10
0
K+ (μM)
10.0
7.5
5.0
2.5
0.0
Cl- (μM)
20
15
10
5
0
SO42- (μM)
800
700
600
500
400
300
200
100
0
DIC (μM)
2200
1950
1700
1450
1200
950
700
Si (μM)
75
65
55
45
35
25
15
5
1
10
100
Discharge (m3 s−1)

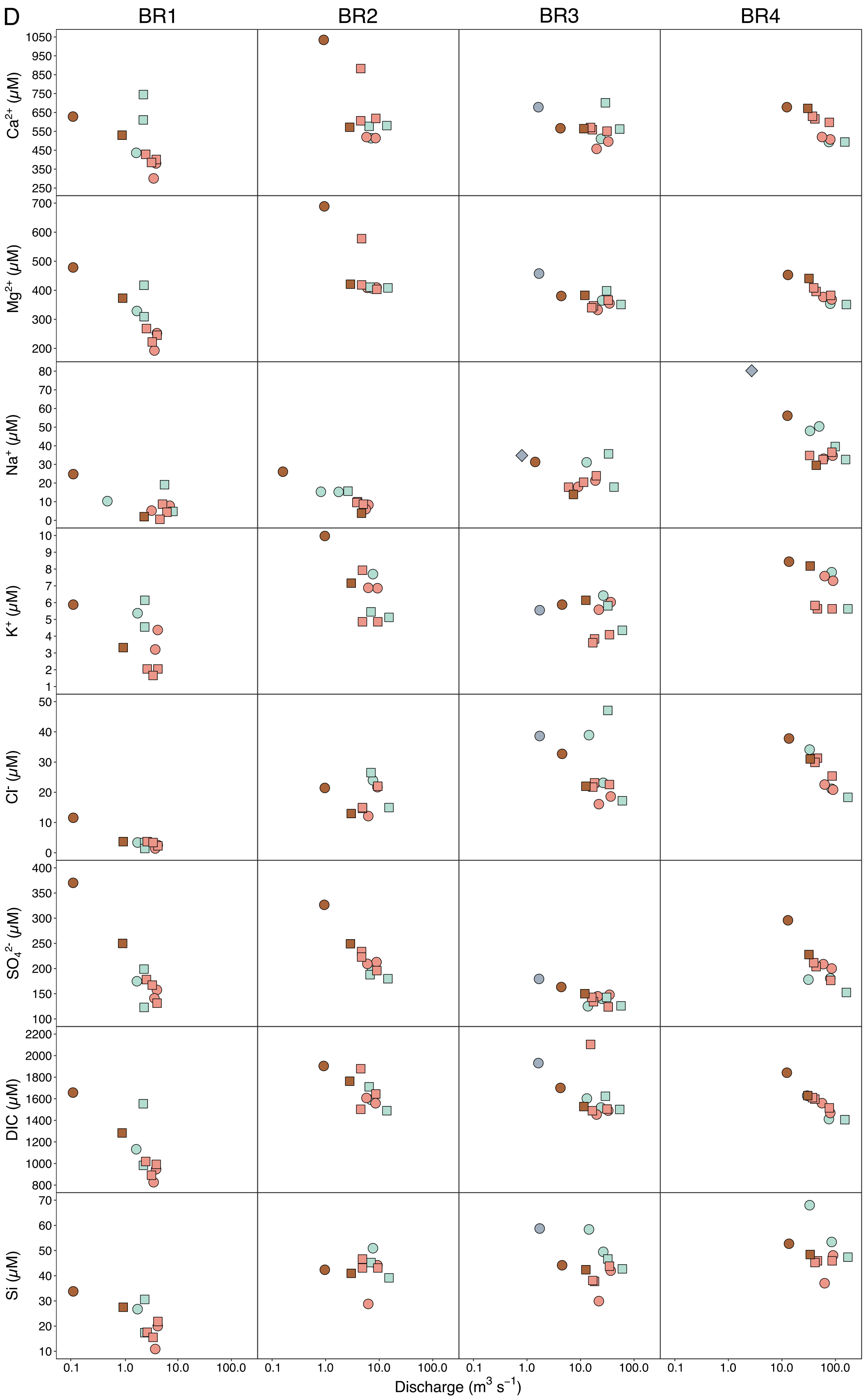
D
BR1
BR2
BR3
BR4
Ca^{2+} (μM)
1050
950
850
750
650
550
450
350
250
Mg^{2+} (μM)
700
600
500
400
300
200
Na^{+} (μM)
80
70
60
50
40
30
20
10
0
K^{+} (μM)
10
9
8
7
6
5
4
3
2
1
Cl^{-} (μM)
50
40
30
20
10
0
SO$_4^{2-}$ (μM)
400
350
300
250
200
150
100
DIC (μM)
2200
2000
1800
1600
1400
1200
1000
800
Si (μM)
70
60
50
40
30
20
10
0.1
1.0
10.0
100.0
Discharge (m^3 s^{-1})

Figure A2.6. Semi-log CQ relationships of cations (Ca^{2+}, Mg^{2+}, Na^{+}, K^{+}), anions (Cl^{-}, SO_4^{2-}), dissolved inorganic carbon (DIC) and Si for sampling sites along the (A) Sunwapta (SR), (B) Athabasca (AR), (C) North Saskatchewan (NSR), and (D) Bow (BR) rivers. Note different y-axis scales.

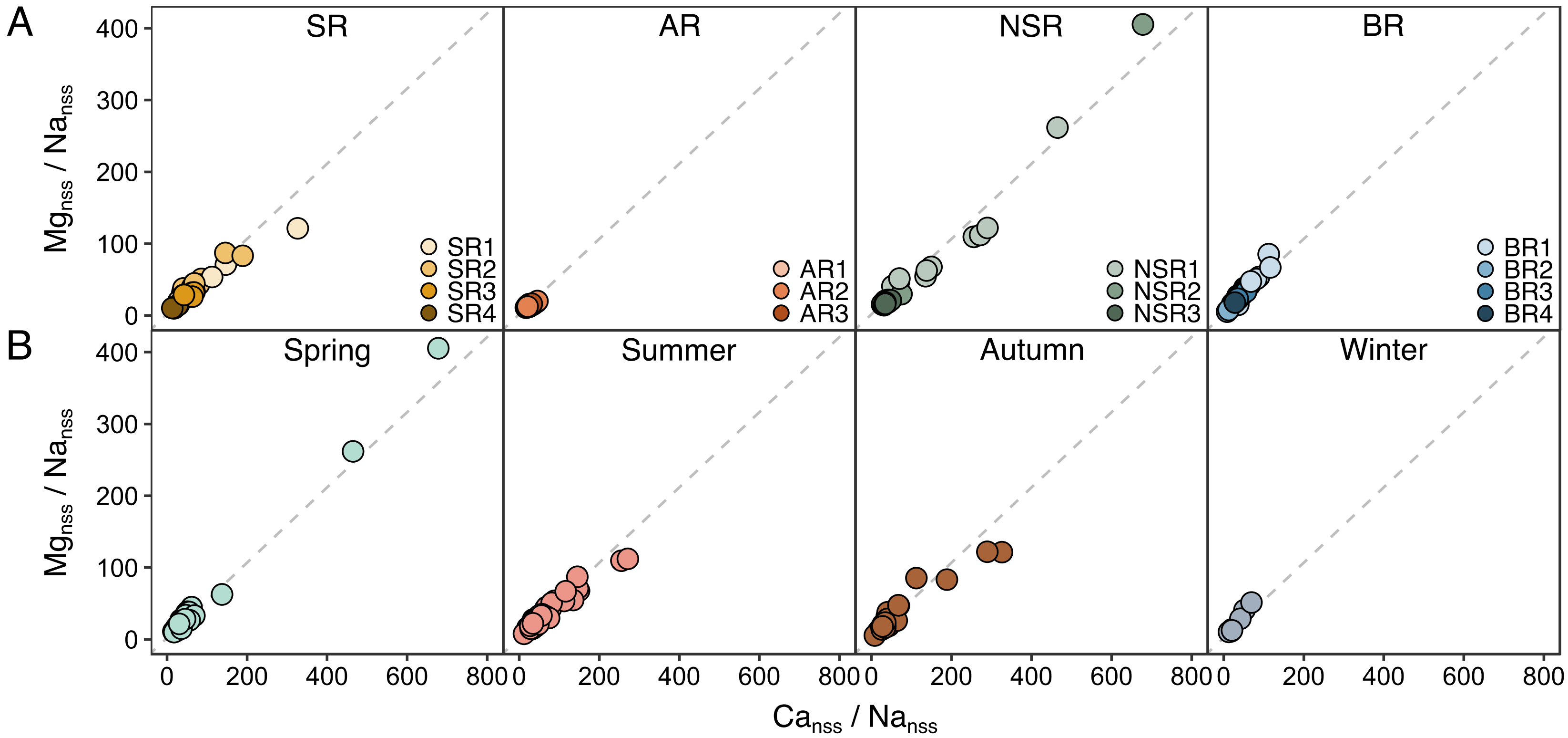

Figure A2.7. Mixing diagrams of non-sea salt (nss) molar Ca/Na concentrations versus molar Mg/Na concentrations by (A) river and (B) season. In panel (A), rivers are SR (Sunwapta River), AR (Athabasca River), NSR (North Saskatchewan River), and BR (Bow River), and colors are related to sampling sites. The dashed grey line is the line of best fit.

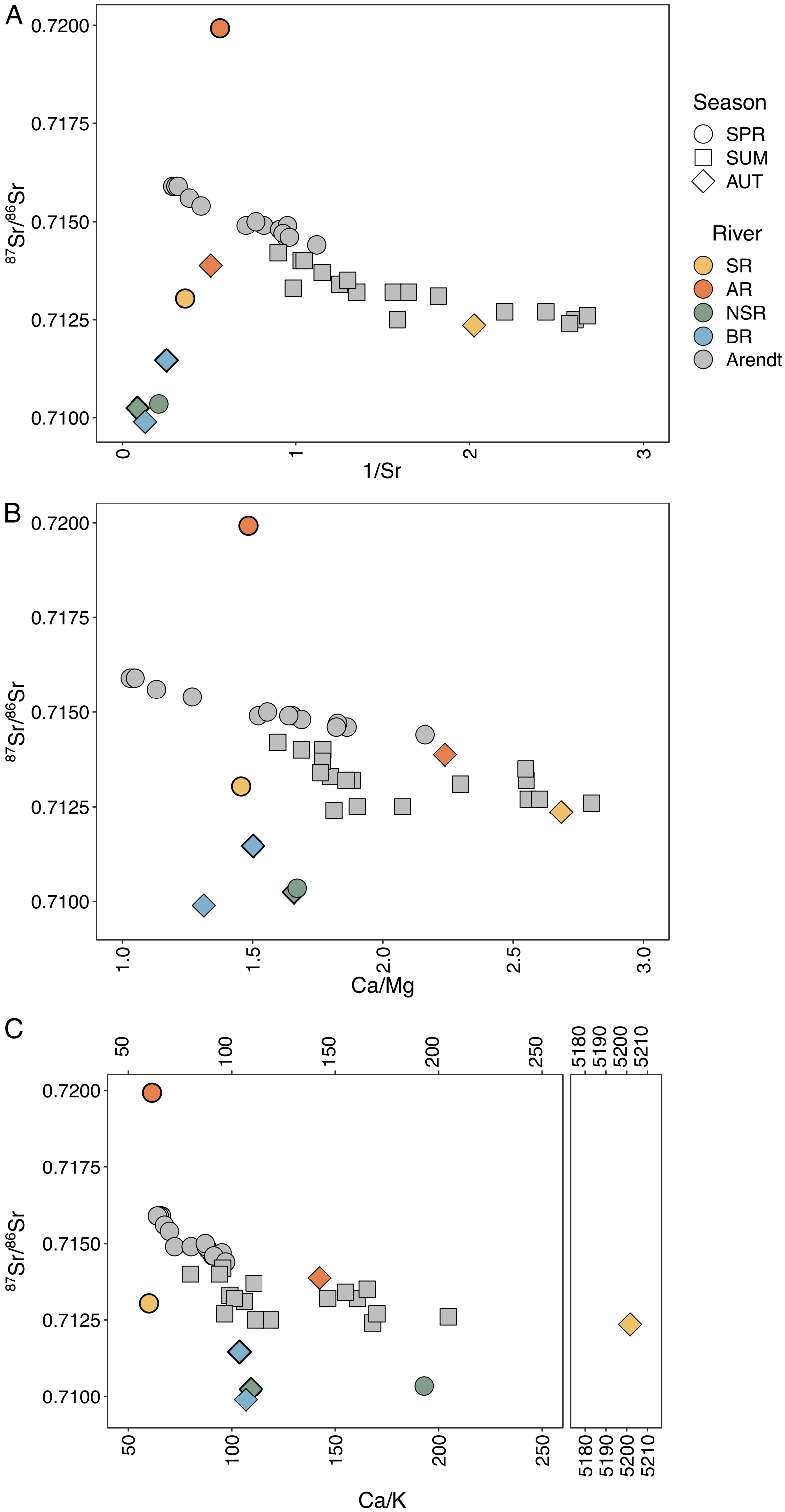

Figure A2.8. Molar ratios versus $^{87}Sr/^{86}Sr$, including (A) the inverse concentration of Sr (μM^{-1}), and (B) molar Ca^{2+}/Mg^{2+} and (C) molar Ca^{2+}/K^{+} ratios. Thick black outlines denote downstream sites. Grey data were collected proximal to sampling site SR1 and published in Arendt et al. (2016).

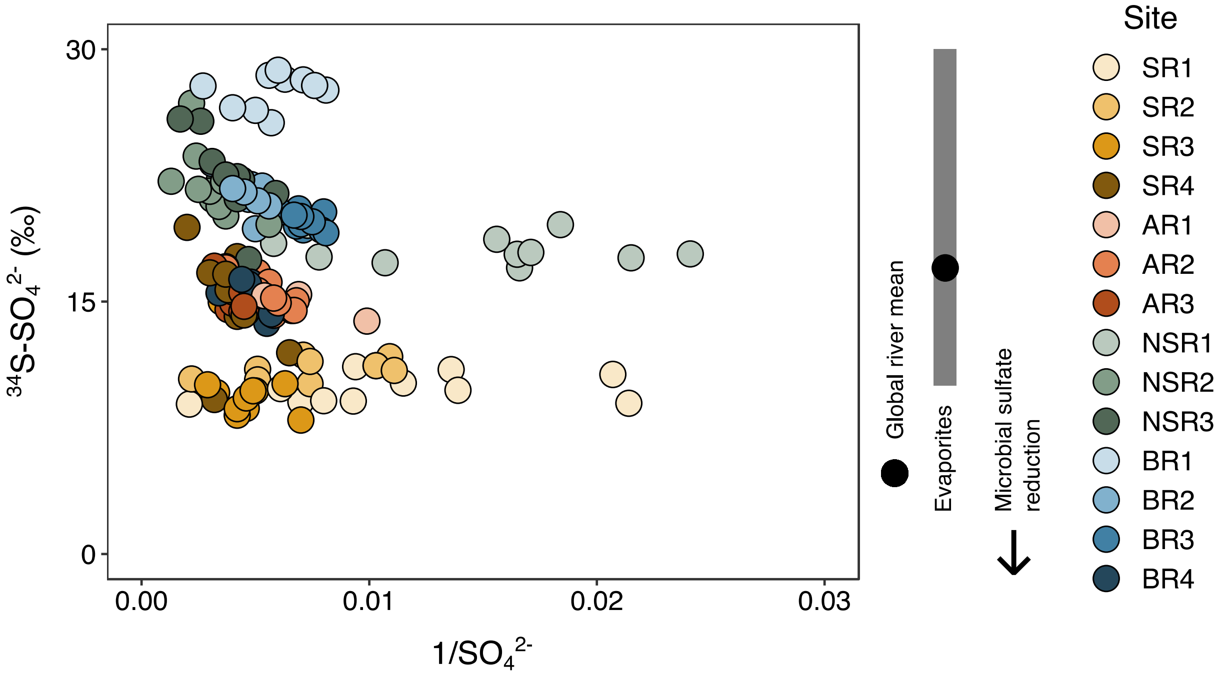

Figure A2.9. Inverse SO_4^{2-} concentration versus δ^{34}S-SO$_4$ (‰ VCDT) for sampling sites along the Sunwapta (SR), Athabasca (AR), North Saskatchewan (NSR), and Bow (BR) rivers. Range of δ^{34}S-SO$_4$ (VCDT) for the global river mean, global evaporites, and microbial sulfate reduction are shown on the right. Figure adapted from Burke et al. (2018) and Relph et al. (2021) with global data from Burke et al. (2018).

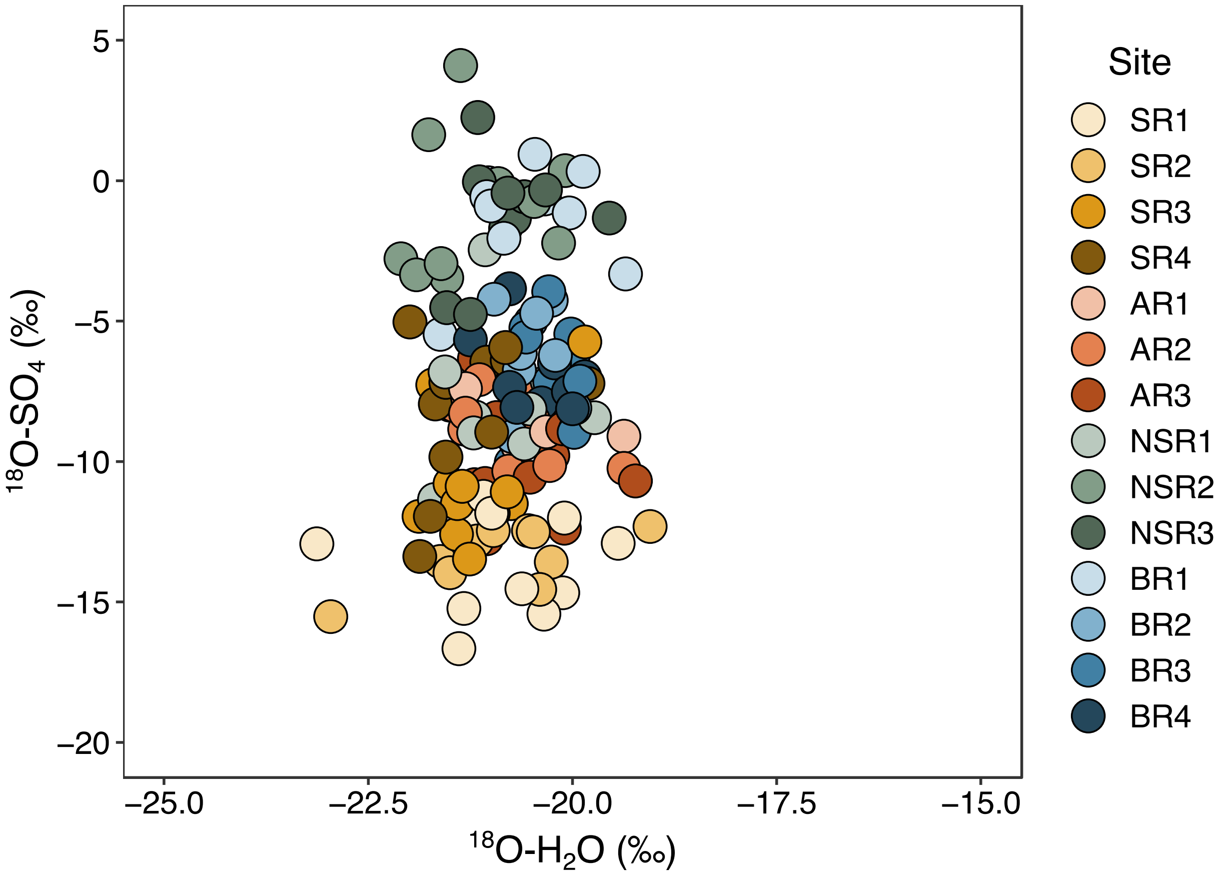

Figure A2.10. $\delta^{18}O\text{-}H_2O$ (‰ VSMOW) versus $\delta^{18}O\text{-}SO_4$ (‰ VSMOW) for sampling sites along the Sunwapta (SR), Athabasca (AR), North Saskatchewan (NSR) and Bow (BR) rivers.

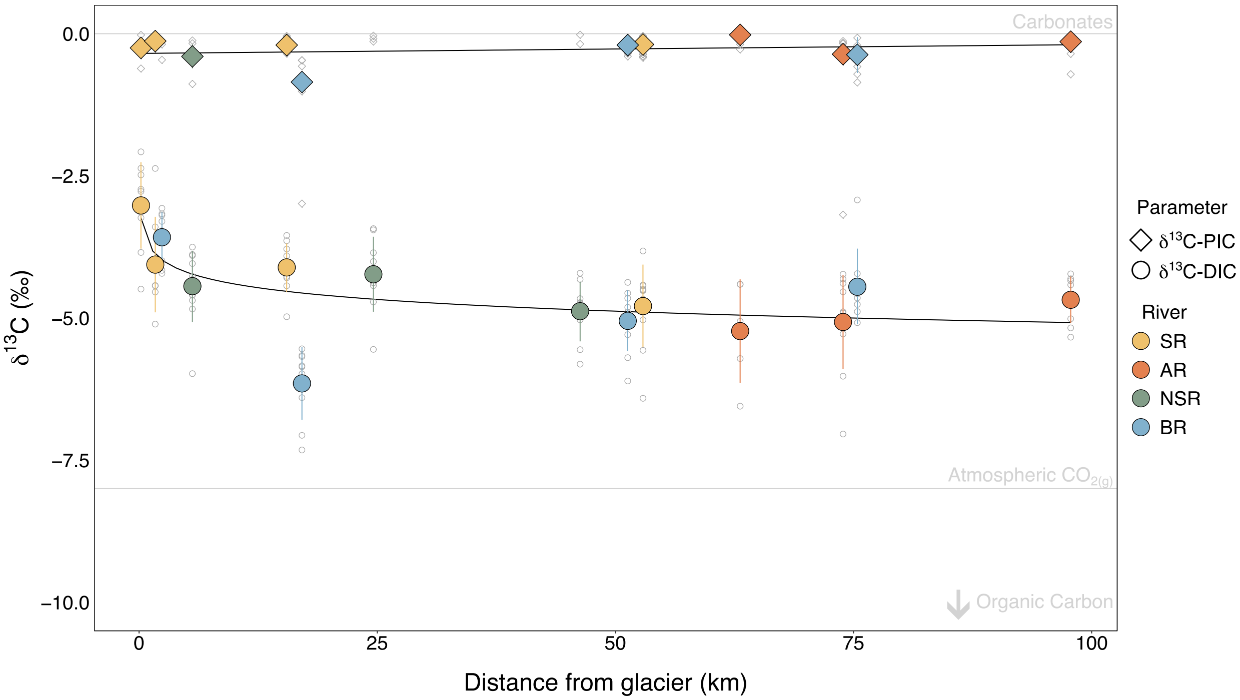

Figure A2.11. $\delta^{13}C$ (‰) signatures of dissolved inorganic carbon (DIC; circles) and particulate inorganic carbon (PIC; diamonds) with downriver distance from source glaciers (km) along the Sunwapta (SR), Athabasca (AR), North Saskatchewan (NSR), and Bow (BR) rivers. Colored symbols are means with the standard deviation as bars, while individual datapoints are seen outlined in grey.

Appendix 3. Supporting information for Chapter 4 “Removal of total and methyl mercury from North Saskatchewan River water during the production of municipal drinking water in Edmonton, Alberta, Canada”

Table A3.1. Total mercury (THg) concentrations in river water (Raw), Post-Filtration (PF) and Post-Ultraviolet (PUV) treatments and in the on-site holding reservoir (Reservoir) from a pilot study conducted in winter and summer 2003-2004.

DATE	Raw THg ng L^{-1}	PF THg ng L^{-1}	PUV THg ng L^{-1}	Reservoir THg ng L^{-1}
10-Nov-03	0.56			0.15
11-Nov-03	0.45			0.14
12-Nov-03	0.80			0.15
13-Nov-03	0.50			0.16
14-Nov-03	0.46			0.15
15-Nov-03	0.37			0.06
16-Nov-03	0.21			0.21
17-Nov-03	0.27			0.11
18-Nov-03	0.28			0.13
19-Nov-03	0.36			0.14
20-Nov-03	0.34			0.13
Mean	0.42			0.14
SD	0.17			0.04
5-Jan-04	0.36	0.14	0.08	0.07
6-Jan-04	0.26	0.13	0.08	0.08
7-Jan-04	0.26	0.08	0.09	0.04
8-Jan-04	0.32	0.08	0.07	0.04
9-Jan-04	0.57	0.08	0.24	0.24
Mean	0.35	0.10	0.11	0.09
SD	0.13	0.03	0.07	0.08
12-Jul-04	4.92	0.26	0.27	0.34
13-Jul-04	36.21	0.25	0.22	0.24
14-Jul-04	16.23	0.25	0.34	0.32
15-Jul-04	4.53	0.31	0.26	0.35
16-Jul-04	3.35	0.20	0.20	0.24
Mean	13.05	0.25	0.26	0.30
SD	13.96	0.04	0.05	0.05

Table A3.2. Summary of block ANOVA calculated for THg.

	DF	SS	MS	F	P-value
WaterType	5	716.68	143.34	13.71	6.82×10^{-11}
Date	28	342.01	12.22	1.17	0.27
Residuals	140	1463.70	10.46		

Table A3.3. Summary of block ANOVA calculated for MeHg.

	DF	SS	MS	F	P-value
WaterType	5	0.380	0.076	13.92	4.90×10^{-11}
Date	28	0.198	0.007	1.29	0.17
Residuals	140	0.765	0.005		

Table A3.4. Total mercury (THg) and methylmercury (MeHg) concentrations in river water (Raw), filtered river water (FRaw), and in water Post-Clarification (PC), Post-Filtration (PF) and Post-Ultraviolet (PUV) treatments, as well as in the on-site holding reservoir (Reservoir) in 2020-2021.

DATE	Raw THg ng L^{-1}	Raw MeHg ng L^{-1}	FRaw THg ng L^{-1}	FRaw MeHg ng L^{-1}	PC THg ng L^{-1}	PC MeHg ng L^{-1}	PF THg ng L^{-1}	PF MeHg ng L^{-1}	PUV THg ng L^{-1}	PUV MeHg ng L^{-1}	Reservoir THg ng L^{-1}	Reservoir MeHg ng L^{-1}
24-Apr-20	16.44	0.476	1.47	0.063	0.16	0.009	<DL	0.000	0.20	0.001	<DL	<DL
1-May-20	8.87	0.201	0.56	0.051	0.15	0.017	0.17	0.009	0.15	0.004	0.41	0.008
8-May-20	9.62	0.191	1.84	0.070	0.22	0.015	<DL	<DL	0.11	<DL	0.35	0.008
15-May-20	4.47	0.100	1.11	0.049	0.36	0.018	0.08	0.004	0.08	0.004	0.07	0.009
22-May-20	9.19	0.122	1.19	0.039	0.97	0.029	0.30	0.003	0.24	0.003	0.32	0.008
29-May-20	8.75	0.168	2.46	0.069	0.60	0.015	0.77	0.005	0.64	0.004	0.74	0.015
4-Jun-20	2.76	0.241	2.09	0.042	0.66	0.019	0.72	0.013	0.77	0.011	0.99	0.017
12-Jun-20	40.14	0.163	1.59	0.070	0.29	0.026	0.40	0.002	0.37	0.002	0.63	0.007
19-Jun-20	4.20	0.156	1.57	0.098	0.29	0.033	0.35	<DL	0.33	0.010	0.62	0.014
26-Jun-20	4.95	0.107	1.23	0.049	0.88	0.026	0.59	0.006	0.46	0.001	0.50	0.006
3-Jul-20	11.54	0.928	2.06	0.066	0.32	0.010	0.55	0.006	0.41	0.005	0.50	0.021
8-Jul-20	9.33	0.175	1.99	0.064	0.32	0.024	0.39	0.002	0.40	<DL	0.32	0.005
17-Jul-20	7.08	0.116	1.48	0.058	2.25	0.046	0.34	<DL	0.39	<DL	0.58	<DL
24-Jul-20	14.15	0.229	1.76	0.090	0.35	0.030	0.40	<DL	0.42	<DL	0.90	<DL
31-Jul-20	3.37	0.083	0.90	0.040	0.33	0.029	0.35	0.003	0.38	0.001	0.39	0.007
7-Aug-20	2.09	0.070	0.63	0.040	0.27	0.027	0.20	0.008	0.16	0.003	0.24	0.002
14-Aug-20	2.00	0.047	0.73	0.028	0.21	0.016	0.44	0.003	0.20	0.003	0.33	<DL
21-Aug-20	3.01	0.055	0.51	0.013	0.27	0.014	0.37	<DL	0.38	0.002	0.37	<DL
28-Aug-20	1.06	0.029	0.57	0.018	0.17	0.014	0.17	<DL	0.17	<DL	0.22	<DL
4-Sep-20	0.55	0.022	0.20	0.016	0.19	0.013	0.10	<DL	0.15	<DL	0.45	<DL
18-Sep-20	0.66	0.023	0.22	0.013	0.16	0.010	0.10	<DL	0.17	<DL	0.13	<DL
2-Oct-20	0.54	0.017	0.24	<DL	0.33	0.013	0.21	<DL	0.12	<DL	0.16	<DL
16-Oct-20	0.62	0.021	0.30	0.009	0.28	0.017	0.37	<DL	0.21	<DL	0.19	0.014
30-Oct-20	1.22	0.024	0.22	0.004	0.58	0.016	0.20	<DL	0.21	<DL	0.23	0.005
27-Nov-20	1.68	0.038	0.34	0.009	1.13	0.023	0.32	<DL	0.36	<DL	0.43	<DL
18-Dec-20	0.66	0.014	0.42	0.009	0.57	0.013	0.28	<DL	0.23	<DL	0.24	<DL
22-Jan-21	0.49	0.018	0.23	0.008	0.48	0.009	0.23	<DL	0.18	<DL	0.22	<DL
26-Feb-21	0.80	0.027	0.26	0.008	0.38	0.016	0.19	0.004	0.21	<DL	0.41	<DL
26-Mar-21	0.71	0.025	0.54	0.017	0.32	0.003	0.18	<DL	0.19	<DL	0.29	<DL
Mean	5.89	0.134	0.99	0.038	0.47	0.019	0.30	0.002	0.29	0.002	0.39	0.005
SD	7.98	0.183	0.70	0.028	0.42	0.009	0.19	0.003	0.16	0.003	0.23	0.006

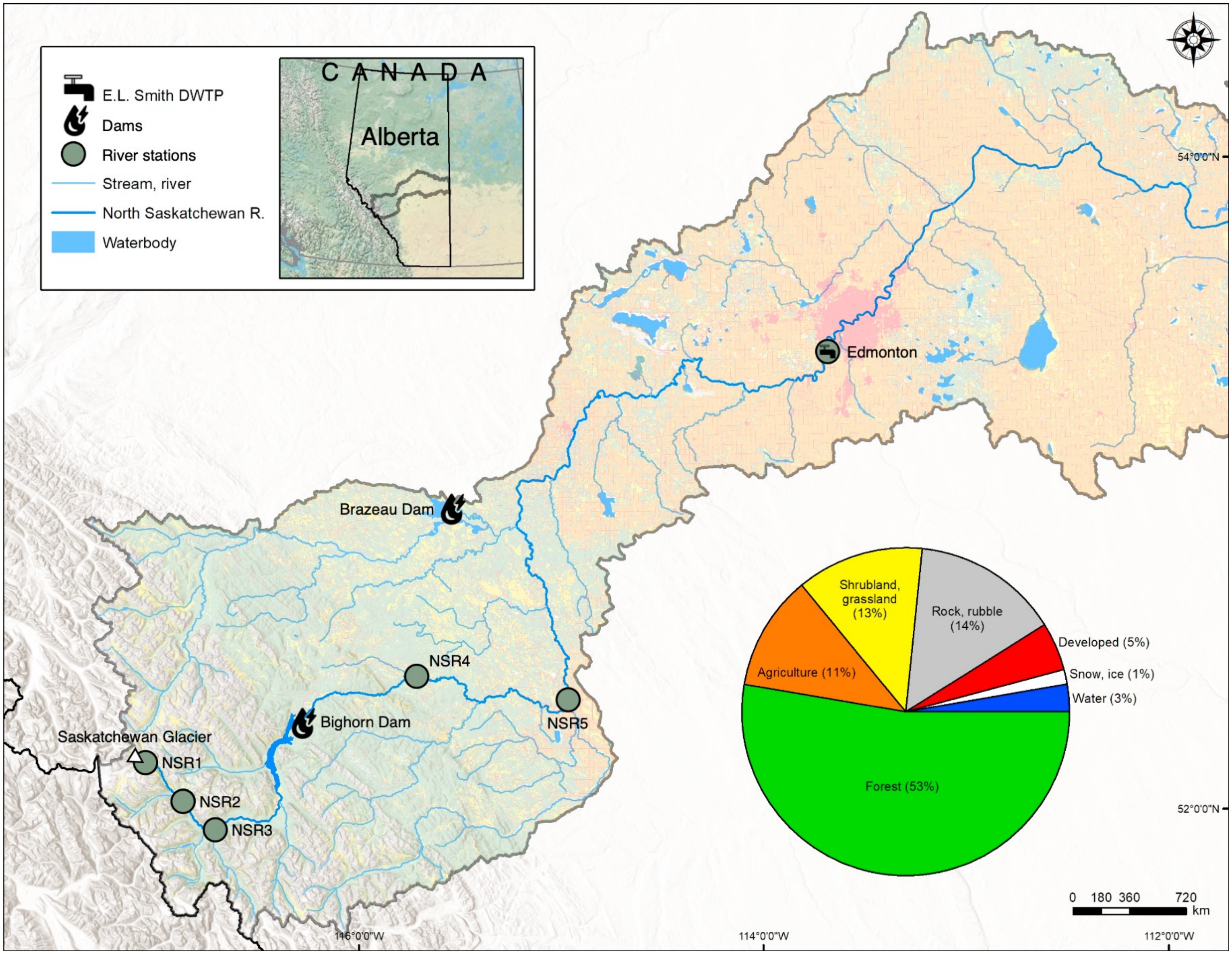

Figure A3.1. Map of the North Saskatchewan River (NSR) in Alberta, with major landmarks shown. The river flows from its origins at the Saskatchewan Glacier in Banff National Park near NSR1 downriver to Edmonton and beyond. Color of the map associates to percent forest, agriculture, shrub or grassland, rock or rubble, developed, snow or ice, and water as shown in the pie chart.

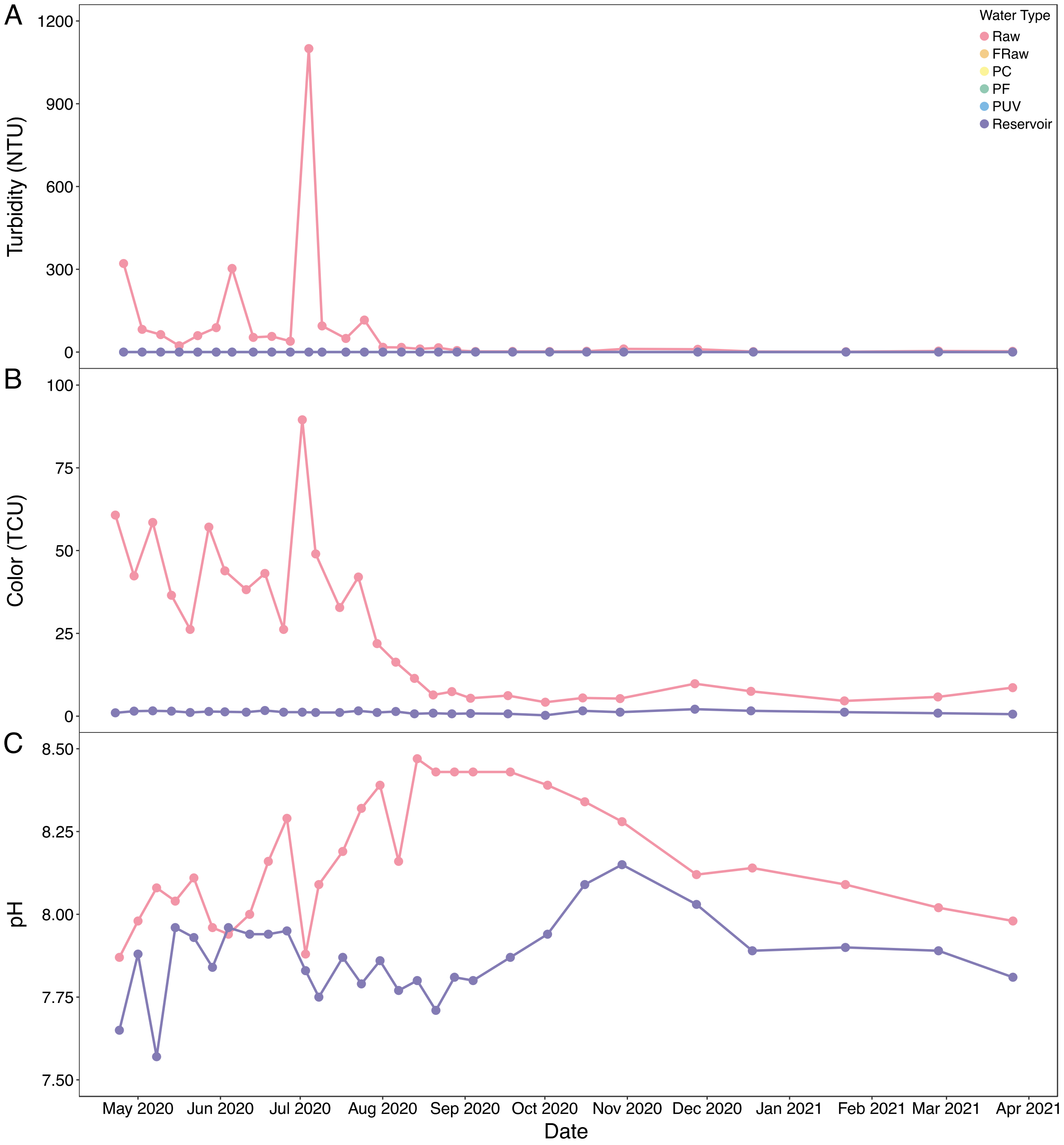

Figure A3.2. (A) Turbidity, (B) Color, and (C) pH in raw river water (Raw), in water Post-Ultraviolet Treatment (PUV; turbidity only) and in the on-site holding reservoir (Reservoir). No data were available for water Post-Clarification (PC) or Post- Filtration (PF) treatment on the days we sampled, or for filtered Raw river water (FRaw).

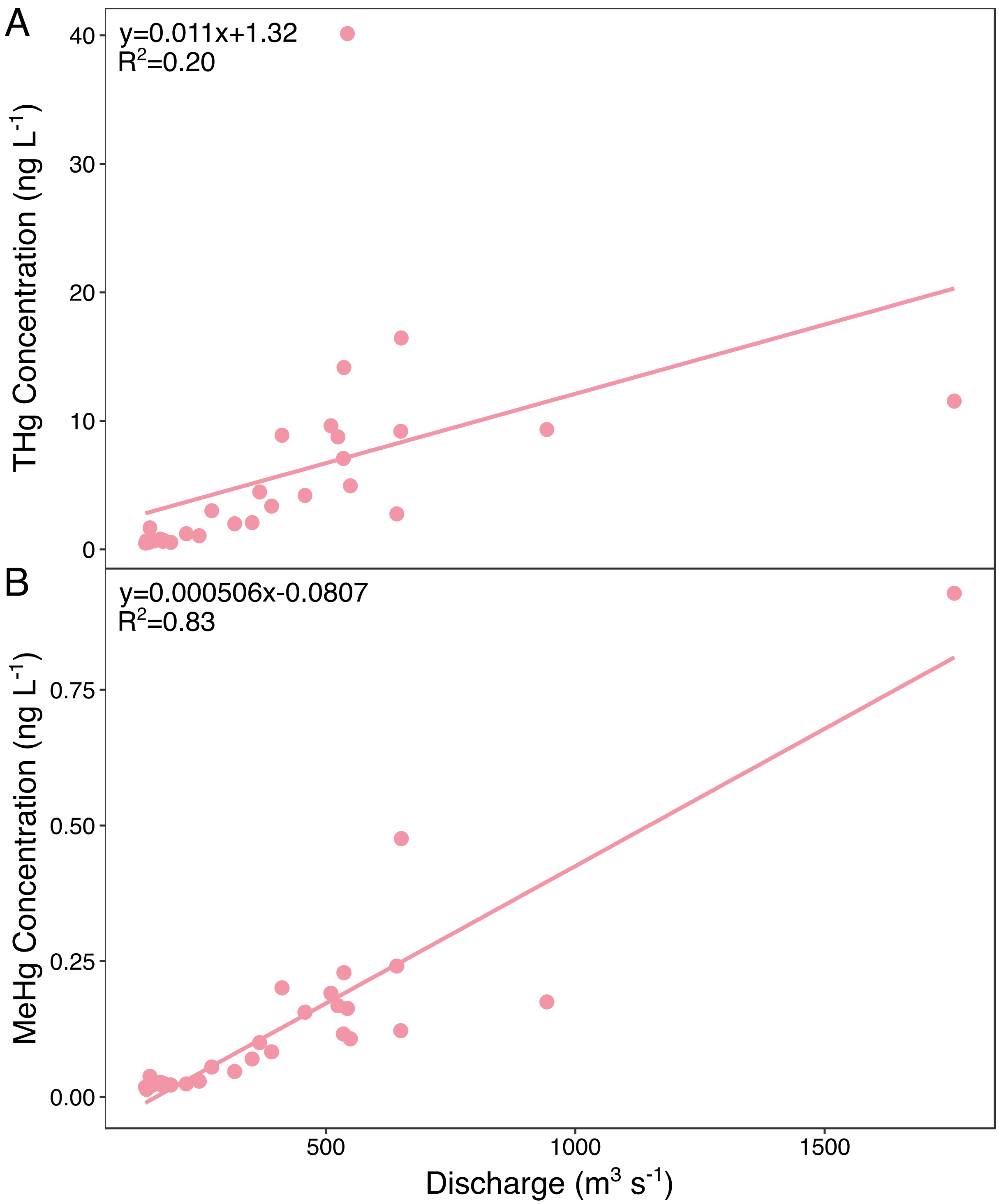

Figure A3.3. Discharge-concentration graphs for (A) THg and (B) MeHg for the North Saskatchewan River at Edmonton. Linear regression formulae and coefficient of determinations are shown in the top right of each graph.

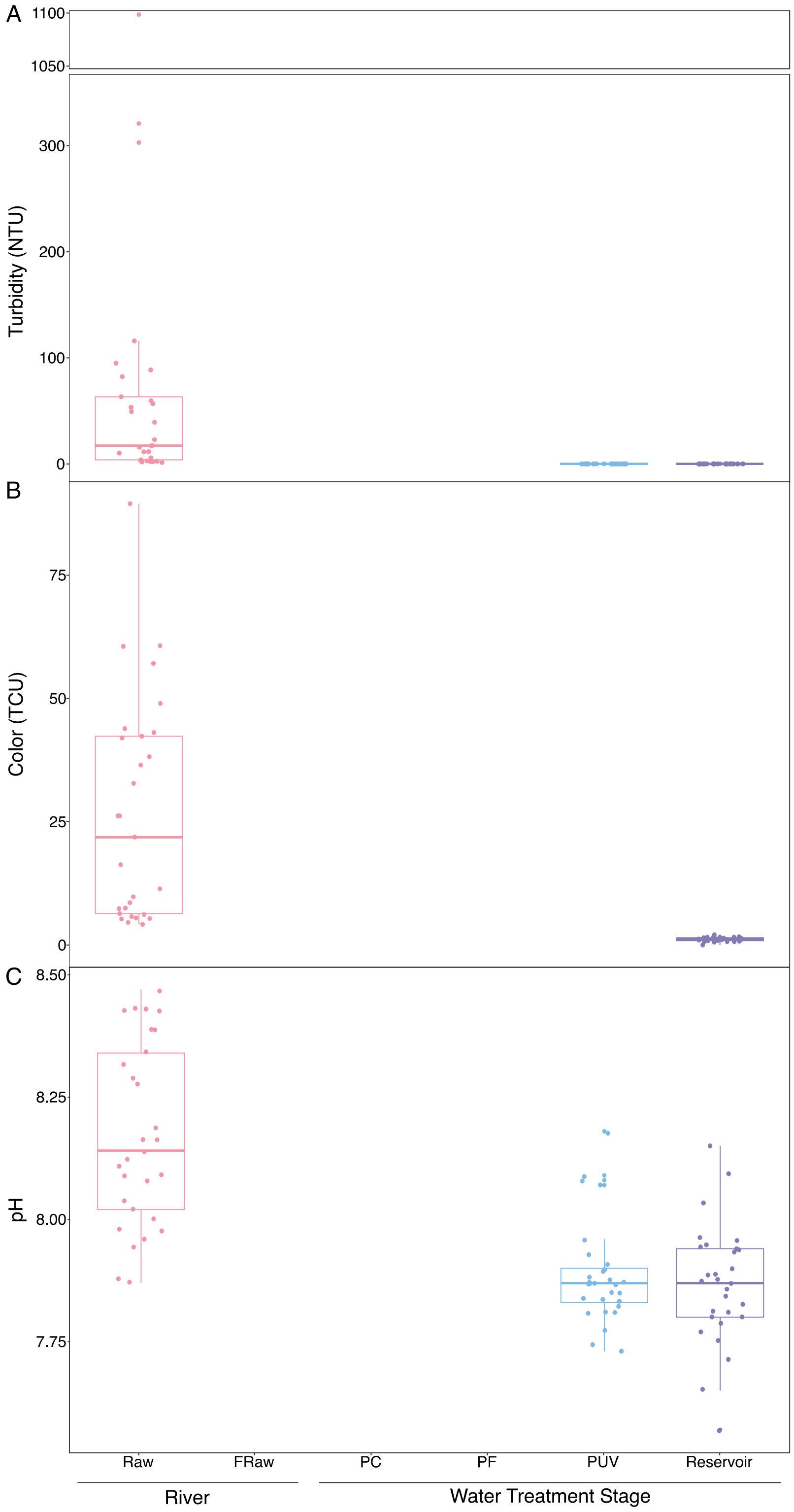

Figure A3.4. (A) Turbidity, (B) Color, and (C) pH in raw river water (Raw), in water Post-Ultraviolet Treatment (PUV) and in the on-site holding reservoir (Reservoir). No data were available for water Post-Clarification (PC) or Post-Filtration (PF) treatment on the days we sampled, or for filtered Raw river water (FRaw).